Open Research Online

The Open University's repository of research publications
and other research outputs

The Dynamics of Periodically Forced Systems

Thesis

How to cite:

Dando, Paul (1993). The Dynamics of Periodically Forced Systems. PhD thesis. The Open University.

For guidance on citations see FAQs.

© 1993 Paul Dando

Version: Version of Record

Copyright and Moral Rights for the articles on this site are retained by the individual authors and/or other copyright owners. For more information on Open Research Online's data policy on reuse of materials please consult the policies page.

oro.open.ac.uk

DX 176218
UNRESTRICTED.

The Dynamics of Periodically Forced Systems

Paul Dando

A thesis submitted for the degree of Doctor of Philosophy in the Department of Mathematics of The Open University.

31 January 1993

Author's no: M7044420.
Date of submission: 2 February 1993.
Date of award: 5 May 1993.

ProQuest Number: C359720

All rights reserved

INFORMATION TO ALL USERS
The quality of this reproduction is dependent upon the quality of the copy submitted.

In the unlikely event that the author did not send a complete manuscript
and there are missing pages, these will be noted. Also, if material had to be removed,
a note will indicate the deletion.

ProQuest C359720

Published by ProQuest LLC (2019). Copyright of the Dissertation is held by the Author.

All rights reserved.
This work is protected against unauthorized copying under Title 17, United States Code
Microform Edition © ProQuest LLC.

ProQuest LLC.
789 East Eisenhower Parkway
P.O. Box 1346
Ann Arbor, MI 48106 – 1346

Abstract

The classical and quantum dynamics of a one-dimensional atomic system perturbed by a periodic electric field of frequency, Ω, in the regimes of high and low field frequency is studied.

At high frequencies various ionization mechanisms are considered in both dynamics. We show that for systems having analytic potentials, and for sufficiently high frequencies, the classical system can ionize through regular orbits, in contradistinction to the driven Coulomb system.

An area-preserving map is constructed which approximates the classical motion well at high frequencies; explicit quantisation of this map, in terms of the Fourier components of the classical motion, provides a very efficient means of obtaining approximate solutions to the one-dimensional, time-dependent Schrödinger equation. The Morse oscillator is considered in detail: the classical map is found to agree well with the numerical solution of Hamilton's equations. Classical and quantal ionization probabilities are compared and circumstances delineated where they agree.

Comparisons of various theoretical models with experimental data for the ionization of excited hydrogen atoms in low frequency microwave fields are used to distinguish between tunnelling *through* and classical escape *over* the slowly oscillating barrier and between one- and many-state dynamical processes. Formulae used to interpret low frequency laser multi-photon ionization data are found not to describe the experimental data which are best reproduced by the new semiclassical model presented here. Ranges of validity of other models are delineated.

A new analytic approximation for the solutions of the two-state equations of motion is obtained and used to predict the positions and widths of each member of the infinite set of resonances between any finite value of Ω and 0. This analysis shows why recent experiments on the microwave ionization of hydrogen atoms by low frequency fields failed to observe any resonances.

Contents

List of Figures v

List of Tables vii

Acknowledgements viii

Introduction 1

1 Classical Theory 8

1.1 Introduction 8

1.2 Hamiltonian dynamics 10

1.2.1 Conservative Hamiltonian systems 11

1.2.2 Time-dependent canonical transformations 12

1.2.3 Angle-action variables 13

1.3 The Hamiltonian and gauge transformations 17

1.3.1 The Hamiltonian for a hydrogen atom in a microwave field 17

1.3.2 The Hamiltonian for a one-dimensional system 19

1.3.3 Gauge transformations 20

1.3.4 The dipole gauge Hamiltonian 21

1.3.5 The acceleration gauge Hamiltonian 22

1.4 Low frequency behaviour: the adiabatic Hamiltonian 22

1.4.1 The adiabatic Hamiltonian 22

1.4.2 The breakdown of adiabatic invariance 24

1.5 Resonant motion: the resonance overlap condition 25

1.6 High frequency behaviour: the mean-motion Hamiltonian 28

1.6.1 The mean-motion Hamiltonian 28

1.6.2 Sudden field switch 31

1.6.3 Adiabatic field switch 32

1.6.4 Breakdown of adiabatic invariance 34

1.7 Classical area-preserving maps 35

1.7.1 The general classical map 35
1.7.2 The mean motion map 38
1.7.3 Local behaviour and the standard map 39

2 Quantal theory **40**
2.1 Introduction 40
2.2 The Schrödinger equation and gauge transformations 40
2.3 Solving the Schrödinger equation 42
2.3.1 Finite difference methods 42
2.3.2 Basis expansion methods 43
2.3.3 Floquet theory 44
2.4 Inclusion of the continuum 46
2.4.1 A discrete representation 46
2.4.2 The Sturmian basis 47
2.4.3 Projection operators and decay factors 48
2.4.4 A semiclassical ionization mechanism 50
2.5 Low frequency theories 52
2.5.1 The adiabatic basis expansion 52
2.5.2 Expansion on unperturbed basis states and Floquet theory 54
2.6 High frequency theories 55
2.6.1 Compensated energy representation 56
2.6.2 The Kramers-Henneberger transformation and stabilization 57
2.7 The quantal map 60
2.7.1 Derivation of the general quantal map 60
2.7.2 Dynamical Photonic Localization 63

3 The Morse oscillator in a high-frequency field **68**
3.1 Introduction 68
3.2 Application to the Morse oscillator 69
3.2.1 The resonance overlap condition 70
3.2.2 Mean-motion 70
3.2.3 Predicted behaviour 72
3.3 Numerical methods 74
3.3.1 Classical calculations 75
3.3.2 Quantal calculations 76
3.4 Accuracy of the classical map 77
3.5 Classically chaotic region 78
3.5.1 Localization 83

3.6 Intermediate frequency region 84
3.6.1 Adiabatically switched fields 84
3.6.2 Suddenly switched fields 85
3.7 Mean-motion region 87
3.8 Conclusions 89

4 Low frequency behaviour I: the tunnelling regime **91**
4.1 Introduction 91
4.2 The unperturbed hydrogen atom 94
4.3 The hydrogen atom in a static electric field: the Stark effect 96
4.3.1 Quantal perturbation theory 97
4.3.2 A uniform semiclassical approach 99
4.3.3 The classical critical field 105
4.4 The hydrogen atom in a slowly varying electric field 106
4.4.1 Keldysh-Faisal-Reiss theory 106
4.4.2 Ammosov-Delone-Kraĭnov theory 107
4.4.3 An adiabatic model 108
4.5 The experiment 109
4.6 Numerical methods 111
4.7 Comparison of theories with experiment 113
4.8 Conclusions 121

5 Low frequency behaviour II: resonances **122**
5.1 Introduction 122
5.2 Approximate solution for the two-state system 123
5.2.1 Semiclassical approximations 126
5.2.2 Bloch representation 126
5.3 Mean probabilities and resonance widths 130
5.3.1 Frequency dependence of the solution 133
5.3.2 Resonance widths 135
5.4 Conclusions 136

A Gauge invariance of the resonance overlap condition **137**

B Sudden ionization: classical **140**

C Sudden ionization: quantal **141**

D Uniform approximations **143**

E Evaluation of action and tunnelling integrals **145**

E.1 Evaluation of the action integral I_ξ 145

E.2 Evaluation of the action integral I_η 146

E.3 Evaluation of the tunnelling integral $A(E)$ 147

E.4 Evaluation of the quantal correction function $\Phi(x)$ 147

E.5 Evaluation of the resonance widths Γ_R^{SC} 148

F Asymptotic form for resonance widths **149**

References **152**

List of Figures

1.1 Simple potential and phase curves. 11
1.2 Phase curves in angle-action representation for librational motion. 15
1.3 Area enclosed by a phase curve in (q,p)- and (θ,I)-representations. 15
1.4 Representation of angle-action variables upon a semi-infinite cylinder. . . 16
1.5 Phase curves in the angle-action representation for rotational motion. . . 17
1.6 The field switch envelope $\lambda(t)$. 20
1.7 Increase of the resonance island width with F. 27
1.8 Graphs of the mean-potential for $V(q) = (1 - e^{-q})^2$. 30
1.9 Graphs of the mean-potential for $V(q) = -1/(1 + q^2)$. 30
1.10 Motion in the potential $V(q) = (1 - e^{-q})^2$ with increasing α. 33
1.11 Motion in the potential $V(q) = -1/(1 + q^2)$ with increasing α. 33

3.1 Dependence of β_{CH} and β_{SUD} on Ω for $\mathcal{A}_0 = 0.5$. 73
3.2 Dependence of β_{CH} and β_{AD} on Ω for $\mathcal{A}_0 = 0.5$. 74
3.3 Classical ionization probabilities at $\Omega = 5\omega$ and varying β 79
3.4 Classical and quantal ionization probabilities for $\Omega = 5\omega$. 80
3.5 Classical and quantal ionization probabilities for $\Omega = 5\omega$. 81
3.6 Classical and quantal bound state populations for $\Omega = 5\omega$, $\beta = 0.08$ $\mathcal{A}_0 = 0.5$ and $\mathcal{A}_s = 1500$. 81
3.7 Dependence of classical and quantal ionization probabilities with β for $\Omega = 5\omega$. 82
3.8 Variation of threshold fields required to produce 10% ionization with Ω. . 83
3.9 Values of β required for 10% and 50% ionization for $12\omega \leq \Omega \leq 20\Omega$. . . . 85
3.10 Surface-of-section plot for $\Omega = 15\omega$, $\beta = 11.5$ and a sudden switch. 86
3.11 Dependence of the classical ionization probability with β for $\Omega = 15\omega$. . . 86
3.12 Variation of the classical ionization probability with β for $\Omega = 30\omega$ and an adiabatic switch. 87
3.13 Variation of the classical ionization probability with β for $\Omega = 30\omega$ and a sudden switch. 88

4.1 Potential for the ξ-motion, V_ξ. 101
4.2 Potential for the η-motion, V_η. 101
4.3 Graph of universal and static ionization curves. 110
4.4 Ionization probability for $n_0 = 24$. 114
4.5 Ionization probability for $n_0 = 25$. 114
4.6 Ionization probability for $n_0 = 26$. 115
4.7 Ionization probability for $n_0 = 27$. 115
4.8 Ionization probability for $n_0 = 28$. 115
4.9 Ionization probability for $n_0 = 29$. 116
4.10 Ionization probability for $n_0 = 30$. 116
4.11 Ionization probability for $n_0 = 31$. 116
4.12 Ionization probability for $n_0 = 32$. 117
4.13 Ionization probability for $n_0 = 27$ and $F_0 \leq 0.13$. 118
4.14 Scaled 10% threshold field for $24 \leq n_0 \leq 32$. 119
4.15 Ionization probabilities at $n_0 = 1$ and $\Omega_0 = 0.02$. 120
4.16 Ionization probabilities at $n_0 = 5$ and $\Omega_0 = 0.02$. 120

5.1 Sketch of the motion of the vector $s(t)$. 128
5.2 Graphs showing $|a_n|^2$ as a function of τ for $\Omega_0 = 0.1$ and $F_0 = 0.121$. . . . 130
5.3 Graphs showing $\overline{P}(n)$ as a function of Ω_0 for $n = 38$ and $F_0 = 0.121$. . . . 132
5.4 Graphs showing $\overline{P}(n)$ as a function of Ω_0 for $n = 38$ and $F_0 = 0.121$. . . . 132
5.5 Graphs showing some values of ψ and Φ_w as a function of Ω_0 for $n = 38$ and $F_0 = 0.121$. 134
5.6 Graphs showing the variation of various functions near the resonance at $\Omega_0 \simeq 0.011544688470691$. 135

F.1 Contour used to evaluate the integral $I(\Omega_0)$. 149

List of Tables

1.1 Relationships between dependent variables and generating functions. . . . 13

3.1 Comparison ionization probabilities obtained using the classical maps with those obtained by exact numerical integration at $\Omega = 5\omega$. 77

3.2 Comparison ionization probabilities obtained using the classical maps with those obtained by exact numerical integration at $\Omega = 15\omega$. 78

4.1 Comparison of exact an approximate semiclassical ionization probabilities. 112

4.2 Zeros of the exponential factor in the ADK-formula. 119

5.1 Values of the coefficients used in the energy level approximation. 125

Acknowledgements

The knowledge that this is the one page that will, for certain, be read by everyone who is foolish enough to pick up this thesis makes writing it one of the more difficult tasks. It is at this point that I think back over my years as a student and remember those people who have had a profound influence on my academic development. The list is endless and to mention each by name would require a separate volume. It is therefore necessary to exercise some restraint and hope that in the process I do not inadvertently offend anyone. Of course, in true film star style, I could just say 'Thank you' to everyone who knows me. However, that would be rather avoiding the issue so, with no more ado and apologies to anyone that I may have missed but thinks that they deserve a mention, here goes.

First and foremost I wish to express my deep gratitude to Dr Derek Richards for suggesting the research topic and supervising the work presented in this thesis. Without Derek's constant help, enthusiasm and encouragement this thesis would probably not have seen the light of day. I would also like to thank Derek for providing some of the figures which grace chapters 1 and 5 and for the classical low frequency calculations presented in chapter 4.

Several colleagues at other institutions should also be thanked. In particular, Professor Peter Koch of the State University of New York, Stony Brook, for supplying the experimental data for the low frequency microwave ionization of hydrogen atoms presented in chapter 4, Dr John Leopold of The Fritz Haber Molecular Dynamics Research Centre, Hebrew University, Jerusalem for useful discussions, and Dr Ken Taylor and Dr Tania Monteiro of Royal Holloway and Bedford New College, University of London, for helpful discussions and for allowing me leave from my present post to complete this thesis. I would also like to thank Margaret Halley, Dr Pat O'Mahony, Dr Hermann Marxer and Dr Francisca Mota Furtado for their help and encouragement during my time at Royal Holloway.

On the technical side, I would like to thank the staff of the Academic Computing Service at the Open University and, in particular, Steve Daniels and Marilyn Moffat for solving the wide variety of problems I encountered with both UNIRAS and LaTeX.

A special mention should also go to my parents, Les and Sheila, my sister, Lisa, and

her husband, Steve, for their support and encouragement throughout my many years as a student; I am sure they all will be relieved to learn that I can now get a 'proper' job !

Finally, I would like to thank all my friends and colleagues at the Open University for making my three years in Milton Keynes a more bearable experience. I have neither the time nor the space to mention them all here but I am sure they know who they are. However, a special mention should go to June Barrow-Green, Dr Geoff Cooper, Michaela Cottee, Dr Jonathan Crellin, Rob Crighton, Fran Jennings, Liz May, Dr Jonathan Myles, Nadine Ramaram and Jeremy Robson; they know why.

The work presented in this thesis was supported by a studentship from the Open University.

Introduction

In recent years, much work has been devoted to the study of nonlinear dynamics and chaos. A system is regarded as chaotic when its long-time evolution depends so sensitively upon the initial conditions that it becomes *de facto* unpredictable and it has become increasingly clear that virtually all systems which are not obviously integrable are prone to chaos, even seemingly simple systems with few degrees of freedom. Indeed, if we allow time-dependent systems, we can even observe chaos in systems with only one degree of freedom.

The study of classically chaotic systems has become one of the most popular and rapidly growing subfields in many areas of physics. In plasma physics, for example, it is relevant to the study of the confinement of charged particles in electromagnetic fields, such as particles in an accelerator (see, for instance, Rechester and Rosenbluth 1978, Month and Herrera 1979 and Jowet *et al.* 1985) whilst in astrophysics it plays an important role in our understanding of the great quantity of observed data on white dwarfs (Angel 1977) and the study of the stability of our solar system (Wisdom 1987). Atomic physics provides several examples of simple, yet non-trivial, systems which are observable in the laboratory and whose classical motion exhibits all the chaotic features currently causing excitement. Many of these examples are essentially of a quantal nature and, because the linear Schrödinger equation that governs the quantal dynamics contains neither the local instability of the nonlinear classical equations of motion that allow for the onset of chaos nor the sensitivity to small changes in the initial conditions, there is a need to understand the manifestations of classical chaos in quantum mechanics, a problem which reduces to a study of the correspondence principle in a regime where the classical motion is irregular.

The development of quantum theory in the early decades of this century revolutionized physics. The seemingly unshakeable concept of a particle moving along a trajectory, sharply defined and uniquely determined by its initial position and momentum coordinates, was replaced by a description of electrons as wave packets whose position and momentum carry inherent uncertainties; classical mechanics could no longer be regarded as providing a correct description of the dynamics at the atomic level. However, estab-

lishing a correspondence between classical and quantum mechanics remained one of the fundamental problems of physics. Whilst solutions to particular problems, such as the quantization of simple systems have been found, many questions remain unanswered and, together with the rapid growth of interest in classically chaotic systems and the continued search for manifestations of chaos in quantum mechanics, the field of semiclassical mechanics has taken on a new and crucial importance. After decades in the wilderness, classical mechanics is now being reinstated as a relevant theory for the study of atomic systems.

Two examples of atomic systems whose classical motion is chaotic involve highly excited hydrogen atoms in the presence of strong fields, in one case a periodically oscillating electric field and in the other in a uniform magnetic field. Each of these systems may be readily studied both theoretically and experimentally and can thus give insight into the relationship between classical and quantal dynamics when the classical motion is irregular.

An excited hydrogen atom in a homogeneous magnetic field provides an example of a time-independent system of two degrees of freedom for which the classical dynamics exhibits a transition from regularity to chaos and its study has yielded several surprising results. For dominantly regular or dominantly chaotic classical motion, the short-ranged correlations in the quantum spectra have been directly linked to the shorter classical periodic orbits. The quantum mechanical energy level spectra has also been related to periodic orbits via a semiclassical series formula, with the information contained in a comparatively few isolated orbits being sufficient to describe the spectra with remarkable accuracy, even for the relatively low lying states: further details of current work in this field can be found in the review by Friedrich and Wintgen (1989).

Highly excited hydrogen atoms in a microwave field provide a physical realization of a time-dependent system for which the classical motion is chaotic; it is the study of this latter system which motivates the work presented in this thesis.

The microwave ionisation of highly excited hydrogen atoms, first observed by Bayfield and Koch (1974), provided a new challenge for theorists. Quantal perturbation theory, which had previously been used to describe multiphoton ionization experiments, proved to be woefully inadequate for studying this new phenomenon, with between 50 and 100 orders perturbation theory being needed to describe the microwave ionization process. The first theoretical study to provide reasonable agreement with the threshold fields observed experimentally by Bayfield and Koch (1974) and Bayfield *et al.* (1977) was provided by Leopold and Percival (1979) who carried out a purely classical, numerical simulation of the dynamics of a periodically driven Kepler system. Subsequently, the onset of ionization in the quantal atom was linked to the onset of stochasticity in the

corresponding classical system, see Meerson *et al.* (1979).

Since then, the microwave ionization of highly excited hydrogen atoms has provided a rich source of study for experimentalists and theorists alike. In recent years, the experiments of Koch and co-workers, see van Leeuwen *et al.* (1985) and Galvez *et al.* (1988) and references therein, have considerably refined the original experiments to produce very accurate measurements, whilst the experiments of Bayfield *et al.* (1989 and references therein) have shown the way towards direct comparison with quantal calculations by restricting the electron to move collinearly with the field, so producing quasi one-dimensional atoms.

From a theoretical viewpoint, the ionization dynamics of an excited hydrogen atom in a microwave field is complicated and incompletely understood. There are no rigorous theories to provide a guide to the system behaviour and, moreover, there are many parameters defining an individual experiment or calculation so it is very difficult to obtain an overall picture of the dynamical response. The two parameters defining the applied field, the field strength, F, and frequency, Ω, together with the initial principle quantum number, n_0, are the main system parameters, but it is convenient to measure these in terms of the scaled field strength, F_0, and frequency, Ω_0, see equation (1.1), page 9 below; the classical ionization probabilities satisfy scaling laws (see Leopold and Percival 1979) and depend only upon the parameters F_0 and Ω_0 and *not* upon F, Ω and n_0 separately. Other important parameters are the initial distribution of substates, the interaction time, the shape of the field envelope, $\lambda(t)$ in equation (1.27) below, and the strength of the static field, if present. Classically, the numerical integration of Hamilton's equations is relatively straightforward provided regularisation is used to remove the Coulomb singularity (see Leopold and Richards 1985, Rath 1990). The quantal study, however, is further complicated by the need to include the continuum, that is the region of phase space where the classical motion ceases to be bound, and the addition of a further parameter, Planck's constant, to parameter space. In addition, for the large quantum numbers of interest here, solving the three-dimensional Schrödinger equation numerically is prohibitively expensive and probably not possible on the computers currently available.

For these reasons, following Jensen (1984), much of the recent theoretical interest has been devoted to the study of the one-dimensional atom, equation (1.26) below; this problem, being computationally much simpler, allows quantal calculations to be performed on relatively modest computers, provided approximations to the continuum are made. One of the main findings of these theoretical studies, together with the recent experiments of Koch and co-workers, is that there are at least six distinct ranges of the scaled field frequency (see, for instance, Koch 1990) in which the dynamics of the problem, both one- and three-dimensional, has quite different characteristics and needs different theoretical

models. The boundaries of these regions are approximate; some depend on both n_0 and Ω_0, but for the values of n_0 currently used are given by the following inequalities.

R1 *The tunnelling regime*, $\Omega_0 \lesssim 0.07$: at these very low field frequencies, experimentally observed threshold fields lie systematically below the corresponding classical values. Comparisons of experimentally obtained ionization probabilities with those calculated using various theoretical models (see Sauer *et al.* 1992 and chapter 4 below) have shown that for values of the coupling strength $C_s = n_0 F_0 \Omega_0 < 0.12$, transitions between adjacent states can be neglected and the atom ionises from the initial level via quantal penetration of the slowly oscillating potential barrier; this ionization mechanism has no classical analogue.

R2 *The low-frequency regime*, $0.05 \lesssim \Omega_0 \lesssim 0.3$: in this region the experimental ionization curves exhibit a great deal of structure which is not reproduced by classical simulations (see Richards *et al.* 1989b). One-dimensional quantal models have, however, reproduced this structure fairly accurately. Richards *et al.* (1989b) have shown that in this regime the quantal dynamics is well described by relatively few adiabatic states and that resonances between these states are responsible for the observed behaviour; this mechanism cannot be reproduced by classical dynamics. As C_s increases so does the required number of adiabatic states: for $C_s > 1.5$ many states are needed and although the the quantum resonances persist there are so many that classical dynamics provides a good estimate of the average quantal behaviour. An equivalent explanation is given by Blümel and Smilansky (1987, 1990) who link the experimental structure to 'unresolved clusters of many Floquet avoided crossings', see also Breuer *et al.* (1989).

R3 *The semi classical regime*, $0.1 \lesssim \Omega_0 \lesssim 1.2$: here there is broad agreement between threshold fields obtained using classical three-dimensional simulations and experimental results, see van Leeuwen *et al.* (1985), except at the low-order resonances, $\Omega_0 = r/s$ for integers $r < s$. Off resonance agreement is usually good for all field strengths: on or near resonance, detailed agreement is not so good although theoretical studies by Jensen *et al.* (1989a) and Leopold and Richards (1993b) have linked quantal resonance effects to classical phase space structures.

R4 *The transition regime*, $1 \lesssim \Omega_0 \lesssim 2$: in this region the agreement between experimental and classically computed threshold fields begins to break down; quantal effects both lowers the experimentally observed threshold fields and raises them above the classical values, depending upon circumstances.

R5 *The high-frequency regime*, $\Omega_0 > 2$: here there is a clear divergence of the three-dimensional classical and experimental threshold fields (see Galvez *et al.* 1988, Bayfield *et al.* 1989); for long exposure times, the classical thresholds *decrease* slowly with Ω_0, as $\Omega_0^{-1/3}$, while the experimental and quantal thresholds *increase* approximately linearly with Ω_0. This 'quantal suppression of classical chaos' was first predicted by Casati *et al.* (1984). The theoretical reasons for these differences are still the source of some controversy. Casati *et al.* (1988) described the underlying dynamics producing the observed behaviour via the theory of 'dynamical photonic localization' and pointed to the existence of a critical field strength, the 'delocalization border', below which the quantal wave function is 'exponentially localized' in photon states, at least near the initial state, and above which there is 'diffusive' ionization. An alternative theoretical explanation has been proposed by Leopold and Richards *et al.* (1989). Here, it was shown that the one-dimensional quantum dynamics is dominated by relatively few quasi-resonant states, that is those states whose energy differs from that of the initial state by an integer number of the photon energy, and that this drastically reduces the effective density of states so making the classical and quantum dynamics quite different.

R6 *The photoelectric effect*, $\Omega_0 \gtrsim 0.5n_0$: at these very high field frequencies the photon energy rises above the threshold for one-photon ionization, $\hbar\Omega > 0.5\mu e^4/(n\hbar)^2$, and all vestiges of classical behaviour disappear, at least for weak field intensities, see Koch (1990).

Whilst these boundaries have been determined for hydrogen, it seems likely that other systems will behave similarly. In this thesis we concentrate on the dynamical response of a one-dimensional system in frequency regimes R1, R2 and R5.

The remainder of this thesis is organized as follows. In chapter 1 we study the classical motion of an atomic system of one-degree of freedom in the presence of an periodic electric field via the Hamiltonian formulation of dynamics. Following Leopold and Richards (1991), we provide a rigorous derivation of the Hamiltonian of a hydrogen atom moving through a region containing a periodic electric field, give the generalization of this to an arbitrary one-dimensional system and derive equivalent representations in which the dynamical response can be more conveniently studied when the field frequency is either very high or very low. For low frequency fields we show how a related conservative system can be used as a starting point in the study of the more complex time-dependent problem. At high frequencies, we obtain an estimate of the critical field strength required for the onset of chaotic motion and show that, for some systems, classical ionization can take place through regular orbits, in contradistinction to the periodically driven Coulomb

potential. In addition, we construct an area-preserving map which is applicable to a wide variety of one-dimensional systems and which reproduces the exact dynamics remarkably accurately at high frequencies.

Chapter 2 discusses some aspects of the corresponding quantal system. We review some of the techniques which have been used to date to solve the time-dependent Schrödinger equation and highlight the problem of including the interaction with the continuum. In the low frequency regime we show how the quantal motion may be efficiently described using the adiabatic basis representation of Richards (1987). Studies of the quantum dynamics of a hydrogen atom in the presence of a high frequency periodic field have yielded two important, yet controversial, theoretical explanations for the discrepancies between classical and quantum dynamics in this regime of field frequency; 'stabilization' and 'localization': we review some of the more important results in both of these fields of study. We end the chapter by providing an explicit quantization of the general classical map, derived in chapter 1, which provides us with an efficient means of numerically solving the one-dimensional time-dependent Schrödinger equation at high field frequencies.

In chapter 3 we apply the classical theory developed in chapter 1 to the specific case of the Morse potential in the presence of a high frequency field. The Morse potential is often used to model molecular interactions with periodic electric fields (see Walker and Preston 1977 and Goggin and Milonni 1988); its analytic properties mean that its response to a high-frequency periodic field is distinctly different to that of the Coulomb potential. By both numerically integrating the equations of motion and iterating the classical map, which we find mimics the exact dynamics fairly accurately, we show that, at sufficiently high frequencies, the driven Morse oscillator can ionize classically via regular orbits. In addition we provide comparisons between ionization probabilities obtained by iterating the classical and quantal maps and, for the Morse potential in a high frequency field, delineate circumstances where there is agreement between classical and quantal dynamics.

Chapters 4 and 5 both consider excited hydrogen atoms in a low-frequency microwave field. In chapter 4 we compare ionization probabilities calculated using various theoretical models with those obtained experimentally. These comparisons allow us to distinguish between tunnelling through and classical escape over the slowly oscillating barrier, formed by the combination of the Coulomb potential and the periodic electric field, and between one- and many-state dynamical processes. In particular, we find that theories which are often used to interpret data for low frequency multi-photon ionization experiments fail to describe the experimental data presented here. We find that the new semiclassical model, derived in chapter 4, reproduces the experimental data remarkably well and delineate ranges of validity of other models.

In chapter 5 we re-investigate the quantal resonance behaviour experimentally observed in the low frequency regime. By obtaining a new, accurate and tractable solution of the two-state equations of motion, we are able, for the first time, to obtain approximations to the resonance widths as $\Omega_0 \to 0$. In particular we show that the width of the resonance at $\Omega_0 \simeq p^{-1}$ is approximately $p^{-5/2}e^{-Cp}$, C being a positive constant, and that for the quantum numbers and frequencies dealt with in chapter 4 they are too narrow to be observed.

Our conclusions are given at the end of each of the chapters 3, 4 and 5 where most of the new results are presented.

Chapter 1

Classical Theory

1.1 Introduction

In this chapter we study the classical motion of an atomic system of one degree of freedom in the presence of a periodic electric field. For moderate field strengths, the classical motion of such a system is complicated as there is no general theory available to describe how a given system will behave. Clearly, the response of the system depends upon a variety of parameters, the applied field frequency, Ω, field strength, F, initial principal action, I_0, and the interaction time being the main system parameters. Fortunately, numerical solutions of Hamilton's equations are relatively easy to obtain for specific systems and so it is not too difficult to explore limited regions of parameter space in order to build up an approximate picture of the dynamical response.

In recent years, classical dynamics has played an important role in the theoretical study of the microwave ionization of highly excited hydrogen atoms. Indeed, the first theoretical study to provide reasonable agreement with the ionisation thresholds reported by Bayfield and Koch (1974) and Bayfield *et al.* (1977) was provided by Leopold and Percival (1978, 1979) who, reasoning that because of the high principal quantum numbers involved, $63 \leq n_0 \leq 69$, classical methods could be applied to the problem, carried out a purely classical numerical simulation of the dynamics of a periodically driven Kepler system. An important result of this work was the observation that ionisation occurs classically via unstable trajectories which do not lie on invariant tori; orbits on invariant tori do not ionize. In subsequent studies, Delone *et al.* (1978) gave the new name 'diffusive ionization' to this process while Meerson *et al.* (1979) linked the onset of microwave ionization in the quantal atom to the onset of stochasticity in the corresponding classical system. It was further noted by Leopold and Percival (1979) that the classical ionization probabilities satisfy scaling laws and depend only upon the scaled field strength and

frequency,

$$F_0 = \frac{(n_0\hbar)^4}{\mu^2 e^6} F, \quad \Omega_0 = \frac{(n_0\hbar)^3}{\mu e^4}\Omega, \quad \text{with} \quad I_0 = n_0\hbar, \tag{1.1}$$

and not upon F, Ω and I_0 separately; in equation (1.1), μ and e are the reduced mass and charge of the electron respectively and $2\pi\hbar$ is Planck's constant. The scaled field, F_0, is the ratio of the applied field strength to the mean Coulomb field while the scaled frequency, Ω_0, is the ratio of the applied field frequency to the unperturbed classical frequency; together, these provide a possible means of experimentally measuring quantal effects (see Koch *et al.* 1989). Throughout this thesis we shall, where possible, use the scaled variables defined in equation (1.1) when considering the microwave ionization of excited hydrogen atoms.

Following the success of these early theoretical studies, many authors have used classical dynamics to model the microwave ionization process. For the hydrogen atom, these studies have often considered the simpler one-dimensional model given by equation (1.26) below (see, for example, Jensen 1984, Leopold and Richards 1985 and Casati *et al.* 1988), although two-dimensional (Leopold and Richards 1986) and three-dimensional (Rath 1990) calculations have also been made. Classical models have also been used to study other periodically forced atomic systems. In particular, Walker and Preston (1977) and Goggin and Milonni (1988) have considered the classical response of the periodically driven one-dimensional Morse oscillator.

In this chapter we study some aspects of the classical motion of an arbitrary one-dimensional system in the presence of a harmonic field. We begin in section 1.2 by providing a brief overview of the Hamiltonian formulation of dynamics for a system of one degree of freedom. In particular, we introduce the concepts of time-dependent canonical transformations and angle-action variables.

In section 1.3 we derive the Hamiltonian functions for both the one- and three-dimensional hydrogen atom in the presence of a microwave field and generalize this work to provide a Hamiltonian for an arbitrary system of one degree of freedom in the presence of a periodic forcing term. The one-dimensional Hamiltonian so obtained does not always provide us with the most convenient description of the motion, particularly for very high or very low frequency fields. In such circumstances we show how time-dependent canonical transformations can be used to obtain equivalent Hamiltonians which provide a more useful description of the dynamics.

The regime of low field frequency is discussed in section 1.4. We show that in the adiabatic limit, $\Omega \to 0$, where the action is an approximate constant of the perturbed motion, it is possible to use a related conservative system, the adiabatic Hamiltonian, to describe the dynamics.

In section 1.5 we concentrate on the high frequency regime and in particular we con-

sider resonant motion, where the applied field frequency is an integer multiple of the unperturbed classical frequency. For such fields, we show how the Chirikov (1979) resonance overlap condition can be used to estimate the field strength required for the onset of chaotic motion. We find that this estimate depends crucially upon the smoothness of the potential and that for analytic potentials other ionization mechanisms may become important at very high frequencies. We investigate two such mechanisms in section 1.6 where we derive the 'mean-motion' Hamiltonian which provides a good approximation of the motion in very high frequency fields.

Finally, in section 1.7, we generalize the work of Casati *et al.* (1988) on the Kepler map and Graham and Höhnerbach (1990, 1991) on the Morse map, to derive an area-preserving map which is applicable to a wide variety of one dimensional systems and provides us with an efficient means of obtaining solutions to Hamilton's equations when the field frequency is high.

1.2 Hamiltonian dynamics

In this section we provide a brief overview of the Hamiltonian formulation of dynamics for a system of one-degree of freedom: generalizations to higher dimensional systems can be found, for example, in Goldstein (1980).

Suppose we have a particle of mass, μ, moving in the one-dimensional, time-independent potential, $V(q)$; the *Hamiltonian function* or *Hamiltonian* for such a system is defined to be

$$H_0(q,p) = \frac{1}{2\mu}p^2 + V(q), \tag{1.2}$$

where q is known as the *generalized coordinate* and p as its *conjugate momentum*. The pair (q,p) are called *conjugate* variables and define a point in two-dimensional phase space representing the state of the system. During a particular motion of the system, (q,p) trace out a continuous curve in phase-space named a *phase curve*: a typical potential, $V(q)$, and its phase curves are sketched in figure 1.1.

The time evolution of the conjugate variables, (q,p), is described by *Hamilton's equations* of motion:

$$\frac{\mathrm{d}q}{\mathrm{d}t} = \frac{\partial H_0}{\partial q}, \qquad \frac{\mathrm{d}p}{\mathrm{d}t} = -\frac{\partial H_0}{\partial q}. \tag{1.3}$$

Note that the variable q *need* not describe the configuration of the system nor *need* p represent a physical momentum, though they frequently do have this meaning.

The Hamiltonian, H_0, has no explicit time-dependence and so its value is always conserved: for the systems of interest in this thesis its value is equal to the energy, E. Henceforth, we shall refer to H_0 as the *unperturbed* Hamiltonian for which we shall assume that Hamilton's equations of motion have known solutions.

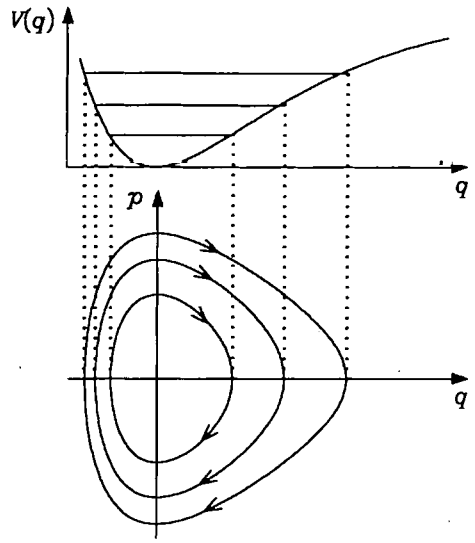

Figure 1.1 Sketch of a typical potential, $V(q)$, and its phase curves.

In general, we shall be considering one-dimensional systems in the presence of an periodic field for which we assume the Hamiltonian can be written in the form

$$H(q,p,t) = H_0(q,p) + H_1(q,p,t), \tag{1.4}$$

where H_1 represents a time-dependent perturbation. Hamilton's equations of motion for the system described by H are then given by equation (1.3) but with H replacing H_0. Note that H now depends explicitly on the time, t, and so its value is no longer conserved.

The general theory of time dependent Hamiltonians is difficult and only for special classes of time-dependent systems does a general theory exist. However, it is sometimes possible to consider the motion of a related conservative system or to use the solutions of the unperturbed system, H_0, as the starting point for finding approximate solutions to a more complex time-dependent system: for these reasons we first consider the motion described by the conservative Hamiltonian, H_0.

1.2.1 Conservative Hamiltonian systems

The contours of the conservative Hamiltonian, H_0, are invariant sets of the system. Hamiltonian systems have *fixed points* which are also invariant sets. The fixed points occur whenever the gradient of the Hamiltonian is zero:

$$\left(\frac{\partial H_0}{\partial q}, \frac{\partial H_0}{\partial p}\right) = \nabla H_0 = 0, \qquad \text{(fixed point)}. \tag{1.5}$$

At fixed points the system is in equilibrium. The location and nature of the fixed points allow us to determine an overall description of the motion. For one-dimensional conservative Hamiltonian systems only elliptic and hyperbolic fixed points can occur: elliptic

fixed points occur when the potential function, $V(q)$ is at a minimum whilst hyperbolic fixed points occur at the maxima of $V(q)$. Hyperbolic fixed points are joined by phase curves, called *separatrixes*, that divide phase space into different invariant regions with different types of motion.

For conservative one-dimensional systems, the motion is usually periodic. Two different types of periodic motion can occur.

1. When the velocity, $\dot{q}$ always has the same sign the motion is said to be a *rotation*.
2. When $\dot{q}$ changes sign the motion is said to be a *libration*.

For rotational motion, it is often more convenient to choose the coordinate q in the range $[0, 2\pi]$ with the ends of the range identified. The Hamiltonian, $H_0(q,p)$, is then 2π-periodic in q.

1.2.2 Time-dependent canonical transformations

The coordinates, (q,p), used to formulate the problem do not always provide us with the most convenient representation in which to study the evolution of a Hamiltonian system. Other equivalent Hamiltonians, for which the equations of motion take on a more convenient form, can be obtained by making a *canonical transformation* to a new set of conjugate variables, (Q,P). Such transformations may be time-dependent and may be applied to either the conservative Hamiltonian, H_0, or the time-dependent Hamiltonian, H, and are particularly useful for two reasons. Firstly, they preserve the form of Hamilton's equations and secondly they are *area-preserving*, that is the Jacobian determinant of the transformation is unity,

$$\frac{\partial(Q,P)}{\partial(q,p)} = \frac{\partial Q}{\partial q}\frac{\partial P}{\partial p} - \frac{\partial Q}{\partial p}\frac{\partial P}{\partial q} = 1. \tag{1.6}$$

This area-preserving property can be used to infer the existence of a function, $F_1(Q,q,t)$, (see, for example, Goldstein 1980, chapter 9) which generates the transformation $(q,p) \rightarrow (Q,P)$ via

$$p = \frac{\partial F_1}{\partial q}, \qquad P = -\frac{\partial F_1}{\partial Q}. \tag{1.7}$$

The function, F_1 is called a *generating function*: note that it is only defined up to an additive constant.

In the (Q,P)-representation the Hamiltonian is

$$K(Q,P,t) = H(q,p,t) + \frac{\partial F_1}{\partial t}(Q,q,t), \tag{1.8}$$

where q and p are expressed in terms of Q and P, *after* taking the time derivative, and the equations of motion are,

$$\frac{\mathrm{d}Q}{\mathrm{d}t} = \frac{\partial K}{\partial P}, \qquad \frac{\mathrm{d}P}{\mathrm{d}t} = -\frac{\partial K}{\partial Q}. \tag{1.9}$$

The form of the generating function, F_1, requires q and Q to be independent variables and thus does not exist for certain important classes of transformation, such as coordinate transformations in configuration space. However, other generating functions can be found by considering (P,q), (Q,p) or (P,p) as independent variables. There are four different types of generating function depending upon the choice of independent variable: $F_1(Q,q,t)$, $F_2(P,q,t)$, $F_3(Q,p,t)$ and $F_4(P,p,t)$. The relationships between the dependent variables and the various generating functions are summarized in table 1.1 and the new Hamiltonian is given by

Table 1.1 Table showing how the dependent variables are related to the various generating functions.

Generating function	Dependent variables q	p	Q	P
$F_1(Q,q,t)$		$\partial F_1/\partial q$		$-\partial F_1/\partial Q$
$F_2(P,q,t)$		$\partial F_2/\partial q$	$\partial F_2/\partial P$	
$F_3(Q,p,t)$	$-\partial F_3/\partial p$			$-\partial F_3/\partial Q$
$F_4(P,p,t)$	$-\partial F_4/\partial p$		$\partial F_4/\partial P$	

$$K(Q,P,t) = H(q,p,t) + \frac{\partial F_j}{\partial t}, \quad (j = 1,2,3,4). \tag{1.10}$$

Canonical transformations are used in many areas of classical mechanics, in particular the Hamilton-Jacobi theory, which is extensively explained in Goldstein (1980) and briefly but elegantly by Landau and Lifshitz (1976), and are the classical equivalent of unitary transformations often used in quantum mechanics.

1.2.3 Angle-action variables

The variables used to formulate a problem are not always the best for solving it. Indeed, for the systems of interest in this thesis, we will often use the solution of a relatively

simple system as the starting point for finding the solution to a more complex system. In such circumstances it is best to choose variables so that the solution of the simpler problem is expressed in the simplest possible way: for the bounded motion of conservative Hamiltonian systems these variables are called *angle-action variables.*

For Hamiltonians of one-degree of freedom, such as H_0 of equation (1.2) above, the motion is usually periodic in time and may be either librational or rotational. First we consider librational motion.

Librational motion

The theory of angle-action variables requires that the phase curve be closed but not a separatrix. Specifically, we consider the unperturbed Hamiltonian, H_0 of equation (1.2), with typical potential and phase curves shown by figure 1.1. In (q,p)-representation the phase curve of energy, E, is represented by the two-valued function

$$p(q,E) = \pm\sqrt{2\mu(E - V(q))}. \tag{1.11}$$

The multivaluedness of this function is clearly unsatisfactory, so we seek a new pair of variables, (θ, I), with the properties:

1. each phase curve is labelled uniquely by I, which is constant along that curve;
2. each point on the phase curve is labelled by a single-valued function of θ.

In the (θ, I)-representation, the contours are lines of constant I, so that the Hamiltonian is independent of θ and, since I is constant, θ increases linearly with time. This is expressed in Hamilton's equation of motion:

$$\frac{\mathrm{d}I}{\mathrm{d}t} = -\frac{\partial H_0}{\partial \theta}, \qquad \frac{\mathrm{d}\theta}{\mathrm{d}t} = \frac{\partial H_0}{\partial I} = \text{ constant.} \tag{1.12}$$

The angle-action variables are obtained by making θ increase by 2π in each period. Then θ is named the *angle variable* and I the *action variable.* The phase curves in the angle action representation are thus straight lines parallel to the θ-axis, as shown in figure 1.2.

The time-dependence of θ is given directly by Hamilton's equation (1.12),

$$\theta = \omega(I)t + \theta_0, \quad \text{where} \quad \omega(I) = \frac{\partial H_0}{\partial I} \tag{1.13}$$

is the angular frequency of the motion and θ_0 is an arbitrary constant. The dependence of the angle variable upon q is more complicated to derive and is given by

$$\theta(q) = \frac{\partial}{\partial I}\int_{q_0}^{q} \mathrm{d}q'\, p(q', I). \tag{1.14}$$

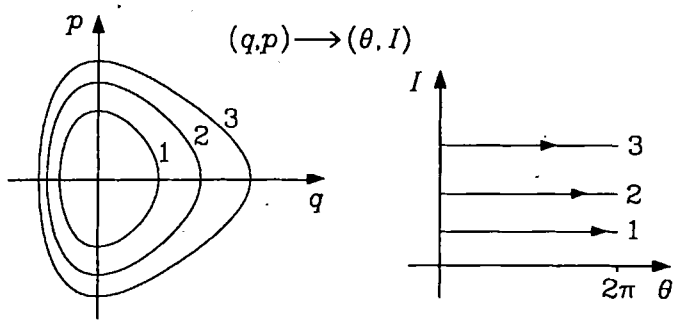

Figure 1.2 Phase curves in angle-action representation for librational motion.

Note that care must be exercised when evaluating $\theta(q)$ using equation (1.14) because $p(q, I)$ is a multivalued function of q.

The Hamiltonian, H_0, in angle-action representation is obtained by comparing the area enclosed by a phase curve during one full period in the (q,p)-representation with the corresponding area in the (θ, I)-representation; as the transformation $(q,p) \rightarrow (\theta, I)$ is canonical, these two areas are the same, see figure 1.3:

$$\mathcal{A}(E) = \oint \mathrm{d}q\, p(q,E) = 2\int_{q_1(E)}^{q_2(E)} \mathrm{d}q\, \sqrt{2\mu(E - V(q))} = \int_0^{2\pi} \mathrm{d}\theta\, I = 2\pi I, \qquad (1.15)$$

where $V(q_i) = E$, $i = 1, 2$. Thus, for librational motion, the action variable is propor

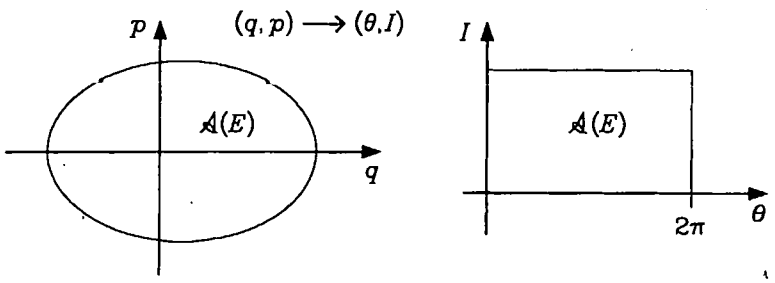

Figure 1.3 Area enclosed by a phase curve in (q,p)- and (θ, I)-representations.

tional to the area and, as a function of the energy, E, is given by

$$I(E) = \frac{1}{\pi}\int_{q_1}^{q_2} \mathrm{d}q \sqrt{2\mu(E - V(q))}, \qquad (1.16)$$

which is a monotonic increasing function of E within each invariant region. By inverting equation (1.16) we can obtain the Hamiltonian, $H_0(I) = E$, as a function of the action. For potentials where there is a minimum energy, E_0, below which motion is impossible, the phase curves in the (q,p)-representation reduce to a point and $I(E_0) = 0$; the action then has a natural boundary at $I = 0$.

The action variable has the same dimensions as angular momentum; the angle variable is dimensionless and usually represents an angle in configuration space. Since the points

(θ, I) and $(\theta + 2\pi, I)$ label the same points in phase space, the (θ, I) coordinates can be represented upon a semi-infinite cylinder, where θ is the angle around the cylinder and I is the coordinate along its axis, see figure 1.4: on this cylinder, q and p are both

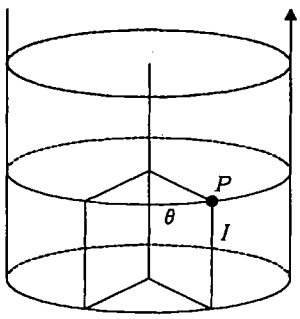

Figure 1.4 Representation of angle-action variables upon a semi-infinite cylinder.

2π-periodic functions of the angle variable,

$$q(\theta + 2\pi, I) = q(\theta, I), \qquad p(\theta + 2\pi, I) = p(\theta, I). \tag{1.17}$$

A separatrix divides phase space into invariant regions which contain phase curves with different properties. Within each such invariant region either all motions are periodic or none are. When the motion is periodic, angle-action variables may be defined but they are *not* defined on the separatrix itself nor are the angle-action variables in different invariant regions related.

Rotational motion

For rotational motion, the phase curves on the plane are not closed and the coordinate, $q(t)$, is a continuously increasing or continuously decreasing function of time. The Hamiltonian is then periodic in q and, for convenience, we suppose this period to be 2π, $H_0(q + 2\pi, p) = H_0(q, p)$.

As before, we require that each phase curve is labelled by an action, I, and each point on a phase curve is labelled by a variable, θ, that is linear in time as in equation (1.13): the phase curves in each representation are shown in figure 1.5. The action is then given as a function of the energy by equating the areas between phase curves in the (q, p) and (θ, I)-representations:

$$I(E) = \frac{1}{2\pi} \int_0^{2\pi} \mathrm{d}q\, p(q, E), \tag{1.18}$$

where $p(q, E)$ is a function of q given by the solution to the energy equation, $H_0(q, p) = E$, which usually has more than one solution; for a Hamiltonian given by equation (1.2) there are two solutions corresponding to the different signs of the square root and representing

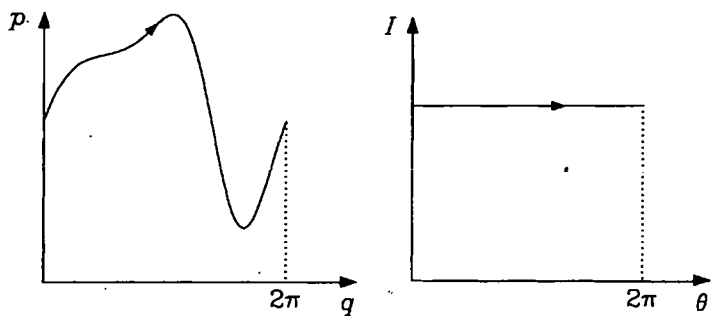

Figure 1.5 Phase curves in the angle-action representation for rotational motion.

rotations in opposite directions. Thus for each energy there are, in this case, two actions defined by equation (1.18), corresponding to each direction of the motion.

Different choices of horizontal axis give actions differing from equation (1.18) by additive constants. Thus, unlike librational motion, for rotations there is no natural boundary for the action and any arbitrary constant may be added to it.

The form of the equation for $\theta(q)$ is identical to equation (1.17) above but since $p(q, I)$ is a single-valued function for rotations, $\theta(q)$ is a continuously increasing or decreasing function of q.

Semiclassical methods: quantization of the action variable

We shall often be concerned with providing quantizations of particular classical systems: for a one-dimensional system expressed in terms of angle-action variables, this is achieved using the prescription,

$$I = \left(n + \frac{\alpha}{4}\right)\hbar, \qquad (n = 0, 1, 2, \ldots), \tag{1.19}$$

where $2\pi\hbar$ is Planck's constant and α is the Maslov index (see Percival 1977). The value taken by the Maslov index depends subtly upon the topology of phase-space: for our purposes we simply note that $\alpha = 2$ for librations and $\alpha = 0$ for rotations give the correct quantization conditions for motion in a one-dimensional system.

1.3 The Hamiltonian and gauge transformations

1.3.1 The Hamiltonian for a hydrogen atom in a microwave field

There are currently two sets of experiments which subject an excited hydrogen atom to a microwave field but which produce these fields in different ways. Here, we follow Leopold and Richards (1991) and derive the equations of motion for both sets of experiments.

The Koch experiment

In the experiments of Koch and co-workers (see Koch 1982, Koch 1990 together with section 4.5 below) an excited hydrogen atom, initially prepared in a microcanonical ensemble of substates, moves through a microwave cavity with a linearly polarized field in the $\hat{z}$ direction of the motion. If $S_{\rm L}$ is the laboratory rest frame, with coordinate axes $0XYZ$, then the electric field in $S_{\rm L}$ is assumed to comprise static, F_s, and oscillatory components:

$$\boldsymbol{E}' = [F_s + \Lambda(z)F_m \sin(\Omega t + \delta)]\,\hat{\boldsymbol{z}}, \tag{1.20}$$

where $\Lambda(z)$ represents a smoothly varying envelope which is zero outside some finite region, positive inside this region with $\Lambda'(z) \geq 0$ for $z \leq 0$ and $\Lambda'(z) \leq 0$ for $z \geq 0$; usually $\Lambda(z)$ is an even function of z: in current experiments $F_s = 0$. In the reference frame $S_{\rm H}$ moving with constant velocity V with origin at the nucleus of the hydrogen atom, the vector and scalar potentials of this field are, on using the Lorentz transformation (see Landau and Lifshitz 1971 §24), and assuming $V \ll c$,

$$A_z = \frac{cF_m}{\Omega}\Lambda(z+Vt)\cos(\Omega t+\delta) + \frac{V}{c}(z+Vt)F_s, \quad A_x = A_y = 0, \tag{1.21}$$

$$\phi = -(z+Vt)F_s - \frac{VF_m}{\Omega}\Lambda(z+Vt)\cos(\Omega t+\delta), \tag{1.22}$$

where $0xyz$ are the coordinates in S_H with $0Z$ parallel to $0z$ and c is the speed of light. Assuming that $\Lambda(z+Vt)$ varies little over the atomic diameter, it may be replaced by the function $\Lambda(Vt) = \lambda(t)$ of time only to give the Hamiltonian,

$$H = \frac{1}{2\mu}\left(\boldsymbol{P} - \frac{eF_m}{\Omega}\lambda(t)\hat{\boldsymbol{z}}\cos(\Omega t+\delta)\right)^2 - eF_s z - \frac{e^2}{r}, \tag{1.23}$$

$$\boldsymbol{P} = \boldsymbol{p} + \frac{e}{c}\boldsymbol{A} \simeq \boldsymbol{p} + \frac{eF_m}{\Omega}\lambda(t)\hat{\boldsymbol{z}}\cos(\Omega t+\delta), \tag{1.24}$$

where $(\boldsymbol{P}, \boldsymbol{r})$ are the conjugate variables.

The Bayfield experiment

The experiments of Bayfield (1987) and co-workers are different. The excited hydrogen atoms move through a wave-guide perpendicular to its axis; the wave-guide is excited to the $\rm TE_{10}$ mode and, in addition to this field, there is also a magnetic field present perpendicular to both the wave-guide and the direction of the motion. In the moving frame, $S_{\rm H}$, the electric field is perpendicular to $V\hat{\boldsymbol{z}}$ and the vector and scalar potentials of the combined field are,

$$\boldsymbol{A} = \frac{cF_m}{\Omega}\hat{\boldsymbol{x}}\sin\left(\frac{\pi t}{T}\right)\cos(\Omega t+\delta), \qquad \phi = -F_s x, \tag{1.25}$$

where T is the time of passage through the wave-guide, about 23.6 ns in the Bayfield *et al.* (1989) experiments. The Hamiltonian is therefore the same as that given in equation (1.23) except that $\hat{z}$ is now in the direction perpendicular to the beam velocity and $\lambda(t) = \sin(\pi t/T)$.

In the Bayfield experiments the hydrogen atoms are prepared in an extremal Stark state, $n_0 \gg 1, n_e = n_2 - n_1 = n_0 - 1, m = 0$: the electron is confined close to the field axis and its motion is well described by a one dimensional Hamiltonian which may be written in the form,

$$H(z,P,t) = \frac{1}{2\mu}P^2 - \frac{e^2}{z} - eF_s - \frac{eF_m}{\mu\Omega}\lambda(t)\cos(\Omega t + \delta), \qquad z \geq 0. \tag{1.26}$$

At this point it should be noted that the form usually used by theorists to model the Bayfield experiments also neglects the static field, F_s, see, for example, Casati *et al.* (1988).

1.3.2 The Hamiltonian for a one-dimensional system

We now provide a generalization of the Hamiltonians derived in the previous section to obtain a Hamiltonian which describes an arbitrary one-dimensional system, described by the potential $V(q)$, in the presence of an oscillating electric field. In particular, we wish to model the Koch experiments, and so we neglect the static field and re-write Hamiltonian (1.23) in the form,

$$H_m(q,p,t) = H_0(q,p) + p\lambda(t)\frac{F}{\mu\Omega}\cos(\Omega t + \delta), \tag{1.27}$$

$$H_0(q,p) = \frac{1}{2\mu}p^2 + V(q), \tag{1.28}$$

where μ is the reduced mass of the system, $F = eF_m$ and Ω the applied field amplitude and frequency, δ the field phase and (q,p) are the conjugate variables: henceforth we shall refer to equation (1.27) as the *momentum gauge* Hamiltonian. Note that the change of sign preceeding the cosine in equation (1.27) simply corresponds to a change in the definition of the field phase, δ, and has no effect on the dynamics. Whilst the derivation of Hamiltonian (1.27) was carried out with a microwave field in mind, it should be noted that the same Hamiltonian can be used to describe laser excitation of ground state hydrogen atoms, provided suitable changes in the parameters are made.

The time-dependent field envelope function, $\lambda(t)$, represents the finite extent of the field in the laboratory: typically, it is zero for a time $t < 0$ and for $t > 0$ rises monotonically to unity over a prescribed time, T_a, remains at unity for many field periods and finally decreases monotonically to zero at time $t = T_m$. In general, it is important to include this envelope in any theoretical model because, for the experimental work carried out to date, the field is rarely switched on suddenly. Typically, $\lambda(t)$ takes the form

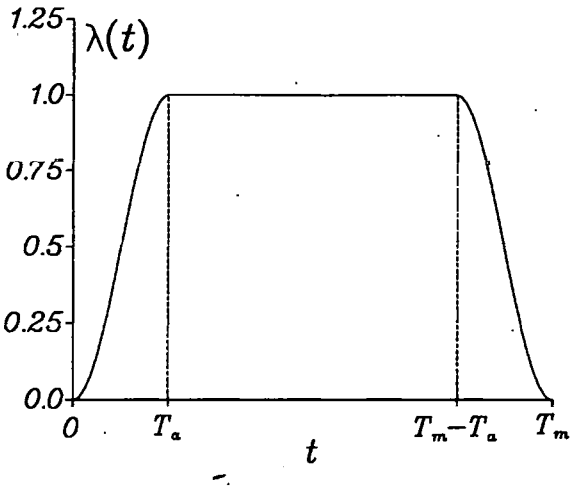

Figure 1.6 Typical variation of the field-switch function, $\lambda(t)$, with t for $0 \leq t \leq T_m$.

shown in figure 1.6: note that this differs from a typical laser pulse which may have no flat portion to the envelope.

In order to accurately model experiments it is essential to incorporate the variation of $\lambda(t)$ into any theoretical model because adiabatically and suddenly switched fields produce different effects. Classically, the initial conditions are usually chosen to lie on an invariant torus of the unperturbed system. When the field is switched on adiabatically, the ensemble of initial conditions evolves onto a single invariant torus of the perturbed system; a sudden switch, on the other hand, projects each different initial condition onto a different initial torus of the perturbed system. Moreover, if the field is switched on suddenly the field phase, δ, plays an important role in the dynamics, see section 1.6 below; it is then necessary to average results over δ. For an adiabatic switch, on the other hand, the field phase has little effect on the dynamics, as is shown by the results presented in chapter 3.

The phase space of the unperturbed system, $H_0(q,p)$ of equation (1.28), is assumed to comprise a bounded and an unbounded region between which there is a single separatrix of energy E^S. Typically, the potential, $V(q)$, will take the form shown by the solid lines of figures 1.8 and 1.9, see page 30 below. It is also assumed that the frequency, $\omega(E)$, of the unperturbed motion decreases with increasing energy. An orbit ionizes by crossing the separatrix and remaining in the unbounded region until $t \geq T_m$.

1.3.3 Gauge transformations

The Hamiltonian of equation (1.27) does not always provide us with the most convenient description of the motion, particularly when the field frequency is very high or very low. Other equivalent Hamiltonians can be obtained by making a general time-dependent

linear transformation in phase space,

$$P = p + a(t), \qquad Q = q + b(t), \tag{1.29}$$

produced by the generating function,

$$F_2(P,q) = (P - a(t))(q + b(t)), \tag{1.30}$$

so that in this representation, and on ignoring terms solely dependent upon time, Hamiltonian (1.27) becomes,

$$K(Q,P,t) = \frac{1}{2\mu}P^2 + V(Q - b(t)) + \frac{P}{\mu}\left(\frac{F}{\Omega}\lambda(t)\cos(\Omega t + \delta) - a(t) + \mu\dot{b}(t)\right) - \dot{a}Q. \tag{1.31}$$

This Hamiltonian can be simplified by removing the term linear in P and there are two obvious ways in which this may be achieved. It should also be noted that because the canonical transformation generated by $F_2(P,q)$, equation (1.30), is linear, the Schrödinger equation corresponding to Hamiltonian (1.31) is obtained by replacing the momentum, P, by its quantal operator equivalent, $\hat{P} = -i\hbar\partial/\partial Q$.

1.3.4 The dipole gauge Hamiltonian

For low frequency fields, $\Omega \ll \omega$, a convenient description of the motion is obtained by choosing,

$$a(t) = \frac{F\lambda(t)}{\Omega}\cos(\Omega t + \delta), \qquad b(t) = 0, \tag{1.32}$$

to give the dipole gauge Hamiltonian,

$$H_d(q_1,p_1,t) = \frac{1}{2\mu}p_1^2 + V(q_1) - q_1\frac{F}{\Omega}\frac{\mathrm{d}}{\mathrm{d}t}(\lambda(t)\cos(\Omega t + \delta)), \tag{1.33}$$

where,

$$q_1 = q, \qquad p_1 = p + \frac{F}{\Omega}\lambda(t)\cos(\Omega t + \delta). \tag{1.34}$$

The initial state is almost always described in terms of the conjugate variables, (q_1,p_1), or the angle-action variables, (θ,I), of this representation and in this gauge $p_1 = \mu\dot{q}_1$. Hamiltonian (1.33) reduces to the form usually used to describe the microwave ionization of hydrogen atoms (see, for example, Leopold and Percival 1979, Jensen 1982, 1984, Casati *et al.* 1987b, 1988, Blümel and Smilansky 1987),

$$H_d(q_1,p_1,t) = \frac{1}{2\mu}p_1^2 + V(q_1) + q_1F\lambda(t)\sin(\Omega t + \delta), \tag{1.35}$$

only when the field envelope changes insignificantly during one field period, that is when $\dot{\lambda}/\lambda \ll \Omega$. This condition is satisfied for most experiments performed to date but may not be in future experiments. In particular, Hamiltonian (1.35) describes the dynamics incorrectly when the field is switched-on suddenly.

1.3.5 The acceleration gauge Hamiltonian

For high field frequencies, $\Omega \gg \omega$, the dynamics is best described in the 'acceleration' gauge, obtained by setting

$$a(t) = 0, \qquad b(t) = -\frac{F}{\mu\Omega}\int_0^t \mathrm{d}t'\,\lambda(t')\cos(\Omega t' + \delta), \tag{1.36}$$

to give

$$H_a(q_2, p_2, t) = \frac{1}{2\mu}p_2^2 + V(q_2 - b(t)), \tag{1.37}$$

with

$$p_2 = p, \qquad q_2 = q + b(t). \tag{1.38}$$

This representation is useful when the field frequency is high because the perturbation is $O(\Omega^{-2})$.

It is important to note that the three Hamiltonians just described, equations (1.27), (1.33) and (1.37), provide equivalent descriptions of the dynamics but, for times $0 < t < T_m$, the canonical variables, (p, q), (p_1, q_1) and (p_2, q_2) are different in each of the three gauges.

1.4 Low frequency behaviour: the adiabatic Hamiltonian

In this section it is assumed that the applied field frequency is very much less than the frequency of the unperturbed motion, $\Omega \ll \omega$, so that the dynamics is best described using Hamiltonian (1.33). In this case, the Hamiltonian for the system changes little during one unperturbed period and so the the principle of adiabatic invariance is valid, see Percival and Richards (1982, chapter 9). Classically, this means that the action of the perturbed motion is an approximate constant of the motion and so it is possible to use a related conservative system to understand the dynamics.

1.4.1 The adiabatic Hamiltonian

Consider a Hamiltonian having the general form,

$$H(q_1, p_1, t) = \frac{1}{2\mu}p_1^2 + V(q_1) - f(t)q_1, \tag{1.39}$$

where $f(t)$ varies slowly between finite limits (f_1, f_2). If it is assumed that $\lambda(t)$ varies very little during one field period, so that $f(t) \simeq -F\lambda(t)\sin(\Omega t + \delta)$, then Hamiltonian (1.39) is just the conventional dipole gauge Hamiltonian (1.35).

The related conservative system is described by the unperturbed adiabatic Hamiltonian (see Leopold and Richards 1993a), defined by,

$$H_{AD}(q_1, p_1) = \frac{1}{2\mu}p_1^2 + V(q_1) - \kappa q_1, \tag{1.40}$$

where κ is a constant. It is assumed that for $f_1 \leq \kappa \leq f_2$ the unperturbed system supports bound motion with angle-action variables (θ, I) and generating function $F_2(I, q_1; \kappa)$, parametrically dependent upon κ (see Percival and Richards 1982). In this case the unperturbed motion is periodic with frequency $\omega_{AD}(I, \kappa)$: subsequently it will be useful to define $\omega(I) = \omega_{AD}(I, 0)$ to be the frequency of the field-free system. All phase space variables are 2π-periodic functions of θ, so can be expressed as Fourier series; in particular, since the Hamiltonian is an even function of p_1 and $p_1 = \mu\dot{q}_1$, it may be assumed that the Fourier development of the position coordinate has the form,

$$q_1(\theta, I) = \bar{q}_1(I, \kappa) + \sum_{s=1}^{\infty} Q_s(I, \kappa) \cos s\theta, \tag{1.41}$$

where $\bar{q}_1$ is the mean of q_1 over an unperturbed orbit,

$$\bar{q}_1(I, \kappa) = \frac{1}{2\pi} \int_{-\pi}^{\pi} \mathrm{d}\theta\, q_1(\theta, I). \tag{1.42}$$

The variation of the perturbation of the original system, equation (1.39), is slow if the relative variation of $f(t)$ during one period is small, that is provided,

$$\left| \frac{1}{f} \frac{\mathrm{d}f}{\mathrm{d}t} \right| \ll \omega_{AD}. \tag{1.43}$$

In the case where $f(t) = F \sin(\Omega t + \delta)$ we need the scaled frequency to be small, $\Omega_0 = \Omega/\omega_{AD} \ll 1$.

The time-dependent generating function, $F_2(I, q_1; f(t))$, obtained by replacing κ with $f(t)$ in the generating function for the unperturbed system, produces a time dependent canonical transformation which, when applied to the original system gives the new Hamiltonian,

$$K_1(\theta, I, t) = H_{AD}(I, f(t)) + \frac{\partial F_2}{\partial t}(I, q_1; f), \tag{1.44}$$

where $H_{AD}(I, f)$ is the adiabatic Hamiltonian in angle-action representation. Here the partial derivative of $F_2(I, q_1; f)$ with respect to time, is expressed as a function of the angle-action variables, (θ, I), *after* differentiation with respect to t: as $f(t)$ is a slowly varying function of time this term, being proportional to $\dot{f}$, is small and in the adiabatic limit can be neglected to give the adiabatic Hamiltonian,

$$K_1(\theta, I, t) \simeq H_{AD}(I, f(t)), \quad \text{(adiabatic limit, } \Omega \to 0). \tag{1.45}$$

This approximation is valid provided changes in the classical action are sufficiently small to be neglected and has the correct static field limit as the field frequency tends to zero.

1.4.2 The breakdown of adiabatic invariance

The transformation between Hamiltonians (1.39) and (1.44) is exact provided the initial orbit remains in the region where the angle-action variables are defined. If the original system ionizes then this condition is violated and Hamiltonian (1.44) is no longer valid. Hence, it is assumed that the applied forces are not strong enough to ionize the system.

As the field frequency, Ω, increases from zero, the adiabatic approximation breaks down and the second term of equation (1.44) can no longer be neglected. It is then necessary to use the exact Hamiltonian (1.44) to describe the dynamics. Leopold and Richards (1993a) show how to obtain an expression for the time-dependent generating function, $F_2(I, q_1; \kappa)$, of the unperturbed system and its time derivative. The former can be defined in terms of the integral given by Percival and Richards (1982, page 112),

$$F_2(I, q_1; \kappa) = \int_{q_0}^{q_1} \mathrm{d}q\, p_1(I, q) = \sqrt{2\mu} \int_{q_0}^{q_1} \mathrm{d}q \sqrt{E(I, \kappa) - V(q) + \kappa q}, \tag{1.46}$$

where $E(I, \kappa) = H_{AD}(I, \kappa)$ is the unperturbed energy expressed in terms of the action and $q_0(I, \kappa)$ is the smallest turning point, corresponding to $\theta = 0$. Differentiation with respect to κ gives,

$$\frac{\partial F_2}{\partial \kappa} = \sqrt{\frac{\mu}{2}} \int_{q_0}^{q_1} \mathrm{d}q \, \frac{\partial E/\partial \kappa + q}{\sqrt{E(I, \kappa) - V(q) + \kappa q}}. \tag{1.47}$$

Provided $\delta\kappa$ is sufficiently small, first-order perturbation theory can be used to write,

$$E(I, \kappa + \delta\kappa) = E(I, \kappa) - \bar{q}(I, \kappa)\delta\kappa + O(\delta\kappa^2), \tag{1.48}$$

which is a classical version of the Hellmann-Feynman theorem of quantum mechanics (see McWeeny and Sutcliffe 1969). Thus,

$$\frac{\partial F_2}{\partial \kappa} = \int \mathrm{d}t \, \{q_1(t) - \bar{q}_1(I, \kappa)\}, \tag{1.49}$$

where the integral is evaluated over one orbit of $H_{AD}(I, \kappa)$. Using the Fourier series expansion of equation (1.41) and setting $\theta = \omega_{AD}(I, \kappa)t + \theta_0$ gives,

$$\frac{\partial F_2}{\partial \kappa} = \frac{1}{\omega_{AD}(I, \kappa)} \sum_{s=1}^{\infty} \frac{1}{s} Q_s(I, \kappa) \sin s\theta. \tag{1.50}$$

Returning now to the time-dependent system described by Hamiltonian (1.44) and writing,

$$\frac{\partial F_2}{\partial t} = \frac{\partial F_2}{\partial f} \dot{f} \tag{1.51}$$

gives the following expression for Hamiltonian (1.44),

$$K_1(\theta, I, t) = H_{AD}(I, f(t)) + \dot{f}(t) \sum_{s=1}^{\infty} \frac{Q_s(I, f)}{s\omega_{AD}(I, f)} \sin s\theta. \tag{1.52}$$

This Hamiltonian is exact provided the orbit remains inside the separatrix of the unperturbed system, equation (1.40), defining the boundary of the invariant region in which the variables (θ, I) are defined.

When the field is switched on over many field periods, so that $\dot{\lambda}/\lambda \ll \Omega$ and $f(t) \simeq -F\lambda(t)\sin(\Omega t + \delta)$, Hamiltonian (1.52) becomes,

$$K_1(\theta, I, t) = H_{AD}(I, f(t)) - F\lambda(t)\Omega \sum_{s=1}^{\infty} \frac{Q_s(I, f)}{s\omega_{AD}(I, f)} \sin s\theta \cos(\Omega t + \delta), \qquad (1.53)$$

where other correction terms due to the field envelope are small and may be neglected. The major advantage of this representation is that the perturbation is now proportional to $F\Omega$ rather than just F.

Hamiltonian (1.52) can be treated either classically or quantally: the quantal behaviour is discussed in chapters 3, 4 and 5 below; the classical behaviour is described by Leopold and Richards (1993a) where first order perturbation theory is used to approximate the dynamics.

1.5 Resonant motion: the resonance overlap condition

At higher field frequencies, $\Omega \geq \omega$, and for sufficiently high field strengths, it is possible for the classical system to ionize via chaotic orbits. Chaotic ionization occurs when a significant proportion of the orbits become unstable and the distribution in action satisfies, approximately, a diffusion equation (see Lichtenberg and Lieberman 1983, page 286). For resonant frequencies, $\Omega = r\omega$ for integer r, an estimate of the field strength required for the onset of chaotic motion can be obtained by using the Chirikov (1979) resonance overlap method which estimates the field strength at which adjacent resonance islands intersect.

In order to derive the overlap criterion for the one dimensional system under consideration here, it is convenient to express Hamiltonian (1.27) in terms of the angle-action variables, (θ, I), of the unperturbed system, $H_0(I)$:

$$H(\theta, I, t) = H_0(I) + FV(\theta, I)\lambda(t)\cos(\Omega t + \delta), \qquad V(\theta, I) = \frac{1}{\mu\Omega} p(\theta, I). \qquad (1.54)$$

The perturbation, $V(\theta, I)$, is a 2π periodic function of the angle variable, θ, and hence may be expanded in a Fourier series, so that Hamiltonian (1.54) becomes:

$$H(\theta, I, t) = H_0(I) + F\lambda(t) \sum_{s=-\infty}^{\infty} V_s(I) e^{-is\theta} \cos(\Omega t + \delta), \qquad (1.55)$$

where,

$$V_s(I) = \frac{1}{2\pi} \int_{-\pi}^{\pi} d\theta\, V(\theta, I) \exp(is\theta), \qquad V_{-s} = V_s^*. \qquad (1.56)$$

For sufficiently small fields the Kolmogorov-Arnol'd-Moser (KAM) theorem (see Arnol'd 1978) ensures that the majority of straight-line trajectories in angle-action space are only slightly distorted by the perturbation; the maximum distortion of the trajectories occurs at resonances, $s = \pm r$, where the phase $s\theta - \Omega t$, is stationary. By writing $\theta = \omega(I)t + \theta_0$, we see that this occurs when $\Omega = r\omega(I)$ so that in the vicinity of the resonance at $s = r$ an approximate expression for Hamiltonian (1.55) is,

$$H(\theta, I, t) \simeq H_0(I) + F\lambda(t)|V_r(I)|\cos(r\theta - \Omega t - \delta + \beta_r). \tag{1.57}$$

where $\beta_r(I)$ is the phase of the Fourier component, $V_r(I) = |V_r(I)|e^{-i\beta_r}$. By making a time-dependent canonical transformation,

$$\psi = \theta - \frac{\Omega}{r}t - \frac{\delta}{r} + \frac{\beta_r(J)}{r}, \qquad J = I - I_r, \tag{1.58}$$

by means of the type 2 generating function,

$$F_2(J, \theta, t) = (J + I_r)\left(\theta - \frac{\Omega}{r}t\right) + \gamma(J), \tag{1.59}$$

where I_r is a constant and $\gamma(J)$ a suitable function of J, the new Hamiltonian is obtained:

$$K(\psi, J) = H_0(J + I_r) - \frac{J\Omega}{r} + F\lambda(t)|V_r(J + I_r)|\cos(r\psi). \tag{1.60}$$

The unperturbed Hamiltonian, H_0, is now expanded as a Taylor series to $O(J^2)$; on choosing the constant, I_r, to be the action of the exact resonance, so that $r\omega(I_r) = \Omega$, we obtain the following approximation to Hamiltonian (1.60):

$$K(\psi, J) \simeq \frac{J^2}{2}\omega'(I_r) + F\lambda(t)|V_r(I_r)|\cos(r\psi), \qquad \omega'(I_r) = \frac{\mathrm{d}\omega(I_r)}{\mathrm{d}I}, \tag{1.61}$$

where an irrelevant constant and higher order terms in the expansion of $V_r(I)$ have been neglected: the quantal equivalent of transformation (1.58) is given by Zaslavsky (1981).

Thus, for small perturbations, Hamiltonian (1.54) can be approximated in the vicinity of each resonance by the Hamiltonian of a simple pendulum; trajectories of the system close to the resonances are thus confined to narrow island chains in angle-action space. Between the resonances, the surviving KAM surfaces prevent trajectories from wandering from one resonance to another and so no net change in energy occurs.

In figure 1.7 we sketch the width of the adjacent resonance islands with increasing F. We see that as the perturbation increases, the resonance islands grow wider in action. When the islands are sufficiently large the system can diffuse in action, or equivalently in energy, by wandering from one island chain to another. These transitions occur when the the field is sufficiently strong for the islands generated by adjacent resonances overlap.

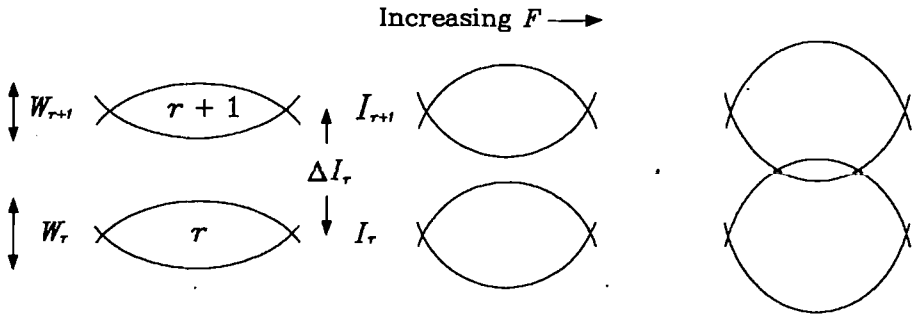

Figure 1.7 Sketch showing how adjacent resonance island widths increase with increasing F, eventually causing them to intersect.

The width of the resonance island in angle action space corresponds to the width of the libration region of the pendulum,

$$W_r = 4\sqrt{F\lambda(t)\frac{|V_r(I_r)|}{\omega'(I_r)}}, \tag{1.62}$$

and the separation of the resonances at r and $r+1$ is given by,

$$\Delta I_r = |I_{r+1} - I_r| \simeq \frac{\omega(I_r)}{r\omega'(I_r)}, \qquad r \gg 1. \tag{1.63}$$

Referring once more to figure 1.7, it is clear that the zeroth-order islands overlap when the island width, W_r, is greater than the separation, ΔI_r. From equations (1.62) and (1.63) we see that this occurs when,

$$16F\lambda(t)|V_r(I_r)|\frac{\mathrm{d}\omega(I_r)}{\mathrm{d}I} > r^{-4}\Omega^2, \qquad r\omega(I_r) = \Omega \qquad (r \gg 1). \tag{1.64}$$

Inequality (1.64) provides an approximate condition for the critical field required to destroy the KAM surfaces between the r and $r+1$ island chains. If the system has an initial energy corresponding to an action lying between I_r and I_{r+1}, then the application of an oscillating field with amplitude greater than the critical field will cause the system to diffuse in action.

In extensive numerical calculations, Chirikov (1979) showed that the overlap condition (1.64) provides a good estimate for the field strength required for global stochasticity. Jensen (1984) argued that secondary island chains, generated by the nonlinear interaction of the primary resonance islands, accelerate the destruction of the confining KAM surfaces and thus estimate (1.64) provides an upper bound on the critical field strength required for the onset of stochastic excitation and ionization of the system; more precise calculations of the island widths and separation for the $r = 1$ and $r = 2$ resonances give values for the critical field approximately 40% lower than that obtained using the simple analysis given here (see Jensen 1984).

For the Hamiltonian of equation (1.27), with $V(\theta, I)$ defined by equation (1.54) above, condition (1.64) suggests that a significant proportion of orbits become chaotic for $F > F_{CH}$ with,

$$F_{CH} = \frac{1}{16\Omega^2}\frac{\omega(I)^4}{|V_r(I)|}\left|\frac{\mathrm{d}\omega(I)}{\mathrm{d}I}\right|^{-1}, \qquad r = [\Omega/\omega], \tag{1.65}$$

where $[x]$ is the integer part of x. In appendix A we show that this criterion is gauge independent, so that Hamiltonians (1.27), (1.33) and (1.37), yield identical expressions for F_{CH}.

The important point to notice in expression (1.65) is that F_{CH} is proportional to $(V_{\Omega/\omega})^{-1}$ and that the rate at which the Fourier components decrease with Ω/ω depends upon the analytic properties of the potential. For analytic potentials, such as the Morse potential which is discussed in detail in chapter 3, V_r decreases faster than any power of r, see equation (3.7) page 70 below; but for potentials with discontinuities in the nth derivative, $V_r \sim r^{-(n+1)}$. Thus, the critical field strength required for chaotic ionization by high frequency fields depends crucially upon the smoothness of the potential: for analytic potentials it increases very rapidly with increasing field frequency whereas for the singular one-dimensional Coulomb potential it decreases.

1.6 High frequency behaviour: the mean-motion Hamiltonian

For high frequency fields, where $\Omega \gg \omega$, the resonance overlap criterion described in section 1.5 can again be used to give an estimate of the field strength required for the onset of chaotic motion. However, chaotic orbits are only significant for very high fields and so other ionization mechanisms may become important at lower field strengths. In this section, two such mechanisms are described, one which occurs when the field is switched on adiabatically, the other when it is switched on suddenly.

1.6.1 The mean-motion Hamiltonian

For high field frequencies the classical dynamics is best described by the Hamiltonian

$$H_a(q_2, p_2, t) = \frac{1}{2\mu}p_2^2 + V(q_2 - b(t)), \tag{1.66}$$

$$b(t) = -\frac{F}{\mu\Omega}\int_0^t \mathrm{d}t'\,\lambda(t')\cos(\Omega t' + \delta), \tag{1.67}$$

which, it should be noted, is exact but remains time-dependent unless $V(q) \equiv 0$. A simplification can be made by noting that during the course of one field period the variables, (q_2, p_2), change very little and that the exact motion consists of a slowly varying

average motion upon which are superimposed small, high-frequency oscillations. Thus, an approximation to Hamiltonian (1.66) can be formed by taking its average over one field oscillation to obtain the mean-motion, or 'dressed', Hamiltonian,

$$\overline{H}(q_2, p_2) - \frac{1}{2\mu}p_2^2 + \overline{V}(q_2), \qquad (1.68)$$

where

$$\overline{V}(q_2) = \frac{\Omega}{2\pi}\int_{-\pi/\Omega}^{\pi/\Omega} \mathrm{d}t\, V(q_2 - b(t)). \qquad (1.69)$$

For many functions, $V(q)$, the integral for the mean-potential, equation (1.69), cannot be evaluated in terms of known functions; the field switch function, $\lambda(t)$, causes further complications. However, when the field is turned on over a large number of field oscillations, so that $\dot{\lambda}/\lambda \ll \Omega$ and $b(t) \simeq -(F\lambda(t)/\mu\Omega^2)\sin(\Omega t + \delta)$, then $\lambda(t)$ may be treated as a constant when computing $\overline{V}$ to produce the mean motion Hamiltonian with the function, $\lambda(t)$, present as a slowly varying parameter,

$$\overline{H}(q_2, p_2; \alpha) = \frac{1}{2\mu}p_2^2 + \overline{V}(q_2, \alpha), \qquad \alpha = \frac{F\lambda(t)}{\mu\Omega^2}, \qquad (1.70)$$

where,

$$\overline{V}(q_2, \alpha) = \frac{1}{2\pi}\int_{-\pi}^{\pi} \mathrm{d}\phi\, V(q_2 + \alpha\sin\phi), \qquad (1.71)$$

and the change of variable, $\phi = \Omega t + \delta$, has been made. The theory of adiabatic invariance can now be used to deduce that the mean-motion action variable is an approximate constant of $\overline{H}$.

The dynamics of Hamiltonian (1.70) is best understood by treating α as a small parameter. The 'space-translated' potential, $V(q_2 + \alpha\sin\phi)$, can then be expanded as a Taylor series in $\alpha\sin\phi$ to give an approximation to Hamiltonian (1.66),

$$H_a \simeq \frac{1}{2\mu}p_2^2 + V(q_2) + \alpha\sin\phi\frac{\partial V}{\partial q_2} + \frac{1}{2}(\alpha\sin\phi)^2\frac{\partial^2 V}{\partial q_2^2} + \frac{1}{6}(\alpha\sin\phi)^3\frac{\partial^3 V}{\partial q_2^3} + O(\alpha^4). \qquad (1.72)$$

Taking a time-average over one field period gives the following approximation to the mean-motion Hamiltonian,

$$\overline{H} \simeq \frac{1}{2\mu}p_2^2 + V(q_2) + \frac{1}{4}\alpha^2\frac{\partial^2 V}{\partial q_2^2} + O(\alpha^4). \qquad (1.73)$$

This approximation can be used to establish some simple properties of the mean-motion potential, $\overline{V}(q_2, \alpha)$, and obtain a qualitative description of the mean-motion for various values of the parameter α.

Using approximation (1.73), it can be seen that $\overline{V}(q) > V(q)$ if $V''(q) > 0$. In figure 1.8, we show the mean potential, $\overline{V}(q)$, equation (1.71), corresponding to a potential of the Morse-type, $V(q) = (1-e^{-q})^2$, for various values of the parameter α: the full curve,

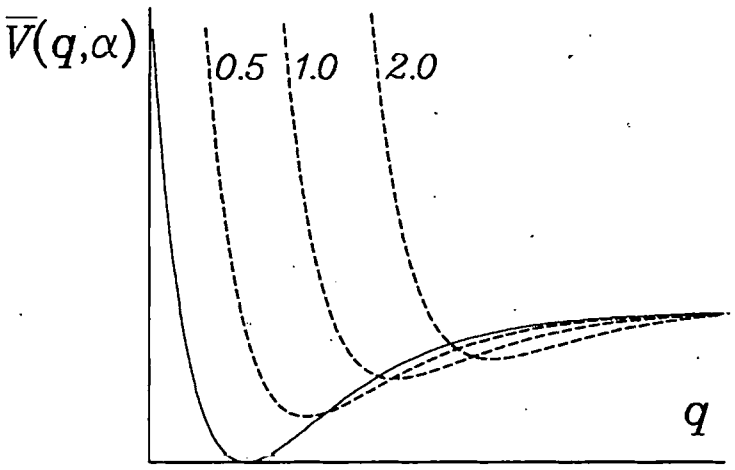

Figure 1.8 Graph of $\overline{V}(q_2, \alpha)$, equation (1.71), corresponding to the potential, $V(q) = (1 - e^{-q})^2$, for various values of the parameter, α. Note that the full curve, with $\alpha = 0$, represents $V(q)$.

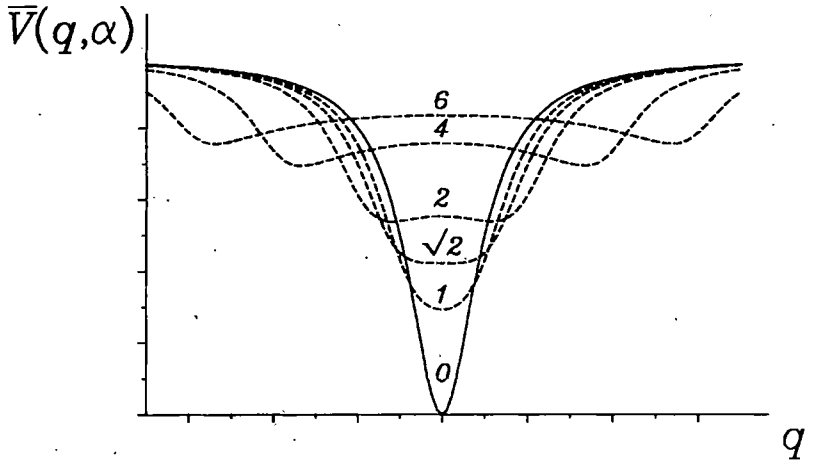

Figure 1.9 Graph of $\overline{V}(q_2, \alpha)$, equation (1.71), corresponding to the potential, $V(q) = -1/(1 + q^2)$, for various values of the parameter, α. Note that the full curve, with $\alpha = 0$, represents $V(q)$.

with $\alpha = 0$, corresponds to the unperturbed potential, $V(q)$. The important point to notice here is that the area under the separatrix of the motion, and hence the action of the mean-motion, must be a decreasing function of α.

A further example is given by the potential $V(q) = -1/(1+q^2)$: the graph of $\overline{V}(q_2, \alpha)$, equation (1.71), corresponding to this potential for various values of the parameter α is shown in figure 1.9. This figure shows that for $\alpha < \sqrt{2}$ the mean potential is qualitatively similar to the unperturbed potential, but that for $\alpha > \sqrt{2}$, the minimum at $q_2 = 0$ becomes a maximum and two other minima are created at $q_2 = \pm q_m$

Because chaotic orbits are significant only for very high fields other ionization mechanisms may become important. Assuming that the mean-motion Hamiltonian accurately describes the dynamics so that there is no chaotic motion, ionization can only occur if the motion crosses the separatrix and, within a time-dependent approximation, there are only two ways in which this can occur. The first is when the field is switched on suddenly; the second when it is switched on adiabatically. In both cases, the dependency of the separatrix of the mean-motion Hamiltonian upon F is needed.

1.6.2 Sudden field switch

For a sudden field switch ionization can occur simply because the phase curve of the initial state intersects the separatrix of the mean-motion Hamiltonian. In this case the field phase, δ, becomes significant. The initial state is a phase curve of H_d in the (q_1, p_1) representation, equation (1.33): at time $t = 0$ each point on this phase curve starts moving on a different phase curve of $\overline{H}$, that is the initial position and momentum are,

$$p_2(0) = p_1 - \frac{F}{\Omega}\cos\delta, \qquad q_2(0) = q_1, \tag{1.74}$$

where (q_1, p_1) lie on the energy contour of $H_d(q_1, p_1) = E_d$, with p_1 given by

$$p_1^2 = 2\mu(E_d - V(q_1)). \tag{1.75}$$

Similarly, the value of the momentum, p_2, on the separatrix of $\overline{H}$, with energy contour $\overline{H}(q_2, p_2) = \overline{E}^S$, is given by,

$$p_2^2 = 2\mu(\overline{E}^S - \overline{V}(q_2, \alpha)). \tag{1.76}$$

By using the approximate mean-motion Hamiltonian (1.73), it may be seen that, for small α, $\overline{V}(q_2, \alpha) \simeq V(q_2) = V(q_1)$. On writing $p_2 = p_1 - (F/\Omega)\cos\delta$, equations (1.34) and (1.38), the following expression is obtained for the value of p_1 at which the initial torus intersects the separatrix of $\overline{H}$,

$$-2p_1\frac{F}{\Omega}\cos\delta + \left(\frac{F}{\Omega}\right)^2\cos^2\delta \simeq 2\mu(\overline{E}^S - E_d). \tag{1.77}$$

In appendix B, this expression is be used to obtain ionization probabilities as functions of the unperturbed dipole energy, E_d, the applied field strength and field frequency for the specific case of the Morse potential. In appendix C it is shown that for any potential the classical and quantal ionization probabilities for this process are similar.

1.6.3 Adiabatic field switch

For slowly switched fields, the variable, α, of equation (1.70), varies slowly with time, $\alpha \rightarrow \alpha(t)$, and the principle of adiabatic invariance ensures that the action, $I(\alpha)$, is an approximate constant of the mean motion. For some potentials, the area under the separatrix, $A(\alpha)$, of $\overline{H}$ is a decreasing function of α; thus there is a critical value, α_c, at which $I = A(\alpha_c)/2\pi$, beyond which bound motion ceases and the system ionizes. An illustration is given in figure 1.10, where an orbit, denoted by the broken curve, is shown in a potential of the Morse-type, $V(q) = (1 - e^{-q})^2$. Here we see that as α increases, the potential changes shape from that in panel A through panel B to panel C, with a corresponding decrease in $A(\alpha)$. Because the action of the mean-motion remains constant the energy of the orbit must gradually increase until, in panel D, it crosses the separatrix and ionizes.

Near the separatrix, the bound frequency, ω, is small, so the ratio, Ω/ω, increases and the accuracy of the mean-motion approximation improves. However the principle of adiabatic invariance breaks down so that α_c, as given above, is only a very rough approximation. In practice, the breakdown of adiabatic invariance affects only a small proportion of orbits and is discussed at the end of this section.

A second example is given by the potential $V(q) = -1/(1+q^2)$, shown schematically in figure 1.11. In this case, the mean-motion Hamiltonian acquires a separatrix at time, $t = t_s$, where $\alpha(t_s) = \sqrt{2}$, and there are two possible outcomes depending upon whether the mean energy, $\overline{E}$, remains greater than the separatrix energy,

$$\overline{E}^S = -(1+\alpha^2)^{-1/2}, \qquad \alpha > \sqrt{2}, \tag{1.78}$$

or whether the mean energy becomes less than $\overline{E}^S$ at some time. As both $\overline{E}$ and $\overline{E}^S$ are complicated functions of α, we can determine whether or not this change occurs only by carrying out detailed calculations. Again, the invariance of the action can be used to obtain a qualitative description of the motion.

As $\alpha(t)$ increases through $\sqrt{2}$ at $t = t_s$, a separatrix is formed when the potential changes shape from that in panel A of figure 1.11, through panel B to panel C. This change alters the nature of the phase curves: for $t < t_s$ there is only one invariant region — note that only energies $\overline{E} < 0$ for which the motion is bounded are considered here — and for $t > t_s$ there are three invariant regions. Imagine an orbit shown schematically by the

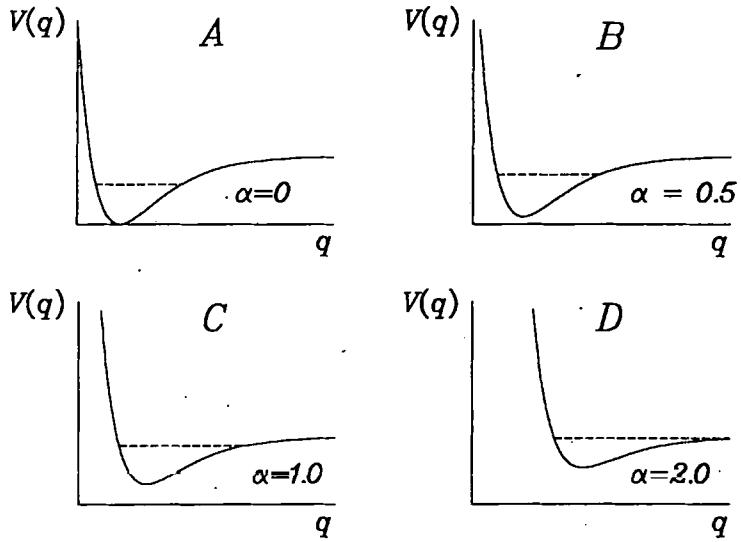

Figure 1.10 Schematic picture of the motion in the potential, $V(q) = (1-e^{-q})^2$ with increasing α. The dotted line marks the energy of the same orbit in each of the panels A to D.

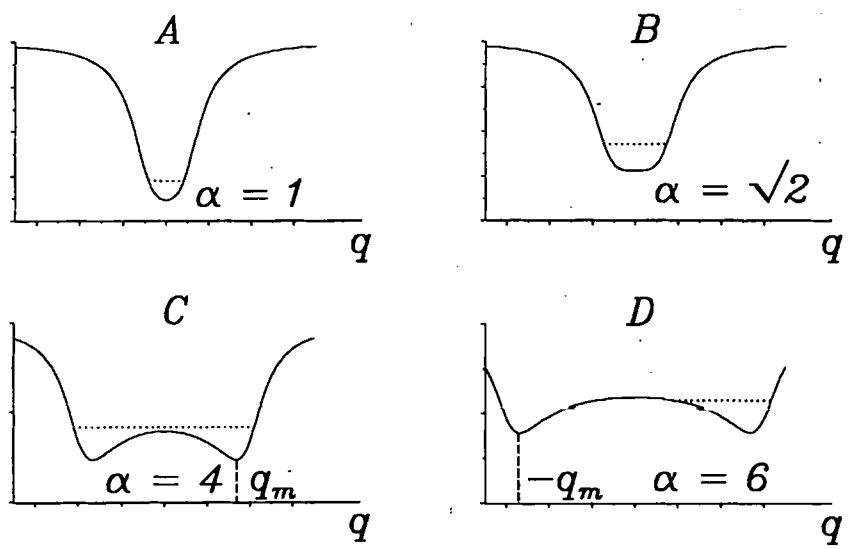

Figure 1.11 Schematic picture of the motion in the potential, $V(q) = -1/(1+q^2)$ with increasing α. The dotted line marks the energy of the same orbit in each of the panels A to D.

dotted line in figure 1.11: as t increases, the action I of this orbit remains approximately constant. For times slightly larger than t_s, the area $A(\alpha)$ under the separatrix will be small so the mean energy of this orbit must satisfy $\overline{E} > \overline{E}^S$. Thus when the separatrix is created, and immediately after, the orbit will begin to oscillate about the two centres at $q_2 = \pm q_m$, so its amplitude and period will increase dramatically.

As t increases further, the area under the separatrix increases, and when the action I satisfies $I \simeq A(t)/2\pi$ we must have $E \simeq \overline{E}^S$. Now it is helpful to imagine the orbit rather than the phase curve. If $\alpha(t)$ increases still further at a time when the particle is not near $q_2 = 0$, then by the next time it reaches the vicinity of $q_2 = 0$ it will find a barrier which it has insufficient energy to cross: it will then start oscillating in one of the two wells centred on $q_2 = \pm q_m$. Because the potential is even, the action variable of this new motion will be approximately $I/2$. Precisely on which side of $q_2 = 0$ the particle ends depends upon the initial conditions and the form of $\lambda(t)$.

1.6.4 Breakdown of adiabatic invariance

The action is an approximate constant of the motion provided that the frequency of the unperturbed motion is not too small. Here, it is found that some orbits behave as though the action is almost constant even though there is a time when the 'frozen' motion has a zero frequency, that is at the instant when the separatrix and mean-motion energy are the same, thus violating a condition required for the principle of adiabatic invariance to hold. This paradox may be resolved by noting that the mathematical proof of the adiabatic invariance of the action variable (see, for example, Percival and Richards 1982, chapter 9) concerns *all* orbits: what happens here is that *some* orbits behave as if the action is an approximate invariant, even though $\omega(t) = 0$ at some instant. The physical reason for this is quite simple: the equations of motion are local in the sense that a particle at point q_2' is not immediately affected by changes at a different point, q_2'', provided the potential at q_2' is unchanged. Therefore, for the example considered in figure 1.11, if $\overline{E}$ is the mean-motion energy and $\overline{E}^S(t)$ the slowly changing separatrix energy, then if $\overline{E}^S(t)$ changes from just below to just above $\overline{E}$ at a time when the particle is at the far turning point, it will not notice the change until it reaches the new turning point near $q_2 = 0$, at which point it will just assume the nature of the motion in the newly created invariant region. Some orbits will, however, will be significantly affected by this small change in $\overline{E}^S(t)$; these will be the orbits which are close to the new unstable fixed point when it is created. Precisely how these orbits are affected is a complicated problem which is not considered here.

The two ionization mechanisms described in this section involve simple properties of time-independent Hamiltonians and clearly have their quantal analogues which, for large

quantum numbers, will give similar ionization probabilities. However, the effectiveness of these mechanisms depends upon the properties of the potential. This is discussed further with reference to the Morse potential in chapter 3 below.

1.7 Classical area-preserving maps

Whilst it is relatively easy to integrate Hamilton's equations numerically, this can prove to be exceedingly time consuming, particularly when one is making a systematic search of parameter space. A more efficient approach is to use a classical map to approximate the dynamical behaviour. The idea of using a map to approximate the dynamics is based on the simple, yet ingenious, idea due to Poincaré of using a stroboscopic classical map to give the change in the dynamical variables over one period of the *external* field. In this section, we generalize the work of Casati *et al.* (1988) on the Kepler map (see also Graham 1988, Nauenberg 1990) and Graham and Höhnerbach (1990, 1991) on the Morse map to derive an area-preserving map which gives the change in the appropriate variables over one *orbital* period and which is applicable to a wide variety of one-dimensional systems. In the next chapter, we shall provide an explicit quantization of this map

1.7.1 The general classical map

Following Richards *et al.* (1989a), we write Hamiltonian (1.27) in terms of the angle-action variables of the unperturbed Hamiltonian, H_0, see equation (1.54) page 25 above, and expand the 2π-periodic perturbation, $V(\theta, I)$, as a Fourier series to obtain Hamiltonian (1.55), namely,

$$H(\theta, I, t) = H_0(I) + F\lambda(t) \sum_{s=-\infty}^{\infty} V_s(I) e^{-is\theta} \cos(\Omega t + \delta). \tag{1.79}$$

First-order perturbation theory then gives the change in the action variable during time, t, to be,

$$\Delta I(\theta_0, t) = iF \sum_{s=-\infty}^{\infty} sV_s(I) e^{-is\theta_0} \lambda(t) \int_0^t dt' \, e^{-is\omega(I)t'} \cos(\Omega t' + \delta), \tag{1.80}$$

where $\theta = \omega(I)t + \theta_0$ and it is assumed that the field envelope, $\lambda(t)$, changes little over the time, t, so that it may be treated as an approximate constant. The following analysis assumes that the perturbation is weak enough for this approximation to ΔI to be reasonable for times comparable to the unperturbed period. In practice, a periodic perturbation causes the invariant tori to break up, but even when this happens, perturbation theory still provides a reasonable approximation to the motion in the vicinity of the unperturbed tori for short times.

In order to progress, it is convenient to express the applied frequency, Ω, in terms of a large integer, r, and a detuning parameter, x:

$$\Omega = \omega(I)(r - x), \quad r \gg 1, \quad |x| < 1/2, \tag{1.81}$$

and to define time in terms of the unperturbed frequency, $t = 2\pi\tau/\omega$. Then for times, $\tau \sim 1$, the integrals of equation (1.80) are dominated by the resonant terms at $s = \pm r$; on ignoring all other terms the following expression for the change in the action variable is obtained,

$$\begin{aligned} \Delta I(\theta_0, \tau) &= rF|V_r(I)|\lambda(\tau)\left(\frac{2\pi\tau}{\omega(I)}\right)\left(\frac{\sin\pi x\tau}{\pi x\tau}\right)\sin(\pi x\tau + r\theta_0 - \delta + \beta_r), \\ &= r\mathcal{F}(r, I)\lambda(\tau)\sin(\pi x\tau + r\theta_0 - \delta + \beta_r), \end{aligned} \tag{1.82}$$

where $\beta_r(I)$ is the phase of the Fourier component, $V_r(I) = |V_r(I)|\exp(-i\beta_r)$, and the first equation defines $\mathcal{F}(r, I)$. Taking an average over the detuning parameter, x, assuming τ large, and using the result,

$$\int_{-1/2}^{1/2} \mathrm{d}x \, \frac{\sin\pi x\tau}{\pi x\tau} \simeq \frac{1}{\tau}, \tag{1.83}$$

gives,

$$\mathcal{F}(r, I) \simeq \frac{2\pi}{\omega(I)} F|V_r(I)|, \tag{1.84}$$

since $r\omega(I) \simeq \Omega$.

The perturbation results, equations (1.82) and (1.84), are now used to approximate the motion by a map: for a suddenly switched field it is convenient to write this map in the form,

$$I_{k+1} = I_k + r(I_k)\mathcal{F}(r(I_k), I_k)\cos\psi_k, \qquad r(I) = \Omega/\omega(I), \tag{1.85}$$

$$\psi_{k+1} = \psi_k + \frac{2\pi\Omega}{\omega(I_{k+1})}, \qquad (\psi = r(I)\theta), \tag{1.86}$$

where the subscript r is now treated as a continuous variable.

One consequence of this construction is that an iterate $I_k \to I_{k+1}$ corresponds to the transformation of the original variable $I(t) \to I(t + T(t))$ through a time interval, $T(I(t), \psi(t))$, dependent upon the initial values of both ψ and I. This poses no problem for the classical map where it is possible to keep track of the time elapsed along any orbit. However, the quantal evolution of the map corresponds to an iterate of a curve in phase space so the correspondence between the original time and the number of iterations is lost. This is a potentially serious problem for the quantization of such maps and is discussed in chapter 2, section 2.7.

In appendix A it is shown that the map (1.85) and (1.86) is gauge independent, so ionization produced by a suddenly switched field, as described by equation (B.6), cannot

be included in this formulation. Neither does it accurately describe the system when the mean-motion has a significantly different frequency to the unperturbed system, although it could clearly be modified to deal with this case, see the discussion in section 1.7.2 below.

There are two problems in using equations (1.85) and (1.86) to approximate the classical motion. First, since the variables (θ, I) are conjugate, the variables (ψ, I) are not and second, the map, being an approximation, is not area-preserving. The first problem is simply dealt with by finding the action variable, $\mathcal{E}$, conjugate to ψ, using the generating function,

$$F_3(I,\psi) = -\frac{H_0(I)\psi}{\Omega}, \quad \omega(I) = \frac{\partial H_0}{\partial I}, \tag{1.87}$$

giving the appropriate action variable $\mathcal{E}$,

$$\mathcal{E} = -\frac{\partial F_3}{\partial \psi} = \frac{H_0(I)}{\Omega} \tag{1.88}$$

which is just the unperturbed energy divided by the applied frequency; in section 2.7 of chapter 2, we shall show how the quantization of this variable approximates the quasi-resonant levels defined by Richards *et al.* (1989a), or the 'photonic-states' of Casati *et al.* (1988). Then, since $\Delta\mathcal{E} \simeq (\omega(I)/\Omega)\Delta I$, the next approximation to equation (1.85) of the classical map is,

$$\mathcal{E}_{k+1} = \mathcal{E}_k + \mathcal{F}(r, I(\mathcal{E}_k))\cos\psi_k, \qquad r = \Omega/\omega(\mathcal{E}_k). \tag{1.89}$$

The map of equations (1.86) and (1.89) is not area-preserving, but is approximated by the generating function,

$$F_2(\mathcal{E}_{k+1}, \psi_k) = \mathcal{E}_{k+1}\psi_k - \mathcal{F}(r(\mathcal{E}_{k+1}), \mathcal{E}_{k+1})\sin\psi_k + 2\pi I(\mathcal{E}_{k+1}) \tag{1.90}$$

and the map produced by this is area preserving:

$$\mathcal{E}_{k+1} = \mathcal{E}_k + \mathcal{F}(r, \mathcal{E}_{k+1})\cos\psi_k, \quad r = \Omega/\omega(\mathcal{E}_{k+1}), \tag{1.91}$$

$$\psi_{k+1} = \psi_k + \frac{2\pi\Omega}{\omega(\mathcal{E}_{k+1})} - \frac{\mathrm{d}\mathcal{F}}{\mathrm{d}\mathcal{E}_{k+1}}\sin\psi_k. \tag{1.92}$$

This is our final approximation to the classical motion.

In order to use this map it is necessary to solve the implicit equation (1.91) for $\mathcal{E}_{k+1}$, but this is generally easier than solving Hamilton's equations and appears to be the necessary consequence of forcing the map to be area-preserving, except in the case of the Coulomb potential for which Kepler's laws ensure that the function $\mathcal{F}$ is independent of $\mathcal{E}$. In chapter 3, it is shown that ionization probabilities given by this map are a very good approximation to those obtained by numerical integration of Hamilton's equations.

Classical ionization is defined to have occurred if the right hand side of (1.89) is larger than the separatrix energy, $\mathcal{E}^S = E^S/\Omega$, so the classical ionization probability from the state of action $\mathcal{E}_k$ per unperturbed period of that level is,

$$P_i^{cl}(\mathcal{E}_k) = \begin{cases} \frac{1}{\pi}\cos^{-1}\left(\frac{\mathcal{E}^S - \mathcal{E}_k}{\mathcal{F}(r,\mathcal{E}_k)}\right) & \mathcal{E}_k + \mathcal{F}(r,\mathcal{E}_k) > \mathcal{E}^S \\ 0 & \text{otherwise.} \end{cases} \tag{1.93}$$

1.7.2 The mean motion map

As was pointed out in the previous section, the map, equations (1.85) and (1.86), is gauge invariant. Consequently, ionization produced by a suddenly switched field, as discussed in section 1.6.2 above and described by equation (B.6) of appendix B, cannot occur. In addition, the unperturbed frequency, $\omega(I)$, occurs in the formulation. However, at very high field frequencies the correct unperturbed motion is that produced by the mean Hamiltonian (1.70), page 29, and so the map will be inaccurate whenever the mean-motion has a significantly different frequency to the unperturbed system.

A more accurate map can be constructed by Fourier-analyzing the potential of the mean-motion, equation (1.71) page 29, and retaining only the lowest harmonics,

$$V(q_2 + \alpha\sin\phi) \simeq \overline{V}(q_2,\alpha) + \overline{V}_1(q_2,\alpha)\sin\phi, \tag{1.94}$$

$$\overline{V}_1(q_2,\alpha) = \frac{1}{2\pi}\int_{-\pi}^{\pi} \mathrm{d}\phi\, V(q_2 + \alpha\sin\phi)\sin\phi, \tag{1.95}$$

so that an approximate Hamiltonian is, for a suddenly switched field,

$$H \simeq \frac{1}{2\mu}p_2^2 + \overline{V}(q_2,\alpha) + \overline{V}_1(q_2,\alpha)\sin(\Omega t + \delta), \tag{1.96}$$

where $\alpha = F/\mu\Omega^2$. This Hamiltonian can be treated in the same manner as the original Hamiltonian in order to produce a map equivalent to that of equations (1.85) and (1.86).

In chapter 3, classical results for the map based upon this Hamiltonian are presented and shown to be in better agreement with exact calculations than the results obtained from the original map, equations (1.91) and (1.92), see table 3.2 and figure 3.13 on pages 78 and 88 respectively. There is, however, a caveat: the mean-motion map is superior if the field is switched on suddenly, but for slowly switched fields an extra term, representing the change in α, is needed and this is not easy to approximate. Indeed, for very high frequency fields the change in α during one orbital period is large and can no longer can be regarded as adiabatic, even for very slow field switches.

For the quantal map, which we shall derive in section 2.7 below, approximation (1.96) becomes important at large α and high frequencies because the number of quasi-resonant states is different according as $\overline{V}$ or V is used and this will produce significant changes in the quantal ionization probabilities.

1.7.3 Local behaviour and the standard map

The dynamics of the map equations (1.91) and (1.92) is difficult to understand. However, by expanding about the initial value $\mathcal{E}_0 = H(I_0)/\Omega$ of $\mathcal{E}$ and defining the new variable:

$$\mathcal{P} = (\mathcal{E} - \mathcal{E}_0), \tag{1.97}$$

the following local approximation to the map of equations (1.91) and (1.92) is obtained:

$$\begin{aligned} \mathcal{P}_{k+1} &= \mathcal{P}_k + \kappa \cos\psi_k, \qquad \kappa = \mathcal{F}(r, I_0), \\ \psi_{k+1} &= \psi_k + T\mathcal{P}_{k+1}, \qquad T = \frac{2\pi\Omega^2}{\omega(\mathcal{E}_0)^3}\frac{\mathrm{d}\omega(I_0)}{\mathrm{d}I}, \end{aligned} \tag{1.98}$$

where higher order terms in the expansion of $\mathcal{F}(r, \mathcal{E})$ have been ignored and an unessential constant has been dropped in the expression for ψ_{k+1}. Thus, the local approximation, equation (1.98), yields the standard map with parameter, $K = \kappa T$, the classical dynamics of which has been studied by several authors (see the review by Chirikov 1979 and references therein). For values of $K \gg 1$, most initial values of ψ lead to chaotic or diffusive motion, with diffusion coefficient $\kappa^2/2$ (see Lichtenberg and Lieberman 1983, page 286). For $K \sim 1$, regular and chaotic trajectories co-exist. This gives a criterion for the onset of chaotic motion, namely $K > 1$, with the same functional form, but a different numerical coefficient, as equation (1.65), page 28, which is based upon the resonance overlap condition:

$$F_{CH}^{map} = \frac{1}{4\pi\Omega^2}\frac{\omega(I_0)^4}{|V_r(I_0)|}\left|\frac{\mathrm{d}\omega(I_0)}{\mathrm{d}I}\right|^{-1}. \tag{1.99}$$

The map (1.98) should provide a reasonable approximation to the motion in the vicinity of the initial action: for the $1d$-hydrogen atom, Casati *et al.* (1988) have compared iterates of the classical Kepler map with the numerical solution of Hamilton's equations and found reasonable agreement.

Chapter 2

Quantal theory

2.1 Introduction

In chapter 1 the classical dynamics of a one-dimensional system in the presence of a periodic field of amplitude F and frequency Ω was studied. Despite the complexity of the problem and the lack of a rigorous theory to describe the behaviour of a given system, numerical solutions of Hamilton's equations are relatively easy to obtain. Thus, it is possible to explore limited regions of parameter space in order to build up an approximate picture of the dynamical response for specific systems.

In this chapter the dynamics of the corresponding quantal system is considered. The study of the quantal dynamics of such a system is far more complicated largely because of the need to include the effects of the continuum, that is the region where the classical motion ceases to be bound. In addition, a further parameter, Planck's constant, has been added to parameter space and again no rigorous theory exists to provide a guide to the behaviour of the system.

2.2 The Schrödinger equation and gauge transformations

In general, the study of a quantal particle moving in a three dimensional potential, $V(\boldsymbol{r})$, under the influence of a classical periodic field described by the vector potential, $\boldsymbol{A}(\boldsymbol{r},t)$, in the Coulomb gauge involves finding the solution, $\Psi(\boldsymbol{r},t)$, of the Schrödinger equation,

$$\mathrm{i}\hbar\frac{\partial\Psi}{\partial t} = \left\{\frac{1}{2\mu}\left(-\mathrm{i}\hbar\nabla - \frac{e}{c}\boldsymbol{A}(t)\right)^2 + V(\boldsymbol{r})\right\}\Psi, \tag{2.1}$$

where e is the electron charge, μ the reduced mass, c the speed of light, $2\pi\hbar$ is Planck's constant, $-\mathrm{i}\hbar\nabla$ is the momentum operator and where, for the reasons discussed in section 1.3.1 above, the spatial variation of the vector potential describing the field has been neglected, $\boldsymbol{A}(\boldsymbol{r},t) \rightarrow \boldsymbol{A}(t)$. As with the classical Hamiltonians described in chapter 1, other equivalent Schrödinger equations may be obtained by making unitary gauge

transformations. By making the transformation,

$$\Psi_d(\boldsymbol{r},t) = \exp\left[-\mathrm{i}\frac{e\boldsymbol{r}.\boldsymbol{A}(t)}{\hbar c}\right]\Psi(\boldsymbol{r},t), \qquad \boldsymbol{E}(t) = -\frac{1}{c}\frac{\partial \boldsymbol{A}}{\partial t}(t), \tag{2.2}$$

the Schrödinger equation (2.1) is transformed to the dipole gauge,

$$\mathrm{i}\hbar\frac{\partial\Psi_d}{\partial t} = \left(-\frac{\hbar^2}{2\mu}\nabla^2 + V(\boldsymbol{r}) - e\boldsymbol{r}.\boldsymbol{E}(t)\right)\Psi_d. \tag{2.3}$$

A third form may be obtained by using the so-called 'Kramers-Henneberger' transformation (see Kramers 1956 page 262 and Henneberger 1968),

$$\Psi_a(\boldsymbol{r},t) = e^{\boldsymbol{a}(t).\nabla}\Psi(\boldsymbol{r},t), \qquad \mu\frac{\mathrm{d}^2\boldsymbol{a}}{\mathrm{d}t^2}(t) = e\boldsymbol{E}(t). \tag{2.4}$$

In this 'space-translated' frame, the acceleration gauge Schrödinger equation is,

$$\mathrm{i}\hbar\frac{\partial\Psi_a}{\partial t} = \left(-\frac{\hbar^2}{2\mu}\nabla^2 + V(\boldsymbol{r}+\boldsymbol{a}(t)) + \frac{1}{2}\mu\dot{\boldsymbol{a}}^2\right)\Psi_a. \tag{2.5}$$

It should be noted that the Schrödinger equations (2.1), (2.3) and (2.5) are all related by time-dependent unitary transformations and therefore make identical physical predictions. However, the operators which correspond to true physical observables differ in all three cases. This should be compared with the corresponding classical situation where the canonical variables (q,p), (q_1,p_1) and (q_2,p_2) of the Hamiltonians (1.27), (1.33) and (1.37), described in section 1.3.3 above, are different in each of the three gauges for times $0 < t < T_m$.

For all but the simplest of cases, there is no known analytic solution to the three dimensional Schrödinger equation and, for the high quantum numbers of interest here, numerical solutions are prohibitively expensive. Thus, attention is usually restricted to the simplified, one-dimensional model which is usually expressed in the dipole gauge,

$$\mathrm{i}\hbar\frac{\partial\Psi}{\partial t} = -\frac{\hbar^2}{2\mu}\frac{\partial^2\Psi}{\partial x^2} + V(x)\Psi - xf(t)\Psi, \qquad f(t) = eE(t), \tag{2.6}$$

or equivalently, using Dirac notation,

$$\mathrm{i}\hbar\frac{\partial}{\partial t}|\Psi(t)\rangle = H|\Psi(t)\rangle, \qquad \Psi(x,t) = \langle x|\Psi(t)\rangle, \tag{2.7}$$

where H is the Hamiltonian or energy operator, obtained from the Hamiltonians discussed in chapter 1 by replacing the momentum variable, p, with its operator equivalent, $-i\hbar\partial/\partial x$. Whilst numerically it is far more efficient to solve equation (2.6) than its full three-dimensional counterpart there are still no known analytic solutions for the systems of interest here. In some circumstances, for instance the hydrogen atom in the presence of a static electric field (see, for example, Bayfield and Pinnaduwage 1985, Bayfield

and Sokol 1988a, 1988b) where the electron is constrained to move along the field axis, the one-dimensional model provides a good approximation to the fully three-dimensional problem. Further simplifications are always made by making approximations the to continuum or neglecting its effect completely.

Much of the work published to date has concentrated on the one dimensional hydrogen atom; the remainder of this chapter concentrates on this specific system and is organized as follows. Firstly, in section 2.3, the various approaches used to solve equation (2.6) are reviewed. In section 2.4 the problem of including the effect of the continuum is highlighted and four different approximations are discussed. Section 2.5 concentrates on the low-frequency regime; in particular, the adiabatic basis expansion (see Richards 1987) is introduced. In section 2.6 the high frequency regime is considered and finally, in section 2.7, we provide an explicit quantisation of the classical map derived in section 1.7 above to give a general quantal which, for high field frequencies, provides a simple and efficient method of obtaining approximate solutions to the one-dimensional Schrödinger equation (2.6).

2.3 Solving the Schrödinger equation

There are two main approaches to obtaining the solution of Schrödinger's equation. One method is to use Finite Difference methods to solve the partial differential equation (2.6) exactly. A more usual approach is expand the time-dependent wave function in terms of an appropriate set of basis functions. Both methods are described in this section.

2.3.1 Finite difference methods

The major advantage of using finite difference methods to solve Schrödinger's equation is that the continuum is automatically taken into account. However, to solve Schrödinger's equation numerically is exceedingly time consuming, even when carried out on supercomputers. The method involves solving the equations on a finite grid and this introduces an added complication; an approximation has to be used to account for the non physical behaviour which may occur if the wave function reaches the edge of the grid: one method is to introduce a complex, or optical, potential (see, for instance, Leforestier and Wyatt 1982) at the edge of the grid to 'absorb' the wave function. For the one-dimensional model of a hydrogen atom, the Coulomb singularity introduces still further difficulties.

The use of a finite difference method for solving the time-dependent one-dimensional Schrödinger equation involves a partial spatial discretization together with the algorithm,

$$\Psi_j^{n+1} = \left(1 - \mathrm{i}\frac{\Delta t H(t+\Delta t/2)}{2\hbar}\right)\left(1 + \mathrm{i}\frac{\Delta t H(t+\Delta t/2)}{2\hbar}\right)^{-1}\Psi_j^n, \qquad (2.8)$$

for unitary time evolution by a step Δt of the wave function at grid-point j: the method is stable for $\Delta t = O((\Delta x)^2)$, where Δx is the separation of consecutive grid-points in the spatial mesh. This procedure leads to a tridiagonal linear system of equations which can be solved by an efficient 'two-sweep' method (Richtmyer 1957).

Finite difference methods have been employed by several authors to study a one-dimensional quantal model of the ground state hydrogen atom, the so-called 'soft-core' model, in the presence of an oscillating electric field, (see for example Bardsley and Comella 1989, Su *et al.* 1990 and Burnett *et al.* 1991) whilst Goggin and Milonni (1988) utilized the finite difference approach in their study of the driven Morse Oscillator.

2.3.2 Basis expansion methods

The more usual approach is to expand the time-dependent wave function $|\Psi(t)\rangle$ in terms of an appropriate set of basis functions in order to reduce the problem to the solution of a set of ordinary differential equations. One method is to use the bound and continuum eigenfunctions of the unperturbed Hamiltonian, $|n\rangle$ and $|k\rangle$ respectively, where

$$H_0|n\rangle = E_n|n\rangle, \qquad \langle n|m\rangle = \delta_{nm}, \tag{2.9}$$

$$H_0|k\rangle = E_k|k\rangle, \qquad \langle k|k'\rangle = \delta(k-k'), \tag{2.10}$$

so that the wave function is then written,

$$|\Psi(t)\rangle = \sum_n a_n(t)|n\rangle + \int \mathrm{d}k\, a_k(t)|k\rangle, \tag{2.11}$$

where the sum is taken over all bound states and the integral over the whole continuous spectrum. On using the orthogonality of both bound and continuum state wave functions the time-dependent Schrödinger equation (2.7) reduces to an infinite set of ordinary differential equations for the amplitudes a_n. For the one-dimensional hydrogen atom these take the form,

$$\mathrm{i}\hbar\frac{\mathrm{d}a_n}{\mathrm{d}t} = E_n a_n - f(t)\left(\sum_{m=1}^{\infty}\langle n|x|m\rangle a_m + \int_0^{\infty}\mathrm{d}k\,\langle n|x|k\rangle a_k\right), \tag{2.12}$$

$$\mathrm{i}\hbar\frac{\mathrm{d}a_k}{\mathrm{d}t} = E_k a_k - f(t)\left(\sum_{m=1}^{\infty}\langle k|x|m\rangle a_m + \int_0^{\infty}\mathrm{d}k'\,\langle k|x|k'\rangle a_{k'}\right). \tag{2.13}$$

However, no analytic solution to equations (2.12) and (2.13) has yet been found and solutions are usually obtained by truncating the sums and integrals and using an approximation to take the coupling with the continuum into account. However, truncating the basis introduces its own problems; for the one-dimensional hydrogenic basis, where there are an infinite number of bound states, the matrix elements $\langle n|x|m\rangle$ are large, as can be

seen by using the Heisenberg correspondence principle to give, for $n \neq m$,

$$\langle n|x|m\rangle \simeq -\frac{\hbar^2}{\mu e^2}\left(\frac{n+m}{2}\right)^2 \frac{J_s'(s)}{s} \simeq -\frac{\hbar^2}{\mu e^2}\frac{0.103(n+m)^2}{|s|^{5/3}}, \quad s = m-n, \tag{2.14}$$

where $J_s(x)$ is an ordinary Bessel function and a standard asymptotic expansion (see Abramowitz and Stegun 1965, equation (9.3.33)) has been used. The matrix elements, equation (2.14), decay slowly as $n \to m+N$, $N \gg 1$; this is caused by the Coulomb singularity and can be overcome by an efficient choice of basis (see the discussion of sections 2.5.1 and 2.6.1 below and, in particular, equation (2.56) on page 55). However, $\langle n|x|m\rangle$ increases as n^2 and this is a more serious problem. For states $n \gg n_0$, the couplings are very large and, as the energy separation decreases as n^{-3}, this means that a very small time-step is required to deal with these states numerically. Blümel and Smilansky (1987) found that when a large number of bound states are strongly coupled, basis truncation may introduce large errors, with satisfactory convergence obtained only with a basis of more than 400 bound states.

In their study of the one-dimensional hydrogen atom in the presence of a microwave field, Casati *et al.* (1984) considered an approximation with a truncated basis of hydrogenic states which excluded the continuum completely. A further simplification was made by neglecting the switch function. Thus equation (2.12), with $V(x) = -1/|x|$ and $f(t) = F\cos\Omega t$, was reduced to,

$$i\hbar\frac{da_n}{dt} = E_n a_n + F\cos\Omega t \sum_{m=n_{min}}^{n_{max}} \langle n|x|m\rangle a_m. \tag{2.15}$$

The total number of states used was about 200 in a typical range $20 \leq n \leq 226$ with n_{min} chosen to lie approximately 20–40 levels below the initially excited state, n_0; a further decrease in n_{min} was shown to have no appreciable influence on the dynamics.

A similar expansion, this time in terms of a basis of unperturbed oscillator states, was used by Walker and Preston (1977) in their study of the quantal response of a driven Morse oscillator far below the dissociation threshold. Again, the continuum and switch function were ignored and sufficient basis states were included to ensure convergence of results; typically, only the lowest twelve oscillator states were required.

2.3.3 Floquet theory

Another frequently used method exploits the time-periodicity of the Hamiltonian to construct the unitary time evolution operator, equation (2.20) below, by numerically integrating the Schrödinger equation for each state in the basis over a single field period, $T = 2\pi/\Omega$; solutions of the Schrödinger equation can then be found at longer times by simply applying the time evolution operator to the initial state. Although this method

has tremendous numerical advantages when the interaction time is large, it only describes the evolution within the bound space since the coupling to the continuum is difficult to include. In addition, it cannot be used to model the effect of the field switch, $\lambda(t)$, which introduces other frequency components, although for $\dot{\lambda} \ll 1$ this effect may be incorporated approximately (see Breuer *et al.* 1989 and references therein). An extensive review of the Floquet approach is given by Chu (1985).

By considering a quantal system driven at frequency Ω and described by the T-periodic Hamiltonian $H(t)$,

$$H(t+T) = H(T), \qquad T = 2\pi/\Omega, \tag{2.16}$$

Shirley (1965) utilized Floquet's (1883) theorem to show that there exists a complete set of states $|\phi_k(t)\rangle$ of the time-dependent Schrödinger equation,

$$\left(H(t) - \mathrm{i}\hbar\frac{\partial}{\partial t}\right)|\Psi(t)\rangle = 0, \tag{2.17}$$

which can be chosen with the property,

$$|\phi_k(t)\rangle = \exp(-\mathrm{i}\epsilon_k t/\hbar)|u_k(t)\rangle, \tag{2.18}$$

$$|u_k(t+T)\rangle = |u_k(t)\rangle, \tag{2.19}$$

where the real parameter, ϵ_k, is called the quasi-energy and where the states, $|u_k(t)\rangle$, are known as the quasi-energy or Floquet states.

In order to describe the time evolution of quantum states subjected to the dynamics defined by $H(t)$, the time evolution operator is used,

$$\hat{U}(t_f, t_i) = \hat{T}\exp\left(-\frac{\mathrm{i}}{\hbar}\int_{t_i}^{t_f} \mathrm{d}t\, H(t)\right), \tag{2.20}$$

where $\hat{T}$ is the time-ordering operator. The time evolution operator, $\hat{U}(t_f, t_i)$, transforms the state, $|\Psi(t_i)\rangle$, at initial time, $t = t_i$, into the state, $|\Psi(t_f)\rangle$, at time, $t = t_f$. Applying $\hat{U}(t_f, t_i)$ to the states, $|u_k\rangle$, over one cycle, T, gives, on using equation (2.19),

$$\hat{U}(t_i + T, t_i)|u_k(t_i)\rangle = \exp(-\mathrm{i}\epsilon_k T/\hbar)|u_k(t_i)\rangle. \tag{2.21}$$

Therefore, the states $|u_k(t_i)\rangle$ diagonalize the one-cycle time-evolution operator $\hat{U}(t_i + T, t_i)$ and, because $\hat{U}$ is unitary, the quasi-energies, ϵ_k, are real and the states, $|u_k\rangle$, are orthogonal and complete. The quasi-energies, ϵ_k, determine the spectrum of $\hat{U}(t_i + T, t_i)$ and hence contain valuable information regarding the dynamical properties of $H(t)$.

As mentioned earlier, the time-evolution operator is usually constructed numerically. The easiest way of achieving this is to expand the time-dependent wave function in terms of a basis consisting of N unperturbed states and then to integrate the resulting set of

differential equations, see for example equation (2.15) above, over one period, T, with N linearly independent initial conditions. For each different initial condition $|\Psi(t_0)\rangle$, a column of the time-evolution operator can be constructed using the relation,

$$|\Psi(t_0+T)\rangle = \hat{U}(t_0+T,t_0)|\Psi(t_0)\rangle. \tag{2.22}$$

The solutions to the Schrödinger equation can then be found at longer times simply by multiplying by $\hat{U}(t_0+T,t_0)=\hat{U}(T)$,

$$|\Psi(t_0+NT)\rangle = \hat{U}(T)^N|\Psi(t_0)\rangle. \tag{2.23}$$

When the effect of the continuum is included, the quasi-energies, ϵ_k, become complex (see Yajima 1982 for a rigorous proof) and the time-evolution operator is no longer unitary: this problem is not addressed here. Instead, we proceed by discussing other methods used to date to model the coupling to the continuum.

2.4 Inclusion of the continuum

As was mentioned at the start of this chapter, one of the major difficulties encountered when solving the Schrödinger equation is the need to approximate the effect of the continuum. In this section we discuss the methods which have been used to date.

2.4.1 A discrete representation

In their study of the one dimensional hydrogen atom in the presence of an oscillating field, Susskind and Jensen (1988) made an expansion of the time dependent wave function in terms of the bound and continuum eigenfunctions of the unperturbed hydrogen atom and introduced a discrete representation of the continuum. Using this method, the authors were able to obtain numerical solutions of the Schrödinger equation. Discretization of the continuum consists of dividing the continuous index, k, into N_c segments in $[0,k_{max}]$, each centred at k_j, $j=1,N_c$, with width Δ_j. The integral over the continuum states in equation (2.12) can then be approximated by,

$$\begin{aligned}\int_0^\infty \mathrm{d}k\,\langle n|x|k\rangle a_k &\simeq \sum_{j=0}^{N_c}\int_{k_j-\Delta_j/2}^{k_j+\Delta_j/2}\mathrm{d}k\,\langle n|x|k\rangle a_k,\\ &\simeq \sum_{j=0}^{N_c}\langle n|x|k_j\rangle a_{k_j}\Delta_j,\end{aligned} \tag{2.24}$$

where it is assumed that $\langle n|x|k\rangle a_k$ varies little on the scale Δ_j. A similar approximation is also applied to equation (2.13) to obtain,

$$\int_0^\infty \mathrm{d}k'\,\langle k|x|k'\rangle a_{k'} \simeq \sum_{j=0,k\neq k_j}^{N_c}\left(\langle k|x|k'\rangle a_{k'}\Delta_j + \int_{k-\Delta_j/2}^{k+\Delta_j/2}\mathrm{d}k'\,\langle k|x|k'\rangle a_{k'}\right). \tag{2.25}$$

However, because the divergence of the matrix elements, $\langle k|x|k'\rangle$, causes numerical difficulties, the authors were forced to neglect the continuum-continuum transitions.

With this scheme, the authors note that the bound states and the discretized continuum can both be treated in the same way by truncating the bound states to a finite number, N_b, and expressing the problem in terms of a large set of ordinary differential equations. If all the Δ_j are chosen to be equal, then this prescription is essentially equivalent to putting the one dimensional hydrogen atom in a large box of length proportional to Δ_j^{-1}.

However, discretizing the continuum introduces two additional constraints. Firstly, if the discretized continuum states are chosen with an equal spacing in k, where $\Delta k = k_{max}/N_c$, then the minimum energy resolution of the discretized continuum is,

$$\Delta E = k_{max}\Delta k \simeq \frac{1}{n_0^2 N_c}, \tag{2.26}$$

and this limits the time of integration. On using the time-energy uncertainty relation, we see that the approximation fails after T_c field periods, where,

$$T_c \simeq \frac{n_0^3\Omega}{n_0^3\Delta E} = \frac{N_c\Omega_0}{n_0}. \tag{2.27}$$

For longer times the number of continuum states, N_c, must be increased in order to resolve the continuum adequately. Secondly, the requirement that $\langle n|x|k\rangle a_k$ varies little on the scale Δ_j introduces an upper limit to the energy considered.

2.4.2 The Sturmian basis

The wave function can be expressed in terms of any complete set of basis functions. For problems involving a one dimensional hydrogen atom in a strong *static* electric or magnetic field the so called Sturmian basis functions have often been used in preference to the hydrogenic eigenfunctions (see, for example, Rotenberg 1970 and Edmonds 1973).

The Sturmian basis has the advantage of being both complete and discrete. These properties make it convenient to use in problems where continuum effects are important without having to deal with the inconveniences which arise through using the hydrogenic continuum wave functions, such as discretizing the continuum or dealing with singular matrix elements. Another advantage of using the Sturmian representation is that the matrix elements are easy to evaluate, being given in terms of simple, algebraic expressions. However, the Sturmian functions have no direct physical significance and in order to interpret the results of Sturmian calculations it is necessary to project back onto the basis of bound and continuum hydrogenic states. In addition, when highly excited bound states and low-energy continuum states play an important role in the dynamics, numerical calculations require at least twice as many Sturmian functions to achieve the same

resolution as carefully chosen bound and discretized continuum states of the hydrogenic basis, see Susskind and Jensen (1988).

For the one-dimensional Coulomb potential, with orbital angular momentum quantum number $l = 0$, the Sturmian functions, $S(x)$, are defined by the eigenvalue equation,

$$-\frac{1}{2}\frac{\mathrm{d}^2 S}{\mathrm{d}x^2} - \frac{\beta}{x}S = E_0 S, \qquad x > 0,\ E_0 < 0,\ \beta > 0, \tag{2.28}$$

with $S(x) = 0$ for $x \leq 0$ and $S(x)$ bounded as $x \to \infty$. The fixed parameter E_0 characterizes a particular basis, $\{S_\beta^{E_0}(x)\}$, with each element of the basis being characterized by the eigenvalue β. In other words, Sturmian functions satisfy a Sturm-Liouville problem where the eigenvalues are the coefficients of the Coulomb potential.

Multiplying by β^{-2} and rescaling x by β reduces equation (2.28) to the Schrödinger equation of the unperturbed hydrogen atom,

$$-\frac{\hbar^2}{2\mu}\frac{\partial^2 \phi_n}{\partial x^2} - \frac{e^2}{x}\phi_n = E_n \phi_n \tag{2.29}$$

with $E_n = E_0 \beta^{-2}$. Therefore, the Sturmian functions are related to the hydrogenic eigenfunctions, ϕ_n, by,

$$S_\beta^{E_0}(x) = C\phi_n(\beta x) \quad \text{with} \quad \int_0^\infty \mathrm{d}x\, S_\beta^{E_0}(x)\frac{2}{x}S_{\beta'}^{E_0}(x) = \delta_{\beta\beta'} \tag{2.30}$$

and where C is a proportionality constant determined by the normalization condition.

A Sturmian basis was used by Casati *et al.* (1987b) in their numerical study of the microwave ionization of highly excited hydrogen. Using up to 600 Sturmian basis functions they solved Schrödinger's equation for a one-dimensional hydrogen atom in an oscillating electric field. By recursively evaluating the hypergeometric functions in the formal expressions for the projection onto the bound states of the hydrogenic basis, the authors were able to study the excitation of bound states in the presence of a strong perturbation. Unfortunately, the complexity of the corresponding expressions for the projection of the Sturmian basis onto the hydrogenic continuum states prevented Casati and coworkers from performing a detailed study of the ionization process. This was remedied by Susskind and Jensen (1988) who derived convenient formulae for the projection of the Sturmian basis onto both the bound and continuum states of the hydrogenic basis, thus enabling them to compare these two different approaches to the solution of Schrödinger's equation.

2.4.3 Projection operators and decay factors

Blümel and Smilansky (1987, 1990) used a quantal one-dimensional model to study the hydrogen atom perturbed by a low frequency field. By using projection operators, the

equations of motion were written in the form of coupled differential equations for the bound and continuum states. By formally integrating equation (2.13) for the continuum states, Schrödinger's equation was reduced to an integro-differential equation in which the kernel describing the bound-continuum transitions was approximated by a combination of decaying exponentials. Continuum-continuum transitions were neglected. Briefly, given the Hamiltonian

$$H(x,t) = H_0(x) - V(x,t), \tag{2.31}$$

$$H_0(x) = \frac{p^2}{2\mu} - \frac{e^2}{x}, \qquad V(x,t) = Fx\sin\Omega t, \tag{2.32}$$

where the energy spectrum of H_0 is given by equations (2.9) and (2.10) above, Blümel and Smilansky used the orthogonality of the states $|n\rangle$ and $|k\rangle$ to obtain equations (2.12) and (2.13) for the amplitudes $a_n(t)$ and $a_k(t)$ respectively. On ignoring continuum-continuum interactions, equation (2.13) was formally integrated to give,

$$b_k(t) = \frac{\mathrm{i}}{\hbar}\int_0^t \mathrm{d}t' \exp(\mathrm{i}E_k t'/\hbar) F \sin\Omega t' \sum_m \langle k|x|m\rangle a_m(t'), \tag{2.33}$$

where $a_k(t) = \exp(-\mathrm{i}E_k t/\hbar) b_k(t)$. Inserting this result into equation (2.12) gives,

$$\begin{aligned} \mathrm{i}\hbar\dot{a}_n(t) &= E_n a_n(t) - F\sin\Omega t \sum_m \Bigg(\langle n|x|m\rangle a_m(t) \\ &+ \frac{\mathrm{i}}{\hbar}\int_0^t \mathrm{d}t' K_{nm}(t-t') F \sin\Omega t' a_m(t') \Bigg) \end{aligned} \tag{2.34}$$

where the kernel, $K_{nm}(t-t')$, is defined by,

$$K_{nm}(s) = \int_0^\infty \mathrm{d}k \, \langle n|x|k\rangle \exp(-\mathrm{i}E_k s/\hbar) \langle k|x|m\rangle, \quad s = t - t' > 0. \tag{2.35}$$

This integro-differential equation is then converted into a set of first-order differential equations by expanding $K(s)$ in a finite series of decaying exponentials. The authors caution that truncation of the basis may produce large errors if not dealt with correctly.

One of the main conclusions of this work is that there exist 'window states' [1], $n_W \sim n_0 F_0^{-1/4}$ such that all ionization occurs from levels in the vicinity of n_W. As noted by Leopold and Richards (1991), it is curious that Blümel and Smilansky's expression for n_W is independent of the applied field frequency. In the low-frequency limit considered by Richards *et al.* (1989b), it is shown that the state $|n_W\rangle$ overlaps most with the adiabatic state at the barrier top whereas in the high-frequency limit, where one- or two-photon ionization is permitted, it is clear that n_W must depend upon the field frequency. Thus, Leopold and Richards (1991) believe that the window states, and hence the decay rates of Blümel and Smilansky are valid only at low frequencies.

[1] The role played by window states in the low-frequency regime is discussed further in section 2.5, below.

2.4.4 A semiclassical ionization mechanism

Following Blümel and Smilansky, Leopold and Richards (1991) also include the continuum using decay factors, providing two approximations to these decay factors both based upon classical perturbation theory. One approximation uses purely classical dynamics, the other uses semiclassical methods. Both these approximations are obtained using the classical Hamiltonian,

$$H(z,P,t) = H_0(z,P,F_s) - \frac{eF_\mu A(t)}{\mu\Omega} P\cos(\Omega t+\delta), \tag{2.36}$$

$$H_0(z,P,F_s) = \frac{1}{2\mu}P^2 - \frac{e^2}{z} - eF_s z, \qquad z \geq 0, \tag{2.37}$$

where F_s represents the constant static field used in the experiments of Bayfield and co-workers (see, for example, Bayfield and Pinnaduwage 1985, Bayfield and Sokol 1988a, 1988b) to maintain the one-dimensional nature of the wave function. The presence of the static field has the effect of lowering the continuum threshold, so that the unperturbed system, H_0, supports only a finite number of bound states and has a potential barrier with saddle energy, $E_s = -2e\sqrt{F_s}$. The time dependent wave function is then expanded in terms of the bound states of the unperturbed Hamiltonian,

$$|\Psi\rangle = \sum_n b_n(t)|n,F_s\rangle \exp[-\mathrm{i}E_n(F_s)t/\hbar)], \tag{2.38}$$

where,

$$H_0(z,P,F_s)|n,F_s\rangle = (E_n(F_s) - \mathrm{i}\mathcal{E}_n(F_s))|n,F_s\rangle, \tag{2.39}$$

to give the usual coupled equations for the amplitudes $b_n(t)$,

$$\mathrm{i}\hbar\frac{\mathrm{d}b_n}{\mathrm{d}t} = -\mathrm{i}\mathcal{E}_n b_n - \frac{ef}{\mu\Omega}\cos(\Omega t+\delta)\sum_m b_m\langle n,F_s|P|m,F_s\rangle \exp[\mathrm{i}(E_n-E_m)t/\hbar], \tag{2.40}$$

where $f = F_\mu A(t)$, $\mathcal{E}_n(F_s)$ are the complex parts of the energy introduced to model the interaction with the continuum and P is now the momentum operator. In deriving expressions for the ionization rates, the following assumptions are made:

1. for times comparable to the unperturbed electron period classical perturbation theory is a reasonable approximation to the exact classical dynamics: this was checked numerically;

2. if the energy becomes greater than the saddle energy, $E_s = -2e\sqrt{F_s}$, then in this time there is a negligible chance of it returning to the neighbourhood of the initial energy;

3. direct ionization occurs only from those states where $\Omega_n = (n^3/n_0^3)\Omega_0 \gg 1$;

4. tunnelling through the barrier gives a negligible decay rate compared with that produced by the periodic field for the quantum numbers of interest, $n_0 \gtrsim 30$; note that this final approximation is not essential.

The classical approximation is obtained by assuming that the field envelope, $A(t)$, varies sufficiently slowly for it to be considered constant. An approximation to the maximum energy change during one period, $T(n)$, of the classical atom initially in a level n is then obtained using classical first order perturbation theory,

$$\max(\Delta E) = e\pi f r z_r(I), \tag{2.41}$$

where $z_s(I)$ are the Fourier components of $z(t)$, $I = n\hbar$ and $\omega(I, F_s)$ are the action and frequency of the unperturbed classical orbit respectively, and $r \simeq \Omega/\omega$. In the presence of a static field, F_s, direct ionization occurs from level n if,

$$\max(\Delta E) > -2e\sqrt{F_s} - E_n(F_s), \tag{2.42}$$

When this condition holds, the total classical ionization probability from level n is,

$$\mathcal{P}_i^{cl} = \frac{\chi}{\pi}, \qquad \cos\chi = \frac{[-2e\sqrt{F_s} - E_n(F_s)]}{\max(\Delta E)}. \tag{2.43}$$

For smaller $\max(\Delta E)$ direct ionization is classically inaccessible and $\mathcal{P}_i^{cl} = 0$. The total classical ionization probability per unit time, P_i^{cl}, is obtained by dividing $\mathcal{P}_i^{cl}$ by the unperturbed period giving a classical estimate for the complex part of the energy for level n of,

$$\mathcal{E}_n^{cl} = \frac{P_i^{cl}\hbar}{2T(n)} = \frac{\Gamma_n}{2} = \frac{\omega_n(F_s)\hbar}{4\pi^2}\chi, \tag{2.44}$$

where Γ_n^{-1} is the lifetime[2] of level n. The authors note that for the high quantum numbers and moderately high fields used in current experiments, equation(2.44) provides a good approximation to the decay factors. However, as the field frequency increases, the number of photons needed for direct excitation to the continuum decreases and semiclassical effects become more important.

The semiclassical approximation is obtained by using WKB wave functions to evaluate the semiclassical transition amplitude, $S_i^{sc}(E, n)$, from a bound level, n, to the continuum state of energy E. The total ionization rate into all the continuum states is then,

$$\mathcal{P}_i^{sc} = \int_{-2e\sqrt{F_s}-E_n}^{\infty} \mathrm{d}E\,|S_n^{sc}|^2 \approx \sum_{k_{min}}^{\infty} J_k(\alpha), \tag{2.45}$$

$$k_{min} = 1 + \left\{\frac{-2e\sqrt{F_s} - E_n}{\Omega\hbar}\right\} \geq 1, \qquad \alpha = \frac{2.58F_0 n_0}{\Omega_0^{5/3}}, \tag{2.46}$$

[2]Further discussion regarding the lifetime of a quantum state in the presence of a static electric field is given at the beginning of chapter 4.

where $J_k(\alpha)$ is a Bessel function of order k, $\{x\}$ is the integer part of x and k_{min} is the minimum number of photons required for direct excitation from level n to the continuum. The final semiclassical expression for the complex part of the energy of level n is,

$$\mathcal{E}_n^{sc} = \frac{\omega(n, F_z)\hbar}{4\pi}\left(\frac{1}{2}(1 - J_0(\alpha)^2) - \sum_{k=1}^{k_{min}} J_k(\alpha)^2\right), \tag{2.47}$$

where the Bessel function addition theorem (see Abramowitz and Stegun 1965, equation (9.1.76)) is used to express the infinite sum as a finite sum. If $k_{min} = 1$, the sum is zero.

In the limit of one-photon ionization with weak fields, $k_{min} = 1$, $\alpha \ll 1$, the authors show that the semiclassical approximation reduces to the Fermi golden rule; in the opposite limit, $k_{min} \gg \alpha \gg 1$, the classical expression (2.44) is recovered. The authors also show that the semiclassical method naturally gives rise to structure in the continuum usually associated with 'above-threshold ionization' peaks in laser ionization of ground state atoms.

2.5 Low frequency theories

As mentioned briefly in section 2.3.2 above, using the hydrogenic basis states can, in some situations, be numerically very inefficient because a large number of basis states are needed to provide an adequate description of the system. In such cases, the one-dimensional Schrödinger equation can only be solved on large computers. One such situation arises when the frequency of the applied field is small compared with the unperturbed atomic frequency, $\Omega_0 \ll 1$. One method which has been used to study the quantal dynamics of an excited hydrogen atom in a low frequency field involves the introduction of an adiabatic basis which we now describe.

2.5.1 The adiabatic basis expansion

Motivated by the need for a numerically efficient one-dimensional quantal method which could be readily extended to include higher-dimensional systems but at the same time retaining the essential physics, Richards (1987) used an approximation, valid for low frequencies, to obtain a set of coupled equations which can be solved using a relatively small, time-dependent, basis. The aim of this approximation was not to obtain quantitative agreement with experimentally obtained ionization probabilities but to describe the qualitative features of the dynamics, in particular the dependence of ionization probabilities upon the various system parameters.

The starting point is the static limit of the one-dimensional system consisting of an electron in a Coulomb and periodic field,

$$H = \frac{1}{2\mu}p^2 - \frac{e^2}{x} - xf(t), \qquad x \geq 0. \tag{2.48}$$

For constant $f < 0$ the spectrum of H is discrete; for $f > 0$, the spectrum is continuous but for large initial quantum numbers, $n_0 \geq 30$, and for energies below the classical saddle,

$$E < E_s(f) = -2e\sqrt{f}, \qquad (f > 0), \tag{2.49}$$

the lifetimes of the resonant states are so long that this part of the spectrum may be considered discrete. Richards (1987) used these adiabatic states as a basis for an expansion of the time-dependent wave function, $|\Psi(t)\rangle$, in the limit where the field frequency is small with respect to the unperturbed energy splitting, that is when $\Omega_0 \ll 1$. The use of these adiabatic states introduces a significant part of the time dependence of the wave function into the basis, thus reducing the number of basis states required. When $f < 0$ then,

$$|\Psi(t)\rangle = \sum_k a_k(t)|k, f\rangle \exp\left(-\frac{\mathrm{i}}{\hbar}\int^t \mathrm{d}t'\, E_k(f(t'))\right), \qquad (f < 0), \tag{2.50}$$

where,

$$H_{AD}(f)|k, f\rangle = E_n(f)|k, f\rangle. \tag{2.51}$$

and H_{AD} is the adiabatic Hamiltonian introduced in section 1.4 of chapter 1 above: the adiabatic states, $|k, f\rangle$, are simply the eigenstates of $H_{AD}(f)$.

When $f > 0$ it is necessary to include the continuum and an expansion similar to that of equation (2.50) is used but with a complex energy term, $\mathcal{E}_n(t)$, included to take into account coupling with the continuum. Inserting this expansion into the time-dependent Schrödinger equation gives the following equation for the transition amplitudes:

$$\frac{\mathrm{d}a_n}{\mathrm{d}t} = -\frac{\mathcal{E}_n(t)}{\hbar}a_n - \dot{f}\sum_p \frac{\langle n, f|\partial H/\partial f|p, f\rangle}{E_n(f) - E_p(f)}a_p \exp\left(\frac{\mathrm{i}}{\hbar}\int_{t_0}^t \mathrm{d}t'\,[E_n(f) - E_p(f)]\right), \tag{2.52}$$

with $\mathcal{E}_n(t) = 0$ when $f < 0$. The major advantage of this representation is that the coupling is now proportional to $F\Omega$ rather than F.

After obtaining approximations to lifetimes, energy levels and matrix elements, equation (2.52) was integrated with initial quantum numbers $n_0 = 30, 60$ and various field strengths. The author was then able to obtain the relative variation of the ionization probability with the system parameters. The main result of these calculations was to show that the ionization probability has a resonant structure clearly associated with the $n_0 \to n_0 + 1$ transition, which is of course absent in the classical approximation.

In chapter 4, we consider the situation where the field frequency is sufficiently small for there to be negligible coupling between states; by using the adiabatic basis and

neglecting the coupling terms, we are able to integrate equation (2.52) to obtain ionization probabilities for the fully three-dimensional hydrogen atom. In chapter 5 we follow Richards *et al.* (1989b) and consider the weak coupling regime in which few states are significantly coupled together; in this case a reasonable approximation to the dynamics is provided by a two-state approximation.

2.5.2 Expansion on unperturbed basis states and Floquet theory

The dynamics of the hydrogen atom in a low-frequency field, $\Omega_0 \lesssim 0.4$, has also been studied by Blümel and Smilansky (1987, 1990) using the one-dimensional quantal model described in section 2.4.3. As mentioned at the end of that section, the major conclusion of this work is that there exist 'window' states, $n_W \sim n_0 F_0^{-1/4}$, such that all ionization occurs from states in the vicinity of n_W. By comparing calculated ionization probability curves with experimental results, Blümel and Smilansky advance a physical picture of 'ionization' as a two step process consisting of excitation from the initial state, $|n_0\rangle$, to states inside the 'window' which then decay with appreciable rates into the continuum. By using the Floquet approach, the authors propose two distinct mechanisms through which excitation to a window state, $|n_W\rangle$, can occur:

1. as the field strength increases the Floquet states, $|u_k\rangle$, broaden until one or more of them has an appreciable overlap with both $|n_0\rangle$ *and* $|n_W\rangle$: the authors claim that this mechanism is responsible for the onset of quantal ionization as a function of the field strength;

2. at certain specific values of the field frequency and strength, two quasi-energy levels, ϵ_μ and ϵ_ν, undergo an avoided crossing[3]; at the avoided crossing, linear combinations of $|u_\mu\rangle$ and $|u_\nu\rangle$ have appreciable overlaps with both $|n_0\rangle$ and $|n_W\rangle$ which leads to an enhanced transfer of probability between the initial state and the ionization window. This mechanism is linked by the authors to sub-ionization threshold structures observed in experimental data.

Breuer *et al.* (1989) have also used the Floquet approach, with a basis consisting solely of bound states, to study the excitation of the one-dimensional hydrogen atom in a low frequency field. Here, the non-monotonic behaviour observed in experimental ionization probabilities is again linked to the behaviour of the Floquet states in the vicinity of avoided crossings of the quasi-energy spectrum.

Note that the theoretical calculations of both Blümel and Smilansky (1987, 1990) and Breuer *et al.* (1989) were carried out using a basis of unperturbed hydrogenic states and

[3]At avoided crossings two quasi-energies become almost equal.

are thus, numerically, far less efficient than calculations carried out using the adiabatic basis discussed in the previous section.

2.6 High frequency theories

When the field frequency is very high, the usual method of solving the time dependent dipole gauge Schrödinger equation (2.3), see page 41, by expanding the wave function in terms of the unperturbed basis functions, as described in section 2.3.2 above, is numerically very inefficient: for $n \gg n_0$, where n_0 is the initial state, the matrix elements, $\langle n|z|m\rangle$, are large, showing a rapid increase with $(m+n)$ see equation (2.14), so that a large number of basis states are required to describe the dynamics in the vicinity of n_0 adequately. In such situations, it is more efficient to use the momentum gauge representation, for which the Hamiltonian is given by equation (1.26), page 19; for convenience we re-write this in the form,

$$H(z,p,t) = \frac{1}{2\mu}p^2 - \frac{e^2}{z} - \frac{F}{\mu\Omega}\lambda(t)\cos(\Omega t+\delta), \qquad z \geq 0. \tag{2.53}$$

On expanding the wave function in terms of the bound states of the unperturbed hydrogen atom

$$|\Psi\rangle = \sum_n b_n(t)|n\rangle \exp[-\mathrm{i}E_n t/\hbar)], \tag{2.54}$$

we obtain the following coupled equations for the amplitudes $b_n(t)$,

$$\mathrm{i}\hbar\frac{\mathrm{d}b_n}{\mathrm{d}t} = -\frac{F\lambda(t)}{\mu\Omega}\cos(\Omega t+\delta)\sum_m b_m\langle n|\hat{p}|m\rangle \exp[\mathrm{i}(E_n - E_m)t/\hbar], \tag{2.55}$$

where $\hat{p}$ is the momentum operator. We now see that for high frequencies these equations have two advantages over those in equation (2.12), page 43, obtained using unperturbed hydrogenic basis states with the dipole gauge Schrödinger equation (2.3):

1. the coupling terms are $O(\Omega^{-1})$ so that the overall coupling between states is reduced;

2. the matrix elements are, on using the Heisenberg correspondence principle,

$$\langle n|\hat{p}|m\rangle \simeq \frac{2\mathrm{i}\mu e^2}{(m+n)\hbar}J_s'(s) \simeq -\frac{\mathrm{i}\mu e^2}{(m+n)\hbar}\frac{0.822\mathrm{sgn}(s)}{|s|^{2/3}}, \quad s = m-n \neq 0, \tag{2.56}$$

which decay more slowly with increasing s than those of z, equation (2.14) above, but decrease with $(m+n)$ rather than increase.

2.6.1 Compensated energy representation

A similar approach was used by Leopold and Richards (1989) in their study of the quantal response of a one-dimensional Hydrogen atom to a high-frequency time-dependent field. By using the conventional dipole gauge Hamiltonian, equation (1.35) given on page 21 above, the authors noted that for high frequency fields a classical orbit comprises segments of ellipses upon which are superimposed small, high-frequency oscillations and conjectured that the quantal dynamics should be similar so that the high n-states should play a relatively unimportant role in the quantum dynamics. This unimportant oscillatory behaviour was removed by using the compensated energy representation of Leopold and Percival (1979). Classically, the rate of change of momentum is given by,

$$\dot{p} = -\frac{\partial H}{\partial z} = \frac{e^2}{z^2} - f(t), \tag{2.57}$$

so that, for large values of z, the rapid oscillations may be removed by introducing the compensated momentum p_c with,

$$p_c(t) = p(t) + a(t), \qquad a(t) = \int \mathrm{d}t\, f(t). \tag{2.58}$$

This new momentum defines the compensated Hamiltonian,

$$H_c = \frac{1}{2\mu} p_c^2 - \frac{e^2}{z}, \tag{2.59}$$

and as this is an approximate constant of the motion, Leopold and Richards (1989) suggested that a basis expansion using the eigenstates of H_c rather than those of H_0 would be numerically more efficient. It should be noted that the compensated Hamiltonian (2.59), is similar to Hamiltonian (2.53) above, but not the same as H_c is an approximation.

Diagonalization of H_c was carried out by introducing the 'compensated energy' states,

$$C_n(z,t) = \langle z|n\rangle \exp[-\mathrm{i}za(t)/\hbar], \quad \dot{a}(t) = f(t), \quad \text{where } H_c C_n(z,t) = E_n C_n(z,t). \tag{2.60}$$

Thus, on writing the wave function as,

$$\Psi(z,t) = \sum_n b_n(t) C_n(z,t) \exp(-\mathrm{i}E_n t/\hbar), \tag{2.61}$$

Leopold and Richards (1989) obtained equations of motion for the amplitudes, $b_n(t)$, similar to those given by equation (2.55) above.

Using this representation, Leopold and Richards (1989) were able to show that, for moderate fields which are slowly switched on and off, only the few quasi-resonant states, n_k, defined by,

$$E_{n_{k+1}} - E_{n_k} \simeq \Omega\hbar, \qquad -M \le k \le N, \tag{2.62}$$

for some suitable M, N, where n_0 labels the initial state (see also Jensen *et al.* 1988), are significantly populated and found that a basis comprising typically between ten and twenty compensated energy quasi-resonant states provided a remarkably good and efficient basis. For $\Omega_0 \gg 1$, many states lie between these quasi-resonant states and thus there is a drastic reduction in the effective density of states leading to differences between classical and quantal behaviour in this frequency region. Even for $n_0 \gg 1$ the differences between the high-frequency classical and quantal motion described by the dipole gauge Hamiltonian (1.35), see page 21, are quite dramatic. By considering a simple model, Leopold and Richards (1989) showed that for moderate values of the principle quantum number, n_0, the classical limit is only achieved for very strong fields for which the ionization times are short. On the other hand, for fixed field strengths and variable n_0, the authors suggest that the classical limit is reached only for $n_0 \gg 3\Omega_0^2$.

2.6.2 The Kramers-Henneberger transformation and stabilization

Other authors have also studied the high field frequency regime. Gavrila and Kaminski (1984) developed a non-perturbative theory to describe electron-atom interactions in intense, high-frequency, laser fields. Briefly, by assuming the laser field to be described by the electrodynamic potential,

$$\boldsymbol{A}(t) = \frac{cF}{e\Omega}\hat{\boldsymbol{e}}\cos\Omega t, \qquad \phi = 0 \tag{2.63}$$

where c is the speed of light and $\hat{\boldsymbol{e}}$ is the polarization vector, and applying the time-dependent Kramers-Henneberger transformation, $\boldsymbol{r} \rightarrow \boldsymbol{r} + \boldsymbol{a}(t)$ (see Kramers 1956, Henneberger 1968 and also equation (2.4), page 41 above) , the authors obtained the acceleration gauge Schrödinger equation,

$$\mathrm{i}\hbar\frac{\partial\Psi}{\partial t} = \left(-\frac{\hbar^2}{2\mu}\nabla^2 + V(\boldsymbol{r}+\boldsymbol{a}(t))\right)\Psi, \tag{2.64}$$

where

$$\boldsymbol{a}(t) = -\frac{e}{\mu c}\int_0^t \mathrm{d}t'\,\boldsymbol{A}(t') = \boldsymbol{a}_0\sin\Omega t, \qquad \boldsymbol{a}_0 = -\frac{F}{\mu\Omega^2}\hat{\boldsymbol{e}}, \tag{2.65}$$

which is the quantal equivalent of the acceleration gauge Hamiltonian (1.37), see page 22 of chapter 1.

At this point there are two problems regarding the Kramers-Henneberger transformation which should be highlighted: firstly, there is no advantage to be gained in employing the Kramers-Henneberger frame to study the one dimensional Coulomb potential; secondly, gauge transformations are only *exact* for constant field envelopes.

Using the Floquet *ansatz*, described in section 2.3.3 above, Gavrila and Kaminski (1984) cast equation (2.64) in the equivalent form of a system of coupled, time-independent differential equations for the Floquet components of the wave function, Ψ,

containing the quasi-energy E which is, in general, complex. By keeping $|a_0| \sim O(1)$ with respect to Ω, an iteration scheme was developed to solve these equations with successive steps containing increasing powers of Ω^{-1}. To the lowest order, the system reduces to the time-independent Schrödinger equation,

$$\left(-\frac{\hbar^2}{2\mu}\nabla^2 + V_0(a_0, r)\right)\Psi_0 = E\Psi_0, \tag{2.66}$$

for the Floquet component, Ψ_0, where,

$$V_0(a_0, r) = \frac{1}{\pi}\int_{-\pi}^{\pi} \mathrm{d}\phi\, V(r + a_0 \sin\phi), \tag{2.67}$$

is the mean or 'dressed' potential. This is the quantal equivalent of the classical mean-motion Hamiltonian described by equation (1.68), see page 29 of chapter 1, with $|a_0| = \alpha\lambda(t)$. To the next order in the iterative procedure, multi-photon processes become possible and an imaginary part is obtained for E together with expressions for the n-photon decay rates.

Using this prescription, Pont and Gavrila (1987) and Pont *et al.* (1988) calculated the levels of a ground-state hydrogen atom interacting with an intense, high-frequency, laser field. The time independence of the Schrödinger equation (2.66) lead the authors to predict that a high-frequency field would not ionize the system. This effect, whereby the ionization probability decreases whilst the field amplitude increases over some interval, the field frequency remaining fixed, has since been termed 'stabilization', although this term is not always clearly defined; the definition of stabilization often differs between papers and occasionally within a single paper.

The theoretical prediction of atomic stabilization has since been a source of great controversy. The described approach assumes that the atom can be exposed to a constant, high intensity, high-frequency field; however, high powered lasers are invariably pulsed so that the effect of the field switch must be taken into account. In addition, the experimental observability of such an effect has also been brought into question (see Bardsley and Comella 1989, Pont and Gavrila 1990) because the states are very short lived at intermediate field strengths and may not survive the build-up of intensity in a true laser field. Recently a vast amount of theoretical and computational effort has been directed towards resolving this controversy. Only a few of the major contributions are mentioned here.

In an attempt to resolve this controversy, several authors (see, for example, Bardsley and Comella 1989, Su *et al.* 1990, Burnett *et al.* 1991, Pont *et al.* 1991) have made time-dependent calculations in the Kramers-Henneberger frame using a simpler one-dimensional atomic model, the so-called 'soft-core' model, $V(x) = -1/\sqrt{1+x^2}$, with the field amplitude either being switched on gradually over a number of field periods

to some constant value, or switched on and off. These calculations provide qualitative confirmation of some of the predictions of stabilization theory in that either the ionization rate, after the initial switch on time, or the total ionization probability after the pulse, is an increasing function for 'small' field strengths but, at higher field amplitudes, reaches a maximum and then decreases.

Tang and Basile (1991) questioned theoretical calculations using a one dimensional model, noting that these may lack many of the fundamental properties of the real three dimensional atom. By numerically integrating both one- and three-dimensional time-dependent soft-core models in the momentum gauge and using a Gaussian envelope for the vector potential (Knight 1993) to switch the field on and off, the authors found that only for extremely short pulses did the system exhibit a significant probability of surviving at the end of the pulse. Further, it was shown that the one dimensional model exhibits a higher survival probability than the three-dimensional. These findings were confirmed by independent numerical studies of the three-dimensional atom by Kulander *et al.* (1991) and Horbatsch (1991).

Time-independent calculations using Floquet methods (see for instance Pont and Gavrila 1990, Dörr *et al.* 1991, Vos and Gavrila 1992) also show that, in some cases, for fixed field frequency, the ionization rate decreases with increasing field strength until some minimum is reached after which it increases. However, there is no reason to suppose that the mechanisms producing these time independent stabilization effects are the same as those which produce time-dependent stabilization.

One of the principal difficulties encountered in the study of these strong field effects has been the lack of good analytic approximations from which physical insight can be obtained. All the results quoted above have been produced by fairly intensive computations which provide little physical insight and, moreover, do not allow for a systematic investigation of parameter space. Indeed, for frequencies high enough to produce one-photon ionization, there appears to be no simple explanation for the observed phenomenon. At lower frequencies, where two photons are required to reach the continuum, recent experimental observations by Jones and Bucksbaum (1991) of highly stable Stark states of barium irradiated by an intense, short-pulse laser field suggest that this phenomenon is best explained in terms of the model presented by Burnett *et al.* (1991) where coupling to excited states is responsible for some of the behaviour. Whether this experimental observation of suppressed ionization is a true manifestation of atomic stabilization as understood from a purely theoretical point of view remains to be seen.

A quite different stabilization mechanism, valid for short pulses has been suggested by Richards (1993). By considering the one-dimensional hydrogen atom in the presence of a high-frequency field, where the interaction time is shorter than, or comparable to, the

classical orbital period and the frequency, Ω, is sufficiently high that one or two photon ionization is possible, the author is able to make analytic approximations to obtain the dependence of the ionization probability on the field strength. For the case where the field frequency is sufficiently high to produce one-photon ionization, the author finds that, after an initial rise, at relatively weak fields, the quantal ionization probability reaches a local maximum at that field for which the energy transfer, $\Omega\hbar$, becomes classically accessible. Thus, in this case, it is seen that stabilization can be interpreted as a 'rainbow' phenomenon, the low intensity side of the maximum being on the dark side of the rainbow with oscillations on the bright side.

From these few examples it seems plausible that there is no single mechanism for stabilization but that different mechanisms occur for different types of fields.

2.7 The quantal map

As has already been seen, solving the time-dependent Schrödinger equation is exceedingly time-consuming when there are many coupled states. For this reason any approximate scheme enabling the time-dependent Schrödinger equation to be integrated with relative ease is welcome. This section considers one such approximate scheme which is applicable for scaled frequencies $\Omega_0 > 2$.

The idea of using a map as an approximate quantal evolution operator for the one-dimensional hydrogen atom perturbed by a periodic field was first introduced by Casati *et al.* (1987a) (see also Casati *et al.* 1988 and Graham 1988 for details). The derivation of this map, the so-called quantum Kepler map, was based upon the construction a classical area-preserving map, which gave the change of the appropriate dynamical variables over one orbital period of the electron, followed by a direct quantization of this map. More recently, Graham and Höhnerbach (1990, 1991) have developed the Morse map using a similar technique in order to study periodically driven molecular vibrations in the Morse potential in both the classical description and its quantal counterpart. In this section, these two specific results are generalized to provide a quantal map applicable to a wide variety of one-dimensional systems (see also Dando and Richards 1990).

2.7.1 Derivation of the general quantal map

In this section the general quantal map is derived by obtaining an explicit quantization of the classical map, given by equations (1.91) and (1.92) on page 37. The connection between quantal operators and classical generating functions is described in detail by Miller (1974): in this case, since our derivation assumes the perturbation to be small, the pre-exponential factor can be ignored and the quantal operator further simplified by

noting that the generating function, equation (1.90) above, is simply the product of the evolution for the 'free' motion, $2\pi I$, and the 'kick', $\mathcal{F}\sin\psi$. Thus,

$$\hat{U} = \exp\left(-\frac{2\pi \mathrm{i} I(\hat{\mathcal{E}})}{\hbar}\right)\hat{P}\exp\left[\frac{\mathrm{i}}{2\hbar}\left(\mathcal{F}(\hat{r},\hat{\mathcal{E}})\sin\psi + \sin\psi\mathcal{F}(\hat{r},\hat{\mathcal{E}})\right)\right] \tag{2.68}$$

where $\hat{\mathcal{E}}$ is the operator conjugate to ψ, $\hat{\mathcal{E}} = -\mathrm{i}\hbar\partial/\partial\psi$, the product has been symmetrized and where $\hat{P}$ is a projection operator onto the bound states, that is those values of $\mathcal{E}$ for which the action $I(\mathcal{E})$ is defined, $\mathcal{E} < \mathcal{E}^S = E^S/\Omega$, where E^S is the separatrix energy. The eigenfunctions of $\hat{\mathcal{E}}$ are approximations to the quasi-resonant states, equation (2.62), in angle-action representation and the eigenvalues of $\hat{\mathcal{E}}$ are the integer labels of these states with the origin chosen, for convenience, to coincide with the initial state, $I_0 = n_0\hbar$. In order to avoid confusion capitals are used for these eigenvalues, so that

$$\mathcal{E}(K) = H_0(n_0\hbar)/\Omega + K\hbar, \quad K = -L, \cdots, M \tag{2.69}$$

where the $M+1$ is the smallest number of photons required for direct excitation from the initial state to the continuum and where L is some lowest level usually chosen to ensure convergence, see Leopold and Richards (1990). One must be careful to avoid confusion between the classical iterates $\mathcal{E}_k$ and the quantal eigenvalues $\mathcal{E}(K)$. Notice that the values of the action variable, I, corresponding to these eigenstates, that is the solutions of the equation $\mathcal{E}_0 + N\hbar = H_0(I)/\Omega$, are not necessarily integer multiples of $\hbar$, that is they do not coincide with the original states of H_0, except possibly at particular values of Ω. Moreover, many states of H_0 may lie between consecutive eigenstates of $\hat{U}$, see for example equation (2.62), page 56 above.

The eigenvalues of $\hat{\mathcal{E}}$ are neither bounded above nor below. This is clearly unphysical but, in most circumstances, unimportant. The higher states are removed by the projection operator, $\hat{P}$; the lower states cause no problem provided they remain insignificantly populated. For the quantal calculations presented in chapter 3, it is found that convergence is achieved before the value of L, equation (2.69), becomes unphysically large. It is also found that L can often be predicted using classical dynamics.

The operation of $\hat{U}$ on the wave function is the quantal equivalent of one iteration of the classical map (1.91) and (1.92). The most significant difference being that for the classical map it is possible to keep track of time along the individual orbits, whereas this is impossible for the quantal map. A quantal state is represented by a classical torus: classically, we can take each point on the torus and follow its time evolution; quantally, each state now lies on a different classical torus having a different fundamental frequency and hence the meaning of time is lost (see also Casati *et al.* 1990, Leopold and Richards 1990).

The Mth iteration of the initial state $|0\rangle$ is then $\hat{U}^M|0\rangle$ and the ionization probability is

$$P_i^q = 1 - \left|\hat{U}^M|0\rangle\right|^2. \tag{2.70}$$

A convenient way of using $\hat{U}$ is to construct its matrix representation in the eigenstates of $\hat{\mathcal{E}}$, that is

$$\langle\psi|N\rangle = \frac{1}{\sqrt{2\pi}}\exp(\mathrm{i}N\psi), \tag{2.71}$$

and an easy way of obtaining the matrix elements of the exponential of an operator is to find each column by solving the set of coupled differential equations

$$\frac{\mathrm{d}U_{NR}}{\mathrm{d}z} = \frac{\mathrm{i}}{2\hbar}\sum_P \langle N|\hat{\mathcal{F}}\sin\psi + \sin\psi\hat{\mathcal{F}}|P\rangle U_{PR}, \tag{2.72}$$

by integrating from $z = 0$ to $z = 1$ with initial conditions $U_{NR}(0) = \delta_{NR}$. Since the right hand side is non-zero only for $P = N \pm 1$ and since the basis of quasi-resonant states is relatively small, it is a quite trivial task to solve these equations. The resultant matrix is, however, unitary so ionization is missing; this is because coupling to the continuum has been removed by including only bound states in equation (2.72), the function $\mathcal{F}(r,\mathcal{E})$ being undefined in the continuum because the action I is defined only for bound motion. For the Morse potential Graham and Höhnerbach (1990, 1991) have overcome this problem by extending the classical unperturbed Hamiltonian, H_0, into the region of unbound motion, $\mathcal{E} > \mathcal{E}^S$, $-\infty < \psi < \infty$, and thus obtain an analytic continuation of $\mathcal{F}(r,\mathcal{E})$ into the continuum. Here, we adopt the semiclassical approximation of Leopold and Richards (1990), outlined in section 2.4.1 above, which mimics the classical ionization of equation (1.93), see page 38, and which we consider to be more realistic as the meaning of the analytic continuation of $\mathcal{F}(r,\mathcal{E})$ is unclear and, moreover, requires the Fourier coefficients to be analytic functions which restricts the class of potentials to those for which the coefficients can be obtained in closed form; the method outlined below is not limited by this constraint.

The basis of our approximation is the classical ionization probability per 'kick', $P_i^{cl}(\mathcal{E}_k)$ of equation (1.93). This can be incorporated into the differential equations (2.72) simply by adding a decay rate $-D(N)U_{NR}/\hbar$ to the right hand side, where $D(N) = P_i^{cl}(\mathcal{E}(N))/2$ with $\mathcal{E}(N)$ the 'energy' of the quasi-resonant level N. A uniform semiclassical approximation to this decay rate is given by equation (2.47) above, with $\alpha = \mathcal{F}(N)/\hbar$, $\mathcal{F}(N) = \mathcal{F}(r(N),\mathcal{E}(N))$.

Thus the final set of equations for the matrix elements U_{NR} are

$$\begin{aligned}
\hbar\frac{\mathrm{d}U_{MR}}{\mathrm{d}z} &= -D(M)U_{MR} + \frac{1}{4}\left(\mathcal{F}(M) + \mathcal{F}(M-1)\right)U_{M-1\,R} \\
\hbar\frac{\mathrm{d}U_{NR}}{\mathrm{d}z} &= -D(N)U_{NR}
\end{aligned} \tag{2.73}$$

$$+ \quad \frac{1}{4}\left([\mathcal{F}(N)+\mathcal{F}(N-1)]\,U_{N-1\,R}-[\mathcal{F}(N)+\mathcal{F}(N+1)]\,U_{N+1\,R}\right)$$

$$\hbar\frac{\mathrm{d}U_{-LR}}{\mathrm{d}z} \;=\; -D(-L)U_{-LR}-\frac{1}{4}\left(\mathcal{F}(-L)+\mathcal{F}(-L+1)\right)U_{-L+1\,R}.$$

These equations can be used to obtain the matrix elements of $\hat{U}$ and then the iterates of the wave function are obtained either by multiplication of the matrix or by finding its eigenvectors. Some results for the application of this map to the Morse oscillator are presented in the next chapter.

2.7.2 Dynamical Photonic Localization

The response of excited hydrogen atoms to a high-frequency microwave field, $\Omega_0 > 1$, has been a source of interest and controversy for both theoreticians and experimentalists since Casati *et al.* (1984), using a quantal one-dimensional model, observed a quantal limitation of classically chaotic motion and predicted that classical and quantal ionization mechanisms are different for a wide range of field strengths. The authors further conjectured that the quantum excitation process is determined by competition between a diffusive process that would be predicted classically and the 'localizing' effects of quantum interference, which tends to suppress the diffusive broadening of the wave function at a maximum spread, the so-called 'localization length'.

Using a curious mixture of classical diffusion theory and quantum mechanics, Casati and co-workers obtained an expression for the localization length in terms of the classical local diffusion coefficient and determined quantitative conditions for diffusive ionization to take place in the quantal system (see the review by Casati *et al.* 1987b for details). In particular, the authors pointed to a 'window' of field strength, determined by the classical chaotic border, F_{CH} defined by equation (1.65), page 28 of chapter 1, below which there is no diffusive motion, and the 'delocalization border', F_D of equation (2.77) below, which defines the critical value of the field strength above which the increase in the classical diffusion coefficient, and hence the localization length, triggers an unending escape of the wave function into the continuum despite the paralyzing effect of quantum interference. It was claimed that within this window of field strength the classical diffusive process is 'frozen' by quantum effects and a quasi-stationary distribution over the unperturbed levels is reached. This phenomenon has since been termed 'dynamical photonic localization'.

An unsatisfactory aspect of this theory was its inability to account for the form of the localized distribution, in particular the chain of equidistant multiphoton peaks in the tail of the steady-state distribution function observed in numerical simulations by Casati *et al.* (1984, 1987b). For this reason, the authors were unable to estimate quantal ionization rates using localization theory.

An alternative theoretical approach, suggested by Casati *et al.* (1987a, 1988), which confirmed the older results and, moreover, allowed for a gross description of the whole distribution, was based upon the construction of the quantum Kepler map. Thus a close connection was established between the hydrogen atom problem and the quantum-kicked-rotator[4], a simple quantal model where the numerically observed quantal limitation of classical chaotic excitation (see, for instance, Casati *et al.* 1979) had been formally related by Fishman *et al.* (1982) and Grempel *et al.* (1984) to Anderson localization, a theory originally developed to describe the effects of disorder on electronic wave functions in a spatially-periodic, one-dimensional, lattice.

A more direct link between the quantum Kepler map and the one-dimensional lattice equation, derived by Shepelyansky (1987), led Casati and co-workers to predict that the localized distribution should be exponential in the number of absorbed photons, the form of the steady-state distribution being 'borrowed' from the results obtained by Chirikov and Shepelyansky (1986) for the quantum-kicked-rotator, namely,

$$\bar{f}_N \simeq \frac{1}{2l_\phi}\left(1+\frac{2|N-N_0|}{l_\phi}\right)\exp\left[-\frac{2|N-N_0|}{l_\phi}\right], \tag{2.74}$$

where $N = [E/\Omega]$ labels the 'photonic state' and is equal to the number photons absorbed by the system, l_ϕ is the photonic localization length and $N_0 = -[n_0/2\Omega_0]$ labels the initial photonic state; here, $[x]$ denotes the integer part of x.. By assuming that $F > F_{CH}$, equation (1.65), so that the classical motion is chaotic and the distribution in action $f(n,\tau)$ obeys, approximately, a Fokker-Planck equation,

$$\frac{\partial f}{\partial t} = \frac{1}{2}\frac{\partial}{\partial n}\left(D_{cl}\frac{\partial f}{\partial n}\right), \qquad (\hbar = 1), \tag{2.75}$$

where D_{cl} is the classical diffusion rate, Casati *et al.* (1988) used a simple heuristic approach to show that, for the hydrogen problem, an estimate for the photonic localization length, l_ϕ, may be obtained by setting it equal to the constant diffusion coefficient of the classical Kepler map,

$$l_\phi \simeq 3.33\left(\frac{F_0}{n_0\Omega_0^{5/3}}\right)^2. \tag{2.76}$$

For $l_\phi \ll N_I$, where $N_I = [n_0/2\Omega_0]$ is the number of photons needed for ionisation from the initial state, the corresponding ionization rate is negligible so that homogeneous exponential localization is expected.

The decreasing tail in the distribution function, $\bar{f}_N$ of equation(2.74), for increasing N shows the 'exponential photonic localization' behaviour which can be expected for $l_\phi \ll N_I$. At higher field strengths, the localization length increases until, at $l_\phi \approx N_I$,

[4]Interest in the quantum-kicked-rotator was originally motivated by the known chaotic dynamics of the corresponding classical system, the standard map discussed in section 1.7 above.

the distribution extends far enough for there to be appreciable transport of action to the continuum and occurs for scaled fields with,

$$F_0 > F_D = \frac{\Omega_0^{7/6}}{\sqrt{6.6 n_0}}, \tag{2.77}$$

where F_D is the 'delocalization border' (see Casati *et al.* 1988).

To account for the experimental cut-off [5], n_c, Brivio *et al.* (1988) defined the ionization probability to be the total probability above the level $n = n_c$ (see also Casati *et al.* 1990). An estimate for the 10% threshold field was then obtained by evaluating the integral[6],

$$\int_{R_c}^{\infty} dR \bar{f}_R = 0.1 \qquad R_c = \frac{1}{2 n_0^2 \Omega} \left(1 - \frac{n_0^2}{n_c^2}\right). \tag{2.78}$$

where $R = |N - N_0|$. It is this border that is often referred to as being the closest to the experimental threshold for 10% 'ionization' and was used to analyze the experimental results of Bayfield *et al.* (1989) and Galvez *et al.* (1988).

At this point, it should be noted that localization theory only describes some 'average' behaviour of the system when $\Omega_0 > 2$ and $l_\phi \ll N_I$. It does not encompass the physics producing the experimentally observed resonances nor does it take into account the effect of the field envelope or the total interaction time: the final-state distribution is given with the field envelope at its maximum value. Nor has it yet treated the case of a static field superimposed with the microwave field so crucial to the quasi-one-dimensional experiments of Bayfield *et al.* (1989) where the good agreement obtained between theoretical predictions and experimental results was claimed to validate the theory of photonic localization. Perhaps more surprisingly, and also somewhat paradoxically for a theory used to understand the ionization process, the continuum, or more significantly the interaction time, does not feature in this theory.

That there is indeed a range of field strengths for which the quantal probabilities are localized but for which the classical system is chaotic is now accepted as theoretically correct. Furthermore, recent experimental results of Galvez *et al.* (1988) and Bayfield *et al.* (1989) confirm that for $\Omega_0 > 2$ the experimental ionization threshold is higher than that predicted by classical dynamics, although no detailed measurements of the excited-state population have yet been made so there is, as yet, no direct experimental evidence for quantal localization. However, the more precise predictions of Casati *et al.* (1988) regarding the underlying dynamics giving rise to the observed behaviour, namely the existence of the delocalization border, F_D, equation (2.77), below which the quantal

[5] Experimentally, 'ionization' often consists of true transport to the continuum *plus* excitation to final n-states above some cut-off n-value, n_c, determined by static electric fields used in the apparatus for particle deflection and detection, see Koch (1990) for details.

[6] An analytic estimate for the integral (2.78) is given by Chirikov (1989).

probability is exponentially localized and above which there is 'diffusive' ionization, are still a source of some controversy.

Leopold and Richards (1989) studied the response of a one-dimensional hydrogen atom to a high-frequency microwave field using the compensated energy representation, described in section 2.6.1 above. For weak fields they found exponential decay of the quantal probabilities, as predicted by Casati *et al.* (1988), but that the range of fields for which this behaviour occurred was not given by the condition $F_0 < F_D$, equation (2.77). Instead, they conjectured that the existence of an approximate selection rule (see Richards *et al.* 1989a), which drastically reduces the density of states, was the main reason for disagreement between classical and quantal dynamics at high-frequencies; the relevant parameter was found to be the reduced action given by,

$$\mathcal{A} = \frac{n_0 F_0}{\Omega_0^{5/3}}. \tag{2.79}$$

For $\mathcal{A} < 1$ transitions between adjacent quasi-resonant states are classically forbidden and the theoretical quantal probabilities were found to be smaller than the classical. For $\mathcal{A} > 1$, it was found that the wave function was spread over many quasi-resonant states but that this was not a sufficient condition for classical dynamics to provide a good description of the motion, thus contradicting the prediction of Casati *et al.* (1988) that for $F_0 > F_D$ the quantal and classical excitation processes will be similar.

A further study by Jensen *et al.* (1989b) found the quantal distributions to be very different to those predicted by localization theory. The authors developed an alternative theory which provided both an estimate of the width of the quantum distribution and a necessary condition for diffusive ionization. Again, the relevant parameter was found to be the reduced action $\mathcal{A}$ of equation (2.79). For $\mathcal{A} < 1$, a two-level approach was used to show that each peak in the distribution is dominated by a *single* photon-state. As $\mathcal{A}$ increases, the height of each succeeding photon peak increases and the two-level model breaks down; the narrow photon peaks are all strongly coupled and the quantum picture is well described by the few quasi-resonant states (see Richards *et al.* 1989a). For $\mathcal{A} \gg 2$, neither the two-level nor the truncated basis theories could be applied. Instead, Jensen and co-workers used the high density of coupled states to write down a set of master equations (see, for example, van Kampen 1981) to describe the transport of probability between the photon resonances, an approach which neglects all interference effects. These master equations were then approximated by a classical Fokker-Planck equation from which the authors concluded that the diffusive description is only valid when $\mathcal{A} \gg 2$. This gives a new criterion for the onset of quantal 'diffusive' ionization:

$$F_0 > F_R \simeq 2.4\Omega_0^{5/3}/n_0. \tag{2.80}$$

Thus, Jensen *et al.* (1989b) predict that dynamical photonic localization theory is only applicable for $F_R/F_D \simeq 0.23 N_I^{1/2} \gg 1$; that is when the number of photon peaks between the initial state and the continuum is large, $N_I \gg 19$. Thus, it would appear that localization theory is only valid at much larger quantum numbers than are accessible in current experiments.

Koch (1990) has made a very careful study of the Galvez *et al.* (1988) and the Bayfield *et al.* (1989) experimental data. For $n_c = 89$ localization theory roughly reproduces the mean behaviour of the experimental data of Galvez *et al.* (1988) but for $n_c = 175$ significantly overestimates the 10% 'ionization' threshold. Both n-cutoff values satisfy the Casati *et al.* (1990) criteria for the applicability of localization theory, $l_\phi \ll N_I$. The author concludes that the photonic localization theory does not quantitatively reproduce experimental data for all conditions so far investigated and that the distribution over final bound atomic states $n \gg n_0$ is not the one 'borrowed' from the kicked-rotator model, given by equation (2.74) above. These conclusions differ from those presented by Bayfield *et al.* (1989).

Whilst localization theory does not agree quantitatively with all experimental and numerical data, it should be recognized that its prediction of the quantal suppression effect, now verified by two independent experiments (Galvez *et al.* 1988 and Bayfield *et al.* 1989) and many calculations (see, for example, Casati *et al.* 1988, Leopold and Richards 1989 and Jensen *et al.* 1989b, Jensen *et al.* 1991), was crucial in drawing both experimental and theoretical attention to the region of high-scaled field frequencies. The elegant route along which Casati and co-workers developed the theory should be also be acknowledged. However, a clear implication is that the present version of photonic localization theory does not correctly describe transport to the final, bound n-levels that are far from the initial level, n_0.

In the next chapter we use the classical and quantal maps, derived above in sections 1.7 and 2.7 respectively, to study the classical and quantal motion of the Morse oscillator in the presence of a periodic, high-frequency, field. We provide further numerical evidence that localization theory, as described in this section, does not describe correctly the quantal evolution of this system.

Chapter 3

The Morse oscillator in a high-frequency field

3.1 Introduction

In this chapter we present results of numerical calculations carried out in the region of high field frequency, $\Omega \gtrsim \omega$. As a model for our discussion we consider the driven Morse oscillator, described by Hamiltonian (3.1) below.

The analytic properties of the Morse potential mean that its response to a high frequency periodic field is distinctly different to that of the one-dimensional Coulomb potential. In particular, we see that the Fourier components of the classical motion, see equation (3.7) below, and hence the critical field strength required for the onset of chaotic ionization, *increase* with increasing field frequency. This means that at very high frequencies, the system may ionize via the mean motion mechanisms discussed in chapter 1, section 1.6 above. By numerically integrating Hamilton's equations of motion, and by iterating the area-preserving map derived in section 1.7 above, we are able to delineate ranges of field frequency, for both suddenly and adiabatically switched fields, for which the classical system ionizes through regular orbits. In addition, by comparing ionization probabilities obtained by iterating both the classical and quantal maps we are able to delineate circumstances where the classical and quantal dynamics agree.

The remainder of this chapter is organized as follows. In section 3.2 we apply the classical theory, described in section 1.5 and 1.6 above, to the driven Morse oscillator. First, we use the resonance overlap condition, equation (1.65) on page 28 above, to obtain a theoretical expression for the critical field strength required for the onset of chaotic ionisation. Next we consider the mean-motion dynamics and obtain expressions for the threshold fields required for the onset of both sudden and adiabatic mean-motion ionisation. By comparing these threshold fields we are able to predict the boundaries of three different regions of field frequency for which the classical ionization mechanisms will be different.

In section 3.3 the numerical methods used to obtain the classical and ionization

probabilities presented in sections 3.5 to 3.7 are described. The classical probabilities are obtained either by numerical integration of Hamilton's equations or by iterating the classical area-preserving maps derived in section 1.7 above; in section 3.4 we discuss the accuracy of these classical maps. The quantal probabilities are obtained by iterating the quantal map described in section 2.7 above.

In sections 3.5 to 3.7 we compare the numerically calculated classical and quantal threshold fields and ionization probabilities with the theoretical values obtained in section 3.2 for each of the three ranges of field frequency delineated in section 3.2. Finally, in section 3.8 we present some conclusions.

3.2 Application to the Morse oscillator

In this section we obtain expressions for the critical field strengths required for classical ionization to take place by each of the mechanisms described in chapter 1 for the specific case of the periodically driven Morse oscillator for which the Hamiltonian corresponding to equation (1.27), see page 19, is given by,

$$H_m = \frac{1}{2\mu}p^2 + V_0(1-\exp[-aq])^2 + p\frac{F}{\mu\Omega}\lambda(t)\cos(\Omega t+\delta). \tag{3.1}$$

The separatrix energy, V_0, and the length scale or 'Morse parameter', a, can be related by introducing the variable $\mathcal{A}_s = \sqrt{2\mu V_0}/a$, which is the action of the separatrix, that is the area under the separatrix divided by 2π. The number of bound states the well can support is the integer part of $\mathcal{A}_s/\hbar$. We also introduce the following dimensionless variables; the scaled energy and field,

$$\varepsilon = \frac{E}{V_0} = \frac{2\mu E}{a^2\mathcal{A}_s^2}, \qquad \beta = \frac{F}{aV_0} = \frac{2\mu F}{a^3\mathcal{A}_s^2}, \tag{3.2}$$

where for bound motion, $0 < \varepsilon < 1$. In terms of these scaled variables, the angle-action variables, (θ, I), of the unperturbed system are,

$$I(\varepsilon) = \mathcal{A}_s(1-\sqrt{1-\varepsilon}), \qquad \exp[-aq(\theta)] = \frac{1-\varepsilon}{1-\sqrt{\varepsilon}\cos\theta}, \tag{3.3}$$

and the unperturbed frequency is,

$$\omega(I) = \frac{\partial H_0}{\partial I} = \frac{a^2}{\mu}(\mathcal{A}_s - I) = \frac{a^2\mathcal{A}_s}{\mu}\sqrt{1-\varepsilon}. \tag{3.4}$$

Henceforth, it will be convenient to describe the initial state of the system using the initial scaled action and energy,

$$\mathcal{A}_0 = I_0/\mathcal{A}_s, \qquad \varepsilon_0 = \mathcal{A}_0(2-\mathcal{A}_0), \tag{3.5}$$

respectively, where I_0 is the initial value of the action variable.

3.2.1 The resonance overlap condition

For a general one-dimensional system, the critical field strength, F_{CH}, for the onset of chaotic motion is given by equation (1.65) on page 28. In order to obtain an expression for F_{CH} for the system under consideration here, we need to calculate the Fourier coefficients; from equation (1.56), page 25, these are,

$$V_k(I) = \frac{1}{2\pi\mu\Omega}\int_{-\pi}^{\pi} \mathrm{d}\theta\, p(\theta, I)e^{\mathrm{i}k\theta} = \frac{\mathrm{i}\sqrt{\epsilon}\omega}{2\pi a\Omega}\int_{-\pi}^{\pi} \mathrm{d}\theta\, \frac{\sin\theta \sin k\theta}{1-\sqrt{\epsilon}\cos\theta}, \tag{3.6}$$

$$V_k(I_0) = \frac{\mathrm{i}}{ak}\left(\frac{\mathcal{A}_0}{2-\mathcal{A}_0}\right)^{k/2}. \tag{3.7}$$

In terms of the scaled variables, equation (3.2), and on substituting equation (3.7) into the expression (1.65) we obtain the scaled critical field strength for the onset of chaotic motion in the periodically driven Morse oscillator:

$$\beta_{CH} = \frac{2\mu F_{CH}}{a^3\mathcal{A}_s^2} = \frac{(1-\mathcal{A}_0)^2}{8r}\left(\frac{2-\mathcal{A}_0}{\mathcal{A}_0}\right)^{r/2}, \qquad r = \frac{\mu\Omega}{\mathcal{A}_s a^2(1-\mathcal{A}_0)}, \tag{3.8}$$

r being the ratio of the applied frequency to the unperturbed frequency. For field strengths, $\beta > \beta_{CH}$, we expect a significant proportion of the motion to be chaotic. However, the analytic properties of the Morse potential mean that the Fourier coefficients, V_r of equation (3.7), decrease rapidly with increasing field frequency with a corresponding increase in the magnitude of β_{CH}, see the full curve of figure 3.1 on page 73: for sufficiently high frequency fields, this means that the classical system may ionize via the mean-motion mechanisms which were discussed in section 1.6 above.

3.2.2 Mean-motion

In section 1.6 above we considered two simple ionization mechanisms which are valid when the mean-motion Hamiltonian (1.68), see page 29, provides an accurate description of the dynamics, one which occurs for sudden field switches and the other for adiabatic switches. Here, we obtain analytic expressions for the critical field strengths required for the onset of both sudden and adiabatic mean motion ionization in the driven Morse oscillator. These enable us to predict the field frequencies at which ionization by the mean-motion mechanisms will predominate.

For the Morse potential, the mean-motion Hamiltonian, see equation (1.68), page 29, becomes

$$\overline{H} = \frac{1}{2\mu}p_2^2 + V_0\{1 - 2I_0(a\alpha)\exp(-aq_2) + I_0(2a\alpha)\exp(-2aq_2)\}, \tag{3.9}$$

where $I_0(x)$ is a modified Bessel function of zero order, not to be confused with the initial action, and $\alpha = F\lambda(t)/\mu\Omega^2$.

For the mean Hamiltonian (3.9), the action of the separatrix is,

$$\overline{\mathcal{A}}_s = \frac{\sqrt{2\mu V_0}}{a}\frac{I_0(a\alpha)}{\sqrt{I_0(2a\alpha)}} = \mathcal{A}_s\frac{I_0(a\alpha)}{\sqrt{I_0(2a\alpha)}}, \tag{3.10}$$

which is a decreasing function of α. Quantally, this means that the number of bound states of the mean Hamiltonian, that is the integer part of $\overline{\mathcal{A}}_s/\hbar$, is also a decreasing function of α. The mean-motion angle-action variables $(\overline{\theta}, \overline{I})$ are,

$$\overline{I}(\overline{\varepsilon}) = \overline{\mathcal{A}}_s - \mathcal{A}_s\sqrt{1-\overline{\varepsilon}}, \tag{3.11}$$

$$\exp[-aq_2(\overline{\theta})] = \frac{1-\overline{\varepsilon}}{I_0(a\alpha) - \sqrt{I_0(a\alpha)^2 - I_0(2a\alpha)(1-\overline{\varepsilon})\cos\overline{\theta}}}, \tag{3.12}$$

where $\overline{\varepsilon} = \overline{E}/V_0$ is the scaled mean-motion energy with $0 < \overline{\varepsilon} \leq 1$ for bound motion, and the mean-motion frequency is,

$$\overline{\omega}(\overline{I}) = \frac{\partial\overline{H}}{\partial\overline{I}} = \frac{a^2}{\mu}(\overline{\mathcal{A}}_s - \overline{I}) = \frac{a^2}{\mu}\mathcal{A}_s\sqrt{1-\overline{\varepsilon}}. \tag{3.13}$$

Firstly, we consider a sudden field switch.

Sudden field switch

For suddenly switched fields, the condition for ionization to occur is given by equation (1.77), see page 31 above,

$$-2p_1\frac{F}{\Omega}\cos\delta + \left(\frac{F}{\Omega}\right)^2\cos^2\delta \simeq 2\mu(\overline{E}^S - E_d). \tag{3.14}$$

In terms of the variables defined in this section, the following expression for the value of p_1 at which the initial torus intersects the separatrix of $\overline{H}$ is obtained:

$$p_1 = a\mathcal{A}_s\left(\frac{\beta^2\cos^2\delta - 4r^2(1-\mathcal{A}_0)^4}{4r(1-\mathcal{A}_0)\beta\cos\delta}\right), \tag{3.15}$$

where $\Omega = \mathcal{A}_s r a^2(1-\mathcal{A}_0)/\mu$ and $F = a^3\mathcal{A}_s^2\beta/2\mu$. In appendix B, equation (3.15) is used to calculate the ionization probability, P_{SUD}, as a function of β, $\mathcal{A}_0$ and r averaged over the field phase, δ. However, by setting $\delta = 0$ and $p_1 = \sqrt{2\mu E} = a\mathcal{A}_s\sqrt{\mathcal{A}_0(2-\mathcal{A}_0)}$, an approximation to the critical field strength required for the onset ionization by the sudden mean-motion mechanism, that is the field strength at which $q_1 = 0$ is the value at which the initial torus intersects the separatrix of $\overline{H}$, can be obtained

$$\beta_{SUD} = \frac{2r(1-\mathcal{A}_0)^3}{1+\sqrt{\mathcal{A}_0(2-\mathcal{A}_0)}}, \tag{3.16}$$

which, for high frequencies, is considerably lower than fields needed for chaotic ionization. This can be seen in figure 3.1 on page 73 where we show the theoretical curves given by

β_{CH} and β_{SUD}, equations (3.8) and (3.16) respectively, for $\mathcal{A}_0 = 0.5$ and $1 \leq r \leq 12$. This type of ionization occurs only because the field is switched on suddenly and the averaging approximation is valid. Similarly, an approximate threshold field for 50% ionization can be obtained by setting $\delta = 0$ and obtaining the value of β in equation (3.15), at which $p_1 = 0$ is the value at which the initial torus intersects the separatrix of $\overline{H}$. This is,

$$\beta_{50} = 2r(1 - \mathcal{A}_0)^2. \tag{3.17}$$

Adiabatic field switch

When the field is switched on adiabatically, the action, $\overline{I}$, equation (3.11), of the mean-motion Hamiltonian (3.9), is an approximate constant of the motion and therefore remains close to its initial value, I_0. The area under the separatrix, $A(\alpha)$, of $\overline{H}$, is

$$A(\alpha) = 2\pi\overline{\mathcal{A}}_s = 2\pi\mathcal{A}_s\left(\frac{I_0(a\alpha)}{\sqrt{I_0(2a\alpha)}}\right), \qquad \alpha = \frac{F\lambda(t)}{\mu\Omega^2}, \tag{3.18}$$

which is a decreasing function of α; note that in equation (3.18), $I_0(x)$ is again a modified Bessel function of zero order. Thus, the critical value of the field strength for adiabatic ionization to occur is given by the value of α at which the area under the separatrix becomes equal to the area under the initial phase curve,

$$\mathcal{A}_0 = \frac{I_0(a\alpha_{AD})}{\sqrt{I_0(2a\alpha_{AD})}}, \qquad \beta_{AD} = 2ar^2(1 - \mathcal{A}_0)^2\alpha_{AD}. \tag{3.19}$$

For $a\alpha_{AD} > 1$, that is $\mathcal{A}_0 < 0.8$, this critical field strength is given to within 5% by

$$\beta_{AD} = \frac{2r^2}{\pi\mathcal{A}_0^4}(1 - \mathcal{A}_0)^2\left(1 + \frac{3\pi}{32}\mathcal{A}_0^4\right)^4, \tag{3.20}$$

on using the asymptotic form given by Abramowitz and Stegun (1965, equation 9.7.1). For high frequencies, β_{AD} is considerably lower than the fields needed for chaotic ionization, β_{CH}. This is shown in figure 3.2, see page 74, where the theoretical curves given by β_{CH} and β_{AD}, equations (3.8) and (3.18) respectively, are depicted for $\mathcal{A}_0 = 0.5$ and $1 \leq r \leq 12$.

3.2.3 Predicted behaviour

By comparing the theoretical threshold fields obtained in sections 3.2.1 and 3.2.2, that is β_{CH}, β_{SUD} and β_{AD} of equations (3.8), (3.16) and (3.20) respectively, we are able to make some predictions about the theoretical classical ionization process at different values of the field frequency. We consider two ways of switching the field on; suddenly and adiabatically.

For a suddenly switched field, we use the values for β_{CH} and β_{SUD}, equations (3.8) and (3.16) respectively, to estimate the values of Ω at which we expect ionization to occur through chaotic orbits and through the mean-motion mechanism. In figure 3.1 the theoretical curves given by β_{CH} (full curve) and β_{SUD} (broken curve) for $\mathcal{A}_0 = 0.5$ and $1 \leq r \leq 14$ are shown. For $\Omega \lesssim 12\omega$, $\beta_{CH} < \beta_{SUD}$ which suggests that classical

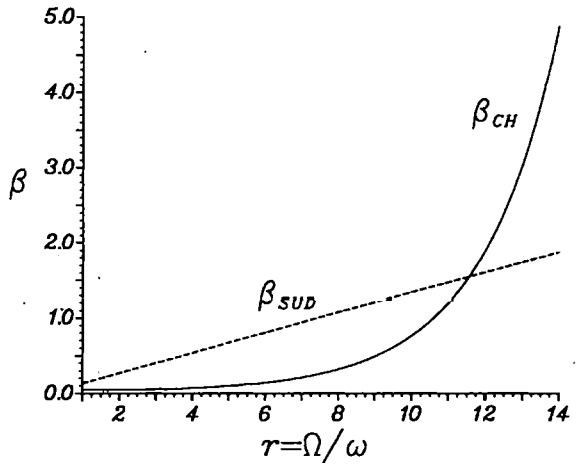

Figure 3.1 Graph showing the dependence of β_{CH} (equation (3.8)), full curve, and β_{SUD} (equation (3.16)), broken curve, with field frequency for $\mathcal{A}_0 = 0.5$.

ionization will occur predominantly through chaotic orbits: for $\Omega > 12\omega$, the onset of classical ionization is expected to occur through the mean-motion mechanism. Indeed, at $\Omega = 5\omega$, $\beta_{CH} \simeq 0.1$ whereas $\beta_{SUD} \simeq 0.67$; for $\Omega = 15\omega$, $\beta_{CH} \simeq 7.89$ and $\beta_{SUD} \simeq 2.01$. By comparing the expressions for β_{CH} and β_{SUD}, given by equations (3.8) and (3.16) respectively, we see that as $\mathcal{A}_0$ increases the value of r at which $\beta_{CH} = \beta_{SUD}$ also increases.

For an adiabatic switch, we use the values for β_{CH} and β_{AD}, equations (3.8) and (3.20) respectively, to delineate the values of the field frequency for which the onset of classical ionization will be due to a significant proportion of the orbits becoming chaotic and those for which the mean-motion mechanism will dominate. In figure 3.2 we show the theoretical curves given by β_{CH} (full curve) and β_{AD} (broken curve) for $\mathcal{A}_0 = 0.5$ and $1 \leq r \leq 27$. For $\Omega \lesssim 24\omega$ the threshold field strength for chaotic motion, β_{CH}, is much less than that required for mean-motion ionization, β_{AD}. For example, when $\Omega = 15\omega$, $\beta_{AD} \simeq 620$ and $\beta_{CH} \simeq 8$. As Ω increases, β_{CH} increases exponentially until, at $\Omega \simeq 25\omega$, $\beta_{AD} = \beta_{CH}$. For $\Omega > 25\omega$, we expect no chaotic ionization and, indeed, at $\Omega = 30\omega$, $\beta_{AD} \simeq 2480$ compared with $\beta_{CH} \simeq 14\,950$. By comparing the expressions for β_{CH} and β_{AD}, given by equations (3.8) and (3.20) respectively, we see that as $\mathcal{A}_0$ increases the value of r at which $\beta_{CH} = \beta_{AD}$ also increases.

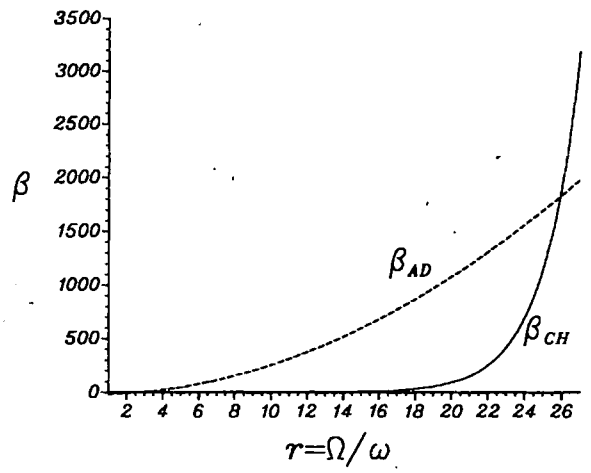

Figure 3.2 Graph showing the dependence of β_{CH} (equation (3.8)), full curve, and β_{AD} (equation (3.20)), broken curve, with field frequency for $\mathcal{A}_0 = 0.5$.

Thus, for field frequencies, $\omega < \Omega \lesssim 12\omega$, we expect all classical ionization to be due to chaotic trajectories for both sudden and adiabatic switches. In the frequency range, $12\omega < \Omega < 24\omega$, we expect all classical ionization to occur through chaotic orbits when the field switch is adiabatic but for suddenly switched fields we expect classical ionization to occur through both the chaotic and mean-motion mechanisms. For very high field frequencies, $\Omega > 24\omega$, we expect all classical ionization to occur through the sudden and adiabatic mean-motion mechanisms. With this in mind, we base our discussion of sections 3.5, 3.6 and 3.7 upon these three different regions of field frequency and in each region we consider the effect of using both sudden and adiabatic switches. In the next section we describe the numerical methods used to obtain the classical and quantal ionization probabilities.

3.3 Numerical methods

In this section, the numerical methods used to obtain the classical and quantal ionization probabilities presented in the following sections of this chapter are described. We restrict our discussion to the case $\mathcal{A}_0 = I_0/\mathcal{A}_s = 0.5$; for fixed frequency ratio, r, and scaled field, β, the classical results are independent of $\mathcal{A}_s$. Further results obtained by varying $\mathcal{A}_0$ show the classical behaviour of this case to be typical. We note that the parameters V_0, a and μ may be varied by changing the value of $\mathcal{A}_s$. In all calculations and the remainder of this chapter we set $a = \mu = \hbar = 1$, so that the integer part of $\mathcal{A}_s$ is then the number of bound states of the quantal system.

3.3.1 Classical calculations

The classical results given in this chapter were obtained either by numerically integrating the equations of motion in the acceleration gauge or by iterating the classical maps described in section 1.7 above; the accuracy of the maps is discussed in section 3.4 below.

The classical ionization probabilities were calculated using the Monte-Carlo method as described by Leopold and Percival (1979). We have assumed that the system was initially on an unperturbed torus of the dipole gauge Hamiltonian, with action given by $\mathcal{A}_0$, and that the initial value of the angle variable, θ_0, was uniformly distributed in $(0, 2\pi)$, but we used a stratified sample of either 200 or 1000 orbits. Each orbit was integrated for a time, T_m, or until the orbit satisfied the ionization conditions detailed below.

The oscillating field was switched on over M_a field periods or a time $T_a = 2\pi M_a/\Omega$, and lasted for M_m field periods or a time T_m. The field envelope function $\lambda(t)$ was of the form,

$$\lambda(t) = \begin{cases} 0, & t \leq 0,\ t \geq T_m, \\ \sin^2 \frac{\pi t}{2T_a}, & 0 \leq t \leq T_a, \\ 1, & T_a \leq t \leq T_m - T_a, \\ \sin^2 \frac{\pi}{2T_a}(T_m - t), & T_m - T_a \leq t \leq T_m, \end{cases} \tag{3.21}$$

and we have assumed that all results are independent of the form of $\lambda(t)$ for T_a sufficiently large. The value of T_m was chosen carefully; sufficiently large to allow time for any chaotic orbits to ionize, but small enough to keep computation time and numerical errors to a minimum. We consider two ways of switching the field on, suddenly ($T_a = 0$) or adiabatically ($T_a \gg 0$).

The main source of error is statistical, although this could be improved by integrating more orbits. If n_i orbits from a sample of N_s ionize, then there is a 66% chance that the ionization probability lies in the range

$$P_i \pm \sqrt{P_i(1 - P_i)/N_s}, \qquad P_i = n_i/N_s, \tag{3.22}$$

and a 95% chance of it lying in twice this width. For $P_i \simeq 0.5$, the statistical uncertainty is about ± 0.035 or $\pm 7\%$ when 200 orbits are used.

Numerical integration of Hamilton's equations

The numerical solution of the equations of motion was carried out using a seventh-order Runge-Kutta-Fehlberg method (see for example Ledermann 1981 page 326). Ionization was said to have occurred once $q(t) > q_{max}$ and $\varepsilon > 1.0$. The value chosen for q_{max} depended upon both the value of Ω and the field switch-on time, T_a. For field frequencies,

$\Omega < 20\omega$, surface-of-section plots (see for example Lichtenberg and Lieberman 1983), suggested a value of $q_{max} = 5$ should be used for all values of T_a, but for $\Omega > 20\omega$, these suggested that $q_{max} = 5$ for $T_a = 0$ and $q_{max} = 15$ for $T_a > 0$ should be used.

Iteration of the classical maps

The area-preserving classical map derived in section 1.7 above,

$$\mathcal{E}_{k+1} = \mathcal{E}_k + \mathcal{F}(r, \mathcal{E}_{k+1}) \cos\psi_k, \quad r = \Omega/\omega(\mathcal{E}_{k+1}), \tag{3.23}$$

$$\psi_{k+1} = \psi_k + \frac{2\pi\Omega}{\omega(\mathcal{E}_{k+1})} - \frac{d\mathcal{F}}{d\mathcal{E}_{k+1}} \sin\psi_k, \tag{3.24}$$

was iterated with

$$\mathcal{F}(r, \mathcal{E}) = \frac{\pi\beta\mathcal{A}_s^2}{\Omega} \left(\frac{\mathcal{A}_s - \sqrt{\mathcal{A}_s^2 - 2\Omega\mathcal{E}}}{\mathcal{A}_s - \sqrt{\mathcal{A}_s^2 - 2\Omega\mathcal{E}}} \right)^{r/2}, \quad r(\mathcal{E}) = \frac{\Omega}{\sqrt{\mathcal{A}_s^2 - 2\Omega\mathcal{E}}}, \tag{3.25}$$

which agrees with the expression used by Graham and Höhnerbach (1990, 1991) in their derivation of the Morse map. For the mean-motion map, $\mathcal{F}(r, \mathcal{E})$ was replaced with its mean-motion counterpart, $\overline{\mathcal{F}}(r, \overline{\mathcal{E}})$:

$$\overline{\mathcal{F}}(r, \overline{\mathcal{E}}) = 2\pi \left[2\overline{\mathcal{A}}_s \frac{I_1(\alpha)}{I_0(\alpha)} - \frac{I_1(2\alpha)}{I_0(2\alpha)} (\Omega + \overline{\mathcal{A}}_s) \right] \left[\frac{\overline{\mathcal{A}}_s - \sqrt{\mathcal{A}_s^2 - 2\Omega\overline{\mathcal{E}}}}{\overline{\mathcal{A}}_s - \sqrt{\mathcal{A}_s^2 - 2\Omega\overline{\mathcal{E}}}} \right]^{r(\overline{\mathcal{E}})/2}, \tag{3.26}$$

where $r(\overline{\mathcal{E}}) = \Omega/\sqrt{\mathcal{A}_s^2 - 2\Omega\overline{\mathcal{E}}}$ and $I_0(x)$ and $I_1(x)$ are modified Bessel functions of zero- and first-order respectively. Note that for small values of α, $\overline{\mathcal{F}}(r, \overline{\mathcal{E}})$ reduces to the expression (3.25) for $\mathcal{F}(r, \mathcal{E})$.

For both maps, the implicit equation (3.23) for $\mathcal{E}_{k+1}$ was solved by supplying the initial estimate $\mathcal{E}_{k+1} = \mathcal{E}_k$ to the NAG routine C05AJF. The modified Bessel functions, $I_0(x)$ and $I_1(x)$ were calculated using the NAG routines S18AEF and S18AFF respectively. Ionization was said to have occurred once $\mathcal{E} > \mathcal{A}_s/2\Omega$. For the reasons given in chapter 1, we only consider the effect of a sudden switch when iterating the classical maps.

3.3.2 Quantal calculations

The quantal results were obtained using the map described in section 2.7 with

$$\mathcal{F}(N) = \frac{\pi\beta\mathcal{A}_s^2}{\Omega} \left[\frac{\mathcal{A}_s - \sqrt{\mathcal{A}_s^2 - 2\mathcal{E}(N)\Omega}}{\mathcal{A}_s + \sqrt{\mathcal{A}_s^2 - 2\mathcal{E}(N)\Omega}} \right]^{\Omega/2\sqrt{\mathcal{A}_s^2 - 2\mathcal{E}(N)\Omega}}, \tag{3.27}$$

$$\simeq \frac{\pi\beta\mathcal{A}_s}{r(1 - \mathcal{A}_0)} \exp(-r(1 - \mathcal{A}_0)), \quad 2\mathcal{E}(N)\Omega \simeq \mathcal{A}_s^2,$$

with $\Omega = r\mathcal{A}_s(1 - \mathcal{A}_0)$ and

$$\mathcal{E}(0) = \frac{\mathcal{A}_s\mathcal{A}_0(2 - \mathcal{A}_0)}{2r(1 - \mathcal{A}_0)}, \qquad \mathcal{E}(N) = \mathcal{E}(0) + N\hbar. \tag{3.28}$$

Notice that if $2\mathcal{E}(N)\Omega \simeq \mathcal{A}_s^2$, that is for states near the separatrix, then $\mathcal{F}(N)$ is practically independent of N and the map is then similar to the quantum Kepler map with $\mathcal{F}(N)$ replacing k (see Leopold and Richards 1990, equation 9) but with a different phase which, because the number of states is finite, remains bound in contradistinction to the quantum Kepler map.

The quantal operator, $\hat{U}$ of equation (2.68), page 61, was constructed by solving the coupled differential equations (2.72), see page 62, using the NAG routine D02CAF. The iterates of the wave function were then obtained by finding the eigenvectors and values of $\hat{U}$ using the NAG routines F02AKF and F04ADF respectively. As with the classical maps, we only consider the effect of a sudden switch when using the quantal map.

3.4 Accuracy of the classical map

In this section the ionization probabilities obtained by iterating the classical maps derived in section 1.7, one given by equations (3.23) and (3.24), the other based upon the approximate mean-motion Hamiltonian of equation (1.96), are compared with those obtained by exact numerical integration of Hamilton's equations. All numerical integration was carried out as described in section 3.3 above.

For field frequencies $\Omega < 12\omega$, figure 3.1 suggests that all classical ionization takes place through chaotic orbits and that the mean-motion mechanism plays little or no part in the dynamics. Thus, it might be expected that probabilities obtained by iterating the classical maps should be in good agreement with those obtained by numerical integration. In table 3.1 we show probabilities at $\Omega = 5\omega$ with varying field strength; all three probabilities agree remarkably well, even at high fields where $P_i \simeq 0.9$. Other comparisons, see for instance figure 3.8, suggest that the map is accurate down to $\Omega = 2\omega$.

Table 3.1 Comparison of classical ionization probabilities obtained by integrating Hamilton's equations, P_i^{cl}, using the area-preserving map, P_i^{map}, and the mean-motion map, P_i^{mn}, for $\Omega = 5\omega$, a sudden field switch and 1500 field oscillations. In each case, 1000 orbits were used with $\mathcal{A}_s = 100$ and $\mathcal{A}_0 = 0.5$.

β	0.05	0.055	0.06	0.07	0.08	0.09	0.10	0.12	0.14	0.16
P_i^{cl}	0.06	0.11	0.23	0.41	0.56	0.62	0.73	0.86	0.91	0.94
P_i^{map}	0.09	0.15	0.27	0.40	0.52	0.54	0.73	0.77	0.87	0.93
P_i^{mn}	0.09	0.12	0.23	0.39	0.52	0.62	0.85	0.94	0.95	0.97

For field frequencies, $\Omega > 12\omega$, figure 3.1 suggests that the mean motion Hamiltonian of equation (3.9) is the correct approximation. Table 3.2 shows similar results to table 3.1

but at the higher frequency, $\Omega = 15\omega$. Here it can be seen that for $P_i < 0.3$ the mean-map is a far better approximation than the map based upon the unperturbed motion, but for $P_i > 0.5$ there is little difference between the two. Other comparisons, see for instance

Table 3.2 Comparison of classical ionization probabilities obtained by integrating Hamilton's equations, P_i^{cl}, using the area-preserving map, P_i^{map}, and the mean-motion map, P_i^{mn}, for $\Omega = 15\omega$, a sudden field switch and 2500 field oscillations. In each case, 200 orbits were used with $\mathcal{A}_s = 100$ and $\mathcal{A}_0 = 0.5$.

β	2.0	3.0	4.0	5.0	10.0	20.0	30.0	40.0	50.0	60.0
P_i^{cl}	0.02	0.10	0.19	0.27	0.55	0.78	0.90	0.93	0.95	0.97
P_i^{map}	0.00	0.00	0.00	0.00	0.25	0.79	0.89	0.96	0.97	0.99
P_i^{mn}	0.03	0.13	0.19	0.27	0.54	0.76	0.87	0.91	0.95	0.94

figure 3.13 on page 88, also show the mean map to be a far better approximation at higher field frequencies.

The agreement shown here between the ionization probabilities obtained by iterating the maps and numerically integrating Hamilton's equations is not unexpected; Casati *et al.* (1988) have shown that the classical Kepler map mimics the exact dynamics fairly accurately whilst Graham and Höhnerbach (1990, 1991) compare results obtained by iterating the classical Morse map for the same parameter values studied in exact classical calculations by Walker and Preston (1977) and find good quantitative agreement.

From these comparisons we conclude that the classical map mimics the exact dynamics remarkably well, but that at high field frequencies and weak fields it is necessary to use the mean motion Hamiltonian to define the unperturbed motion. This suggests that a quantal map based upon these classical maps should also be a good approximation to the exact quantal solution.

3.5 Classically chaotic region

For field frequencies, $\Omega < 12\omega$, all classical ionisation takes place through chaotic orbits. Figure 3.3 shows the variation in P_i with scaled field strength, β, when $\Omega = 5\omega$, for which $\beta_{CH} \simeq 0.097$, and various values of switch-time, M_a, and field phase, δ: all ionization probabilities were calculated by exact numerical of the equations of motion as described in section 3.3 above. The similarities between the four curves suggest that the ionization probabilities, P_i, are almost independent of the field phase and not very sensitive to the field switch-on time. Additionally, the relatively low value of β required for ionization

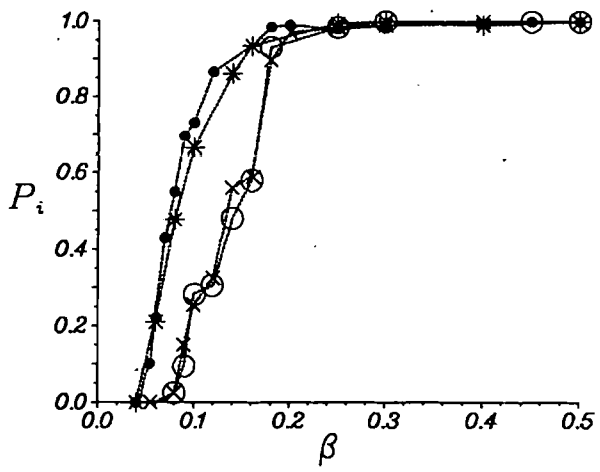

Figure 3.3 Graph showing the dependence of the classical ionization probability, P_i, with β for varying field switch-on times and field phase for $\Omega = 5\omega$, $\mathcal{A}_0 = 0.5$ and $\mathcal{A}_s = 100$. The sudden switch, $M_a = 0$ with $M_m = 1500$, are shown by full circles ($\delta = 0$) and asterisks ($\delta = \pi/2$). The adiabatic switch, $M_a = 500$ with $M_m = 2500$, are shown by crosses ($\delta = 0$), and open circles ($\delta = \pi/2$). All ionization probabilities were obtained by numerical integration of Hamilton's equations.

compared with $\beta_{SUD} \simeq 0.67$ means that all classical ionization takes place through chaotic orbits.

In figure 3.4 we compare various ionization probabilities, obtained by iterating the classical and quantal maps, as functions of β for $\Omega = 5\omega$ and the long time of 1500 field periods. The quantum mechanical probabilities shown in figure 3.4 are complicated to describe as these now depend upon $\mathcal{A}_s$. We see that for $\mathcal{A}_s = 100$ the classical (crosses) and quantal (full curve) are quite different, with the quantal probabilities approaching the classical probabilities with increasing $\mathcal{A}_s$. The reason for this is quite simple. The approximate number of quasi-resonant levels is $N_{QR} \simeq \mathcal{A}_s(1 - \mathcal{A}_0)/2r$, so that for $\mathcal{A}_s = 100$, $N_{QR} \simeq 5$, and this is a very small number of states. As N_{QR}, that is $\mathcal{A}_s$, increases we expect the quantal probabilities to approach the classical probabilities (which are independent of $\mathcal{A}_s$ for fixed $\mathcal{A}_0$).

There are two main differences between the classical and quantal probabilities shown in figure 3.4. First, we note that even at $\mathcal{A}_s = 1500$ there are many oscillations in the quantal probabilities, though it is not known whether these are real or a consequence of using a map — for the quantum Kepler map, it has been shown (Leopold and Richards 1990) that similar oscillations are a property of the map and the mechanism producing these is also present in the Morse map. Second, the quantal probabilities are smaller than the classical probabilities: it is not immediately clear whether this is a real difference in the bound-state dynamics or due to the different manner in which ionization is treated

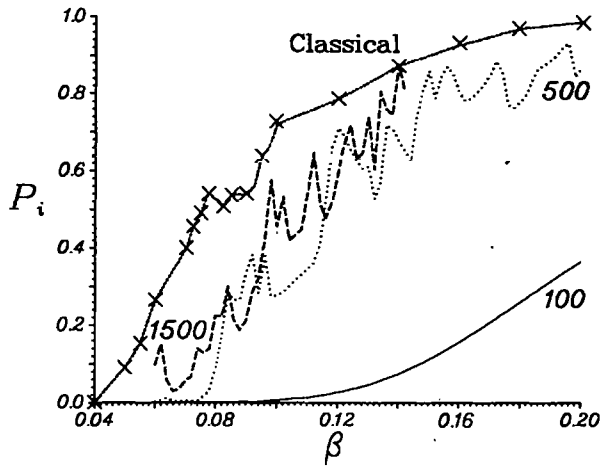

Figure 3.4 Graph showing the dependence of the ionization probability with β for $\Omega = 5\omega$ and $\mathcal{A}_0 = 0.5$. Probabilities shown by the crosses were obtained from the classical map using 1000 orbits with $\mathcal{A}_s = 100$; those shown by the full, dotted and broken curves from the quantal map with $\mathcal{A}_s = 100$, 500 and 1500 respectively. A sudden switch was used with $M_m = 1500$.

in the classical and quantal systems. On doubling the quantal decay rates probabilities are obtained which differ insignificantly from those in figure 3.4, which suggests that the bound-state dynamics is responsible for the differences.

The results shown in figure 3.4, for $\mathcal{A}_s = 500$ and 1500 ($N_{QR} = 25$ and 75 respectively) suggest that for long interaction times the classical limit is well beyond physically realistic values of $\mathcal{A}_s$. In figure 3.5 we show quantal probabilities for $\mathcal{A}_s = 3000$ ($N_{QR} = 150$) and $\mathcal{A}_s = 5000$ ($N_{QR} = 250$). At these high values of $\mathcal{A}_s$ there are fewer oscillations in the quantal probabilities and, for $\mathcal{A}_s = 5000$, the agreement between classical and quantal probabilities is quite good. In particular, the local minimum observed in the classical probabilities at $\beta \simeq 0.08$ is reproduced in both sets of quantal calculations. For $\beta \gtrsim 0.12$, the quantal probabilities for $\mathcal{A}_s = 5000$ lie systematically above the classical. This is due to the value of $-L$, equation (2.69), being too small which leads to an unphysical loss of probability, or 'ionization', from the bottom of the basis. This also accounts for the apparent agreement between the classical and quantal probabilities for $\mathcal{A}_s = 3000$ in this region. These results suggest that the quantal map is correct in the classical limit, albeit for unphysically large values of $\mathcal{A}_s$, and justifies the use of the semiclassical decay rates discussed in chapter 2, section 2.4.4 above.

In figure 3.6 we compare the classical and quantal bound-state populations in the case $\Omega = 5\omega$, $\beta = 0.08$, $\mathcal{A}_s = 1500$ after 1500 field periods for which $P_i^{map} = 0.5$: superimposed on this is the classical ionization probability per iteration, given by-equation (1.93) on page 38, as a function of N, which is seen to be significant only for $N \gtrsim 64$. There are two points to notice in this comparison. First, the overall agreement between classical

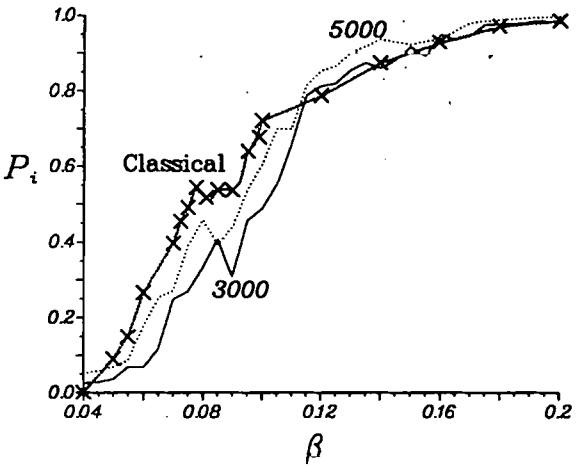

Figure 3.5 As for figure 3.4 with quantal probabilities for $\mathcal{A}_s = 3000$ and 5000 shown by the full and dotted curves respectively. Probabilities shown by the crosses were obtained from the classical map using 1000 orbits.

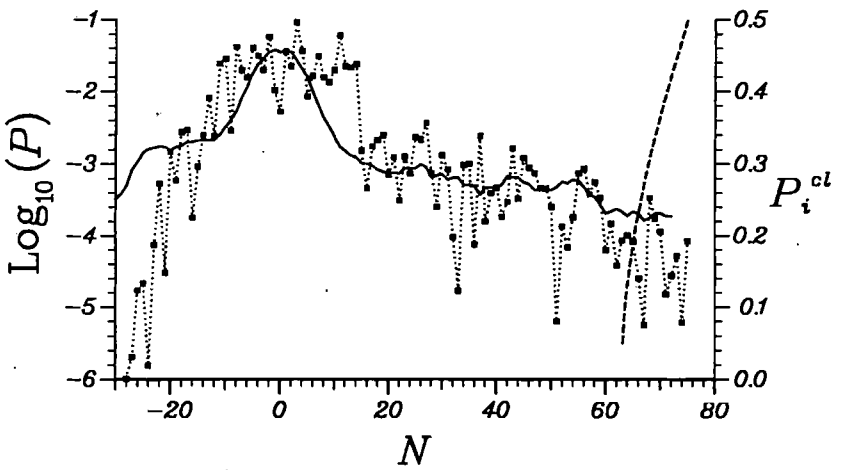

Figure 3.6 Comparison of classical (full curve) and quantal (full circles) bound state populations for the case $\Omega = 5\omega$, $\beta = 0.08$, $\mathcal{A}_0 = 0.5$ and $\mathcal{A}_s = 1500$ for a sudden switch with $M_m = 1500$. The broken curve represents the classical ionization probability, P_i^{cl} of equation (1.93). The classical probabilities were obtained from the map using 10000 orbits.

and quantal probabilities is quite good; the large plateau centred on $N = 0$ is due to the classical resonance island, though it is unclear why the quantal plateau should extend to larger values of N. The lower edge of this island, at $N \simeq -10$, marks the lower edge of both classical and quantal probabilities. Indeed we have found that the lower limit of the quantal basis can be estimated well by classical dynamics: as r passes through integer values, the value of L, see equation (2.69), page 61, changes dramatically according as the resonance island is above or below the initial state. The probabilities for $10 < N < 50$, that is the classically chaotic region, are in broad agreement, with the quantal results oscillating about the less structured classical probabilities. However, for $N > 50$ the quantal probabilities are generally significantly smaller and it is precisely from this region that direct-ionization occurs, as can be seen from the broken curve. This explains why the classical and quantal ionization probabilities differ in this model.

As the interaction time decreases, the field producing a given ionization probability increases so direct ionization occurs from a wider band of states. In figure 3.7 we show the equivalent of figure 3.4, but for only 100 field periods, and it is seen that at $\mathcal{A}_s = 1000$ there is good agreement between the classical and quantal probabilities, that the field producing 10% ionization is considerably larger and that the quantal probabilities have less structure.

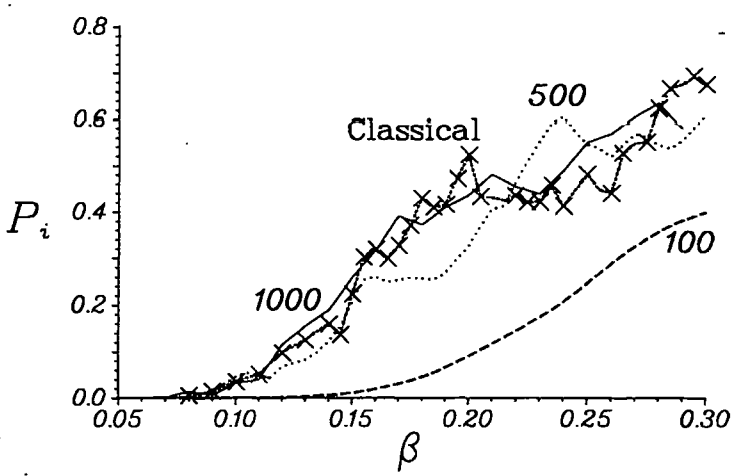

Figure 3.7 Graph showing the dependence of the ionization probability with β for $\Omega = 5\omega$ and $\mathcal{A}_0 = 0.5$. Probabilities shown by the crosses were obtained from the classical map using 1000 orbits with $\mathcal{A}_s = 100$; those shown by the broken, dotted and full curves from the quantal map with $\mathcal{A}_s = 100$, 500 and 1000 respectively. A sudden switch was used with $M_m = 100$.

Our numerical calculations show that the classical probabilities are insensitive to small variations in the applied frequency. The quantal probabilities of the map, however, show a fairly erratic dependence upon Ω: the reasons for this are given in Leopold and Richards (1990), and Casati *et al.* (1990) suggest that these fluctuations ought to be aver

aged over to obtain the correct result. The effect of such fluctuations is seen in figure 3.8 where we show the threshold fields required to produce 10% ionization as a function of $r = \Omega/\omega$. The classical results are shown by the crosses (numerical integration) and the broken curve (map); these threshold fields both follow the chaotic boundary, β_{CH}, of equation (3.8), but are always lower. The data shown in figures 3.1 and 3.2 suggests that in the frequency range $2\omega \leq \Omega \leq 8\omega$ classical ionization is dominated by chaotic dynamics. In fact, the corresponding values of β_{SUD} range from 0.27 at $\Omega = 2\omega$ to 1.07

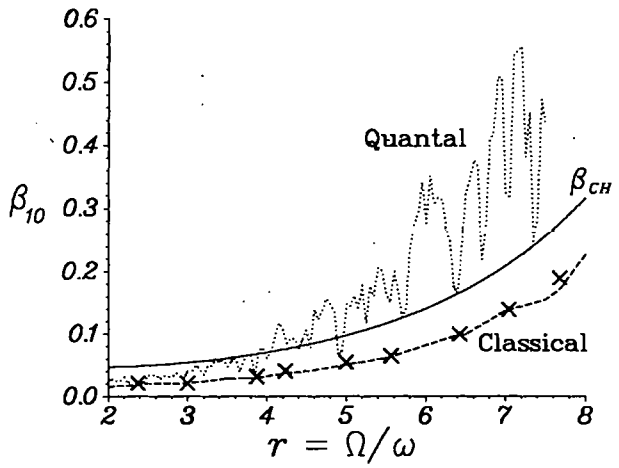

Figure 3.8 Graph showing the variation in the threshold fields, β_{10}, required to produce 10% ionization with Ω and $A_0 = 0.5$. The threshold fields shown by the crosses were obtained by numerical integration of Hamilton's equations, those by the broken curve from the classical map and those by the dotted curve from the quantal map with $\mathcal{A}_s = 100$. A sudden switch was used with $M_m = 1500$ and $\delta = 0$. The full curve represents the theoretical values β_{CH}, equation (3.8).

at $\Omega = 8\omega$, higher than any value needed for chaotic ionization.

The quantal threshold fields are quite different: they are close to the classical threshold fields for $\Omega < 3\omega$ but for larger frequencies they show very large fluctuations, which are not very surprising because the number of quasi resonant states is small; for instance at $\Omega = 6\omega$, $N_{QR} = 4$, so we should expect resonances and little resemblance to the classical behaviour. It is a matter for future calculations to determine whether or not these fluctuations are real or an artifact of the map: the work of Leopold and Richards (1990, 1991) suggests that more exact calculations will remove at least some of these fluctuations.

3.5.1 Localization

The localization theory of Casati *et al.* (1987b, 1988) has been used to obtain estimates of the field strengths required for the onset of quantal ionization (see also section 2.7.2 above). In this section we apply this theory to the periodically driven Morse oscilla-

tor and compare the theoretical field strength for the onset of quantal ionization, β_L, equation (3.30) below, with those obtained by iterating the quantal map.

The estimate of the field strength required for the onset of quantal ionization is obtained (see Casati *et al.* 1987b, Casati *et al.* 1988) by setting the localization length, l_ϕ, equal, approximately, to the classical diffusion constant, and then equating $l_\phi/2$ to $\max(N)$. For the driven Morse oscillator, l_ϕ is given by,

$$l_\phi \simeq \frac{1}{2}\mathcal{F}(N)^2 \simeq \frac{\pi^2\beta^2\mathcal{A}_s^2}{2r^2(1-\mathcal{A}_0)^2}\exp[-2r(1-\mathcal{A}_0)]; \tag{3.29}$$

see also Graham and Höhnerbach (1990, 1991): note that for the parameters of figure 3.6, $l_\phi \simeq (109\beta)^2$. On setting $l_\phi/2 = \max(N) = \mathcal{A}_s(1-\mathcal{A}_0)/2r$, we obtain an approximate quantal ionization threshold, in the same spirit as Casati *et al.* (1987b, 1988),

$$\beta_L = \left(\frac{2r(1-\mathcal{A}_0)^3}{\mathcal{A}_s}\right)^{\frac{1}{2}} \frac{\exp[r(1-\mathcal{A}_0)]}{\pi}, \qquad \beta > \beta_{CH}. \tag{3.30}$$

In most cases we have considered the exponential distribution given by equation (2.74) on page 64, that is $P(N) = l_\phi^{-1}\exp(-2N/l_\phi)$, is a rather poor fit to that produced by the Morse-map, and deteriorates as the interaction time increases. Despite this poor fit, the localization threshold, β_L, sometimes agrees reasonably well with our numerical thresholds, β_N, and sometimes does not; for example at $\mathcal{A}_0 = 0.5$, $\Omega = 5\omega$ if $\mathcal{A}_s = 500$ then $\beta_L = 0.19$ and $\beta_N = 0.14$, but for $\mathcal{A}_s = 100$, $\beta_L = 0.43$ and $\beta_N = 0.21$. This should be contrasted with the agreement obtained by Bayfield *et al.* (1989) for the hydrogen atom. Both of these comparisons are for short interaction times with $M_m = 100$ field periods: for longer times there is no agreement. We therefore conclude that the localization theory, as presented by Casati *et al.* (1987b, 1988) provides a poor description of the quantum dynamics in the high frequency regime.

3.6 Intermediate frequency region

At intermediate frequencies, $12\omega < \Omega < 20\omega$, the classical dynamics is more complicated. Here, ionization probabilities are more dependent upon the field switch-on time and, for sudden switches, the field phase. When an adiabatic switch is used, all classical ionization is through chaotic orbits; for a sudden switch there is evidence, see figures 3.10 and 3.11, that ionization can occur through both chaotic and mean-motion mechanisms.

3.6.1 Adiabatically switched fields

For an adiabatic switch, with $M_a = 500$ and $M_m = 3500$, the comparison between β_{CH} and the numerically calculated classical threshold fields required for 10% and 50%

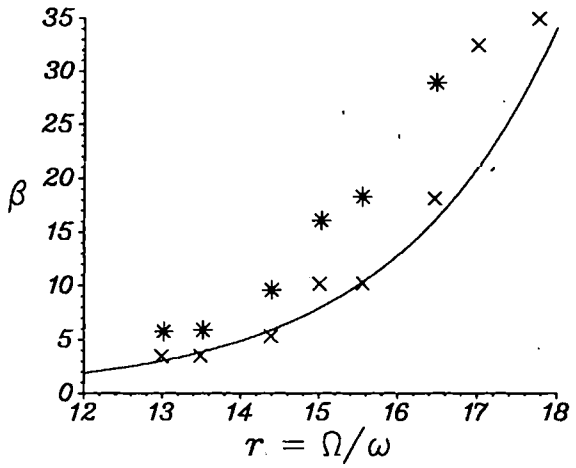

Figure 3.9 Values of β required for 10% (crosses) and 50% (asterisks) ionization for $12\omega \leq \Omega \leq 20\Omega$ with $\mathcal{A}_0 = 0.5$ and $\mathcal{A}_s = 100$. The field was switched on adiabatically with $M_a = 500$, $M_m = 1500$ and $\delta = 0$. The full curve represents the theoretical values β_{CH}, equation (3.8).

ionization for $12\omega \leq \Omega < 18\omega$ and $\delta = 0$ is shown in figure 3.9. Again, there is good agreement between the numerical thresholds and β_{CH}, suggesting that chaotic ionization is prevalent in these cases, a view reinforced by considering the relevant values of β_{AD}, which range from 396 at $\Omega = 12\omega$ to 890 at $\Omega = 18\omega$.

3.6.2 Suddenly switched fields

For suddenly switched fields, with intermediate frequencies, some orbits ionise because their initial tori cross the mean-motion separatrix, whilst others become unstable and ionize chaotically. This behaviour is shown by the surface-of-section plot, figure 3.10. Here $\Omega = 15\omega$ and $\beta = 11.5$; we show one orbit, with $\theta_0 = 1.25\pi$, ionizing via separatrix-crossing whilst a second orbit, with $\theta_0 = 0.69\pi$ ionizes chaotically. The same behaviour, again at $\Omega = 15\omega$, is seen by examining the results shown in figure 3.11. The probabilities indicated by the crosses were obtained by integrating 200 orbits with 20 different values of θ_0 and 10 different values of δ, all chosen as described above. The full curve shows the theoretical ionization probability, P_{SUD}, as calculated in equation (B.6) of appendix B. For $\beta < \beta_{CH} \simeq 8$, there is good agreement between the theoretical and numerically calculated probabilities which suggests that here there ought to be agreement between classical and quantal ionization probabilities. In this region the classical map of equation (3.23) and (3.24) underestimates the ionization probability, see table 3.2, but the map based on the mean-motion, equation (1.96), provides a more accurate description.

As β increases, some classical chaotic ionization occurs and hence, for a given β, the

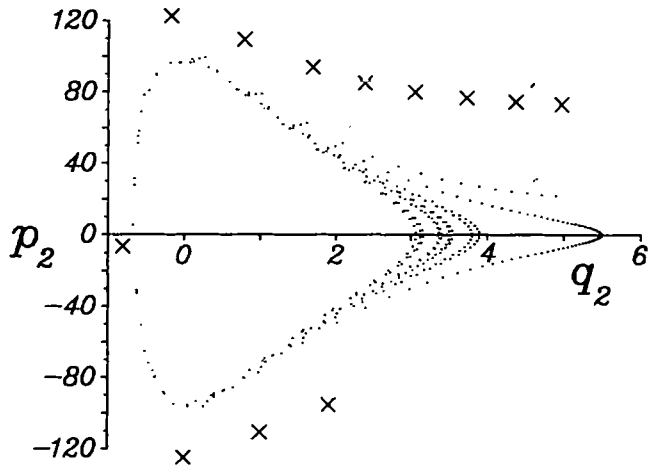

Figure 3.10 Surface-of-section plot for $\Omega = 15\omega$, $\mathcal{A}_0 = 0.5$, $\mathcal{A}_s = 100$, $\beta = 11.5$ and a sudden switch with $\delta = 0$. The orbit with initial angle variable $\theta_0 = 1.25\pi$, shown by the crosses, ionizes through the mean-motion mechanism; that with $\theta_0 = 0.69\pi$, shown by the dots, ionizes chaotically.

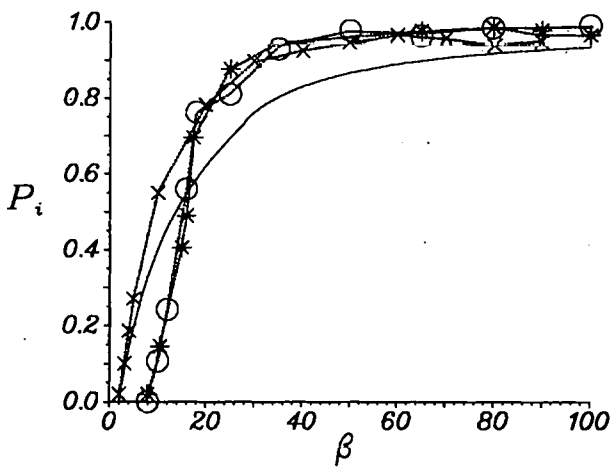

Figure 3.11 Graph showing the dependence of the classical ionization probability with β for $\Omega = 15\omega$, $\mathcal{A}_0 = 0.5$ and $\mathcal{A}_s = 100$ with various values of M_a, M_m and δ. The asterisks and open circles represent the ionization probabilities obtained using an adiabatic switch with $M_a = 500$ and $M_m = 3500$ for $\delta = 0$ and $\delta = \pi/2$ respectively. The crosses represent the ionization probabilities obtained using a sudden switch with $M_m = 2500$, averaged over the field phase. The full curve represents the theoretical probabilities, P_{SUD}, as calculated in appendix B.

computed ionization probability is higher than that given by the theoretical curve. In figure 3.11 we also show the computed classical ionization probabilities for an adiabatic switch of $M_a = 500$ with $\delta = 0$ and $\delta = \pi/2$: both require higher values of β for 10% ionization than a suddenly switched field, because all classical ionization occurs through chaotic orbits when the field is adiabatically switched.

In this case we should not expect classical and quantal ionization probabilities to agree except when $\mathcal{A}_s$ is huge, simply because the selection rule picking out the quasi-resonant states dramatically decreases the density of states. The classical dynamics does, however, suggest that the mean-motion Hamiltonian is the correct zero-order approximation to the dynamics and this ought to be taken into account in any approximate quantal description, especially as it leads to a reduction of the number of bound states.

3.7 Mean-motion region

At very high frequencies, $\Omega \geq 20\omega$, numerical calculations suggest that the mean-motion approximation provides a good description of the classical dynamics for both adiabatic and suddenly switched on fields. This is slightly lower than the theoretical values shown by figure 3.2 which suggest that, for adiabatic switches with $20\omega \leq \Omega < 25\omega$, β_{CH} is still significantly less than β_{AD}. In figure 3.12 we show the variation in the classical ionisation probability, P_i, with increasing β for $\Omega = 30\omega$ and an adiabatic switch of $M_a = 3000$, $M_m = 7000$. Here, the theoretical threshold field is $\beta_{AD} \simeq 2475$, whereas $\beta_{CH} \simeq 14\,950$.

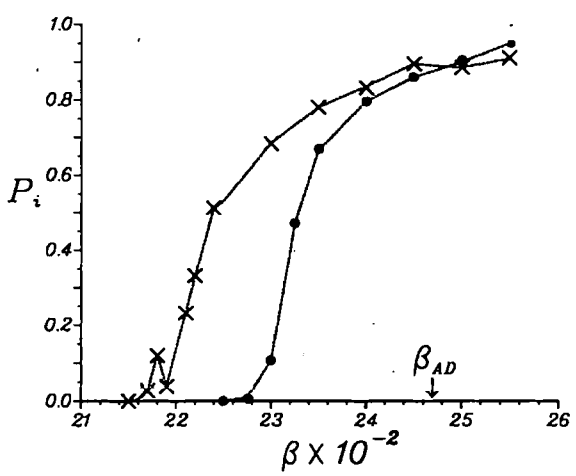

Figure 3.12 Graph showing the variation of the classical ionization probability with β for $\Omega = 30\omega$, $\mathcal{A}_0 = 0.5$ and $\mathcal{A}_s = 100$. An adiabatic switch was used with $M_a = 3000$, $M_m = 7000$ (crosses) and $M_m = 6000$, $M_m = 13\,000$ (full circles). In both cases the field phase, $\delta = 0$.

In theory, no classical ionization should take place for $\beta < \beta_{AD}$ and there should be 100% ionisation for $\beta > \beta_{AD}$. The discrepancy between the actual and theoretical dynamical

behaviour is caused by switching the field on too quickly. In figure 3.12 we also show the classical ionization probabilities obtained for an adiabatic switch with $M_a = 6000$ and $M_m = 13000$ and these show better agreement with the theoretical behaviour. Whilst switching the field on over longer time intervals improves the agreement with theory, true adiabatic conditions are difficult to achieve as the period of the classical motion increases towards infinity with increasing field amplitude, leading to a breakdown of adiabatic invariance.

At high field frequencies, the classical map, equations (3.23) and (3.24), greatly overestimates the 10% ionization threshold, giving $\beta_{10} \simeq 37000$. This is because the map is gauge invariant so ionization due to the mean-motion mechanism is absent. In this frequency range, the map based upon the mean-motion Hamiltonian (1.96) is a far better approximation. This is seen in figure 3.13 where probabilities with a sudden switch, $\Omega = 30\omega$ and $M_m = 1000$ are shown, and it will be noticed that the field strengths needed to ionize the system are considerably smaller than for an adiabatic switch. Here, the crosses show the results obtained from the numerical integration of 200 orbits consisting of 20 values of θ_0 and 10 values of δ, chosen as before, and the asterisks show the results obtained using the mean-motion map; the full curve shows the theoretical probabilities, P_{SUD}, equation (B.6) of appendix B. Again, there is good agreement between

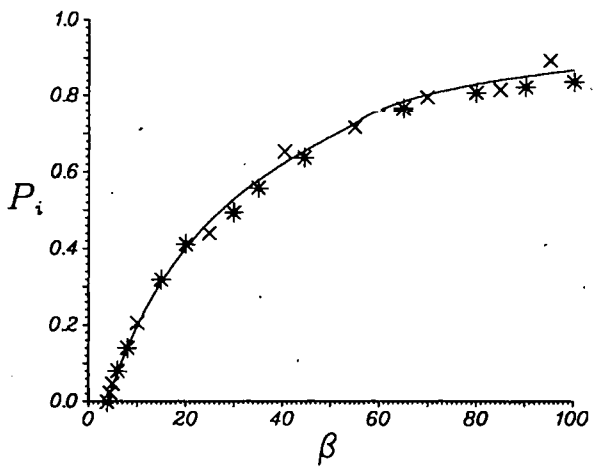

Figure 3.13 Graph showing the variation of the classical ionisation probability with β for $\Omega = 30\omega$, $\mathcal{A}_0 = 0.5$ and $\mathcal{A}_s = 100$. A sudden switch, averaged over the field phase, was used with $M_m = 1000$. The crosses depict results obtained by numerically integrating Hamilton's equations and the asterisks show results obtained by using the classical mean-motion map. The full curve shows the theoretical ionization probabilities, P_{SUD}, as calculated in appendix B.

the theoretical and the numerically calculated probabilities. In this limit the analysis of appendix C shows that the classical and quantal ionization probabilities are similar.

In the very high frequency region if $\Omega/\omega > \mathcal{A}_s(1 - \mathcal{A}_0)/2$ the quantal and classical

ionization mechanisms are fundamentally different, for the quantal description allows for direct single-photon transitions into the continuum, a process not allowed in classical dynamics. This mechanism is present in the quantal maps described in section 2.7, but the distortion due to the mean-motion clearly becomes important so only the map based on the mean-motion, equation (1.96), is accurate.

3.8 Conclusions

In this chapter we have studied the response of the Morse potential to a high frequency field. The analytic properties of the Morse potential mean that, for sufficiently high frequency fields, classical ionization can occur through regular orbits, in contradistinction to the driven Coulomb potential.

We have compared ionisation probabilities obtained by iterating the classical area-preserving map with those obtained by exact numerical integration and find that, for the driven Morse potential, the map mimics the exact dynamics remarkably well. Further, we have shown that the quantization of this map provides a very simple and efficient method of obtaining approximate solutions to the time-dependent Schrödinger equation.

We have also compared ionization probabilities obtained by iterating the classical and quantal maps. For the classical system we show that there are three possible ionization mechanisms; chaotic ionization dominates for physically realistic fields and frequencies and for this there is no quantal counterpart for the quantum numbers of current interest as an approximate selection rule drastically reduces the density of states. We further show that the localization theory proposed by Casati *et al.* (1987b, 1988) does not provide a correct description of the quantal evolution of the driven Morse potential.

The two other classical ionization mechanisms, which become significant at high-frequencies, do not involve chaotic orbits and have quantal analogues so classical and quantal ionisation probabilities are similar. For suddenly switched high frequency fields ionization can occur simply by a momentum transfer due to a gauge change; in appendix C we show that classical and quantal probabilities for this mechanism are the same, apart from interference effects.

For an adiabatically switched high-frequency field the classical system can ionize by a process involving the adiabatic invariance of the mean-motion which gradually 'squeezes' the phase curve into the unbounded region of phase space. Similar dynamics effects the quantal system, but in this case direct transitions into the continuum may be possible from the eigenstates of the classical adiabatic Hamiltonian, and the squeezing now brings these states nearer to the continuum into which they may decay more easily: the combination of these two effects needs to be considered in detail, but it seems likely that

at these very high frequencies quantal ionization probabilities are larger than classical ionization probabilities.

Chapter 4

Low frequency behaviour I: the tunnelling regime

4.1 Introduction

We now concentrate on the regime of low field frequency; for excited states of the hydrogen atom in a 9.9 GHz microwave field, this means that the scaled frequency, $\Omega_0 \lesssim 0.03$. Due to the availability of experimental data for the microwave ionization of hydrogen (see section 4.5 below) this chapter concentrates exclusively on this particular system.

Quantally, the dynamics can be described by the equations of motion (2.52), page 53, derived in chapter 2 using a basis of adiabatic states (see also Richards 1987); for the purposes of this chapter it is convenient to recast these in the form given by Richards *et al.* (1989b),

$$\frac{\mathrm{d}a_n}{\mathrm{d}\bar{t}} = -\frac{\mathcal{E}_n(f)}{\hbar\omega_{at}(n_0)}a_n - n_0F_0\Omega_0\cos(\Omega_0\bar{t})\sum_{p\neq n}a_p\frac{M_{np}(f)}{\Delta E_{np}(f)}\exp\left[\mathrm{i}\int_0^{\bar{t}}\mathrm{d}t'\Delta E_{np}(f)\right], \quad (4.1)$$

where,

$$\Delta E_{np} = (E_n(f) - E_p(f))(n_0\hbar)^3/\mu\hbar e^2, \quad (4.2)$$

$$M_{np} = \langle n, f|z|p, f\rangle\mu e^2/(n_0\hbar)^2, \quad (4.3)$$

with Ω_0 and F_0 the scaled frequency and field strength respectively, $\omega_{at}(n_0)$ the classical orbital frequency and $\bar{t} = \mu e^4 t/(n_0\hbar)^3$ the rescaled time. The classical motion is best described by the adiabatic Hamiltonian (1.40) given on page 22 of chapter 1, provided the ionization probability per field period is small.

In the scaled units used in equation (4.1), both M and ΔE are of order unity, so it is clear that the most important parameters are the scaled frequency, Ω_0, and the coupling strength, $C_s = n_0F_0\Omega_0$, which determines how many states are needed to describe the quantal motion adequately. By comparing the different theoretical models discussed in this chapter with experimental data, see section 4.7 below, we can determine the values

of C_s for which the validity of each model holds: three different ionization mechanisms are found to predominate.

1. For small values of the coupling strength, $C_s \lesssim 0.12$, transitions between adiabatic states can be neglected. In this case the system can only ionize by tunnelling through the slowly moving barrier, formed by the interaction between the Coulomb potential and the oscillating field; this mechanism has no classical analogue.

2. For slightly larger values of the field strength, for which $0.12 \lesssim C_s \lesssim 0.16$, the potential barrier is lowered and classical 'over-the-barrier' escape can occur.

3. For $C_s \gtrsim 0.16$ transitions between adiabatic states become important. In this case an atom, in an initial state with principle quantum number n_0, can be excited to a level $n > n_0$: ionization can then occur from level n either by tunnelling through, or by classical escape over, the slowly moving barrier.

In this chapter we are interested in the first mentioned situation where C_s and Ω_0 are both small so that transitions between states can be neglected; in this case equation (4.1) reduces to,

$$\frac{\mathrm{d}a_{n_0}}{\mathrm{d}t} = -\frac{\mathcal{E}_{n_0}(t)}{\hbar} a_{n_0}, \tag{4.4}$$

where n_0 labels the initial state. We compare and contrast numerical results obtained using this model both with those obtained using other theoretical models and with experimental data.

The realization that a quantal particle could traverse a classically impenetrable static potential barrier arose early in the development of quantum mechanics. However, there has been continuing interest in, and some controversy over, quantum mechanical tunnelling (see, for instance, the reviews by Hauge and Støvneng 1989, and Olkhovsky and Recami 1992). Questions which have been raised include the definition of tunnelling times and how a non-stationary barrier is traversed.

Several theories based on the original work of Keldysh (1965), and later Faisal (1973) and Reiss (1980), have addressed the tunnelling ionization of atoms in an oscillating electric field (see also Perelomov *et al.* 1968, Delone and Kraĭnov 1985, Ammosov *et al.* 1986). The so-called Keldysh-Faisal-Reiss (KFR) theory has been used to apply tunnelling interpretations to some intense-laser multiphoton ionization (LMPI) experiments, often with noble gas atoms and their ions (see, for example, Baldwin and Boreham 1981, Yergeau *et al.* 1987, Chin *et al.* 1988, Perry *et al.* 1988, Augst *et al.* 1989, Gibson *et al.* 1990, Xiong and Chin 1991, Augst *et al.* 1991). However, given that tunnelling rates increase exponentially with the field amplitude (see Landau and Lifshitz 1977, §77)

and that, according Petite *et al.* (1987) and Gibson *et al.* (1990), the absolute determination of relevant peak intensities greater than $10^{12}\,\mathrm{Wcm}^{-2}$ in focussed laser beams is difficult even to within a factor of two, LMPI experiments have not provided *sensitive* tests of dynamic tunnelling theory. Indeed, Augst *et al.* (1989) even ascribed the term 'tunnelling ionization' to LMPI experiments that were analysed with a model based on classical over-the-barrier escape.

Recently, Sauer *et al.* (1992) have used data from the microwave ionization of excited hydrogen atoms to make direct comparisons between experiment and theory. Microwave technology facilitates precise determination of the field amplitude and pulse shape (see Sauer *et al.* 1991 and section 4.5 below), a major advantage over LMPI experiments. By comparing their experimental ionization probabilities with those obtained from theoretical calculations, the authors were able to distinguish between tunnelling ionization, classical escape over the slowly oscillating barrier and between one- and many-state dynamical processes. They found that formulae based on the KFR-theory, often used to model laser tunnelling ionization experiments, failed to describe their data, which were best reproduced by the new semiclassical model presented in section 4.3.2 below.

The objective of this chapter is to utilize approximate expressions for the complex part of the resonant energy, $\mathcal{E}_n$, in order to evaluate the amplitudes, a_n, of equation (4.4), and hence obtain the probability of ionization due to tunnelling. We use as a model the three-dimensional hydrogen atom which enables us to draw comparisons both with available data obtained from microwave experiments (see Sauer *et al.* 1992) and other existing theories allowing us, for the first time, to give conditions where tunnelling theories are valid.

In section 4.2, we give a brief description of the Schrödinger equation for the unperturbed, three-dimensional hydrogen atom in parabolic coordinates. In section 4.3 the effect of a uniform static electric field on the unperturbed hydrogen atom is considered. We show how classical and quantal methods have been used to address the problem and provide a new semiclassical approximation for the ionization probability.

In section 4.4 the hydrogen atom in a slowly varying field is discussed. We show how the static tunnelling rates derived in section 4.3 can be used to obtain ionization probabilities in the presence of an oscillating field. We also provide a brief description of KFR and related theories.

In addition to models which involve tunneling, an *adiabatic* model is also considered in section 4.4. This model assumes transitions to adjacent states of the adiabatic basis followed by classical over-the-barrier escape and is complementary to tunnelling.

In section 4.5 the microwave experiment is described and in section 4.6 we give details of the numerical methods used to calculate the ionization probabilities which are

presented in section 4.7. Finally, in section 4.8, we present some conclusions.

4.2 The unperturbed hydrogen atom

The Schrödinger equation in cartesian coordinates (x, y, z) for the unperturbed, three-dimensional hydrogen atom is,

$$\left(-\frac{\hbar^2}{2\mu}\nabla^2 - \frac{e^2}{r}\right)\Psi = E\Psi, \tag{4.5}$$

where μ is the reduced mass, e the electron charge, $\nabla^2 = \partial^2/\partial x^2 + \partial^2/\partial y^2 + \partial^2/\partial z^2$ is the Laplacian operator and where $r^2 = x^2 + y^2 + z^2$. Owing to the O(4) symmetry of the fieldless hydrogen problem, equation (4.5) can be separated in many different coordinate systems: the solution of Schrödinger's equation in terms of parabolic coordinates is particularly useful when investigating problems where there is an axial symmetry, as when a static electric field is present. Moreover, separability of the Schrödinger equation in parabolic coordinates is maintained when the atom is placed in a static electric field; this situation is addressed in the next section.

The parabolic coordinates, (ξ, η, ϕ), are connected with the cartesian coordinates, (x, y, z), by the relations,

$$\begin{aligned} \xi &= r + z, \qquad \eta = r - z, \qquad \phi = \tan^{-1}(y/x), \\ x &= \sqrt{\xi\eta}\cos\phi, \qquad y = \sqrt{\xi\eta}\sin\phi, \qquad z = \frac{1}{2}(\xi - \eta), \end{aligned} \tag{4.6}$$

with $r = \frac{1}{2}(\xi + \eta)$, and where $0 \leq \phi < 2\pi$ with ξ and η defined on the semi-infinite interval $0 \leq \xi, \eta < \infty$. In these coordinates the Laplacian operator is,

$$\nabla^2 = \frac{4}{\xi + \eta}\left[\frac{\partial}{\partial\xi}\left(\xi\frac{\partial}{\partial\xi}\right) + \frac{\partial}{\partial\eta}\left(\eta\frac{\partial}{\partial\eta}\right)\right] + \frac{1}{\xi\eta}\frac{\partial^2}{\partial\phi^2}, \tag{4.7}$$

and $V = -e^2/r = -2e^2/(\xi + \eta)$. The Schrödinger equation (4.5) is then,

$$-\frac{\hbar^2}{2\mu}\left\{\frac{4}{\xi + \eta}\left[\frac{\partial}{\partial\xi}\left(\xi\frac{\partial\Psi}{\partial\xi}\right) + \frac{\partial}{\partial\eta}\left(\eta\frac{\partial\Psi}{\partial\eta}\right)\right] + \frac{1}{\xi\eta}\frac{\partial^2\Psi}{\partial\phi^2}\right\} - \left(E + \frac{2e^2}{\xi + \eta}\right)\Psi = 0. \tag{4.8}$$

In order to solve equation (4.8) a solution is sought in the form,

$$\Psi(\xi, \eta, \phi) = \frac{\chi_1(\xi)}{\sqrt{\xi}}\frac{\chi_2(\eta)}{\sqrt{\eta}}\exp(im\phi), \tag{4.9}$$

where m is the magnetic quantum number. Substituting equation (4.9) into equation (4.8) and effecting the separation gives the following equations for χ_1 and χ_2,

$$\frac{\mathrm{d}^2\chi_1}{\mathrm{d}\xi^2} + \left(\frac{\mu}{2\hbar^2}E + \frac{\mu e^2}{\hbar^2\xi}\beta_1 - \frac{m^2 - 1}{4\xi^2}\right)\chi_1 = 0, \tag{4.10}$$

$$\frac{\mathrm{d}^2\chi_2}{\mathrm{d}\eta^2} + \left(\frac{\mu}{2\hbar^2}E + \frac{\mu e^2}{\hbar^2\eta}\beta_2 - \frac{m^2 - 1}{4\eta^2}\right)\chi_2 = 0, \tag{4.11}$$

where β_1 and β_2 are the separation constants related by the constraint,

$$\beta_1 + \beta_2 = 1. \tag{4.12}$$

It should be noted that both β_1 and β_2 are functions of the energy.

In order to proceed, we restrict attention to the discrete energy spectrum, $E < 0$, and introduce the dimensionless quantities,

$$n = \frac{e^2}{\hbar}\sqrt{-\frac{\mu}{2E}}, \quad \rho_1 = \frac{\mu e^2}{n\hbar^2}\xi, \quad \rho_2 = \frac{\mu e^2}{n\hbar^2}\eta. \tag{4.13}$$

In terms of these variables, equations (4.10) and (4.11) can be re-written in the form,

$$\frac{\mathrm{d}^2\chi_i}{\mathrm{d}\rho_i^2} + \left(-\frac{1}{4} + \frac{1}{\rho_i}\left(\frac{|m|+1}{2} + n_i\right) + \frac{1-m^2}{4\rho_i^2}\right)\chi_i = 0, \quad (i = 1, 2), \tag{4.14}$$

where,

$$n_1 = -\frac{1}{2}(|m|+1) + n\beta_1, \qquad n_2 = -\frac{1}{2}(|m|+1) + n\beta_2. \tag{4.15}$$

Examination of equation (4.14) shows that the functions, χ_i, behave as $\exp(-\rho_i/2)$ for $\rho_i \gg 1$ and as $\rho_i^{(|m|+1)/2}$ for $\rho_i \ll 1$, so solutions are sought of the form,

$$\chi_i(\rho_i) = \exp(-\rho_i/2)\rho_i^{(|m|+1)/2}W_i(\rho_i), \tag{4.16}$$

where the functions $W_i(\rho_i)$ are the regular solutions of the equation,

$$\rho_i\frac{\mathrm{d}^2W_i}{\mathrm{d}\rho_i^2} + (|m|+1-\rho_i)\frac{\mathrm{d}W_i}{\mathrm{d}\rho_i} + n_iW_i = 0, \tag{4.17}$$

which may be recognized as the equation for the confluent hypergeometric function (see Abramowitz and Stegun 1965, chapter 13); the solutions which are finite at the origin are,

$$W_i = M(-n_i, |m|+1, \rho_i), \tag{4.18}$$

where n_i must be a non-negative integer. Thus, each stationary state of the discrete spectrum is determined in parabolic coordinates by three integers: the parabolic quantum numbers, n_1 and n_2, and the magnetic quantum number m. For a principle quantum number, n, we have,

$$n = n_1 + n_2 + |m| + 1. \tag{4.19}$$

The wave function $\Psi_{n_1n_2m}$ of the discrete spectrum is then of the form,

$$\Psi_{n_1n_2m} = A_{n_1n_2m}f_{n_1m}(\mu e^2\xi/n\hbar^2)f_{n_2m}(\mu e^2\eta/n\hbar^2)\exp(\mathrm{i}m\phi), \tag{4.20}$$

where $A_{n_1n_2m}$ is the normalization constant and the functions f_{n_1m} and f_{n_2m} are defined by,

$$f_{pm}(\rho) = M(-p, |m|+1, \rho)\exp(-\rho/2)\rho^{(|m|+1)/2}, \quad (p = n_1, n_2). \tag{4.21}$$

In the next section we discuss the modifications to the unperturbed hydrogen atom, described by equation (4.5), in the presence of a static electric field.

4.3 The hydrogen atom in a static electric field: the Stark effect

The Schrödinger equation for a hydrogen atom in a uniform electric field F parallel to the z-axis is,

$$\left(-\frac{\hbar^2}{2\mu}\nabla^2 - \frac{e^2}{r} + Fz\right)\Psi = E\Psi, \tag{4.22}$$

where F is the field strength.

As mentioned in the previous section, equation (4.22) is also separable in parabolic coordinates, defined by equation (4.6) above. Effecting the separation with the product *ansatz* (4.9) gives the following equations for χ_1 and χ_2:

$$\frac{\mathrm{d}^2\chi_1}{\mathrm{d}\xi^2} + \left(\frac{\mu E}{2\hbar^2} + \frac{\mu e^2}{\hbar^2\xi}\beta_1 - \frac{m^2-1}{4\xi^2} - \frac{\mu F}{4\hbar^2}\xi\right)\chi_1 = 0, \tag{4.23}$$

$$\frac{\mathrm{d}^2\chi_2}{\mathrm{d}\eta^2} + \left(\frac{\mu E}{2\hbar^2} + \frac{\mu e^2}{\hbar^2\eta}\beta_2 - \frac{m^2-1}{4\eta^2} + \frac{\mu F}{4\hbar^2}\eta\right)\chi_2 = 0. \tag{4.24}$$

where β_1 and β_2 are again related by constraint (4.12). These equations describe the properties of the hydrogen atom in the presence of a *static* electric field F: equation (4.23) is the radial Schrödinger equation for bound motion in a ξ potential, shown schematically for $m^2 > 1$ in figure 4.1, page 101; equation (4.24) represents the motion in an η-potential which diverges to $-\infty$ as $\eta \to \infty$, see figure 4.2, page 101.

It is important to realize that the potential, $V = -e^2/r + Fz$, possesses a barrier whose height and width depend upon the external electric field. Classically, the presence of the electric field has little effect on the dynamics, merely reducing the ionization threshold; ionization occurs when the energy of the electron exceeds the barrier maximum. Quantally, the problem is rather more subtle. In the field free case with $E < 0$, both the ξ- and η-potentials support bound states. However, in the presence of an electric field, whilst the ξ-potential still supports bound states, the energy spectrum of the η-motion is continuous; the electron tunnels through the potential barrier leaving the atom ionized. One way of representing this effect is to introduce a phenomenological decay rate into equation (4.22); the wave function, Ψ, then represents a *resonant* state. Such states can be characterized by a resonant energy and a width; as the resonant energy increases so does the corresponding width, with the result that the initially narrow resonance becomes wider as the classical saddle is approached. The energy, $E(n,F)$, of the resonant state corresponding to a bound level, n, of the unperturbed system is then complex and is written,

$$E(n,F) = E_R(n,F) - \mathrm{i}\frac{\Gamma_R(n,F)}{2}, \qquad \Gamma_R \geq 0, \tag{4.25}$$

where the real values E_R and Γ_R correspond to the position and width of the resonant state respectively. On relating Γ_R to the phenomenological decay term, $\mathcal{E}_n$, of equation (4.4), $\Gamma_R(n,F) = 2\mathcal{E}_n(F)$, we see that the static field ionization probability, $P_i^{st}(n,F)$, of an initial level, n, is

$$P_i^{st}(n,F) = 1 - |a_n|^2 = 1 - \exp[\Gamma_R(n,F)t/\hbar], \qquad a_{n_0} = 1. \tag{4.26}$$

When calculating the Stark energy, E, equations (4.23) and (4.24) are treated as one-dimensional Schrödinger equations with discrete bound states. One approach is to numerically integrate equations (4.23) and (4.24) and then use constraint (4.12) to obtain the energy E as a function of the field strength, F (see, for instance, Damburg and Kolosov 1983). In practice, this treatment is quite elaborate due to the particular properties of the differential equation (4.24). The subsequent calculations are thus numerically too intensive for the application we have in mind here where the principle quantum number is large, $n \gtrsim 20$. In addition, quantal perturbation theory, semiclassical approaches and classical methods have all been employed and we proceed by describing each of these three methods in turn.

4.3.1 Quantal perturbation theory

The Stark effect furnished the first example for the application of quantal perturbation theory, carried out by Schrödinger (1926) who obtained the formula for the linear Stark energy levels,

$$E = -\frac{\mu e^4}{2\hbar^2 n^2} + \frac{3}{2}\frac{F\hbar^2}{\mu e^2} n(n_1 - n_2), \tag{4.27}$$

already known from the calculations of Schwarzschild (1916) and Epstein (1916) based on the old quantum theory. Since then, several authors have studied the series expansion for the Stark levels, the first two terms of which are given by equation (4.27). The derivation of higher order terms is non trivial and the continuous energy spectrum of the η-motion means that any perturbative approach will produce a series which is merely an asymptotic expansion: after a certain point in the series, which becomes later as the perturbation is reduced in magnitude, the terms increase rather than decrease and the series does not converge.

To overcome some of these difficulties, Damburg and Kolosov (1983) found it convenient to use a modified procedure. Using the transformation $(\xi,\eta) \rightarrow (\rho_1,\rho_2)$ defined by equation (4.13) and seeking solutions for χ_1 and χ_2 of the form given in equation (4.16), the authors were able to cast equation (4.17) in the form,

$$\rho_i \frac{\mathrm{d}^2 W_i}{\mathrm{d}\rho_i^2} + (|m| + 1 - \rho_i)\frac{\mathrm{d}W_i}{\mathrm{d}\rho_i} + \left(\lambda_i - \frac{1}{2}(|m|+1)\right)]W_i = (-1)^{i+1}(\rho_i^2/4\mathcal{R})W_i, \quad (i = 1,2), \tag{4.28}$$

where,

$$\mathcal{R} = \frac{\mu e^6}{n^3 \hbar^4 F}, \qquad \lambda_i = n\beta_i. \tag{4.29}$$

The energy is then obtained from the separation constants,

$$E = -\frac{\mu e^4}{2\hbar^2}(\lambda_1 + \lambda_2)^{-2}. \tag{4.30}$$

For F sufficiently small, $\mathcal{R}$ is a large parameter and a solution of equation (4.28) is sought in the form of a power series expansion in $\mathcal{R}^{-1}$,

$$W_i = \sum_{l=0} W_i^{(l)} \mathcal{R}^{-l}, \qquad \lambda_i = \sum_{l=0} \lambda_i^{(l)} \mathcal{R}^{-l}. \tag{4.31}$$

Thus Damburg and Kolosov (1983) obtain a series in F for the Stark energy: to fifth order in F_0 this is,

$$\begin{aligned} E_0^{DK} &= -\frac{1}{2} + \frac{3F_0}{2n}(n_1 - n_2) - \frac{F_0^2}{16n^2}\{17n^2 - 3(n_1 - n_2)^2 - 9m^2 + 19\} \\ &+ \frac{3F_0^3}{32n^3}(n_1 - n_2)\{23n^2 - (n_1 - n_2)^2 + 11m^2 + 39\} \\ &- \frac{F_0^4}{1024n^4}\{5487n^4 + 35182n^2 - 1134m^2(n_1 - n_2)^2 \\ &+ 1806n^2(n_1 - n_2)^2 - 3402n^2m^2 + 147(n_1 - n_2)^4 - 549m^4 \\ &+ 5754(n_1 - n_2)^2 - 8622m^2 + 16211\} \\ &+ \frac{3F_0^5}{1024n^5}(n_1 - n_2)\{10563n^4 + 90708n^2 + 220m^2(n_1 - n_2)^2 \\ &+ 98n^2(n_1 - n_2)^2 + 772n^2m^2 - 21(n_1 - n_2)^4 + 725m^4 \\ &+ 780(n_1 - n_2)^2 + 830m^2 + 59293\} + O(F_0^6), \end{aligned} \tag{4.32}$$

where $E_0 = (n\hbar)^2 E/\mu e^4$ is the scaled energy and F_0 is the scaled field strength.

Asymptotic formula for the resonance width

Standard perturbation theory only gives an expression for the real part of the energy eigenvalue. In order to obtain an expression for the imaginary part, Damburg and Kolosov (1983) used a uniform asymptotic approach, as described in appendix D, using the Airy equation (see Abramowitz and Stegun 1965, chapter 10) as the comparison equation. In this way, the authors obtained an asymptotic formula for Γ_R:

$$\begin{aligned} \Gamma_R &= \frac{(4R)^{2n_2+m+1}\exp(-2R/3)}{n^3 n_2!(n_2+m)!} \\ &\times \left(1 - \frac{F_0}{4n}\left(34n_2^2 + 34n_2m + 46n_2 + 7m^2 + 23m + \frac{53}{3}\right) + O(F_0^2)\right), \end{aligned} \tag{4.33}$$

where

$$R = \frac{n(-2E_0^{DK})^{3/2}}{F_0}. \tag{4.34}$$

For ground state hydrogen ($n = 1$, $n_1 = n_2 = m = 0$), the first term of equation (4.33) reduces to the form given by Landau and Lifshitz (1977, §77).

Semiempirical formula for the resonance width

By analysing their numerical results and re-writing the multiplier $1-\alpha F_0+O(F_0^2)$ of equation (4.33) as $\exp(-\alpha F_0)$, Damburg and Kolosov (1983) obtained the following semiempirical formula for Γ_R,

$$\begin{aligned}\Gamma_R^{DK} &= \frac{(4R)^{2n_2+m+1}}{n^3 n_2!(n_2+m)!} \\ &\times \exp\left[-\frac{2}{3}R-\frac{F_0}{4n}\left(34n_2^2+34n_2m+46n_2+7m^2+23m+\frac{53}{3}\right)\right].\end{aligned} \tag{4.35}$$

In section 4.7 we compare numerically calculated ionization probabilities, $P_i^{DK}(n_0,F_0)$, obtained using the Damburg and Kolosov (DK) formula (4.35) both with those obtained experimentally and those obtained numerically using the semiclassical model which we now derive.

4.3.2 A uniform semiclassical approach

The starting point for our semiclassical approach is the Hamiltonian,

$$H=\frac{1}{2\mu}p^2-\frac{e^2}{r}+zF. \tag{4.36}$$

As before, the equations of motion associated with equation (4.36) are separable in parabolic coordinates defined in equation (4.6) above. Effecting the separation, we obtain the equations,

$$\frac{1}{2\mu}p_\xi^2+\left(\frac{I_\phi^2}{8\mu\xi^2}-\frac{e^2\beta_1}{2\xi}+\frac{F}{8}\xi\right) = \frac{E}{4}, \tag{4.37}$$

$$\frac{1}{2\mu}p_\eta^2+\left(\frac{I_\phi^2}{8\mu\eta^2}-\frac{e^2\beta_2}{2\eta}-\frac{F}{8}\eta\right) = \frac{E}{4}, \tag{4.38}$$

where I_ϕ is a constant equal to the action of the ϕ-motion, and where, as before, β_1 and β_2 are related by constraint (4.12). Replacing p_ξ and p_η with their quantal operator equivalents and carrying out the quantization of I_ϕ in the standard way,

$$I_\phi=m\hbar, \tag{4.39}$$

we obtain the following Schrödinger equations,

$$\frac{\mathrm{d}^2\chi_1}{\mathrm{d}\xi^2}+\left(\frac{\mu E}{2\hbar^2}+\frac{\mu e^2\beta_1}{\hbar^2\xi}-\frac{m^2}{4\xi^2}-\frac{\mu F}{4\hbar^2}\xi\right)\chi_1 = 0, \tag{4.40}$$

$$\frac{\mathrm{d}^2\chi_2}{\mathrm{d}\eta^2}+\left(\frac{\mu E}{2\hbar^2}+\frac{\mu e^2\beta_2}{\hbar^2\eta}-\frac{m^2}{4\eta^2}+\frac{\mu F}{4\hbar^2}\eta\right)\chi_2 = 0. \tag{4.41}$$

It should be noted that with this method we do not retrieve exactly equations (4.23) and (4.24); the m^2-1 term has been replaced by m^2. This apparent anomaly was

explained by Langer (1937) who noted that application of standard WKB formulae to radial Schrödinger equations, such as equations (4.23) and (4.24) above, yields a solution which becomes infinite at the origin and so is not the desired wave function. However, by making the substitution, $r = e^x$, $\psi = e^{x/2}u(x)$, where r and ψ represent the radial coordinate and wave function respectively, Langer noted that a Schrödinger equation is obtained to which WKB methods are directly applicable. By Langer-transforming the basic equations (4.23) and (4.24), Gallas *et al.* (1982) obtained precisely equations (4.40) and (4.41); note that the main effect of the Langer transformation is to replace the m^2-1 term by m^2. Thus, equations (4.40) and (4.41) are the correct equations to use for the semiclassical approximation.

Equations (4.40) and (4.41) are Schrödinger equations for motion in the potentials,

$$V_\xi(\xi) = -\frac{e^2\beta_1}{2\xi} + \frac{m^2\hbar^2}{8\mu\xi^2} + \frac{F}{8}\xi, \tag{4.42}$$

$$V_\eta(\eta) = -\frac{e^2\beta_2}{2\eta} + \frac{m^2\hbar^2}{8\mu\eta^2} - \frac{F}{8}\eta. \tag{4.43}$$

Schematic views of the potentials for $m^2 > 0$ are given in figures 4.1 and 4.2. The negative parts of the ξ- and η-axes have no physical meaning but are of considerable help in the mathematical formulation. As shown in figure 4.1, the motion along the ξ-coordinate is confined for all values of the field strength: classically the particle is bound to oscillate between the turning points $0 \leq \xi_2 < \xi_1$ and quantization of the motion can be carried out in the standard way,

$$I_\xi = \frac{\sqrt{2\mu}}{\hbar}\int_{\xi_2}^{\xi_1} \mathrm{d}\xi\,\sqrt{E/4 - V_\xi(\xi)} = (n_{1\xi} + 1/2)\pi. \tag{4.44}$$

The motion in the η-coordinate, shown in figure 4.2, is much more complicated and the source of all difficulties in studying the Stark effect. For physically meaningful energies, that is those lower than the classical saddle energy, the classical motion near the nucleus is bounded between $0 \leq \eta_1 < \eta_2$ whilst quantally the electron may tunnel through the barrier. Since it is necessary to explicitly include the barrier, uniform methods are needed.

We need the wave functions at energies below the saddle energy, $E^S = 4V_\eta^{max}$, so there are three real turning points, $\eta_1(E) \ll \eta_2(E) < \eta_3(E)$, see figure 4.2. In appendix D we describe the general idea of using the comparison equation method to obtain a uniform approximation to the solution of the one-dimensional Schrödinger equation. For the system under consideration here, there are two nearby turning points, $\eta_2(E)$ and $\eta_3(E)$ of figure 4.2, which coalesce as the energy, E, of the system approaches E^S. It is necessary to include these two turning points explicitly in the comparison equation. In this case,

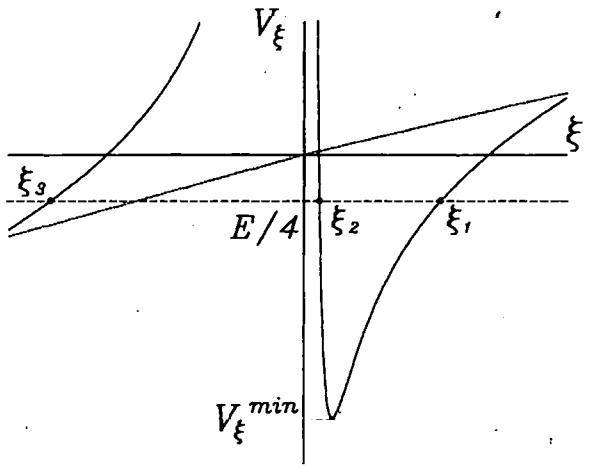

Figure 4.1 Potential, V_ξ, for the ξ-motion defined by equation (4.42).

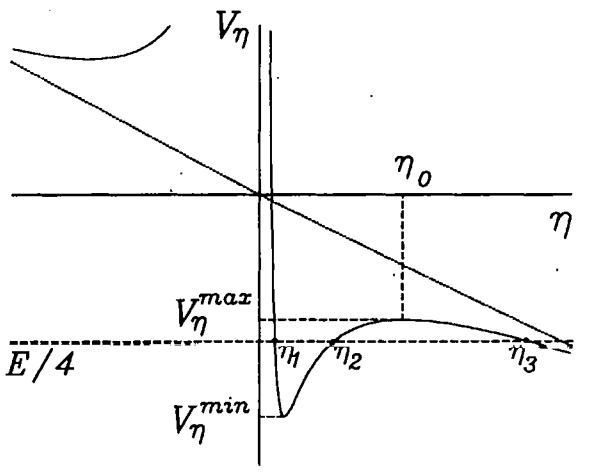

Figure 4.2 Potential, V_η, for the η-motion defined by equation (4.43).

an appropriate comparison function is,

$$Q_0(\sigma) = -A + \sigma^2/4, \tag{4.45}$$

where A is positive for energies below the barrier top and negative for energies above the barrier. The comparison equation can then be written in the form,

$$\frac{\mathrm{d}^2\phi}{\mathrm{d}z^2} + (z^2/4 - a)\phi = 0, \quad \sigma = z\sqrt{\hbar}, \quad A = \hbar a, \tag{4.46}$$

the solutions of which may be expressed in terms of parabolic cylinder functions, $\phi = W(a, \pm z)$ (see Abramowitz and Stegun 1965, equation (19.1.3)).

Here, we are only interested in systems with $E < E^S$: in this case, there are two close turning points, $\eta_2 < \eta_3$, and it is convenient to define A so that $\sigma(\eta_2) = -2\sqrt{A}$ and $\sigma(\eta_3) = 2\sqrt{A}$ with,

$$A(E) = \frac{1}{\pi}\int_{\eta_2}^{\eta_3} \mathrm{d}\eta\, \sqrt{-Q_\eta(\eta)}, \quad Q_\eta(\eta) = 2\mu\left\{E/4 - V_\eta(\eta)\right\}. \tag{4.47}$$

The wave function is then given by,

$$\chi_2(\eta, E) = \left(\frac{\sigma^2/4 - A}{Q_\eta(\eta)}\right)^{1/4} \left\{\alpha W(a, z) + \beta W(a, -z)\right\}, \tag{4.48}$$

where we have written $z = \sigma(\eta)/\sqrt{\hbar}$, $a = A(E)/\hbar$ and where $\sigma(\eta)$ is given by equation (D.11),

$$\frac{\sigma}{4}\sqrt{\sigma^2 - 4A} - A\ln\left(\frac{\sigma + \sqrt{\sigma^2 - 4A}}{2\sqrt{|A|}}\right) = \int_{\eta_3}^{\eta} d\eta'\, \sqrt{Q_\eta(\eta')}, \quad \sigma > 0, \tag{4.49}$$

$$\frac{s}{4}\sqrt{s^2 - 4A} - A\ln\left(\frac{s + \sqrt{s^2 - 4A}}{2\sqrt{|A|}}\right) = \int_{\eta}^{\eta_2} d\eta'\, \sqrt{Q_\eta(\eta')}, \quad s > 0, \tag{4.50}$$

where $s = -\sigma$.

In order to proceed further, we need to impose appropriate boundary conditions. We assume that the wave function is delta-function normalized in energy, $\langle E'|E\rangle = \delta(E - E')$, and that it has the asymptotic form, see Landau and Lifshitz (1977),

$$\chi_2(\eta, E) \to \left(\frac{2\mu}{\pi\hbar p_\eta}\right)^{1/2} \sin\left(\frac{1}{\hbar}\int_{\eta_3(E)}^{\eta} \mathrm{d}\eta'\, \sqrt{Q_\eta(\eta')} + \delta(E)\right), \tag{4.51}$$

where the phase shift, $\delta(E)$, determines the behaviour of the wave function.

At the left-hand turning point, $\eta = \eta_1(E)$, we can again use uniform methods, this time with the Airy equation (see Abramowitz and Stegun 1965, chapter 10) as the comparison equation, to obtain the following approximation to the wave function in the inner region, $\eta_1(E) \ll \eta \ll \eta_2(E)$,

$$\chi_2(\eta, E) = \gamma\left(\frac{\hbar}{Q_\eta(\eta)}\right)^{1/4} \cos\left(\frac{1}{\hbar}\int_{\eta_1(E)}^{\eta} \mathrm{d}\eta'\, \sqrt{Q_\eta(\eta')} - \frac{\pi}{4}\right), \tag{4.52}$$

where γ is a constant to be determined.

Matching the asymptotic form of the solution, equation (4.48), to the small-η solution, equation (4.52), gives the following relations between α, β and γ,

$$\gamma_1 \sin\alpha_1 = \frac{\alpha}{k(a)^{1/2}} \quad , \gamma_1 \cos\alpha_1 = \beta k(a)^{1/2} \quad , \gamma_1 = \gamma, \tag{4.53}$$

with the phase $\alpha_1(E)$ given by,

$$\alpha_1(E) = I_\eta + \frac{1}{2}\Phi(a), \tag{4.54}$$

where, by analogy with equation (4.44) for the ξ-motion, we have written

$$I_\eta = \frac{\sqrt{2\mu}}{\hbar}\int_{\eta_1}^{\eta_2} \mathrm{d}\eta \sqrt{E/4 - V_\eta(\eta)}, \tag{4.55}$$

and where the functions Φ and k are,

$$\Phi(x) = x(1 - \ln|x|) + \arg\Gamma(1/2 + \mathrm{i}x), \tag{4.56}$$

$$k(x) = 1/\{\sqrt{1 + \exp(2\pi x)} + \exp\pi x\}. \tag{4.57}$$

The function $\Phi(x)$ is odd, positive for $x > 0$, and has a single maximum of $\Phi \approx 0.15$ at $x = 0.18$. In appendix E we give expressions to be used in the numerical evaluation of $\Phi(x)$ and also evaluate I_η in terms of complete elliptic integrals.

Matching the solution (4.48) to the asymptotic form (4.51) for $\eta \gg \eta_3$ gives,

$$\delta(E) = \frac{\pi}{4} + \frac{1}{2}\Phi(a) + \alpha_2(E), \tag{4.58}$$

where,

$$\gamma_2 \sin\alpha_2 = \alpha\sqrt{k}, \quad \gamma_2 \cos\alpha_2 = \beta/\sqrt{k}, \quad \gamma_2 = \left(\frac{2\mu}{\pi^2\hbar^3}\right)^{1/4}. \tag{4.59}$$

On using equations (4.53), (4.58) and (4.59) we obtain the following expression for the phase shift:

$$k(E)^2 = \tan(\delta(E) - \pi/4 - \Phi(a)/2)\cot\alpha_1(E), \tag{4.60}$$

with $\alpha_1(E)$ given by equation (4.54).

Energy levels and resonance widths

Various definitions of resonant energies and widths exist, all of which yield numerically similar results for narrow resonances. Damburg and Kolosov (1983) and Gallas *et al.* (1982) use the Breit Wigner parametrization of the asymptotic phase shift, $\delta(E)$, (see also Landau and Lifshitz 1977 §145) to determine the resonance parameters E_R and

Γ_R. Here, we follow Richards (1987) and employ the maxima of the time-delay function (see also Connor and Smith 1981),

$$\tau = 2\hbar \frac{\mathrm{d}\delta}{\mathrm{d}E}. \tag{4.61}$$

The real part, E_R, of the resonant energy are those energies at which the time-delay has local maxima; the corresponding resonance widths are then defined by,

$$\Gamma_R = 2\mathcal{E}_R = \frac{4\hbar}{\tau(E_R)}. \tag{4.62}$$

On using equation (4.60) we find that the time delay is given by,

$$\tau(E) = \hbar \frac{\mathrm{d}\Phi(E)}{\mathrm{d}E} + 2\hbar \frac{k^2\alpha_1' + kk' \sin 2\alpha_1}{\cos^2 \alpha_1 + k^4 \sin^2 \alpha_1}. \tag{4.63}$$

For all levels below the barrier top, $\alpha_1(E)$ and its derivative are well-behaved functions of E: for states well below E^S, the tunnelling integral, A of equation (4.47), is large so that k, equation (4.57) is small. Therefore, in this region the local maxima of τ are at the roots of $\alpha_1(E) = (n_2 + 1/2)\pi$, that is,

$$I_\eta + \frac{1}{2}\Phi(a) = (n_2 + 1/2)\pi. \tag{4.64}$$

The resonant energy is then found by solving equations (4.64) and (4.44) subject to constraint (4.12). The resonance width, Γ_R^{SC}, is then, on using equation (4.63),

$$\Gamma_R^{SC} = 2\mathcal{E}_R = 4\left(\frac{2}{k^2}\frac{\mathrm{d}\alpha_1}{\mathrm{d}E} + \frac{\mathrm{d}\Phi}{\mathrm{d}E}\right)^{-1}, \qquad E = E_R, \tag{4.65}$$

$\mathcal{E}_R$ being the complex part of the energy.

In appendix E we show how to express the action integrals I_η, I_ξ, the tunnelling integral, A, and the resonance widths, Γ_R, in terms of complete elliptic integrals.

Numerical considerations

Numerical calculation of the energy levels and resonance widths, whilst straightforward in principle, is far from trivial. Firstly we have to solve equations (4.44) and (4.64) to obtain values for the energy levels, E, and one of the separation constants, say β_1[1]. Herein lies the problem: the integral, I_η of equation (4.64), is only defined for energies $E < E^S$ and standard two dimensional root finding techniques invariably attempt to evaluate I_η for $E > E^S$, particularly for substates with energies lying just below the classical saddle energy, E^S. Whilst it is possible to extend the definition of I_η to energies $E > E^S$ (see Callaс *et al.* 1982 for details) our chief interest here is in states lying below

[1]Note that the second separation constant, β_2, is then obtained using constraint (4.12).

the classical saddle. To this end we need an estimate, for each substate, of the critical field strength required to give $E \simeq E^S$ and for this we use the classical critical field, F_c^{cl}: the method used for calculating F_c^{cl} is given in the next section. Further details of our numerical approach for obtaining semiclassical approximations to the energy levels and resonance widths are given in section 4.6 below.

4.3.3 The classical critical field

Banks and Leopold (1978a, 1978b) used an exact classical treatment based on the assumption of adiabatic invariance of the actions to find explicit expressions for the critical ionization energy, E_c^{cl}, and critical field, F_c^{cl}, and to calculate Stark shifts for all values of the electric field up to F_c^{cl}. In their treatment of this problem, the authors separate the classical Hamiltonian (4.36) using a method similar in spirit to that described in section 4.3.2 above[2] to obtain equations (4.37) and (4.38). Classically, the total energy, E^{cl}, must lie in the range,

$$4\max(V_\xi^{min}, V_\eta^{min}) \leq E^{cl} \leq 4V_\eta^{max} \leq 0, \tag{4.66}$$

where V_ξ and V_η are given by equations (4.42) and (4.43) respectively. For any value of $E^{cl} = 4V_\xi = 4V_\eta$ in this region the equations $E^{cl} = 4V_\xi$ and $E^{cl} = 4V_\eta$ each have three real roots, ξ_1, ξ_2, ξ_3 and η_1, η_2, η_3 respectively (see also figures 4.1 and 4.2, page 101). The classical critical ionization energy is defined by $E_c^{cl} = 4V_\eta^{max}$ which implies $\eta_2 = \eta_3$. The energy E^{cl} and the separation constants β_1, β_2, are related implicitly to the actions I_ξ, I_η and I_ϕ and the electric field F. By imposing the condition $\eta_2 = \eta_3$ in exact classical calculations relating I_ξ and I_η to E, β_1, β_2, F, I_ϕ and the six real roots, Banks and Leopold obtain expressions for the classical critical field, F_c^{cl}, and critical energy, E_c^{cl}, in terms of the functions, $\Phi_c(u,v)$ and $\mathcal{E}_c(u,v)$, which are scale invariant forms of the electric field and the energy respectively. These functions are dimensionless and independent of the total action, $I = I_\xi + I_\eta + I_\phi$, but dependent on the dimensionless ratios $u = I_\eta/I$ and $v = I_\phi/I$. The critical field and critical energy are then written,

$$F_c^{cl} = \frac{\mu^2 e^6}{I^4}\Phi_c(u,v), \qquad E_c^{cl} = -\frac{\mu^2 e^4}{2I^2}\mathcal{E}_c(u,v). \tag{4.67}$$

The authors are then able to obtain values of F_c^{cl} and E_c^{cl} and of Stark shifts by using a polynomial fit to the functions $\Phi_c(u,v)$ and $\mathcal{E}_c(u,v)$. Their results are in very good agreement with quantal calculations of Stark shifts for strong fields obtained using the quantal asymptotic method of Damburg and Kolosov (1983) described in section 4.3.1 above.

[2]Banks and Leopold (1978a, 1978b) use the coordinates $\xi = (r+z)/2$, $\eta = (r-z)/2$.

4.4 The hydrogen atom in a slowly varying electric field

We may begin to explore the tunnelling ionization probability in the presence of a slowly oscillating field by integrating the static tunnelling rate for each substate, Γ_R^{DK} of equation (4.35) or Γ_R^{SC} of equation (4.65), over one oscillation of the external field to obtain a fractional loss of population per field period,

$$W(\boldsymbol{n}) = \frac{1}{2\Omega_0\hbar}\int_0^{2\pi} \mathrm{d}\tau\, \Gamma_R(\boldsymbol{n}, F_0 \sin\tau), \tag{4.68}$$

where we have written $\tau = \Omega_0 \bar{t}$, $\boldsymbol{n} = (n, n_1, m)$ denotes the substate and where we allow for the oscillatory nature of the field by writing $F = F_0 \sin\tau$. After N field oscillations, the ionization probability for each substate is,

$$P_i(\boldsymbol{n}, F_0) = 1 - \exp[-NW(\boldsymbol{n})]. \tag{4.69}$$

The total ionization probability, $P_i(n, F_0)$ is then obtained by averaging equation (4.69) over the microcanonical distribution:

$$P_i(n, F_0) = \frac{1}{n^2}\sum_{m=1-n}^{n-1}\sum_{n_1=0}^{n-|m|-1} P_i(\boldsymbol{n}, F_0). \tag{4.70}$$

In section 4.7 we compare ionization probabilities obtained using the semiclassical approximation, P_i^{SC}, and the Damburg and Kŏlosov (1983) formula, P_i^{DK}, with experimental ionization probabilities, P_i^{expt}. We also consider two other approximations; the adiabatic method, described in section 4.4.3, and the Keldysh-Faisal-Reiss theory described next.

4.4.1 Keldysh-Faisal-Reiss theory

A quantal theory often used to describe intense laser multiphoton ionization (LMPI) and above-threshold ionization (ATI) data is based on a theory due to Keldysh (1965). The Keldysh theory was the first attempt to describe ionization by an oscillating field for a range of frequencies from the tunnelling limit ($\gamma \ll 1$) to the multiphoton ionization (MPI) limit ($\gamma \gg 1$) where the 'Keldysh parameter', γ, is the ratio of the tunnelling time to the external field period; for the hydrogen atom this is,

$$\gamma = \frac{\Omega}{n_0 F} = \frac{\Omega_0}{F_0}, \tag{4.71}$$

where n_0 is the initial state and where Ω_0 and F_0 are the scaled frequency and field strength respectively. The double inequalities are consistent with Keldysh's original presentation although one finds in the LMPI literature $\gamma < 1$ (rather than $\gamma \ll 1$) being called the 'tunnelling regime' (see, for instance, Augst *et al.* 1989).

Since then, the Keldysh theory has been modified by several authors, most notably Faisal (1973) and Reiss (1980) and is now known as the 'Keldysh-Faisal-Reiss' (KFR) theory.

In essence, the KFR theory assumes that a single matrix element connects the initial atomic bound state $|\Psi_0\rangle$ to an unbound (dressed) state, $|\Psi_f\rangle$. The final state $|\Psi_f\rangle$ is assumed to be the Volkov state which is the exact solution of the Schrödinger equation for an unbound electron moving with momentum, $\boldsymbol{p}$, in a time-varying electric field with no other potential present;

$$\Psi_f(\boldsymbol{r},\boldsymbol{p},t) = \langle \boldsymbol{r}|\Psi_f\rangle = C\exp\left[\frac{\mathrm{i}}{\hbar}\left(\boldsymbol{p}.\boldsymbol{r} - \int_0^t \mathrm{d}t'\,\frac{p^2}{2\mu} + H_A(t')\right)\right], \tag{4.72}$$

where C is a normalization constant and H_A is the interaction Hamiltonian,

$$H_A(t) = -\frac{e}{\mu c}\boldsymbol{p}.\boldsymbol{A}(t) + \frac{e^2}{2\mu c^2}A(t)^2, \tag{4.73}$$

with $\boldsymbol{A}$ the vector potential of the electric field, $\boldsymbol{F}(t) = (e/c)\partial\boldsymbol{A}/\partial t$. Quantal first-order perturbation theory gives the ionization probability at time, t, as,

$$P_i^{KFR}(t) = \left|\frac{1}{\hbar}\int_0^t \mathrm{d}t'\,\langle\Psi_f|H_A|\Psi_0\rangle\right|^2, \tag{4.74}$$

which can be written,

$$P_i^{KFR}(t) = \left|\frac{1}{\hbar}\int_0^t \mathrm{d}t'\exp\left(\frac{\mathrm{i}}{\hbar}\int_0^{t'}\mathrm{d}t''\left(\frac{p^2}{2\mu} + H_A(t'')\right)\right)\langle\boldsymbol{p}|H_A(t')|\Psi_0\rangle\right|^2, \tag{4.75}$$

where $\langle\boldsymbol{r}|\boldsymbol{p}\rangle = \exp(\mathrm{i}\boldsymbol{p}\cdot\boldsymbol{r}/\hbar)$. In the KFR theory, the initial state is chosen to be a single bound state, $|\Psi_0\rangle = \exp[\mathrm{i}E_0t/\hbar]|0\rangle$, where E_0 is the energy of the eigenstate, $|0\rangle$. Note that the use of first-order perturbation theory assumes that coupling to intermediate states can be neglected and hence only the initial and final states appear in the formulation. Therefore, KFR-theory cannot provide a correct description of the quantal motion when other bound states play a significant role in the dynamics.

4.4.2 Ammosov-Delone-Kraĭnov theory

As mentioned in the previous section, one important approximation made by the KFR theory is to assume that the final state wave function is the Volkov state, equation (4.72), thereby neglecting the long-range effect of the Coulomb potential on the ionized electron. Consequently, for the hydrogen atom in a low frequency field, P_i^{KFR}, equation (4.75), does not reduce to the correct formula for the probability of static field ionization (see Landau and Lifshitz 1977, §77) in the limit $\Omega \to 0$. Perelomov *et al.* (1968) corrected this by using a final state wave function which does include the effect of the Coulomb

interaction on the ionized electron. However, analytic expressions for the tunnelling ionization probability in an alternating field were only obtained for a few specific states of the hydrogen atom. By starting from the expression obtained by Perelomov *et al.* (1966) for the ionization probability for states of the hydrogen atom, Ammosov *et al.* (1986) derived an expression for the probability of ionization due to tunnelling for arbitrary states of complex atoms and atomic ions. For a particular substate of the hydrogen atom the Ammosov-Delone-Kraĭnov (ADK) tunnelling ionization probability is,

$$\begin{aligned} P_i^{ADK}(\boldsymbol{n}, F_0) &= \frac{\mu e^4}{\hbar^3 n^3}\left(\frac{3}{\pi^3}\right)^{1/2}\left(\frac{(2l+1)(l+|m|)!}{(|m|)!(l-|m|)!}\right)\left(\frac{n-l}{n+l}\right)^{l+1/2} \\ &\times (n^2-l^2)^{-n}\left(\frac{4n}{F_0}\right)^{2n-|m|-3/2}\exp\left[-2n\left(\frac{1}{3F_0}-1\right)\right], \end{aligned} \tag{4.76}$$

where $\boldsymbol{n} = (n, l, m)$ denotes the substate and F_0 is the scaled field strength. Note that the result given by Ammosov *et al.* (1986) contains misprints and errors; equation (4.76) is our corrected version which agrees with the result obtained for hydrogen atoms by Delone and Kraĭnov (1985, equation 9.24). The total ionization probability for a given initial principle quantum number, n_0, and scaled field strength, F_0, can be obtained by summing equation (4.76) over all the substates of the microcanonical distribution, that is,

$$P_i^{ADK}(n, F_0) = \frac{1}{n^2}\sum_{l=0}^{n-1}\sum_{m=-l}^{l} P_i^{ADK}(\boldsymbol{n}, F_0). \tag{4.77}$$

4.4.3 An adiabatic model

By way of contrast with the models described thus far, all of which involve tunnelling through the slowly moving barrier, we also consider an adiabatic model for which the ionization process consists of a rapid transition from an initial level, n_0, to the level $n_0 + 1$, followed by classical over-the-barrier escape.

For a static electric field, the classical system ionizes if the field strength, F, is greater than the classical critical field, F_c^{cl}, given by equation (4.67) in section 4.3.3 above. Now consider an oscillating field. In the very low frequency limit, we assume that the field is oscillating sufficiently slowly for it to be considered simply as a static field which changes sign: this allows us to apply results from static field theory. Now, from equations (1.37) and (1.38), page 99, we see that changing the direction of the static field, $F \to -F$, simply interchanges the ξ- and η-motions: this means that a field, F, has the same effect on the parabolic substate, $\boldsymbol{n} = (n_1, n_2, m)$, as a field, $-F$, on the substate, $\boldsymbol{n} = (n_2, n_1, -m)$. Thus we can assume that the adiabatic critical field of an atom in a

substate $\boldsymbol{n} = (n_1, n_2, m)$ is equal to,

$$F_c^{adia}(\boldsymbol{n}) = \frac{\mu^2 e^6}{(\hbar n)^4} \min\{\Phi_c(u_2, v), \Phi_c(u_1, -v)\} \quad \text{where} \quad u_1 = \frac{n_1}{n},\ u_2 = \frac{n_2}{n},\ v = \frac{m}{n} \tag{4.78}$$

and $n = n_1 + n_2 + |m| + 1$ is the principle quantum number. As mentioned in section 4.3.3 above, the scale invariant form of the electric field, $\Phi_c(u, v)$, is dimensionless and independent of n, depending only upon the dimensionless ratios, $u = n_2/n$ and $v = m/n$. Thus, $F_c^{adia}(n)$ depends only upon the principle quantum number, n, through the n^{-4} term in the prefactor and so decreases rapidly with increasing n.

Provided the interaction time extends over many field oscillations, the classical system will ionize for $F > F_c^{adia}$. By considering a microcanonical ensemble of initial conditions, we obtain the adiabatic ionization probabilities denoted by the full curve in figure 4.3, where, for comparison we also show the static field ionization curve, P_i^{st}; note that because the adiabatic and the static field ionization probabilities are both calculated classically, they depend only upon the scaled field, F_0, and not upon n_0 and F separately. The two curves shown in figure 4.3 are quite different with P_i^{st} lying below the full curve throughout the range of F_0 shown. Indeed, the adiabatic probability is unity for $F_0 \gtrsim 0.2$ whereas $P_i^{st} < 1.0$ for $F_0 \lesssim 0.38$; this is because, for a given parabolic substate, $\boldsymbol{n} = (n_1, n_2, m)$, $F_c^{adia}(\boldsymbol{n}) \leq F_c^{cl}(\boldsymbol{n})$. Indeed, if we consider the extremal Stark state, $\boldsymbol{n} = (0, n-1, 0)$, we find that $n^4 F_c^{cl}(\boldsymbol{n}) \simeq 0.38$ whereas $n^4 F_c^{adia}(\boldsymbol{n}) \simeq 0.13$.

As the coupling strength increases, $C_s \gtrsim 0.12$, transitions between adiabatic basis states become important and a simple classical model of the atom can no longer be applied. Instead, we assume a crude model for the ionization process, consisting of a rapid transition from an initial level, n_0, to the level, $n_0 + 1$, followed by classical over-the-barrier escape. Further, we assume that this ionization mechanism can be approximated by classical dynamics. It then follows that the ionization probability, P_i^{adia}, can be obtained from the full curve of figure 4.3 simply by rescaling the field, $F_0 \rightarrow \left(\frac{n_0}{n_0+1}\right)^4 F_0$.

In section 4.7 we compare the ionization probabilities obtained numerically using P_i^{ADK}, P_i^{SC} and P_i^{DK} with those given by the adiabatic model, P_i^{adia}, and those obtained experimentally, P_i^{expt}. In the next section the experimental method is described.

4.5 The experiment

For completeness we now describe the method used to obtain the experimental data shown, for example, by the solid line of figure 4.4. All experiments were carried out by Professor Koch's group at the State University of New York, Stony Brook.

The experimental apparatus has been described previously by Richards *et al.* (1989b) and Koch *et al.* (1989). Briefly, H^+-Xe electron-transfer collisions produce a 17 keV beam

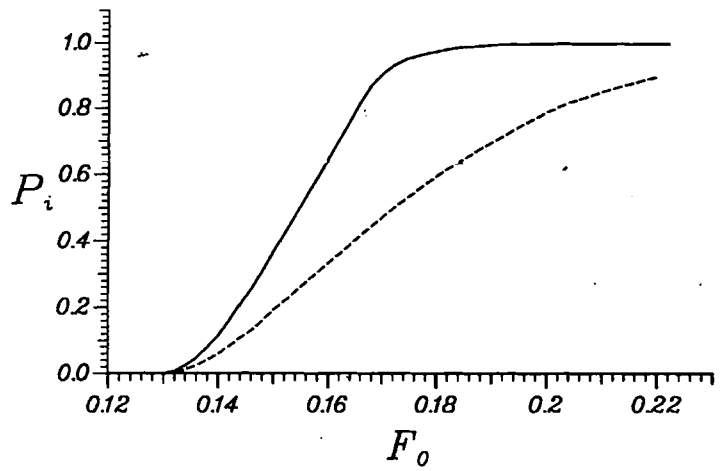

Figure 4.3 Graph showing the dependence of the ionization curve, P_i^{uni} (full curve) and the static field ionization curve, P_i^{st} (broken curve) upon the scaled field strength, F_0.

of neutral hydrogen atoms. A fraction of about 10^{-5} is in a particular parabolic state with initial quantum number, $n_0 = 7$ from which $^{12}C^{16}O_2$ laser double-resonance excitation takes place to an extremal parabolic state in an n_0-manifold between 24 and 32. After excitation to this substate the beam passes through a weak electric field which has no effect on n_0 but does 'scramble' the substates. Previous work using static field ionization as a diagnostic tool just before the microwave cavity has shown that the atomic substate distribution entering the cavity corresponds classically to a microcanonical ensemble of initial orbits with fixed initial principle action, see van Leeuwen *et al.* (1985). The initial phase of the microwave field is averaged over by the experiment.

The 4.96 cm long, 5.32 cm diameter cylindrical microwave cavity resonates CW in the TM_{020} mode at 9.908 GHz. The 0.63 cm thick end caps have 0.26 cm diameter holes on axis to pass the 0.09 cm diameter beam. The field distribution is calculated numerically after Halbach and Holsinger (1976). In the atom's rest frame, the pulse, $\lambda(t)$, is turned on and off in 22 cycles (0.05 to 0.95), and remains constant (> 0.95) for 250 cycles.

In this experiment, ionization means true ionization plus excitation to bound states above an apparatus-determined cut-off n-value, n_c (see, for instance Richards *et al.* 1989b, Koch *et al.* 1989, Koch *et al.* 1992). Experimental insensitivity to variations of n_c values in the range $75 \leq n_c \leq 90$ (in other words, far above n_0) along with calculations, justifies the assumption that true ionization completely dominates for the low frequencies of interest here.

The most important aspect of this experiment is that the frequency of the microwave cavity, Ω_c, is fixed and the *scaled* frequency, Ω_0, is changed only by varying the initial

principle quantum number, n_0; the relation between the two frequencies is,

$$\Omega_0 = \Omega_c/\omega_{at}(n_0) = (\Omega_c/\mathrm{GHz})(0.00533757 n_0)^3, \qquad \omega_{at}(n) = \mu e^4/(n\hbar)^3. \tag{4.79}$$

Thus, the scaled frequency can only be sampled at discrete values.

All experimental data presented in section 4.7 below have the same relative 5% absolute amplitude uncertainty but the *relative* amplitude uncertainty between data for different values of n_0 is even smaller.

4.6 Numerical methods

In this section the methods used to obtain the numerical results presented in section 4.7 below are described. In all calculations and for the remainder of this chapter we use atomic units so that $\mu = e = \hbar = 1$.

The DK-formula and semiclassical ionization probabilities were obtained by evaluating expressions (4.70) and (4.69) using $\Gamma_R = \Gamma_R^{DK}$, equation (4.35), and $\Gamma_R = \Gamma_R^{SC}$, equation (4.65), respectively. For each substate of the microcanonical ensemble, denoted by the quantum numbers (n,n_1,m), we first calculated the classical critical field, F_c^{cl}. For those states with $F > F_c^{cl}$ we set $P_i(n, F_0) = 1$ because their ionization occurs on a time scale significantly less than the total interaction time. This gives an upper bound to the ionization probability and should be a good approximation for the pulse length of the microwave experiment considered here; for very short pulses, however, it would overestimate the ionisation probability. Other substates were treated as described below.

For the quantal perturbation probabilities, $P_i^{DK}(n_0, F_0)$, denoted by the crosses in, for example, figure 4.4, numerical evaluation of the resonance widths was facilitated by replacing the factorials in the prefactor of (4.35) with the fourth-order Stirling's formula (see Abramowitz and Stegun 1965, equation (6.1.37)). Numerical evaluation of the integral in equation (4.68) was then carried out using the NAG routine `D01AJF`.

Numerical calculation of the semiclassical ionization probabilities, $P_i^{SC}(n_0, F_0)$, denoted by the asterisks in, for example, figure 4.4, was less straightforward as exact numerical evaluation the the integral in equation (4.68) proved to be too time consuming. Instead, we used a modified procedure to obtain an approximation to the integral. First we note that the resonance widths, Γ_R^{SC} can be written in the form,

$$\Gamma_R^{SC} = \exp\left\{-n_0\left(A_0 + A_1 F_0 \sin\tau + A_2 F_0^2 \sin^2\tau + \cdots\right)\right\}, \tag{4.80}$$

where we have written $\tau = \Omega_0 t$ and where A_0, A_1 and A_2 are constants which are to be calculated for each substate. The integral may then be written as,

$$I = 2\exp(-n_0 A_0)\int_0^{\pi/2} du\, \exp\left(-n_0 A_1 F_0 \cos u - n_0 A_2 F_0^2 \cos^2 u + \cdots\right). \tag{4.81}$$

The major contribution to this integral will come from close to $u = 0$, so we can approximate $\cos u$ by its Taylor expansion and extend the upper limit of the integral to ∞. On neglecting terms $O(F_0^2)$ we obtain a linear approximation,

$$I_{lin} = 2\sqrt{-\frac{\pi}{2n_0 A_1 F_0}}\exp[-n_0(A_0 + A_1 F_0)],. \qquad A_1 < 0. \tag{4.82}$$

Including the terms $O(F_0^2)$ gives the following quadratic approximation:

$$I_{quad} = 2\sqrt{-\frac{\pi}{2n_0(A_1 F_0 - 2A_2 F_0^2)}}\exp[-n_0(A_0 + A_1 F_0 + A_2 F_0^2)]. \tag{4.83}$$

In table 4.1 we compare semiclassical ionization probabilities calculated using the quadratic approximation (4.83), P_i^{app}, with those obtained by numerically calculating integral (4.68) using the NAG routine D01AJF, P_i^{num}, for $n_0 = 25$ ($\Omega_0 = 0.02353$) and a range of F_0. We see that the agreement between the exact and approximate probabilities is remarkably good; the quadratic approximation (4.83) is thus used in the evaluation of all semiclassical ionization probabilities presented in the next section.

Table 4.1 Table comparing values for the semiclassical ionization probabilities obtained by numerical evaluation of integral (4.68) using the NAG routine D02AJF, P_i^{num}, with those obtained using the the quadratic fit, I_{quad}, equation (4.83), P_i^{app}, for $n_0 = 25$ ($\Omega_0 = 0.02353$) and $0.11 \leq F_0 \leq 0.128$.

F_0	0.110	0.112	0.114	0.116	0.118	0.120	0.122	0.124	0.126	0.128
P_i^{ex}	0.000	0.000	0.002	0.008	0.022	0.049	0.087	0.133	0.186	0.244
P_i^{app}	0.000	0.000	0.002	0.008	0.023	0.050	0.087	0.134	0.187	0.245

To obtain the semiclassical resonance widths, we begin by solving equations (4.44) and (4.64) coupled by constraint (4.12). Firstly, equation (4.64) was solved using the NAG routine C05ADF for 15 different values of the real part of the energy between $E_{min} = 4\max(V_\eta^{min}, V_\xi^{min})$ and $E_{max} = 4V_\eta^{max}$ to obtain 15 values of $\beta_2(E)$. The NAG routine E02BEF was then used to fit a cubic spline to these 15 points, thus giving an approximation to the function $\beta_2(E)$. Next, the real part of the resonant energy was obtained by solving equation (4.44), again using the NAG routine C05ADF, with the value of $\beta_1(E) = 1 - \beta_2(E)$ obtained from the cubic spline fit using the NAG routine E02BBF. In each case, the action integrals, I_ξ and I_η were evaluated in terms of complete elliptic integrals using the method described in appendix E; the Carlton symmetrized forms of the complete elliptic integrals were calculated using the NAG routines S21BBF, S21BCF and S21BDF. Having obtained the real part of the resonant energy, the tunnelling integral, $A(E)$ of equation (4.47) was evaluated, as described in appendix E and finally the resonance width was obtained.

The ADK ionization probabilities were obtained using formula (4.77). As for the calculation of the DK ionization probabilities, the factorials in the prefactor were replaced with the fourth-order Stirling's formula.

4.7 Comparison of theories with experiment

In figures 4.4 to 4.12 we compare experimentally obtained ionization probabilities (full curve) for the hydrogen atom ($n_0 = 24, \ldots, 32$ respectively) with those obtained using the semiclassical approximation of section 4.3.2 (asterisks), the Damburg and Kolosov (1983) quantal perturbation formula of section 4.3.1 (crosses), the adiabatic model described in section 4.4.3 (broken curve) together with those obtained from classical Monte-Carlo calculations (full squares). We exploit the precise calibration of the microwave amplitude to distinguish finely between the different theoretical ionization mechanisms and, in particular, between models involving tunnelling and models involving classical over-the-barrier escape. All experimental data presented in this section have the same 5% absolute amplitude uncertainty but the *relative* amplitude uncertainty between data for different values of n_0 is even smaller.

Firstly, we note that the classical ionization probabilities, P_i^{MC}, always underestimate P_i^{expt} with the discrepancy increasing with decreasing n_0. For the lower values of n_0, this discrepancy near the onset of ionization is quantitatively similar to that for classical *versus* tunnelling ionization in a static electric field. For example, the fields measured by Koch and Mariani (1981) that produce static ionization rates in the range $\Gamma_K = 10^5$–$10^8\,\mathrm{s}^{-1}$ for individual substates with $n_0 = 30, 40$ are from 8% to 17% smaller than the corresponding classical critical field, F_c^{cl} (see Banks and Leopold 1978b).

Ionization probabilities, P_i^{adia}, denoted by the broken curve in figures 4.4–4.12 and obtained using the adiabatic model described in section 4.4.3 above, agree fairly well with experimental probabilities for $n_0 \geq 29$ but less well at lower n_0, with the agreement being rather poor for $n_0 \leq 26$. The agreement for $n_0 \geq 31$ is particularly good for $P_i^{expt} \gtrsim 0.2$, a trend which is repeated at lower values of n_0. Indeed, close inspection of figures 4.4–4.12 shows that the disagreement of both P_i^{adia} and P_i^{MC} with P_i^{expt} decreases with increasing values of F_0 which suggests a growing importance of dynamic couplings between bound states as F_0 increases.

In contrast, ionization probabilities obtained using the semiclassical model, P_i^{SC}, denoted by the asterisks, reproduce the experimental ionization curves remarkably well for $n_0 \leq 29$; the agreement of P_i^{expt} with ionization probabilities obtained using the DK-formula model, P_i^{DK}, denoted by the crosses, is less impressive for this range of n_0. In fact, for $n_0 \leq 27$, one may clearly distinguish between the semiclassical and the

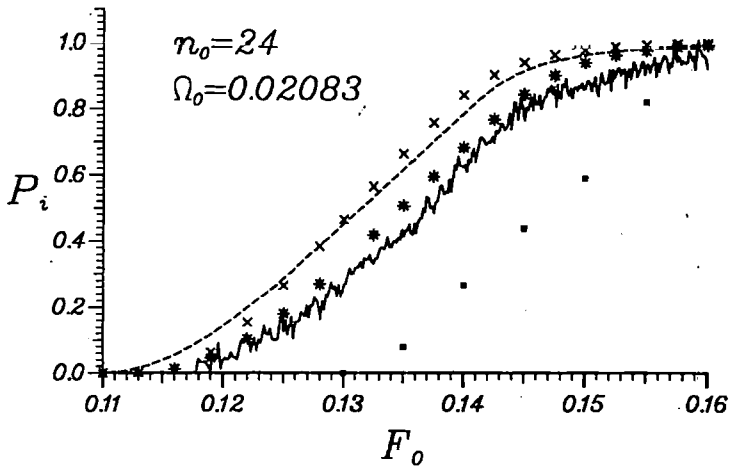

Figure 4.4 Comparison of experimental ionization probabilities (full curve) with those obtained numerically using the semiclassical model described in section 4.3.2 (asterisks), the DK formula, equation 4.35 (crosses) and the adiabatic model described in section 4.4.3 (broken curve) for $n_0 = 24$ ($\Omega_0 \simeq 0.02083$). Also shown are the classical ionization probabilities, P_i^{MC} (full circles).

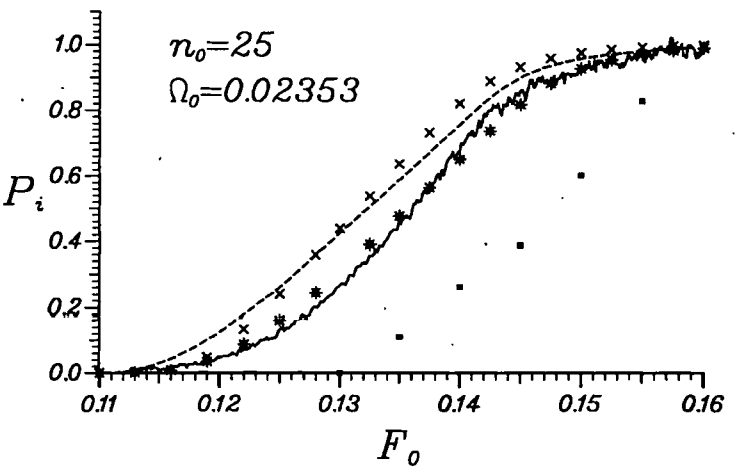

Figure 4.5 As for figure 4.4 with $n_0 = 25$ ($\Omega_0 \simeq 0.02353$).

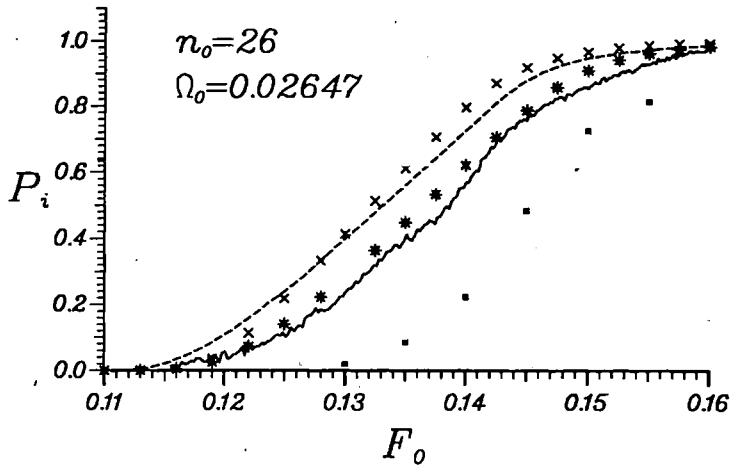

Figure 4.6 As for figure 4.4 with $n_0 = 26$ ($\Omega_0 \simeq 0.02647$).

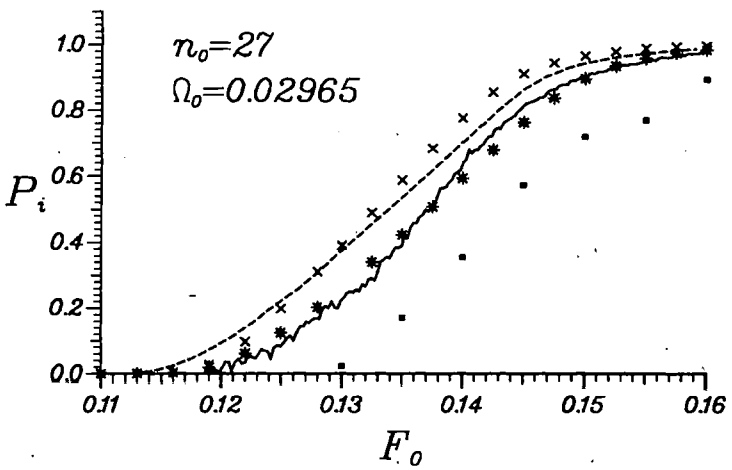

Figure 4.7 As for figure 4.4 with $n_0 = 27$ ($\Omega_0 \simeq 0.02965$).

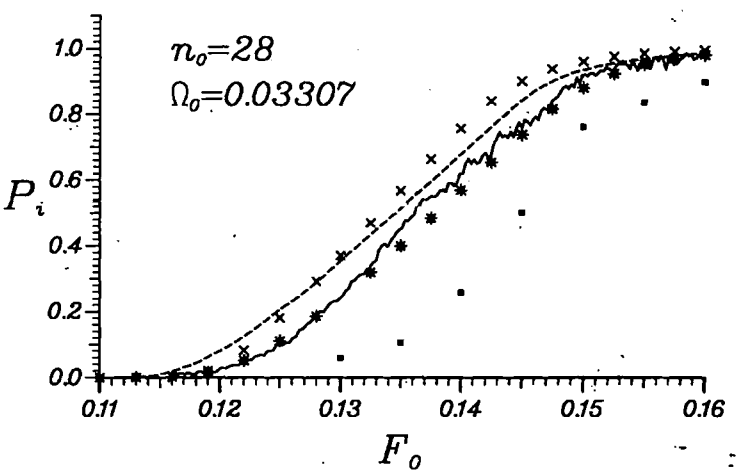

Figure 4.8 As for figure 4.4 with $n_0 = 28$ ($\Omega_0 \simeq 0.03307$).

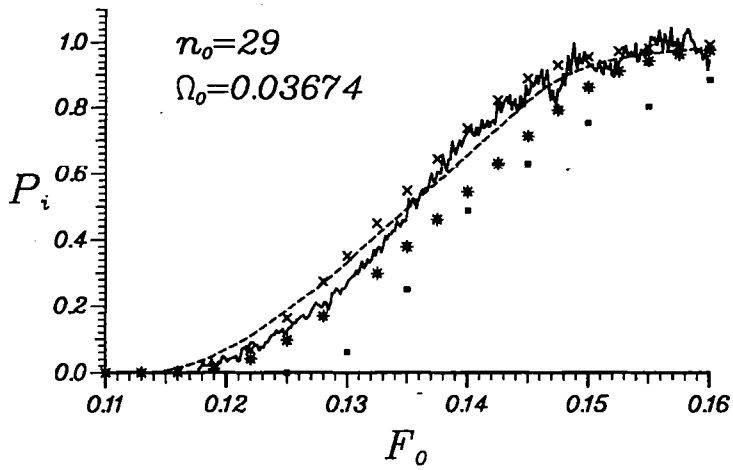

Figure 4.9 As for figure 4.4 with $n_0 = 29$ ($\Omega_0 \simeq 0.03674$).

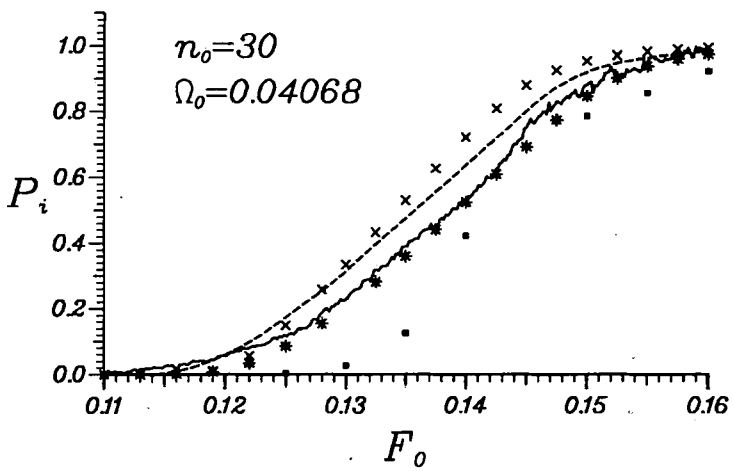

Figure 4.10 As for figure 4.4 with $n_0 = 30$ ($\Omega_0 \simeq 0.04068$).

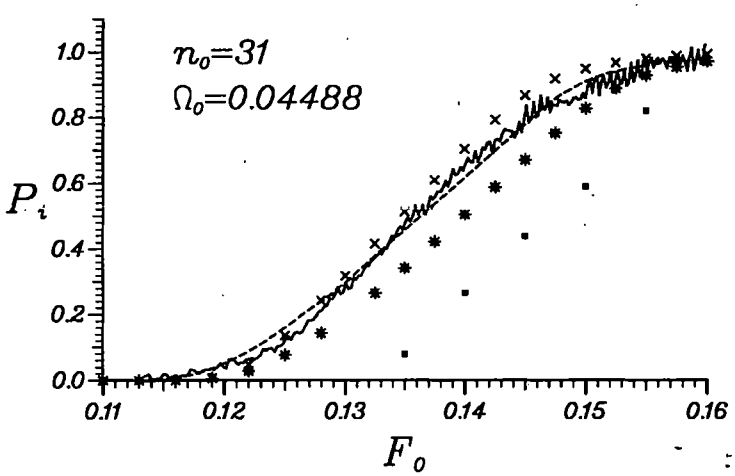

Figure 4.11 As for figure 4.4 with $n_0 = 31$ ($\Omega_0 \simeq 0.04488$).

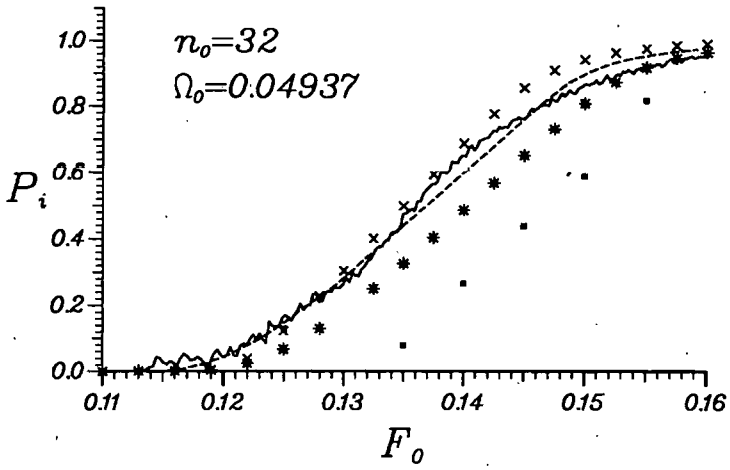

Figure 4.12 As for figure 4.4 with $n_0 = 32$ ($\Omega_0 \simeq 0.04937$).

DK-formula model calculations as the latter yields curves having a shape different from the experimental curves. This may be seen more clearly in figure 4.13 which shows the ionization curves for $n_0 = 27$ but with $P_i \leq 0.4$ and $F_0 \leq 0.13$ and where, for clarity, the adiabatic and classical probabilities have been omitted. Even allowing for the 5% absolute amplitude uncertainty, we see that a small global adjustment of the experimental amplitude does not change this trend. Both of these models involve tunnelling, but the DK-formula model is clearly inferior, see figures 4.4–4.9 and 4.13 in particular. This is in part due to the DK-formula, equation (4.33), overestimating Γ_R; experiments by Koch and Mariani (1981) with some $|m| < 3$ substates of $n_0 = 30, 40$ have shown the DK-formula to work reasonably well for near extremal substates (that is substates with $n_1 = n - 1$ or $n_1 = 0$) but to overestimate the resonance width for other substates by at least an order of magnitude.

The apparent agreement between the DK-formula model and experiment observed for higher values of n_0, see for example figure 4.11 for $n_0 = 31$, is accidental. At higher values of n_0, Ω_0 and hence the coupling strength, $C_s = n_0 F_0 \Omega_0$, increases; the initial level, n_0, is then significantly coupled to the adjacent $(n_0 + 1)$-level, with a consequent increase in ionization probability. Hence, at some value of n_0 the experimental microwave ionization curve will lie accidentally near the DK-formula curve.

Figure 4.14 compares the experimental $F_{expt}(10)$, shown by the full curve, with calculated $F_0(10)$ values, $F_0(X)$ being the field amplitude at which $X\%$ ionization occurs. The 3D classical Monte Carlo calculations, $F_0^{MC}(10)$ denoted by the full squares, only start to approach $F_{expt}(10)$ for the higher values of n_0. At the low end, not only is the $\gtrsim$10% disagreement significant, but the trend is wrong: with decreasing n_0 the classical 10% threshold field, $F_0^{MC}(10)$, rises whereas $F_{expt}(10)$ gently falls.

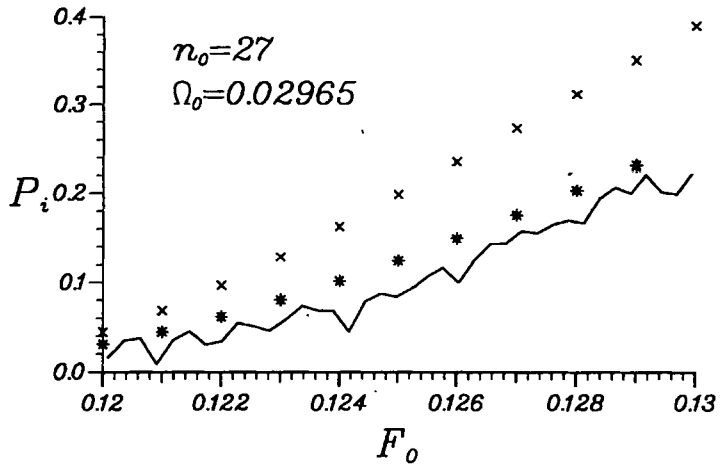

Figure 4.13 Comparison of experimental ionization probability (full curve) with those calculated numerically using the semiclassical model, P_i^{SC}, (asterisks) and the DK-formula, P_i^{DK} for $P_i \leq 0.4$ and $F_0 \leq 0.13$ at $n_0 = 27$ ($\Omega_0 = 0.0297$).

The 10% threshold field, $F_0^{adia}(10)$, of the adiabatic model, denoted by the open circles, are in close agreement with $F_{expt}(10)$ only for $n_0 \geq 29$ which shows that for the 9.9 GHz field considered here, the ionization mechanism in this model is wrong for the lower n_0 values.

In contrast, 10% threshold fields, $F_0^{SC}(10)$, obtained using the semiclassical model and shown by the asterisks, agree best with $F_{expt}(10)$ only for $n_0 \leq 29$. Though close, the DK-formula threshold field, $F_0^{DK}(10)$ denoted by the crosses, are less than $F_{expt}(10)$ for $24 \leq n_0 \leq 29$. Note that both of these models produce 10% threshold fields which decrease monotonically with decreasing n_0 whereas $F_{expt}(10)$ peak mildly near $n_0 = 28$.

Figures 4.4–4.13 together with figure 4.14 suggest strongly that for hydrogen atoms exposed to about 300 oscillations of a 9.9 GHz field tunnelling becomes the dominant ionization mechanism for $C_s \lesssim 0.12$, corresponding to $n_0 \leq 28$ or $\Omega_0 \leq 0.033$; at higher values of C_s, and consequently n_0 and Ω_0, coupled-state ionization mechanisms become important. Notice, that for an initial principle quantum number, $n_0 = 28$, the classical electron hits the moving barrier $(2\Omega_0)^{-1} = 15$ times per half period of the oscillating field, which sets a time scale for tunnelling to become important.

We now proceed by describing the ionization probabilities, P_i^{ADK}, obtained using the ADK formula given by equation (4.76) of section 4.4.2 above. Calculation of the 10% threshold field, $F_0^{ADK}(10)$ using the ADK-formula yields values nearly a factor of two below $F_{expt}(10)$ for $n_0 = 24$–32. Since the tunnelling ionization rate depends exponentially on F_0, this produces a *huge* discrepancy in P_i. Alternatively, evaluating P_i^{ADK} at $F_{expt}(10)$ values gives ionization probabilities above 0.97, far too high.

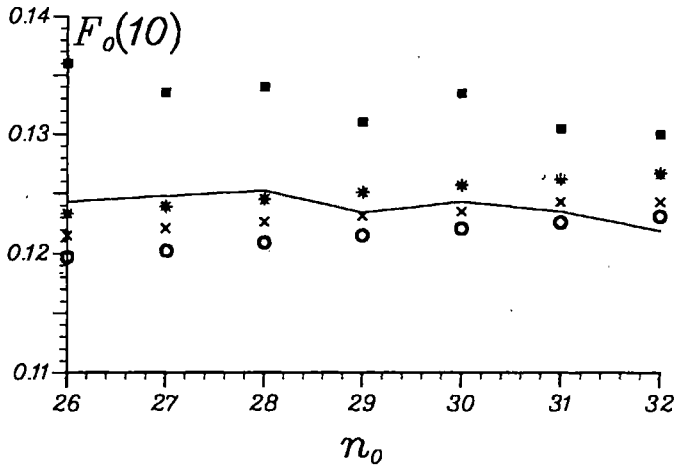

Figure 4.14 Comparison of the scaled 10% threshold fields, $F_0(10)$, calculated using classical Monte-Carlo methods (full squares), the DK-formula (crosses), the semiclassical model (asterisks) and the adiabatic model (open circles) for $24 \leq n_0 \leq 32$. The full curve represents the experimental 10% threshold field, $F_{expt}(10)$.

The main reason for the failure of the ADK-formula is simple. For $n_0 \gg 1$ and $l = m = 0$, the ADK-tunnelling rate formula, equation (4.76), can be written in the form,

$$P_i^{ADK}(n_0, F_0) \simeq \sqrt{\frac{3}{\pi {n_0}^9}} \exp\left[-n_0 \left\{ \left(\frac{2}{3F_0} - 2\right) + \left(2 - \frac{3}{2n_0}\right) \ln\left(\frac{F_0}{4}\right) \right\}\right]. \qquad (4.84)$$

The field amplitude at which the exponential factor is zero is clearly important: for large n_0 this ought to be the scaled classical critical field, ${n_0}^4 F_c^{cl}(n_0, n_1, m)$. In table 4.2 we

Table 4.2 Values of F_0 at which the exponential factor in the ADK-formula, equation (4.84), is zero for various values of n_0.

n_0	20	50	100	500	1000	10000
F_0	0.0677	0.0661	0.0656	0.0652	0.0652	0.0651

give the F_0-values at which the exponential factor in equation (4.84) is zero for various values of n_0. We see that the exponential factor in the ADK-formula has its zero at $F_0 \simeq 0.065$ whereas F_c^{cl} gives a value of $F_0 \simeq 0.13$. For $n_0 \approx 1$ this leads to small errors but these increase dramatically with increasing n_0. In figure 4.15 we compare the three ionization probabilities P_i^{ADK} (broken curve), P_i^{DK} (full curve) and P_i^{SC} (dotted curve) for $n_0 = 1$; the ionization curves produced by the three different models are similar. This should be contrasted with figure 4.16 which shows the same three curves as figure 4.15

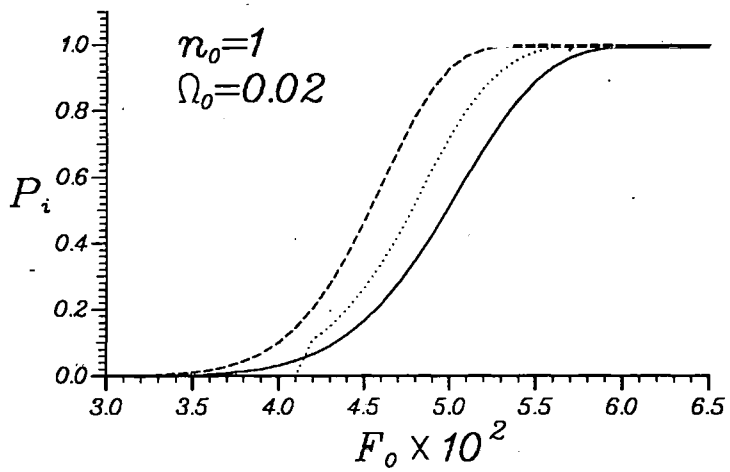

Figure 4.15 Comparison of the ADK-formula ionization probabilities, P_i^{ADK} (broken curve), with those obtained using the DK-formula, P_i^{DK} (full curve) and the semi-classical model (dotted curve) at $n_0 = 1$ and $\Omega_0 = 0.02$.

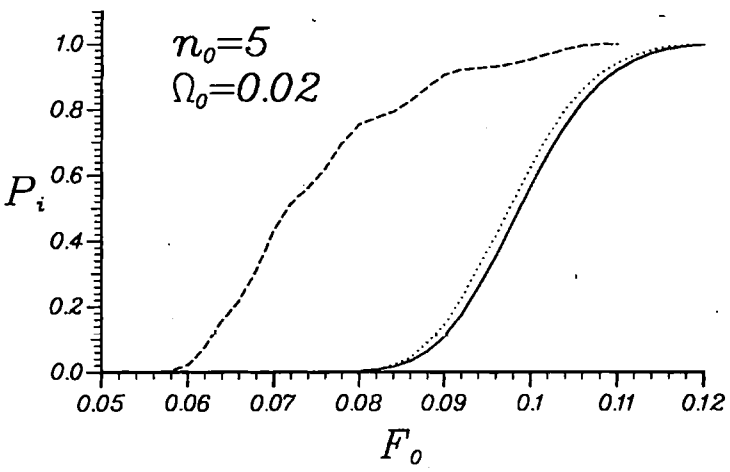

Figure 4.16 As figure 4.15 with $n_0 = 5$ and $\Omega_0 = 0.02$.

but at $n_0 = 5$. Even at these relatively small values of n_0, the ionization probabilities obtained using the ADK-formula model are significantly lower than those obtained using either the DK-formula or the semiclassical model and this discrepancy increases with increasing n_0. Note that even at these low values of n_0, P_i^{SC} and P_i^{DK} show remarkable agreement. Therefore the assertion (see Augst *et al.* 1991, page 863) that the validity of the ADK formula improves with increasing principle quantum number is wrong.

4.8 Conclusions

In this chapter we have made direct comparisons between experimental ionization probabilities obtained for the microwave ionization of excited hydrogen atoms and those obtained numerically using different theoretical models. These comparisons clearly show that for $C_s \lesssim 0.12$ or, equivalently, $n_0 \lesssim 28$, $\Omega_0 \leq 0.033$, coupling between states can be neglected; ionization occurs when the electron tunnels through the slowly moving barrier. Moreover we find that KFR-type formulae, which are often used to interpret low-frequency LMPI data, fail to reproduce the experimental data presented here whereas ionization probabilities obtained using our new semiclassical model show remarkable agreement with those obtained experimentally for $n_0 \lesssim 29$. Unfortunately, evaluation of the semiclassical ionization probabilities can only be achieved numerically and is far from straightforward, see the discussion in section 4.6 for a measure of the complexity involved. Clearly, it would be advantageous if the semiclassical resonance energies and widths could be expressed as a formula: this, however, is a matter for future work and not considered in this thesis.

For $C_s > 0.16$ ($n_0 > 29$) our study shows that coupling to other states becomes important and this must be incorporated into any theoretical model; this situation is considered in the next chapter where we use a two-state approximation to obtain a solution to equation (4.1) for $n_0 \gtrsim 29$.

Chapter 5

Low frequency behaviour II: resonances

5.1 Introduction

In this chapter we discuss the effect of a low frequency periodic electric field on an excited hydrogen atom in the regime where the scaled frequency, Ω_0, lies in the range $0.05 \leq \Omega_0 \leq 0.2$. For this range of scaled frequency, the experimental ionization curves show a great deal of structure which is not reproduced by classical simulations of the ionization process.

By using a quantal one-dimensional model together with the adiabatic basis, see Richards (1987) and also section 2.5.1 above, Richards *et al.* (1989b) were able to show that resonances between a few adiabatic states were responsible for various features in the experimental ionization curves. Although the experiments were performed on three dimensional atoms the comparison gave fairly conclusive evidence that many of the observed features can be understood using a one-dimensional model. Other calculations using an unperturbed basis have also been published but, because of the very large number of states involved, it is not easy to obtain analytic estimates from such calculations. Breuer *et al.* (1989) studied this problem using Floquet methods and an unperturbed basis and showed, numerically, that the resonances described in Richards *et al.* (1989b) can be related to near degeneracies in the quasi energy spectrum, a similar explanation is given in the earlier work of Blümel and Smilansky (1987, 1990) who associated the resonances with 'unresolved clusters of many Floquet avoided crossings'; further discussion of these studies can be found in section 2.5.2 of chapter 2.

At first sight the results presented in chapter 4 (see also Sauer *et al.* 1992) seem to contradict the theory presented by Richards (1987) and Richards *et al.* (1989b) which showed that there are resonances whenever $1/\Omega_0 \simeq p$, where p is a large integer, see equation (5.13) below, and that at these frequencies the ionization probability is enhanced. Thus, according to this theory we should expect to see an infinite series of resonances as $\Omega_0 \to 0$. However, in chapter 4, where we studied the lower frequency

range, $0.02 \leq \Omega_0 \leq 0.05$, we demonstrated that, for $\Omega_0 \lesssim 0.03$ and initial principal quantum number $n_0 \leq 28$, the simple semiclassical theory, presented in section 4.3.2, sufficed to explain the experimental results but, more important, no resonance effects were observed, see, for example, the experimental curve denoted by the full line in figure 4.4 on page 114 above (see also Sauer *et al.* 1992). The reason that these are not seen is simply that as Ω_0 decreases the resonance width becomes very narrow and in any experiment which samples the frequency too coarsely they will not be seen; in the experiments described in chapter 4 only the discrete scaled frequencies $\Omega_0 = (0.011469 n_0)^3$, with $24 \leq n_0 \leq 32$, were sampled.

Richards *et al.* (1989b) showed numerically that the resonance widths decrease with frequency, but the approximate theory of that paper gave only the positions of the resonances. In order to obtain resonance widths it is necessary to understand how the solutions of Schrödinger's equation depend upon the driving frequency, so one needs accurate solutions in a tractable form. In this chapter we provide such a solution of the two-state equations of motion which we use to obtain approximations to the resonance widths as $\Omega_0 \to 0$. In particular we show that the width of the resonance at $\Omega_0 \simeq p^{-1}$ is approximately $p^{-5/2} c^{-Cp}$, C being a positive constant, and that for the quantum numbers and frequencies dealt with by Sauer *et al.* (1992) and chapter 4 above they are too narrow to be observed.

The remainder of this chapter is organized as follows. Section 5.2 is devoted to obtaining an accurate analytic solution to the two-state equation, valid for low frequency perturbations. This is achieved by re-writing Schrödinger's equation in terms of the Bloch equation and then transforming this into a form in which first order perturbation theory is valid. In section 5.3 we use this approximation to obtain expressions for both the position and width of the resonances. Finally, in section 5.4, we present some conclusions.

5.2 Approximate solution for the two-state system

For the low field frequencies considered in this chapter, the classical motion is most conveniently described using the dipole gauge Hamiltonian (1.35), see page 21 above; for the one-dimensional hydrogen atom in the presence of a low frequency electric field we write this as,

$$H(z,p,t) = \frac{1}{2\mu} p^2 - \frac{e^2}{z} - zF \sin \Omega t, \qquad z \geq 0. \tag{5.1}$$

Note that here we have neglected both the field envelope, $\lambda(t)$, and the field phase, δ; for a slowly switched sinusoidal field this approximation produces insignificant errors provided the driving frequency is small compared to the unperturbed frequency of the system and the system starts at $t = 0$, that is when the perturbation is zero. When the

scaled frequency is small the classical electron executes many oscillations of its Kepler orbit during each field period so it is appropriate to use the adiabatic basis defined by the conservative adiabatic Hamiltonian given by equation (1.40) on page 22, namely,

$$H_{AD}(z,p,f) = \frac{1}{2\mu}p^2 - \frac{e^2}{z} - zf, \quad z \geq 0, \tag{5.2}$$

where f is a parameter. In section 1.4.1 we showed that the angle-action variables defined by this Hamiltonian define a new representation which becomes time-dependent if f is replaced by $F\sin\Omega t$; then Hamiltonian (5.1) becomes, Leopold and Richards (1993a),

$$K(\theta,I,t) = H_{AD}(I,f) + F\Omega\sum_{s=1}^{\infty}\frac{Q_s(I,f)}{s\omega_{AD}(I,f)}\sin s\theta\cos\Omega t, \qquad f = F\sin\Omega t, \tag{5.3}$$

where

$$H_{AD}(I,f) = H_{AD}(z(\theta,I,f),p(\theta,I,f),f) \quad \text{with} \quad \omega_{AD}(I,f) = \frac{\partial H_{AD}}{\partial I} \tag{5.4}$$

being the frequency of the conservative motion defined by the Hamiltonian (5.2), and where $Q_s(I,f)$ is the sth Fourier component of $z(\theta,I,f)$. In the following we shall approximate these by their field free values,

$$Q_s(I,f) \simeq Q_s(I,0) = -\frac{2I^2}{\mu e^2}\frac{J_s'(s)}{s}. \tag{5.5}$$

As already noted in chapter 1, the advantage of this representation is that the perturbation is proportional to $F\Omega$ rather than just F.

In this angle-action representation the eigenfunctions of H_{AD}, that is solutions of $H_{AD}|n,f\rangle = E_n(f)|n,f\rangle$, have the form

$$\langle\theta|n,f\rangle = (2\pi)^{-1/2}e^{in\theta}, \qquad \text{with} \quad E_n(f) = H_{AD}(n\hbar,f). \tag{5.6}$$

For all the numerical results presented in this chapter we use the expressions for $E_n(f)$ derived by Richards (1987), namely,

$$\left(n+\frac{3}{4}\right)^2 E_n(f) = -\frac{\mu e^4}{\hbar^2}\left(\frac{1}{2}+\sum_{j=1}^{5}e_j^+\beta^j\right) \qquad 0 \leq f, \tag{5.7}$$

$$\left(n+\frac{3}{4}\right)^2 E_n(f) = -\frac{\mu e^4}{\hbar^2}\left(\frac{1}{2}+\sum_{j=1}^{3}e_j^-\beta^j\right) \qquad f \leq 0, \tag{5.8}$$

where the coefficients, $e_j^{\pm}$, are given in table 5.1 and where β is a dimensionless parameter defining the field strength,

$$f = \beta\left(\frac{c}{n+\frac{3}{4}}\right)^4, \qquad -1 \leq \beta \leq 1, \qquad c = \frac{4}{3\pi}\frac{\sqrt{2\mu e^3}}{\hbar} = 0.60\,\text{au}: \tag{5.9}$$

Table 5.1 Values of the coefficients, $e_j^{\pm}$, used in the energy level approximation, equations (5.7) and (5.8).

j	1	2	3	4	5
e_j^+	1.947 (-1)	1.474 (-2)	4.509 (-3)	2.061 (-3)	1.148 (-3)
e_j^-	1.946 (-1)	1.410 (-2)	2.606 (-3)	—	—

our analysis suggests that the precise form chosen for $E_n(f)$ is of no significance. Using the adiabatic basis, equation (5.6), and the Hamiltonian (5.3) we can re-derive the equations of motion for the time-dependent amplitudes, $a_n(t)$ and $a_{n+1}(t)$, see equations (2.52) on page 53 and also Richards (1987): in the low frequency limit only two adiabatic states are significantly coupled and these equations become,

$$\frac{\mathrm{d}}{\mathrm{d}\tau}a_{n+1} = k(\tau)\exp\left\{\frac{\mathrm{i}}{\Omega_0}\int_0^\tau \mathrm{d}\tau\,\mathcal{E}(f)\right\}a_n, \qquad \tau = \Omega t \tag{5.10}$$

$$\frac{\mathrm{d}}{\mathrm{d}\tau}a_n = -k(\tau)\exp\left\{-\frac{\mathrm{i}}{\Omega_0}\int_0^\tau \mathrm{d}\tau\,\mathcal{E}(f)\right\}a_{n+1}, \tag{5.11}$$

where,

$$k(\tau) = \frac{FQ_1}{2\Delta E}\cos\tau \simeq -0.325\frac{nF_0}{\mathcal{E}}\cos\tau, \qquad \mathcal{E} = \frac{\Delta E(f)}{\omega(n)\hbar} = \frac{E_{n+1}(f) - E_n(f)}{\omega(n)\hbar}, \tag{5.12}$$

where $f(t) = F\sin\tau$ and Ω_0 is small. In section 5.3 below we shall need to know how the solutions of these equations depend upon the various system parameters, Ω_0, F_0 and n so here we note that $\mathcal{E}$ is independent of Ω_0, is a very slowly varying function of n and only weakly dependent upon F_0. The main dependence upon n comes from k and upon Ω_0 from the large Ω_0^{-1} factor in the exponent; for small frequencies this is the cause of all complications.

The two-state approximation is clearly valid provided k is small, which is normally the case when n is small as $F_0 < 0.13$. If n is large then k may also be large but even then a two-state approximation is valid provided Ω_0 is sufficiently small because the rapid oscillations in the exponent prevent growth of a_{n+1}.

Richards *et al.* (1989b) showed that the solution to these equations has resonances at the frequencies

$$\Omega_0 \simeq \frac{n(n+1/2)}{(n+1)^2 p} \quad (p \text{ a large integer}), \tag{5.13}$$

which is just the condition for the energy between adjacent unperturbed states to be an integer multiple of the photon energy . However, the approximation used to obtain the resonance positions gave their widths to be zero so in order to determine the widths of these resonances a more accurate solution to equations (5.10) and (5.11) is required.

5.2.1 Semiclassical approximations

Analytic approximations to the two-state equations which deal adequately with the high frequency oscillations are difficult to obtain. Semiclassical approximations to equations similar to these have been derived by Crothers and co-workers in the context of diabatic two-state collisions, see for instance Crothers and Hughes (1977) and Crothers (1976). This type of approximation begins by converting the two first-order equations into the second-order equation

$$\frac{\mathrm{d}^2}{\mathrm{d}\tau^2}a_{n+1} - \frac{1}{\Omega_0}\left(\mathrm{i}\mathcal{E} + \frac{\Omega_0}{k}\frac{\mathrm{d}k}{\mathrm{d}\tau}\right)\frac{\mathrm{d}}{\mathrm{d}\tau}a_{n+1} + k(\tau)^2 a_{n+1} = 0. \tag{5.14}$$

Since Ω_0 is small the Ω_0^{-1} term dominates except at those times at which $k(\tau) \simeq 0$, that is when the coupling is small. Uniform approximations[1] to this equation fail for the current problem because the original equations are unitary and this endows special properties onto equation (5.14) which are not shared by any comparison equation which could be used as a basis for a uniform approximation. As a consequence all the uniform approximations we could find failed to satisfy unitarity.

5.2.2 Bloch representation

In order to proceed we reformulate the equations of motion and then transform the new equations into a form in which the coupling is sufficiently weak for first-order perturbation theory to provide an accurate approximation. This procedure is carried out using the Pauli matrices, see for instance Landau and Lifshitz (1977, §55):

$$\sigma_1 = \begin{pmatrix} 0 & 1 \\ 1 & 0 \end{pmatrix}, \qquad \sigma_2 = \begin{pmatrix} 0 & -\mathrm{i} \\ \mathrm{i} & 0 \end{pmatrix}, \qquad \sigma_3 = \begin{pmatrix} 1 & 0 \\ 0 & -1 \end{pmatrix}, \tag{5.15}$$

having the commutator relations $[\sigma_j, \sigma_k] = 2\mathrm{i}\varepsilon_{jkl}\sigma_l$, and making the associations

$$|n, f\rangle \leftrightarrow \begin{pmatrix} 1 \\ 0 \end{pmatrix} \quad \text{and} \quad |n+1, f\rangle \leftrightarrow \begin{pmatrix} 0 \\ 1 \end{pmatrix}. \tag{5.16}$$

Then, if only two states dominate, Hamiltonian (5.3) may be written in terms of these matrices:

$$K = \frac{1}{2}\left(E_{n+1}(f) + E_n(f)\right)\mathrm{I}_2 - \frac{1}{2}\Delta E(f)\sigma_3 - k(t)\Omega\hbar\sigma_2. \tag{5.17}$$

where I_2 is the unit 2×2 matrix.

The motion produced by this Hamiltonian is most easily described in terms of the mean values of the Pauli matrices,

$$s_k(t) = \langle t|\sigma_k|t\rangle, \quad k = 1, 2, 3 \tag{5.18}$$

[1] Uniform approximations are described in appendix D.

with $|t\rangle$ being the wave function at time t:

$$|t\rangle = a_{n+1}|n+1, f\rangle \exp\left\{-\frac{\mathrm{i}}{\hbar}\int_0^t \mathrm{d}t\, E_{n+1}(t)\right\} + a_n|n, f\rangle \exp\left\{-\frac{\mathrm{i}}{\hbar}\int_0^t \mathrm{d}t\, E_n(t)\right\}. \quad (5.19)$$

In the Schrödinger representation the matrices, σ_k, have no explicit time dependence so the equations of motion for their mean values are

$$\frac{\mathrm{d}s_k}{\mathrm{d}t} = \frac{\mathrm{i}}{\hbar}\langle t|[K, \sigma_k]|t\rangle, \quad k = 1, 2, 3. \quad (5.20)$$

Using scaled units we can write these equations in the vector form

$$\frac{\mathrm{d}\boldsymbol{s}}{\mathrm{d}\tau} = \zeta(\tau)\begin{pmatrix} 0 & \cos\psi & -\sin\psi \\ -\cos\psi & 0 & 0 \\ \sin\psi & 0 & 0 \end{pmatrix}\boldsymbol{s} = -\zeta(\tau)\boldsymbol{M}\times\boldsymbol{s}, \quad (5.21)$$

where

$$\zeta(\tau) = \sqrt{4k^2 + (\mathcal{E}/\Omega_0)^2} \gg 1 \quad \text{and} \quad \tan\psi = \frac{2\Omega_0 k(\tau)}{\mathcal{E}(\tau)} \ll 1. \quad (5.22)$$

These equations have the same form as those normally associated with a two state atom, see for example Allen and Eberly (1975, page 39), but because we start with an adiabatic basis all the coefficients of s_k are time-dependent and some are varying very rapidly so the usual approximations, for example the rotating wave approximation, cannot be used.

The components of $\boldsymbol{s}$ are related to the original amplitudes by introducing real variables A, B, α and β such that $a_n(\tau) = Be^{\mathrm{i}\beta}$ and $a_{n+1}(\tau) = Ae^{\mathrm{i}\alpha}$ to give

$$s_1(\tau) + \mathrm{i}s_2(\tau) = 2AB\exp\mathrm{i}\left(\alpha - \beta - \frac{1}{\Omega_0}\int_0^\tau \mathrm{d}\tau\, \mathcal{E}(\tau)\right), \qquad s_3(\tau) = B^2 - A^2. \quad (5.23)$$

In particular the probabilities of being in the two states are

$$|a_n|^2 = B^2 = \frac{1}{2}(1 + s_3(\tau)), \qquad |a_{n+1}|^2 = A^2 = \frac{1}{2}(1 - s_3(\tau)). \quad (5.24)$$

Equation (5.21) provides a more graphic picture of the motion than the original equations of motion. Since $s_1^2 + s_2^2 + s_3^2 = 1$ the vector $\boldsymbol{s}(t)$ moves on the unit sphere; instantaneously it is rotating rapidly, with angular speed $\zeta(\tau) \gg 1$, about the slowly moving vector,

$$\boldsymbol{M}(\tau) = (0, \sin\psi, \cos\psi), \quad (5.25)$$

which itself oscillates slowly about the z-axis with small amplitude, periodic oscillations in the Oyz-plane. Note that because $\psi = O(\Omega_0)$, $\boldsymbol{M}$ is almost parallel to the z-axis. The combined motion is sketched in figure 5.1.

It is clear that the motion would appear simpler if viewed from the slowly moving reference frame with the new z-axis along $\boldsymbol{M}$. Thus we define a new vector, $\boldsymbol{x}$, by the

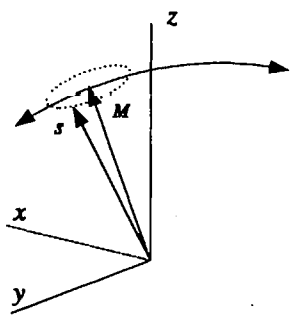

Figure 5.1 Diagram showing the how the motion of s comprises the rapid rotations about M, which itself is executing slow, periodic, small amplitude oscillations about the z-axis in the Oyz-plane.

equation $\boldsymbol{x} = \mathsf{R}_1(\tau)\boldsymbol{s}$, where R_1 is the time-dependent matrix

$$\mathsf{R}_1 = \begin{pmatrix} 1 & 0 & 0 \\ 0 & \cos\psi & -\sin\psi \\ 0 & \sin\psi & \cos\psi \end{pmatrix}, \tag{5.26}$$

in which the equations of motion take the simpler form

$$\frac{\mathrm{d}\boldsymbol{x}}{\mathrm{d}\tau} = \begin{pmatrix} 0 & \zeta & 0 \\ -\zeta & 0 & -\dot{\psi} \\ 0 & \dot{\psi} & 0 \end{pmatrix} \boldsymbol{x}, \quad \text{where} \quad \dot{\psi} = \frac{\mathrm{d}\psi}{\mathrm{d}\tau}. \tag{5.27}$$

Since $\zeta = O(\Omega_0^{-1})$ and $\dot{\psi} = O(\Omega_0)$ the dominant motion of $\boldsymbol{x}$ is a rapid rotation about the new z-axis with angular speed ζ; this suggests a final transformation

$$\boldsymbol{x} = \mathsf{R}_2(\tau)\boldsymbol{w} \quad \text{with} \quad \mathsf{R}_2 = \begin{pmatrix} \cos\eta & \sin\eta & 0 \\ -\sin\eta & \cos\eta & 0 \\ 0 & 0 & 1 \end{pmatrix} \tag{5.28}$$

and where

$$\eta(\tau) = \int_0^\tau \mathrm{d}\tau\, \zeta(\tau) = \frac{1}{\Omega_0} \int_0^\tau \mathrm{d}\tau\, \sqrt{\mathcal{E}^2 + 4\Omega_0^2 k^2}. \tag{5.29}$$

We shall see later that η is approximately the angle rotated by the original vector, $\boldsymbol{s}$. This brings the equations of motion to the final form

$$\frac{\mathrm{d}\boldsymbol{w}}{\mathrm{d}\tau} = \dot{\psi}\boldsymbol{a} \times \boldsymbol{w}, \quad \boldsymbol{a} = (\cos\eta, \sin\eta, 0), \quad \boldsymbol{w}_0 = \pm \begin{pmatrix} 0 \\ -\sin\psi_0 \\ \cos\psi_0 \end{pmatrix}, \tag{5.30}$$

where the sign for $\boldsymbol{w}_0 = \boldsymbol{w}(0)$ depends upon which state is initially populated, the upper sign being correct when $a_n(0) = 1$. The angle, ψ_0, is the initial value of ψ and is given by

$$\psi_0 = -\tan^{-1}\left(0.65\frac{\Omega_0 F_0 (n+1)^4}{n(n+\frac{1}{2})^2}\right). \tag{5.31}$$

Again $\boldsymbol{w}(\tau)$ is connected to $\boldsymbol{w}_0$ by a rotation, but as $\dot{\psi} = O(\Omega_0)$ the angle of rotation is small. Moreover the vector $\boldsymbol{a}$ is rotating very rapidly about the z-axis so on average $\boldsymbol{w}$ changes very little: we shall see later that for $\Omega_0 \ll 1$ the angle of rotation Φ_w is very small and, for a fixed τ, decreases very rapidly as $\Omega_0 \to 0$.

The vector, $\boldsymbol{w}$, changes very little and so its motion can be approximated using first-order perturbation theory; so if $\boldsymbol{m}(\tau)$ is the direction of the rotation connecting $\boldsymbol{w}(\tau)$ to $\boldsymbol{w}_0$,

$$\Phi_w(\tau) \simeq \sqrt{I_c^2 + I_s^2}, \qquad \boldsymbol{m}(\tau) \simeq -(I_c, I_s, 0)/\Phi_w \tag{5.32}$$

where

$$I_c + \mathrm{i}I_s = \int_0^\tau \mathrm{d}\tau\, \dot{\psi}(\tau) e^{\mathrm{i}\eta(\tau)}. \tag{5.33}$$

On using the vector representation of a finite rotation, Goldstein (1980, page 165) we obtain the approximate solution to equation (5.30)

$$\boldsymbol{w}(\tau) = \boldsymbol{w}_0 \cos\Phi_w + \boldsymbol{m}(\boldsymbol{m}\cdot\boldsymbol{w}_0)(1-\cos\Phi_w) + (\boldsymbol{w}_0 \times \boldsymbol{m})\sin\Phi_w, \tag{5.34}$$

which can also be written in the matrix form, $\boldsymbol{w}(\tau) = \mathsf{W}(\tau)\boldsymbol{w}_0$. The advantage of writing the approximate solution of equation (5.30) in this form is that it preserves unitarity.

Finally, we collect together all the rotations to relate the initial and final values of $\boldsymbol{s}$,

$$\boldsymbol{s}(\tau) = \mathsf{R}(\tau)\boldsymbol{s}(0), \quad \mathsf{R}(\tau) = \mathsf{R}_1(\psi)^{-1}\mathsf{R}_2(\eta)\mathsf{W}(\tau)\mathsf{R}_1(\psi_0). \tag{5.35}$$

Note that the only approximation used in deriving this solution is the approximation of equation (5.32) for Φ_w and $\boldsymbol{m}$. Since R_1 and W are close to the identity it is tempting to assume that a good approximation to $\boldsymbol{s}(\tau)$ is obtained by a simple rotation about the z-axis due to R_2. However, $\boldsymbol{s}(0) = \pm\hat{\boldsymbol{z}}$, so this motion itself does not produce any transitions: these are caused by the small modulations due to R_1 and W which are therefore very important. It is this combination of the rapid rotations of R_2 and the small slow oscillations which causes difficulties in finding accurate solutions and also accounts for their complicated behaviour.

On using equations (5.24) and (5.35) we obtain approximations for the probability, $|a_n|^2$. In figure 5.2 we compare this approximate solution for $|a_n|^2$, the full curve, with that obtained from the numerical integration of the original equations (5.10) and (5.11), the broken curve, for $0 \le \tau \le 2\pi$ with $n = 38$, $\Omega_0 = 0.1$ and $F_0 = 0.12$. The $1/\Omega_0$

oscillations of $|a_n(t)|$ are due to the rotations caused by R_2; the other more complicated variations are produced by R_1 and W. At lower frequencies the approximation is even better; for instance at $\Omega_0 = 0.01$, where there are 100 oscillations, these differences are at worst 2×10^{-7}.

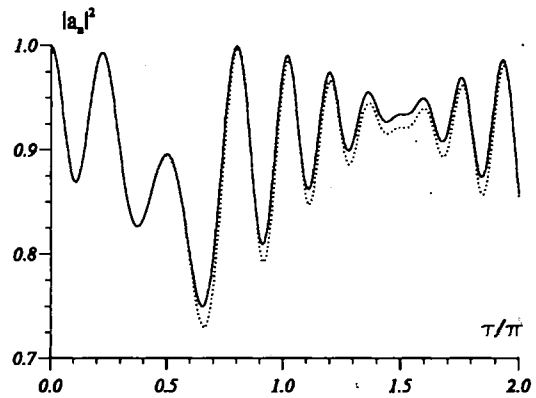

Figure 5.2 Graphs showing $|a_n|^2$ as a function of τ in the case $n = 38$, $\Omega_0 = 0.1$ and $F_0 = 0.121$. The solid line depicts the approximate solution given by equation (5.35), the dotted line is the exact result obtained by solving equations (5.10) and (5.11) numerically.

5.3 Mean probabilities and resonance widths

The equations of motion (5.21) for $\boldsymbol{s}(\tau)$ are linear and have 2π-periodic coefficients and so Floquet's theory can be used to infer that there exists a matrix U relating solutions at the times τ and $\tau + 2\pi$. Thus, we can obtain the long-time behaviour of the system from a knowledge of the solutions at $\tau = 2\pi$:

$$\boldsymbol{s}(\tau + 2\pi) = \mathsf{U}\boldsymbol{s}(\tau) \quad \text{and} \quad \boldsymbol{s}(\tau + 2N\pi) = \mathsf{U}^N \boldsymbol{s}(\tau), \quad \text{for all } \tau. \tag{5.36}$$

Further, since $\boldsymbol{s}$ is confined to lie on the surface of a unit sphere, U represents a rotation through an angle, Φ, in the direction of a unit vector, $\boldsymbol{n}$. On setting $\tau = 0$, so $\mathsf{U} = \mathsf{R}(2\pi)$, and using the vector representation in equation (5.34) we obtain the following expression for $\boldsymbol{s}$ after N field periods,

$$\boldsymbol{s}(2N\pi) = \boldsymbol{s}(0)\cos N\Phi + \boldsymbol{n}(\boldsymbol{s}(0)\cdot\boldsymbol{n})(1 - \cos N\Phi) + (\boldsymbol{s}(0)\times\boldsymbol{n})\sin N\Phi, \tag{5.37}$$

where Φ and $\boldsymbol{n}$ are the angle and direction of the rotation defined by $\mathsf{R}(2\pi)$.

Now suppose that the system is initially in the lower state, $|\vec{n}, f\rangle$; so that, from equation (5.24), $\boldsymbol{s}(0) = (0,0,1)$; the probability of being in the lower state at time

$\tau = 2N\pi$ is then

$$\begin{aligned} P(n,N) &= \frac{1}{2}\left(1 + \boldsymbol{s}(2N\pi)\cdot\hat{\boldsymbol{z}}\right) \\ &= \frac{1}{2}\left(1+n_3^2\right) + \frac{1}{2}\left(1-n_3^2\right)\cos N\Phi, \quad n_3 = \boldsymbol{n}\cdot\hat{\boldsymbol{z}}. \end{aligned} \tag{5.38}$$

The mean probability of staying in the initial state over M field periods is defined to be

$$\begin{aligned} \overline{P}(n) &= \frac{1}{M}\sum_{N=1}^{M} P(n,N) \\ &= \frac{1}{2}\left(1+n_3^2\right) + \frac{1}{2}\left(1-n_3^2\right)\frac{\sin(M\Phi/2)\cos((M+1)\Phi/2)}{M\sin\Phi/2}. \end{aligned} \tag{5.39}$$

If Φ is an integer multiple of 2π then $\overline{P}(n) = 1$; otherwise, if M is sufficiently large the second term is small and we have

$$\overline{P}(n) = \frac{1}{2}\left(1+n_3^2\right), \quad \Phi \neq 2\pi p, \quad M \text{ large}, \tag{5.40}$$

so when $n_3 = 0$, $\overline{P}(n) = \overline{P}(n+1) = \frac{1}{2}$. The continuum enters the equations of motion via decay terms with decay from the upper state being much faster than that from the lower state, see Richards (1987, equation (3.27)). In Richards *et al.* (1989b) it was shown that the inclusion of decay, other than destroying unitarity, does not significantly alter the relative values of $\overline{P}(n)$ and $\overline{P}(n+1)$, so that when $n_3 = 0$ the ionization probability is enhanced, see for instance figure 5 of Richards *et al.* (1989b) which shows how peaks in the ionization probability coincide with the resonance positions computed assuming no decay.

In figures 5.3 and 5.4 we compare the exact and approximate values of $\overline{P}(n)$. The approximate values, depicted by the solid line, are obtained using equation (5.35) to find n_3, while the exact solution is obtained using the Floquet methods described by Richards *et al.* (1989b), see also section 2.3.3 of chapter 2 above. In figure 5.3 we show results in the vicinity of $\Omega_0 = 0.09$ and see that the approximation predicts the position and width of the resonance quite accurately. In figure 5.4 we continue figure 5.3 to lower frequencies and observe that the exact and approximate results are barely distinguishable. We also note that, apart from the regular array of ever narrowing resonances, $\overline{P}(n)$ has a rather erratic behaviour in between resonances: for instance at $\Omega_0 \simeq 0.0515$ and 0.062, $\overline{P}(n) \simeq 1$ while at $\Omega_0 \simeq 0.07$ it is smaller. From equation (5.40) it is clear that all these features are a consequence of the dependence of n_3 upon Ω_0, so we now turn to a more detailed analysis of the behaviour of the approximate solution upon Ω_0.

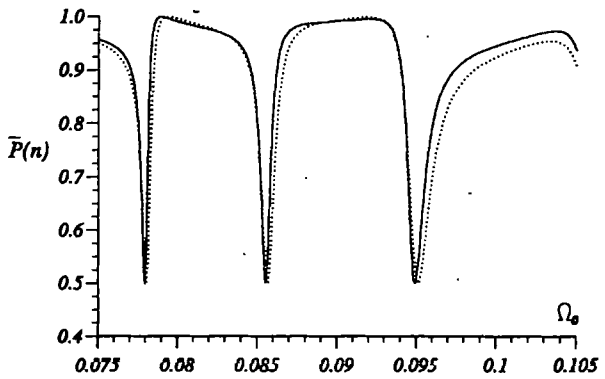

Figure 5.3 Graphs showing $\overline{P}(n)$ as a function of Ω_0 in the case $n = 38$ and $F_0 = 0.121$. The solid line depicts the approximate solution given by equations (5.35) and (5.40), the dotted line is the exact result obtained by solving equations (5.10) and (5.11) numerically.

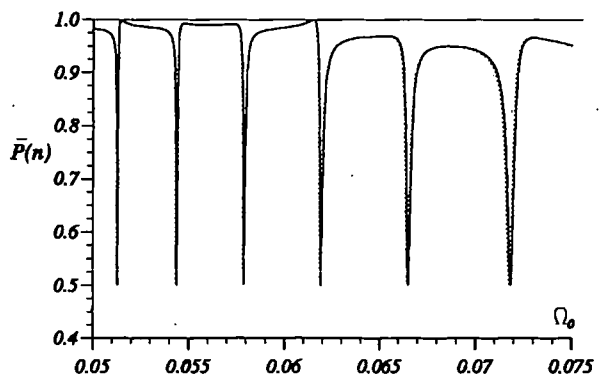

Figure 5.4 As in figure 5.3, but showing $\overline{P}(n)$ over a different frequency range: the solid line depicts the approximate solution and the dotted line is the exact result.

5.3.1 Frequency dependence of the solution

The angle of the rotation, Φ, connecting $\boldsymbol{s}(0)$ to $\boldsymbol{s}(2\pi)$, equation (5.37), is given by the relation

$$\begin{aligned} 2\cos\Phi + 1 &= \mathrm{Tr}(\mathsf{R}) = \mathrm{Tr}(\mathsf{R}_2\mathsf{W}) \\ &= (1+\cos\Phi_w)\cos\eta + \cos\Phi_w \\ &\quad -2m_3\sin\eta\sin\Phi_w + 4m_3^2\sin^2(\Phi_w/2)\sin^2(\eta/2). \end{aligned} \tag{5.41}$$

This relation is exact, but if the approximation defined in equation (5.32) is used then $m_3 = 0$ and the last two terms are zero: henceforth we shall normally assume that $m_3 = 0$.

The direction, $\boldsymbol{n}$, is more difficult to obtain and can only be found by considering the action of R on two linearly independent vectors. Consider the vectors $\boldsymbol{x}_k = \mathsf{R}\boldsymbol{a}_k$, $k = 1, 2, 3$, with $\boldsymbol{a}_k$ the unit vectors along the axes. Then from equation (5.37) we obtain

$$R_{kj} = \boldsymbol{x}_j \cdot \boldsymbol{a}_k = \delta_{kj}\cos\Phi + n_k n_j(1-\cos\Phi) + \varepsilon_{kjl}n_l\sin\Phi, \tag{5.42}$$

so

$$2n_3\sin\Phi = R_{12} - R_{21}. \tag{5.43}$$

Thus, provided $\sin\Phi \neq 0$, $n_3 = 0$ when $R_{21} - R_{12} = 0$ or, on using approximation (5.32) so that $m_3 = 0$,

$$\begin{aligned} 2\cos(\eta/2)\Big\{\sin(\eta/2)\left[(1+\cos\Phi_w)\cos\psi + m_1\sin\Phi_w\sin\psi\right] \\ - m_2\sin\Phi_w\sin\psi\cos(\eta/2)\Big\} &= 0, \end{aligned} \tag{5.44}$$

where $\psi = \psi(0)$ since $\tau = 2\pi$. We now consider the roots of this equation.

One solution is $\cos(\eta/2) = 0$ making η an odd multiple of π; from equation (5.41) we see that this gives $\cos\Phi = -1$ so that $\Phi = \pi$. In this case we cannot use equation (5.43) to find n_3, but instead we have

$$\boldsymbol{n} \propto \boldsymbol{s}(0) + \boldsymbol{s}(2\pi) \quad \text{giving} \quad n_3 = \sqrt{\frac{1+R_{33}}{2}}, \quad (\cos\eta - -1), \tag{5.45}$$

where, for $\cos\eta = -1$ and $m_3 = 0$,

$$\begin{aligned} R_{33} &= \cos 2\psi\cos\Phi_w + m_1\sin 2\psi\sin\Phi_w - 2m_2^2\sin^2(\Phi_w/2)\sin^2\psi \\ &\simeq 1 - 2\psi^2 + 2m_1\psi\Phi_w - \frac{1}{2}\Phi_w^2. \end{aligned} \tag{5.46}$$

Some typical values of ψ and Φ_w are shown in figure 5.5, for the case $n = 38$, $F_0 = 0.121$, as a function of Ω_0. Since both ψ and Φ_w are small we see that $n_3 \simeq 1$ when

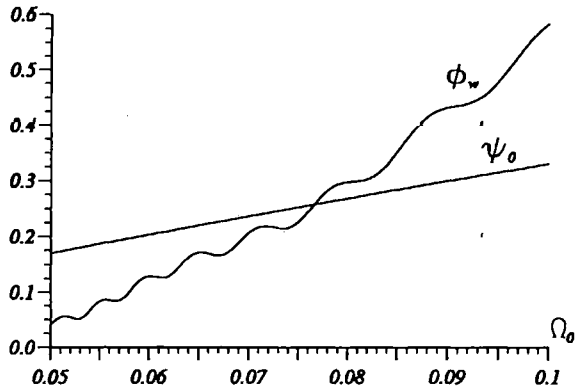

Figure 5.5 Graphs showing some values of ψ, equation (5.31) and Φ_w, equation (5.32) as a function of Ω_0 in the case $n = 38$ and $F_0 = 0.121$.

$\cos\eta \simeq -1$: indeed, for very small Ω_0, $|\Phi_w| \ll \psi \propto \Omega_0$ so in this limit $n_3 \simeq 1 - \frac{1}{2}\psi^2$ and $\overline{P}(n) = 1 - O(\Omega_0^2)$ when $\cos\eta = -1$, that is in between resonances.

The other solution is given by the roots of the equation

$$\sin(\eta/2) = \frac{m_2 \cos(\eta/2) \sin\Phi_w \sin\psi}{(1+\cos\Phi_w)\cos\psi + m_1 \sin\Phi_w \sin\psi}. \tag{5.47}$$

The left hand side of this equation varies between ± 1 as η changes from π to 3π, that is as Ω_0 changes by a quantity Ω_0^2, see equation (5.49) below. On the other hand the right hand side is always very small so the roots must be near $\eta = 2\pi p$, for some large integer p, but to determine the corrections, upon which the behaviour at resonance depend, we need an estimate of Φ_w. In the integral (5.33), from which Φ_w is obtained, the function $\dot{\psi}$ is $O(\Omega_0)$ and 2π-perodic whereas the exponent is monotonic increasing from zero to about $2\pi/\Omega_0 \gg 1$. A good approximation to this integral is obtained by ignoring the term $O(\Omega_0^2)$ in the phase integrand to give the slightly simpler integral

$$I(\Omega_0) = \int_0^{2\pi} \mathrm{d}\tau\, \dot{\psi}(\tau) \exp\left(\frac{\mathrm{i}}{\Omega_0}\int_0^{\tau} \mathrm{d}\tau\, \mathcal{E}(\tau)\right). \tag{5.48}$$

When $\eta = \frac{1}{\Omega_0}\int_0^{2\pi} \mathrm{d}\tau\, \mathcal{E}(\tau) = 2\pi p$, that is $\Omega_0 \simeq 1/p$, we can change variables to express the integral (5.48) in the form $\int_0^{2\pi} \mathrm{d}y\, f(y) e^{\mathrm{i}py}$ where $f(y)$ is a 2π-periodic, analytic function of y. In this case $I(\Omega_0)$ decreases faster than any power of p, that is $|I| < \Omega_0^{-N}$ for any $N > 0$. For other values of Ω_0, I is larger as there is incomplete cancellation of the oscillations. However, we need an estimate of I near the points where $\eta = 2\pi p$, so we shall assume that $I(\Omega_0)$ does not change sufficiently rapidly near here to invalidate this assumption; we demonstrate numerically that this is true in figure 5.6.

In appendix F we show that near a resonance $\Phi_w = |I|$ decreases as $\Omega_0^{1/2}\exp(-C/\Omega_0)$, for some positive constant C. In order to illustrate this behaviour we consider a rather

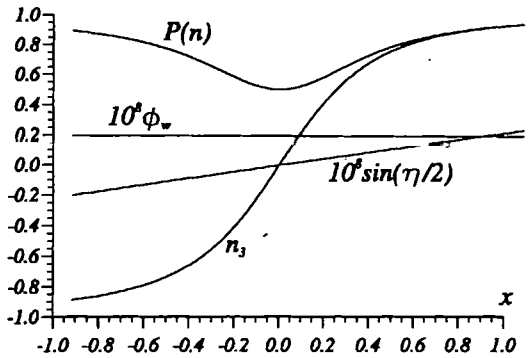

Figure 5.6 Graphs showing the variation of various functions near the resonance at $\Omega_0 \simeq 0.011544688470691$ as a function of $x = (\Omega_0 - 0.011544688470691)^{13}$ for $n = 38$ and $F_0 = 0.121$.

extreme case, the resonance at $\Omega_0 \simeq 0.011544688470691$, having a width of $\delta\Omega_0 \simeq 10^{-13}$. In figure 5.6 we show graphs of $\overline{P}(n)$, n_3, Φ_w and $\sin(\eta/2)$ over the width of the resonance for $n = 38$ and $F_0 = 0.121$.

These numerical results are representative of all cases we have considered and show clearly that Φ_w changes little over the width of the resonance.

We have shown that the positions of the resonances are at the roots of equation (5.47) and we see from the above analysis that $\eta - 2\pi p = O(\Omega_0^{3/2}\exp(-C\Omega_0^{-1}))$. In this case $\cos\eta \simeq 1$ and from equation (5.41) we see that $\Phi \simeq \Phi_w$, and that equation (5.43) is applicable which confirms that the solution of equation (5.47) gives the zeros of n_3 and hence the positions of the minimum of $\overline{P}(n)$, equation (5.40), as shown in figures 5.3 and 5.4. By comparing the graphs in figure 5.5 with those in figures 5.3 and 5.4 we see that this is true for all $\Omega_0 < 0.1$; we have not considered larger frequencies.

5.3.2 Resonance widths

Finally we are in a position to determine the width of the minima of $\overline{P}(n)$ as a function of Ω_0, which is determined by the rate at which n_3 passes through zero as Ω_0 changes. Suppose that Ω_r is a resonance frequency, $n_3(\Omega_r) = 0$; then for a nearby frequency, $\Omega_0 = \Omega_r + \delta\Omega_0$, we have $\delta n_3 = n_3'(\Omega_r)\delta\Omega_0$. The derivative of n_3 at a resonance is obtained by differentiating equation (5.43) to give $n_3' = (\partial\eta/\partial\Omega_0)/\Phi_w$, but from the definition of η, equation (5.29), we have

$$\frac{\partial\eta}{\partial\Omega_0} = -\frac{1}{\Omega_0^2}\int_0^{2\pi} \mathrm{d}\tau \, \frac{\mathcal{E}^2}{\sqrt{\mathcal{E}^2 + 4k^2\Omega_0^2}} \simeq -\frac{2\pi}{\Omega_0^2} \tag{5.49}$$

so that

$$\delta n_3 = -\frac{2\pi\delta\Omega_0}{\Omega_0^2\Phi_w(\Omega_0)}. \tag{5.50}$$

Thus on using the above estimate for $\Phi_w(\Omega_0)$ we see that the width of the resonance decreases as $\Omega_0^{5/2}e^{-C/\Omega_0}$. This very rapid decrease in resonance widths with decreasing frequency is the main reason why none were seen in Sauer *et al.* (1992); for example at $n = 28$, $F_0 = 0.123$, typical of the parameters considered in Sauer *et al.* (1992), there is a resonance at $\Omega_0 = 0.033236$ with a width $\delta\Omega_0 = 2 \times 10^{-5}$, whereas the experiment was at a scaled frequency $\Omega_0 = 0.03307$ while at $n = 24$, $\Omega_0 = 0.02083$, the nearest resonance is at $\Omega_0 = 0.0206$ having a width $\delta\Omega_0 \simeq 10^{-6}$.

5.4 Conclusions

In this chapter we have studied the behaviour of a one-dimensional hydrogen atom in the presence of a low frequency, harmonic electric field in the limit as the field frequency tends to zero. For the small scaled frequencies $\Omega_0 \simeq p^{-1}$, p being a large integer, there are resonances at which the ionization probability is enhanced and we have shown that the width of each resonance is of order $\Omega_0^{5/2}\exp(-C/\Omega_0)$. Our analysis is based upon the two-state approximation to the coupled equations of motion but, since an adiabatic basis is used, this is a good approximation at low frequencies. In order to find the resonance widths we have found a new, accurate solution to these equations. The rapid decrease in the width as $\Omega_0 \to 0$ explains why low frequency resonances were not found in the experiments reported in Sauer *et al.* (1992).

The relationship of this one-dimensional model to a real three-dimensional atom remains an open question. However, it should be noted that a number of quite subtle features seen in experimental results can be explained by this one-dimensional model. For instance, the threshold fields for ionization in both one- and three-dimensional atoms agree remarkably well, provided the scaled field is not too large, while the positions of the resonances near $\Omega_0 = 1/3$, $1/2$ and 1, for example, agree well, as does the classical behaviour near them. Finally, we note that the one-dimensional model provides accurate positions of, and qualitatively accurate behaviour near, the low frequency resonances, see Richards *et al.* (1989b). Thus, it seems reasonable to assume that the result obtained here will be similar to the true resonance width of the three-dimensional atom. However, it is not clear how the equivalent analysis for these atoms should proceed without making further approximations.

Appendix A

Gauge invariance of the resonance overlap condition

In this appendix we show that each of the three Hamiltonians (1.27), (1.33) and (1.37), derived in section 1.7, yield identical expressions for the critical field strength , F_{CH} of equation (1.65) given on page 28 and derived using the Chirikov (1979) resonance overlap condition, above which a significant proportion of orbits become unstable.

The dipole gauge

For convenience, we start with the dipole gauge Hamiltonian, equation (1.33), which we write in the form,

$$H_d(q_1,p_1,t) = H_0(q_1,p_1) + q_1 F \sin\Omega t, \tag{A.1}$$

$$H_0(q_1,p_1) = \frac{1}{2\mu}p_1^2 + V(q_1), \tag{A.2}$$

where, for convenience, we have set $\lambda(t) = 1$ and $\delta = 0$.

As in section 1.5 we express Hamiltonian (A.1) in terms of the angle-action variables, (θ, I), of the unperturbed Hamiltonian, H_0:

$$H_d(\theta,I,t) = H_0(I) + q_1(\theta,I)\sin\Omega t. \tag{A.3}$$

The variable, $q_1(\theta,I)$, is a 2π-periodic function of θ and hence may be expressed as the Fourier series

$$q_1(\theta,I) = \sum_{s=-\infty}^{\infty} Q_s(I)e^{-is\theta}, \tag{A.4}$$

where

$$Q_s(I) = \frac{1}{2\pi}\int_0^{2\pi} d\theta\, q_1(\theta,I)e^{is\theta}, \qquad Q_s = Q^*_{-s} = |Q_s|\exp(-i\gamma_s). \tag{A.5}$$

Substituting equation (A.4) into Hamiltonian (A.3) gives

$$H_d(\theta,I,t) = H_0(I) + \frac{F}{2i}\sum_{s=-\infty}^{\infty} Q_s(I)\{e^{-i(s\theta-\Omega t)} - e^{-i(s\theta+\Omega t)}\}. \tag{A.6}$$

Resonances occur when $s = \pm r$ so that $r\theta = \Omega t$, that is at $\Omega = r\omega$. On ignoring the rapidly varying terms, an approximation to Hamiltonian (A.6) in the vicinity of the resonance at $\Omega = r\omega$ is, on using equation (A.5),

$$H_d(\theta, I, t) \simeq H_0(I) - F|Q_r(I)|\sin(r\theta - \Omega t + \gamma_r). \tag{A.7}$$

The momentum gauge

The momentum gauge Hamiltonian, equation (1.27), is

$$H_m(q, p, t) = H_0(q, p) + \frac{p}{\mu\Omega}\cos\Omega t, \tag{A.8}$$

where the conjugate variables, (q, p) and (q_1, p_1) are related by equation (1.34);

$$p = p_1 - \frac{F}{\Omega}\cos\Omega t, \qquad q = q_1. \tag{A.9}$$

The crucial point here is that the dependency of H_0 upon (q_2, p_2) is given by equation (A.2) with (q_1, p_1) replacing (q_1, p_1); we can therefore use the *same* angle-action variables to write Hamiltonian (A.8) as

$$H_m(\theta, I, t) = H_0(I) + \frac{F}{\mu\Omega}p(\theta, I)\cos\Omega t. \tag{A.10}$$

Now, from Hamilton's equations for the unperturbed motion, we have

$$\dot{q}(\theta, I) = \dot{q}_1(\theta, I) = \frac{\partial H_0}{\partial p} = \frac{p(\theta, I)}{\mu}, \tag{A.11}$$

so that

$$p(\theta, I) = \mu\dot{q}_1(\theta, I) = -\mathrm{i}\mu\omega(I)\sum_{s=-\infty}^{\infty} sQ_s(I)e^{-\mathrm{i}s\theta}, \quad \text{where } \dot{\theta} = \frac{\partial H_0}{\partial I} = \omega(I). \tag{A.12}$$

On using equation (A.12), Hamiltonian (A.10) becomes,

$$H_m(\theta, I, t) = H_0(I) - \frac{\mathrm{i}F\omega(I)}{\Omega}\sum_{s=-\infty}^{\infty} sQ_s(I)\{e^{-\mathrm{i}(s\theta-\Omega t)} + e^{-\mathrm{i}(s\theta+\Omega t)}\}. \tag{A.13}$$

Thus, in the vicinity of the resonance at $s = \pm r$ we obtain an approximation to H_m:

$$H_m(\theta, I, t) \simeq H_0(I) - F|Q_r(I)|\sin(r\theta - \Omega t + \gamma_r). \tag{A.14}$$

The acceleration gauge

The acceleration gauge Hamiltonian, equation (1.37), is

$$H_a(q_2, p_2, t) = \frac{1}{2\mu}p_2^2 + V(q_2 - b(t)), \qquad b(t) = \frac{F}{\mu\Omega^2}\sin\Omega t, \tag{A.15}$$

where,

$$p_2 = p_1 - \frac{F}{\Omega}\cos\Omega t \quad \text{and} \quad q_2 = q_1 - \frac{F}{\mu\Omega^2}\sin\Omega t. \tag{A.16}$$

For high frequencies, an approximation to Hamiltonian (A.15) is given by equation (1.72) given on page 29:

$$H_a(q_2, p_2, t) \simeq H_0(q_2, p_2) + \frac{F}{\mu\Omega^2}\sin\Omega t \frac{\partial V}{\partial q_2}. \tag{A.17}$$

Again the dependency of H_0 upon (q_2, p_2) is given by equation (A.2) with (q_2, p_2) replacing (q_1, p_1) and so again we can use the same angle-action variables to re-write H_a as

$$H_a(\theta, I, t) \simeq H_0(I) + \frac{F}{\mu\Omega^2}\sin\Omega t \frac{\partial V}{\partial q_2}(\theta, I). \tag{A.18}$$

On considering the unperturbed motion we see that the equations of motion are,

$$\dot{p}_2 = -\frac{\partial H_0}{\partial q_2} = -\frac{\partial V}{\partial q_2}, \qquad \dot{q}_2 = \frac{\partial H_0}{\partial p_2} - \frac{p_2}{\mu}, \tag{A.19}$$

and so we have

$$\frac{\partial V}{\partial q_2}(\theta, I) = -\mu\ddot{q_2}(\theta, I) = \mu\omega(I)^2 \sum_{s=-\infty}^{\infty} s^2 Q_s(I) e^{-\mathrm{i}s\theta}, \tag{A.20}$$

where again we have used $\dot{\theta} = \partial H_0/\partial I = \omega(I)$. Substituting equation (A.20) into equation (A.18) gives,

$$H_a(\theta, I, t) \simeq H_0(I) + \frac{F\omega(I)^2}{2\mathrm{i}\Omega^2} \sum_{s=-\infty}^{\infty} s^2 Q_s(I)\{e^{-\mathrm{i}(s\theta - \Omega t)} - e^{-\mathrm{i}(s\theta + \Omega t)}\} \tag{A.21}$$

and so, in the vicinity of the resonance at $s = \pm r$ an approximation to H_a is

$$H_a(\theta, I, t) \simeq H_0(I) - F|Q_r(I)|\sin(r\theta - \Omega t + \gamma_r), \tag{A.22}$$

where $\Omega \simeq r\omega$.

Thus the approximate Hamiltonians, equations (A.7), (A.14) and (A.22) take the same form in each of the three gauges and the gauge-invariance of the overlap criterion, equation (1.65), follows. A similar analysis can be used to prove the gauge invariance of the classical map, equations (1.91) and (1.92).

Appendix B

Sudden ionization: classical

In this appendix, we outline the calculation of the classical ionization probabilities for the Morse potential, described by equation (3.1), when the oscillating field is switched on suddenly. In section 1.6, we obtained the following expression for the value of the momentum, p_1, at which the initial unperturbed torus intersects the separatrix of the mean-motion Hamiltonian,

$$-2p_1\frac{F}{\Omega}\cos\delta+\left(\frac{F}{\Omega}\right)^2\cos^2\delta\simeq 2\mu(\overline{E}^S-E_d). \tag{B.1}$$

In terms of the variables $\mathcal{A}_s$ and $\mathcal{A}_0$, introduced in section 3.2, $2\mu\overline{E}^S = a^2\mathcal{A}_s^2$ and $2\mu E_d = a^2\mathcal{A}_s^2\mathcal{A}_0(2-\mathcal{A}_0)$, which gives,

$$p_1 = a\mathcal{A}_s(1-\mathcal{A}_0)\mathcal{P}, \tag{B.2}$$

$$\mathcal{P} = \frac{(\beta^2\cos^2\delta-4r^2(1-\mathcal{A}_0)^4)}{4r(1-\mathcal{A}_0)^2\beta\cos\delta}, \tag{B.3}$$

and where we have written $\Omega=\mathcal{A}_s r a^2(1-\mathcal{A}_0)/\mu$ and $F=a^3\mathcal{A}_s^2\beta/2\mu$.

We now find the values of the angle variables, $\theta_{1,2}$, at which the intersection takes place by using equations (3.3) and (3.4) to write p_1 in terms of the action-angle variables. Substituting the resulting expression into equation (B.3) gives,

$$\frac{\sqrt{\epsilon}\sin\theta}{1-\sqrt{\epsilon}\cos\theta}=\mathcal{P}, \tag{B.4}$$

Rearranging this and using equation (3.5) to rewrite ϵ in terms of $\mathcal{A}_0$ gives,

$$\sin(\theta_{1,2}+\gamma)=\frac{\mathcal{P}}{\sqrt{\mathcal{A}_0(2-\mathcal{A}_0)(1+\mathcal{P}^2)}},\quad \tan\gamma=\mathcal{P}. \tag{B.5}$$

The difference, $|\theta_1-\theta_2|/2\pi$ is then the ionization probability which can be averaged over the field phase to give our final expression:

$$P_{SUD}(\beta,\mathcal{A}_0,r)=\frac{1}{2\pi^2}\int_0^{2\pi}\mathrm{d}\delta\,\cos^{-1}\left(\frac{\mathcal{P}(\delta)}{\sqrt{\mathcal{A}_0(2-\mathcal{A}_0)(1+\mathcal{P}(\delta)^2)}}\right). \tag{B.6}$$

This is used to compute the theoretical ionization probability curves shown in figures 3.11 and 3.12.

Appendix C

Sudden ionization: quantal

Here we show how the quantal-sudden ionization probability is related to the classical sudden probability of equation (B.6), derived in appendix B, and that in the classical limit they are identical. We assume that for times $t < 0$ the dipole Hamiltonian, equation (1.33) with $F = 0$, describes the system, and for $t > 0$ that the Hamiltonian of equation (1.37) is a good approximation. At $t = 0$ there is a transition in momentum,

$$p_2 = p_1 - (F/\Omega)\cos\delta, \tag{C.1}$$

so that the wave functions $\psi_\pm$ immediately before and after $t = 0$ are related by,

$$\begin{aligned} \psi_+ &= \psi_- \exp\left(-\mathrm{i}\frac{Fq\cos\delta}{\Omega\hbar}\right) \\ &= \sum a_k \overline{\psi}_k(q) + \int_{E^S}^{\infty} \mathrm{d}E\, a(E)\overline{\psi}(E,q) \end{aligned} \tag{C.2}$$

where $\overline{\psi}$ are the eigenstates of $\overline{H}$ and ψ_-, the initial state, is an eigenstate of H_d. Then, assuming that the continuum wave functions are delta-function normalized in energy the ionization amplitude is,

$$a(E) = \int_{-\infty}^{\infty} \mathrm{d}q\, \overline{\psi}^*(E,q)\psi_n(q) \exp\left(-\mathrm{i}\frac{Fq\cos\delta}{\Omega\hbar}\right). \tag{C.3}$$

Since the quantum numbers are large we use the WKB approximations.

$$\overline{\psi}(E,q) = \sqrt{\frac{2\mu}{\pi\hbar p(E,q)}} \sin\left(\frac{1}{\hbar}\int_{a_2(E)}^{q} \mathrm{d}x\, p(E,x) + \varphi(E)\right), \tag{C.4}$$

$$\psi_n(q) = \sqrt{\frac{2\mu\omega(E_n)}{\pi p(E_n,q)}} \sin\left(\frac{1}{\hbar}\int_{a_1}^{q} \mathrm{d}x\, p(E_n,x) + \frac{\pi}{4}\right), \tag{C.5}$$

where a_k, $k = 1, 2$ are the inner turning points. Then the transition amplitude is, on ignoring the rapidly varying terms,

$$\begin{aligned} a(E) &= \frac{\mu}{\pi}\sqrt{\frac{\omega(E_n)}{\hbar}} \int_{a_3}^{b} \mathrm{d}q\, \frac{\exp\left(-\mathrm{i}\frac{Fq\cos\delta}{\Omega\hbar}\right)}{\sqrt{p(E,q)p(E_n,q)}} \\ &\times \cos\left(\frac{1}{\hbar}\int_{a_3}^{q} \mathrm{d}x\, \left(p(E,x) - p(E_n,x)\right) + \varphi(E) - \frac{\pi}{4}\right), \end{aligned} \tag{C.6}$$

where $a_3 = \max(a_1, a_2)$ and b is the outer turning point.

This integral may be evaluated using the stationary phase approximation with the stationary phase points at the real roots, q_1 and q_2, of,

$$\Delta p(q) = p(E, q) - p(E_n, q) = \pm \frac{F \cos\delta}{\Omega}. \tag{C.7}$$

Remembering that $p(q) > 0$ and that $E > E_n$ we see that for each sign of equation (C.7) only one part of the cosine in equation (C.6) contributes and so we have,

$$a(E) = \mu \sqrt{\frac{\omega(E_n)}{2\pi}} \sum_{k=1}^{2} \frac{\exp\left\{\frac{\mathrm{i}}{\hbar}\left(\int_{a_3}^{q_k} \mathrm{d}x\, \Delta p(x) + \varphi(E) - \frac{\pi}{4} - \frac{F q_k \cos\delta}{\Omega}\right) + \mathrm{i}\frac{\pi\sigma_k}{4}\right\}}{\sqrt{p(E, q_k) p(E_n, q_k) |\Delta p'(q_k)|}}, \tag{C.8}$$

where the Maslov indices are $\sigma_1 = 1$ and $\sigma_2 = -1$. The classical limit is obtained by ignoring the interference terms, and on using the relation,

$$p(E, q) p(E_n, q) \Delta p'(q) = \mu V'(q) \Delta p(q), \tag{C.9}$$

where we assume α small so that $\overline{V}(q, \alpha) \simeq V(q)$, we see that,

$$|a(E)|^2 = \frac{\mu\omega(E_n)}{2\pi|\Delta p|}\left(\frac{1}{|V'(q_1)|} - \frac{1}{|V'(q_2)|}\right). \tag{C.10}$$

However, the classical probability is just,

$$P^{cl}(E) = \frac{1}{2\pi}\left|\theta_2'(E) - \theta_1'(E)\right|, \tag{C.11}$$

where θ_k are the two roots of $\mu E(\theta) = p(E_n, q(\theta))\Delta p$ and since,

$$\mu \frac{\mathrm{d}E}{\mathrm{d}\theta} = \Delta p \frac{\mathrm{d}p}{\mathrm{d}\theta} = -\frac{\Delta p}{\omega(E_n)} \frac{\mathrm{d}V}{\mathrm{d}q}, \tag{C.12}$$

the equality of the classical and quantal ionization probabilities in the sudden limit follows.

Appendix D

Uniform approximations

For one-dimensional systems it is often possible to use uniform methods to obtain asymptotic approximations to the solutions of Schrödinger's equation. The essence of uniform approximations is that similar equations have similar solutions, two equations being similar if their order, type and number of turning points are the same. A rigorous exposition of this theory is given by Cherry (1950); here we concentrate on the elementary case needed for this application. The approximate theory starts with the Schrödinger equation which we assume can be written in the form:

$$\frac{\mathrm{d}^2\psi}{\mathrm{d}x^2} + \hbar^{-2}Q(x)\psi = 0, \tag{D.1}$$

where $Q(x)$ is some sufficiently well behaved function of x. For our application, this equation derives from the Hamiltonian,

$$H(p,q) = p^2/2\mu + V(q), \tag{D.2}$$

in which case,

$$Q(x) = 2\mu(E - V(x)), \tag{D.3}$$

where E is the particle energy, μ its mass and V the potential energy. Let,

$$\frac{\mathrm{d}^2\phi}{\mathrm{d}\sigma^2} + \hbar^{-2}Q_0(\sigma)\phi = 0, \tag{D.4}$$

be a comparison equation such that $Q_0(\sigma)$ and $Q(x)$, equation (D.1), have similar turning point structure over the x-range of interest. We should then expect the solutions $\psi(x)$ and $\phi(\sigma)$, of equations (D.1) and (D.4) respectively, to be approximately related by a coordinate stretch and a rescaling; this can be expressed by writing,

$$\psi(x) = f(\sigma)\phi(\sigma), \qquad \sigma = \sigma(x), \tag{D.5}$$

where $f(\sigma)$ and $\sigma(x)$ remain to be determined; naturally, both f, σ and their inverses must be continuous. The function $\sigma(x)$ can be thought of as a non linear, invertible,

scaling of coordinates and $f(\sigma)$ the associated rescaling of the wave function. The forms of the primitive WKB expressions, namely,

$$\psi(x) = Q^{-1/4}(x) \exp\left(\mathrm{i}\int_{x_0}^{x} \mathrm{d}x' \sqrt{Q(x)}\right), \tag{D.6}$$

$$\phi(\sigma) = Q_0^{-1/4}(\sigma) \exp\left(\mathrm{i}\int_{\sigma_0}^{\sigma} \mathrm{d}\sigma' \sqrt{Q_0(\sigma')}\right), \tag{D.7}$$

suggest a solution with,

$$f(\sigma) = \left(\frac{Q_0(\sigma)}{Q(x)}\right)^{1/4}, \tag{D.8}$$

and $\sigma(x)$ implicitly defined by,

$$\int_{\sigma_0}^{\sigma} \mathrm{d}\sigma' \sqrt{Q_0(\sigma')} = \int_{x_0}^{x} \mathrm{d}x' \sqrt{Q(x')}. \tag{D.9}$$

The coordinate scaling, σ, is obtained by substituting equation (D.5) into (D.1) and using (D.4) to give,

$$\frac{\hbar^2}{f}\frac{\mathrm{d}\phi}{\mathrm{d}\sigma}\frac{\mathrm{d}}{\mathrm{d}x}\left(f^2\frac{\mathrm{d}\sigma}{\mathrm{d}x}\right) + \hbar^2\phi\left(\frac{\mathrm{d}^2 f}{\mathrm{d}\sigma^2}\left(\frac{\mathrm{d}\sigma}{\mathrm{d}x}\right) + \frac{\mathrm{d}f}{\mathrm{d}\sigma}\frac{\mathrm{d}^2\sigma}{\mathrm{d}x^2}\right) + \left(Q - Q_0\left(\frac{\mathrm{d}\sigma}{\mathrm{d}x}\right)^2\right)\phi f = 0, \tag{D.10}$$

which can be satisfied to $O(\hbar^2)$ by choosing σ to satisfy,

$$Q_0(\sigma)\left(\frac{\mathrm{d}\sigma}{\mathrm{d}x}\right)^2 = Q(x). \tag{D.11}$$

For $f(\sigma)$ to be well behaved, $\sigma(x)$ must be chosen so that the zeros of $Q(x)$ and $Q_0(\sigma)$ coincide and are of the same type. Note that with f defined by equation (D.9), we have

$$f(\sigma)^2\frac{\mathrm{d}\sigma}{\mathrm{d}x} = 1, \tag{D.12}$$

and the first term of equation (D.10) is zero.

Equations (D.11), (D.8), (D.5) and (D.4) are the important equations for the application of this method. In practice, it is essential that $Q_0(\sigma)$ can be chosen so that the solution to equation (D.4), $\phi(\sigma)$, can be represented in terms of standard functions with known properties.

Appendix E

Evaluation of action and tunnelling integrals

In this appendix we obtain analytic expressions for the integrals I_ξ, I_η and A given by equations (4.44), (4.55) and (4.47) respectively of section 4.3.2, together with the quantal correction function, $\Phi(x)$, equation (4.56) and the resonance widths, Γ_R^{SC} of equation (4.65). The expressions derived in this appendix are used to numerically evaluate of these functions.

E.1 Evaluation of the action integral I_ξ

The action integral of the ξ-motion is given by equation (4.44),

$$\begin{aligned} I_\xi &= \frac{\sqrt{2\mu}}{\hbar}\int_{\xi_2}^{\xi_1} \mathrm{d}\xi\,\sqrt{E/4 - V_\xi(\xi)}, \\ &= \frac{\sqrt{\mu F}}{2\hbar}\int_{\xi_2}^{\xi_1} \mathrm{d}\xi\,\frac{-\xi^2 + \frac{2E}{F}\xi + \frac{4e^2\beta_1}{F} - \frac{m^2\hbar^2}{\mu F\xi}}{\sqrt{-\xi^3 + \frac{2E}{F}\xi^2 + \frac{4e^2\beta_1}{F}\xi - \frac{m^2\hbar^2}{\mu F}}}. \end{aligned} \tag{E.1}$$

Following the notation of Gallas *et al.* (1982), we write this in the form,

$$I_\xi = \frac{\sqrt{\mu F}}{2\hbar}\left(-I_\xi^{(2)} + \frac{2E}{F}I_\xi^{(1)} + \frac{4e^2\beta_1}{F}I_\xi^{(0)} - \frac{m^2\hbar^2}{\mu F}I_\xi^{(-1)}\right), \tag{E.2}$$

where,

$$\begin{aligned} I_\xi^{(j)} &\equiv \int_{\xi_2}^{\xi_1} \mathrm{d}\xi\,\xi^j\left(-\xi^3 + \frac{2E}{F}\xi^2 + \frac{4e^2\beta_1}{F}\xi - \frac{m^2\hbar^2}{\mu F}\right)^{-1/2}, \\ &\equiv \int_{\xi_2}^{\xi_1} \mathrm{d}\xi\,\frac{\xi^j}{\sqrt{(\xi_1-\xi)(\xi-\xi_2)(\xi-\xi_3)}}. \end{aligned} \tag{E.3}$$

The turning points, ξ_1, ξ_2, are the non-negative roots of the cubic equation,

$$-\xi^3 + \frac{2E}{F}\xi^2 + \frac{4e^2\beta_1}{F}\xi - \frac{m^2\hbar^2}{\mu F} \equiv (\xi_1-\xi)(\xi-\xi_2)(\xi-\xi_3) = 0, \tag{E.4}$$

and, as shown in figure 4.1 on page 101, are ordered $\xi_3 < 0 \leq \xi_2 < \xi_1$. Equation (E.2) can be simplified by using the identity,

$$I_\xi = \frac{\sqrt{2\mu}}{\hbar}\int_{\xi_2}^{\xi_1} \mathrm{d}\xi \sqrt{E/4 - V_\xi(\xi)} \equiv \frac{\sqrt{2\mu}}{2\hbar}\int_{\xi_2}^{\xi_1} \mathrm{d}\xi \frac{\xi}{\sqrt{E/4 - V_\xi}}\frac{\mathrm{d}V_\xi}{\mathrm{d}\xi}, \tag{E.5}$$

which is obtained after a trivial integration by parts. From this identity it follows that,

$$I_\xi = \frac{\sqrt{\mu F}}{2\hbar}\left(\frac{1}{2}I_\xi^{(2)} + \frac{2e^2\beta_1}{F}I_\xi^{(0)} - \frac{m^2\hbar^2}{\mu F}I_\xi^{(-1)}\right). \tag{E.6}$$

Combining equations (E.2) and (E.6) and eliminating $I_\xi^{(2)}$ gives,

$$I_\xi = \frac{\sqrt{\mu F}}{2\hbar}\left(\frac{2E}{3F}I_\xi^{(1)} + \frac{8e^2\beta_1}{3F}I_\xi^{(0)} - \frac{m^2\hbar^2}{\mu F}I_\xi^{(-1)}\right). \tag{E.7}$$

The integrals, $I_\xi^{(j)}$, can be evaluated analytically in terms of complete elliptic integrals (see Abramowitz and Stegun 1965, chapter 17), yielding,

$$\begin{aligned} I_\xi^{(0)} &= g_\xi \mathbf{K}(k_\xi), \qquad I_\xi^{(-1)} = \frac{g_\xi}{\xi_1}\mathbf{\Pi}(\xi_1 - \xi_2)/\xi_1, k_\xi), \\ I_\xi^{(1)} &= g_\xi(\xi_3\mathbf{K}(k_\xi) + (\xi_1 - \xi_3)\mathbf{E}(k_\xi)), \end{aligned} \tag{E.8}$$

where $g_\xi^2 = 4/(\xi_1 - \xi_3)$, $k_\xi^2 = (\xi_1 - \xi_2)/(\xi_1 - \xi_3)$ and $\mathbf{E}$, $\mathbf{K}$ and $\mathbf{\Pi}$ are standard complete elliptic integrals of the first, second and third kinds respectively.

E.2 Evaluation of the action integral I_η

For energies $E < E^S$, the action integral of the η-motion, I_η of equation (4.55), may be evaluated in a similar fashion,

$$\begin{aligned} I_\eta &= \frac{\sqrt{2\mu}}{\hbar}\int_{\eta_1}^{\eta_2} \mathrm{d}\eta \sqrt{E/4 - V_\eta(\eta)}, \\ &= \frac{\sqrt{\mu F}}{2\hbar}\left(\frac{2E}{3F}I_\eta^{(1)} - \frac{8e^2\beta_2}{3F}I_\eta^{(0)} - \frac{m^2\hbar^2}{\mu F}I_\eta^{(-1)}\right), \end{aligned} \tag{E.9}$$

where the integrals, $I_\eta^{(j)}$, are defined by,

$$I_\eta^{(j)} \equiv \int_{\eta_1}^{\eta_2} \mathrm{d}\eta \frac{\eta^j}{\sqrt{(\eta - \eta_1)(\eta_2 - \eta)(\eta_3 - \eta)}}, \tag{E.10}$$

with the roots, $0 \leq \eta_1 < \eta_2 < \eta_3$, obtained from,

$$\eta^3 + \frac{2E}{F}\eta^2 + \frac{4e^2\beta_2}{F}\eta - \frac{m^2\hbar^2}{\mu F} \equiv (\eta - \eta_1)(\eta_2 - \eta)(\eta_3 - \eta). \tag{E.11}$$

As before, the $I_\eta^{(j)}$'s can be expressed in terms of complete elliptic integrals:

$$\begin{aligned} I_\eta^{(0)} &= g_\eta \mathbf{K}(k_\eta), \qquad I_\eta^{(-1)} = \frac{g_\eta}{\eta_1}\mathbf{\Pi}((\eta_2 - \eta_1)/\eta_1, k_\eta), \\ I_\eta^{(1)} &= g_\eta(\eta_3\mathbf{K}(k_\eta) - (\eta_3 - \eta_1)\mathbf{E}(k_\eta)), \end{aligned} \tag{E.12}$$

where $g_\eta^2 = 4/(\eta_3 - \eta_1)$ and $k_\eta^2 = (\eta_2 - \eta_1)/(\eta_3 \quad \eta_1)$.

E.3 Evaluation of the tunnelling integral $A(E)$

The tunnelling integral, $A(E)$ of equation (4.47), can also be evaluated in terms of complete elliptic integrals using the method outlined in this appendix:

$$\begin{aligned} A(E) &= \frac{\sqrt{2\mu}}{\pi}\int_{\eta_2}^{\eta_3} \mathrm{d}\eta\,\sqrt{V_\eta(\eta)-E/4}, \\ &= \frac{\sqrt{\mu F}}{2\pi}\left(-\frac{2E}{3F}A^{(1)} - \frac{8e^2\beta_2}{3F}A^{(0)} + \frac{m^2\hbar^2}{\mu F}A^{(-1)}\right), \end{aligned} \tag{E.13}$$

where η_1, η_2, η_3 are again the roots of equation (E.11) and where the $A^{(j)}$'s are defined by,

$$A^{(j)} \equiv \int_{\eta_2}^{\eta_3} \mathrm{d}\eta\,\frac{\eta^j}{\sqrt{(\eta_1-\eta)(\eta_2-\eta)(\eta_3-\eta)}}, \tag{E.14}$$

and may be written in the form,

$$\begin{aligned} A^{(0)} &= g_A\mathbf{K}(k_A), \qquad A^{(-1)} = \frac{g_A}{\eta_3}\mathbf{\Pi}((\eta_3-\eta_2)/\eta_3, k_A), \\ A^{(1)} &= g_A(\eta_1\mathbf{K}(k_A) + (\eta_3-\eta_1)\mathbf{E}(k_A)), \end{aligned} \tag{E.15}$$

where $g_A^2 = 4/(\eta_3-\eta_1)$ and $k_A^2 = (\eta_3-\eta_2)/(\eta_3-\eta_1)$. In evaluating $A(E)$, the branches for the integrals are chosen so that $A(E) > 0$ for $E < E^S$.

E.4 Evaluation of the quantal correction function $\Phi(x)$

The function $\Phi(x)$ given by equation (4.56),

$$\Phi(x) = x(1-\ln|x|) + \arg\Gamma(1/2+\mathrm{i}x), \tag{E.16}$$

is odd, positive for $x > 0$, has a single maximum of $\Phi \approx 0.15$ at $x = 0.18$. For $x \gg 1$ it has the asymptotic expansion,

$$\Phi(x) = 1/24x + 7/2880x^3 + 31/40320x^5 + O(x^{-7}), \tag{E.17}$$

which is accurate to 0.3% for $x > 1$ and 0.04% for $x > 2$. For small x, the formula given by Abramowitz and Stegun (1965, equation (6.1.27)) may be used to evaluate $\arg\Gamma(1/2+ix)$ but more rapid convergence is obtained by rewriting it in the form,

$$\begin{aligned} \arg\Gamma(1/2+\mathrm{i}x) &= x\Psi(1/2) + \sum_{j=0}^{\infty}\left(z_j - \frac{1}{3}z_j^3 + \frac{1}{5}z_j^5 - \tan^{-1}z_j\right) \\ &+ \frac{7}{3}x^3\zeta(3) - \frac{31}{5}x^5\zeta(5), \qquad z_j = \frac{2x}{1+2j}, \end{aligned} \tag{E.18}$$

where $\zeta(m)$ is the Riemann Zeta function (Abramowitz and Stegun 1965, chapter 23) and $\Psi(x) = \Gamma'(x)/\Gamma(x)$.

E.5 Evaluation of the resonance widths Γ_R^{SC}

A semiclassical expression for the resonance widths is given by equation (4.65). Differentiating the function $F_1(E)$, equation (4.60), with respect to E, gives the following expression for Γ_R^{SC}:

$$\Gamma_R^{SC} = 4\left\{\frac{2}{k^2}\left(\frac{\mathrm{d}I_\eta}{\mathrm{d}E} + \frac{1}{2}\frac{\mathrm{d}\Phi}{\mathrm{d}E}\right) + \frac{\mathrm{d}\Phi}{\mathrm{d}E}\right\}^{-1}, \qquad E = E_R, \tag{E.19}$$

with,

$$\frac{\mathrm{d}I_\eta}{\mathrm{d}E} = \frac{1}{\hbar}\sqrt{\frac{\mu}{F}}\left(\frac{1}{2}I_\eta^{(1)} + e^2\frac{\mathrm{d}\beta_2}{\mathrm{d}E}I_\eta^{(0)}\right). \tag{E.20}$$

Since, at resonance $\mathrm{d}I_\xi/\mathrm{d}E = 0$, it follows that,

$$e^2\frac{\mathrm{d}\beta_2}{\mathrm{d}E} = -e^2\frac{\mathrm{d}\beta_1}{\mathrm{d}E} = \frac{I_\xi^{(1)}}{2I_\xi^{(0)}}, \tag{E.21}$$

so that,

$$\frac{\mathrm{d}I_\eta}{\mathrm{d}E} = \frac{1}{\hbar I_\xi^{(0)}}\sqrt{\frac{\mu}{F}}\left(I_\xi^{(0)}I_\eta^{(1)} + I_\eta^{(0)}I_\xi^{(1)}\right), \tag{E.22}$$

where the $I_\xi^{(j)}$'s and $I_\eta^{(j)}$'s are defined by equations (E.3) and (E.10) respectively. Substituting expression (E.22) into equation (E.19) gives our final semiclassical approximation to the resonance widths:

$$\Gamma_R^{SC} = 4\left\{\frac{2}{k^2}\left(\frac{1}{\hbar I_\xi^{(0)}}\sqrt{\frac{\mu}{F}}\left(I_\xi^{(0)}I_\eta^{(1)} + I_\eta^{(0)}I_\xi^{(1)}\right) + \frac{1}{2}\frac{\mathrm{d}\Phi}{\mathrm{d}E}\right) + \frac{\mathrm{d}\Phi}{\mathrm{d}E}\right\}^{-1}. \tag{E.23}$$

Numerical determination of Γ_R^{SC} therefore only requires the determination of $A(E)$ since all the $I_\xi^{(j)}$ and $I_\eta^{(j)}$ are automatically obtained during the calculation of the energy eigenvalue, E_R.

Appendix F

Asymptotic form for resonance widths

In this appendix we derive the asymptotic form of the integral, defined in equation (5.48),

$$I = \int_0^{2\pi} \mathrm{d}\tau\, \dot{\psi} \exp\left(\mathrm{i}\frac{g(\tau)}{\Omega_0}\right), \qquad g(\tau) = \int_0^{\tau} \mathrm{d}\tau\, \mathcal{E}(\tau), \tag{F.1}$$

as a function of Ω_0 as $\Omega_0 \to 0$ at those values of Ω_0 for which the exponent, and hence the integrand, $f(\tau)$, is 2π-periodic. Since $\dot{g} = \mathcal{E}(\tau) > 0$ for all real values of τ there are no real stationary phase points. However, the exponent is stationary at τ_s the complex roots of $\mathcal{E}(\tau) = 0$ and because of the periodicity $\tau_s + 2\pi$ is also a root: it is important to note that these roots are independent of Ω_0.

From the definition of ψ, equation (5.22), we see that the integral can be written in the form

$$I = 2\Omega_0 \int_0^{2\pi} \mathrm{d}\tau \frac{\dot{k}\mathcal{E} - k\dot{\mathcal{E}}}{\mathcal{E}^2 + 4\Omega_0^2 k^2} \exp\left(\mathrm{i}\frac{g(\tau)}{\Omega_0}\right) \tag{F.2}$$

so that near the stationary phase points the integrand has poles, as shown in figure F.1.

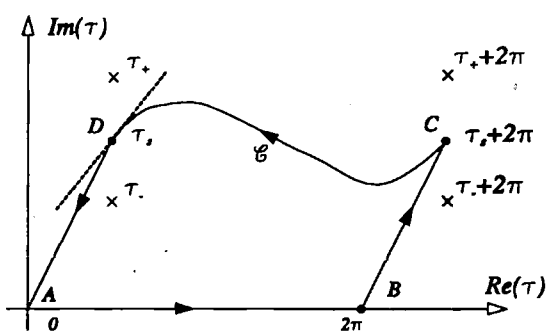

Figure F.1 Diagram showing the relative positions of the contour used to evaluate the integral (F.1), the poles, $\tau_\pm$, the stationary phase points, τ_s, and the stationary path, the dashed line, used to approximate the integral.

Choose the stationary phase point, τ_s, so that $\Im(g(\tau_s)) > 0$ and consider the contour C joining the points $\tau = 0$, 2π, $\tau_s + 2\pi$ and τ_s as shown schematically in figure F.1. Then

because the integrand is periodic the integrals along BC and DA cancel to give,

$$I = \int_0^{2\pi} \mathrm{d}\tau\, f(\tau) = 2\pi \mathrm{i} R(\tau_-) + \int_{DC} \mathrm{d}z\, f(z), \tag{F.3}$$

$R(\tau_-)$ being the residue at τ_-, which is given by,

$$R(\tau_-) = \frac{\mathrm{i}}{2} \frac{\dot{k}\mathcal{E} - k\dot{\mathcal{E}}}{k(\dot{\mathcal{E}} + 2\mathrm{i}\Omega_0 \dot{k})} \exp\left(\mathrm{i}\frac{g}{\Omega_0}\right)\Big|_{\tau=\tau_-} \tag{F.4}$$

$$= \left(-\frac{\mathrm{i}}{2} + O(\Omega_0)\right) \exp\left(-\mathrm{i}\frac{g(\tau_s)}{\Omega_0}\right). \tag{F.5}$$

In order to evaluate the integral along DC we need to expand about both D and C choosing the direction along the path of steepest descent at both ends, but because the integrand is periodic both contributions are obtained by expanding about D, as shown by the dashed line in figure F.1.

Near D we set $\tau = \tau_s + z$ and using the definition (5.22) to expand $\psi(\tau)$ we obtain, using an obvious notation,

$$\tan\psi = \frac{2\Omega_0}{z\dot{\mathcal{E}}_s}\left(k_s + \gamma z + O(z^2)\right), \qquad \gamma = \dot{k}_s - k_s \frac{\ddot{\mathcal{E}}_s}{2\dot{\mathcal{E}}_s}, \tag{F.6}$$

so that near the stationary point,

$$\dot{\psi} = -\frac{2\Omega_0 k_s \dot{\mathcal{E}}_s}{z^2\dot{\mathcal{E}}_s^2 + 4\Omega_0^2 (k_s + z\gamma)^2} + O(z^2) \simeq -\frac{2\Omega_0 k_s \dot{\mathcal{E}}_s}{z^2\dot{\mathcal{E}}_s^2 + 4\Omega_0^2 k_s^2}. \tag{F.7}$$

We use this last approximation because the poles of this function differ from those of the exact function only by $O(\Omega_0^2)$. Now put $z = xe^{\mathrm{i}\beta}$, where x is real and $\beta = \frac{\pi}{4} - \frac{1}{2}\arg(\dot{\mathcal{E}}_s)$, so for the integral along DC we obtain,

$$I_{DC} \simeq -2\Omega_0 k_s \dot{\mathcal{E}}_s \exp \mathrm{i}\left(\beta + \frac{g(\tau_s)}{\Omega_0}\right) \int_{-\infty}^{\infty} \mathrm{d}x\, \frac{1}{x^2\dot{\mathcal{E}}_s^2 e^{2\mathrm{i}\beta} + 4\Omega_0^2 k_s^2} \exp\left(-\frac{|\dot{\mathcal{E}}_s| x^2}{2\Omega_0}\right). \tag{F.8}$$

In order to evaluate this integral consider the Fourier transform of the product,

$$F(y) = \frac{1}{\sqrt{2\pi}} \int_{-\infty}^{\infty} \mathrm{d}x\, e^{\mathrm{i}xy} \frac{e^{-\alpha x^2/\epsilon}}{x^2 + \epsilon^2 a^2}, \tag{F.9}$$

where $\epsilon \ll 1$ and α are real and positive and $\Re(a) > 0$; we need the value of $F(0)$. The Fourier transform of each function in the integrand is readily obtained, so we can express $F(y)$ as the convolution integral,

$$F(y) = \frac{1}{2a\sqrt{2\alpha\epsilon}} \int_{-\infty}^{\infty} \mathrm{d}u\, \exp(-|u|a\epsilon - \epsilon(y-u)^2/4\alpha). \tag{F.10}$$

On setting $y = 0$ and expanding the first, more slowly decaying, exponential we find that,

$$F(0) = \frac{1}{a\epsilon}\sqrt{\frac{\pi}{2}} - \sqrt{\frac{2\alpha}{\epsilon}} + O(1), \tag{F.11}$$

and thus

$$I_{DC} \simeq -\left(\pi + 2ik_s e^{-i\beta}\sqrt{\frac{2\pi\Omega_0}{|\dot{\mathcal{E}}|}}\right)\exp(ig(\tau_s)/\Omega_0). \tag{F.12}$$

On combining this with equations (F.3) and (F.5) we see that

$$I(\Omega_0) = \int_0^{2\pi} d\tau\, \dot{\psi}(\tau)\exp\left(\frac{i}{\Omega_0}\int_0^{\tau} d\tau\, \mathcal{E}(\tau)\right) \simeq -2ik_s\sqrt{\frac{2\pi\Omega_0}{|\dot{\mathcal{E}}|}}\exp i\,(g(\tau_s)/\Omega_0 - \beta) \tag{F.13}$$

so that at the resonant frequencies $|I|$ decreases as $\Omega_0^{1/2}\exp(-C/\Omega_0)$ for some real constant C.

References

Abramowitz M and Stegun I A. 1965. *Handbook of Mathematical Functions.* (New York: Dover).

Allen L and Eberly J H. 1975. *Optical Resonance and Two-Level Atoms.* (London: Wiley-Interscience).

Ammosov M V, Delone N B and Kraĭnov V P. 1986. Tunnel ionization of complex atoms and of atomic ions in an alternating electromagnetic field. *Sov. Phys.-JETP*, **64**, 1191–1194. (*Zh. Eksp. Teor. Fiz.*, **91**, 2008–2013, 1986).

Angel J R P. 1977. Magnetism in White Dwarfs. *Astrophys. J.*, **216**, 1–17.

Arnol'd V I. 1978. *Mathematical Methods of Classical Mechanics.* (Berlin: Springer).

Augst S, Strickland D, Meyerhofer D D, L Chin S and Eberly J H. 1989. Tunneling Ionization of Noble Gases in a High Intensity Laser Field. *Phys. Rev. Lett.*, **63**, 2212–2215.

Augst S, Meyerhofer D D, Strickland D and Chin S L. 1991. Laser ionization of noble gases by Coulomb-barrier suppression. *J. Opt. Soc. Am. B*, **8**, 858–867.

Baldwin K G H and Boreham B W. 1981. Investigation of tunneling processes in laser-induced ionization of argon. *J. Appl. Phys.*, **52**, 2627–2633.

Banks D and Leopold J G. 1978a. Classical Stark ionisation threshold electric field and energy for hydrogenic ions. *J. Phys. B: At. Mol. Phys.*, **11**, L5–L9.

Banks D and Leopold J G. 1978b. Ionisation of highly-excited atoms by electric fields I. Classical theory of the critical field for hydrogenic atoms. *J. Phys. B: At. Mol. Phys.*, **11**, 37–46.

Bardsley J N and Comella M J. 1989. ac Stark effect for short-range potentials with intense electromagnetic fields. *Phys. Rev. A*, **39**, 2252–2255.

Bayfield J E. 1987. Studies of the sinusoidally driven weakly bound atomic electron in the threshold region for classically stochastic behaviour. *Pages 1–33 of:* Pike E R and Sarkar S (eds), *Quantum Measurement and Chaos.* (New York: Plenum).

Bayfield J E and Koch P M. 1974. Multiphoton Ionization of Highly Excited Hydrogen Atoms. *Phys. Rev. Lett.*, **33**, 258–261.

Bayfield J E and Pinnaduwage L A. 1985. Diffusion-like aspects of multiphoton absorption electrically polarized highly excited hydrogen atoms. *Phys. Rev. Lett.*, **54**, 313–316.

Bayfield J E and Sokol D W. 1988a. Excited Atoms in Strong Microwaves: Classical Resonances and Localization in Experimental Final-State Distributions. *Phys. Rev. Lett.*, **61**, 2007–2010.

Bayfield J E and Sokol D W. 1988b. Highly excited hydrogen atoms in strong microwaves. *Pages 315–326 of:* Taylor K T, Nayfeh M H and Clark C W (eds), *Atomic Spectra and Collisions in External Fields.* (New York: Plenum).

Bayfield J E, Gardner L D and Koch P M. 1977. Observation of Resonances in the Microwave-Simulated Multiphoton Excitation and Ionization of Highly Excited Hydrogen Atoms. *Phys. Rev. Lett.*, **39**, 76–79.

Bayfield J E, Casati G, Guarneri I and Sokol D W. 1989. Localization of Classically Chaotic Diffusion for Hydrogen Atoms in Microwave Fields. *Phys. Rev. Lett.*, **63**, 364–367.

Blümel R and Smilansky U. 1987. Microwave Ionization of Highly Excited Hydrogen Atoms. *Z. Phys. D—Atoms, Molecules and Clusters*, **6**, 83–105.

Blümel R and Smilansky U. 1990. Ionization of hydrogen Rydberg atoms in strong monochromatic and bichromatic fields. *J. Opt. Soc. Am. B*, **7**, 664–679.

Breuer H P, Dietz K and Holthaus M. 1989. Low-frequency ionization of excited hydrogen atoms: the Floquet picture. *J. Phys. B: At. Mol. Opt. Phys.*, **22**, 3187–3196.

Brivio G P, Casati G, Perotti L and Guarneri I. 1988. Quantum Suppression of Chaotic Diffusion: Theory and Experiment. *Physica D*, **33**, 51–57.

Burnett K, Knight P L, Piraux B R M and Reed V C. 1991. Suppression of Ionization in Strong Laser Fields. *Phys. Rev. Lett.*, **66**, 301–304.

Casati G, Chirikov B V, Ford J and Izrailev F M. 1979. Stochastic Behaviour in Classical and Quantum Hamiltonian Systems, Como June 1977. *Pages 334–352 of: Lecture Notes in Physics Volume* **93**. (Berlin: Springer).

Casati G, Chirikov B V and Shepelyansky D L. 1984. Quantum Limitations for Chaotic Excitation of the Hydrogen Atom in a Monochromatic Field. *Phys. Rev. Lett.*, **53**, 2525–2528.

Casati G, Guarneri I and Shepelyansky D L. 1987a. Exponential photonic localization for the hydrogen atom in a monochromatic field. *Phys. Rev. A*, **36**, 3501–3504.

Casati G, Chirikov B V, Shepelyansky D L and Guarneri I. 1987b. Relevance of classical chaos in quantum mechanics: the hydrogen atom in a monochromatic field. *Phys. Rep.*, **154**, 77–123.

Casati G, Guarneri I and Shepelyansky D L. 1988. Hydrogen Atom in Monochromatic Field: Chaos and Dynamical Photonic Localization. *IEEE J. Quantum Electron.*, **24**, 1240–1444.

Casati G, Guarneri I and Shepelyansky D L. 1990. Classical Chaos, Quantum Localization and Fluctuations: a Unified View. *(Stat. Phys.* **17***) Physica A*, **163**, 205–214.

Cherry T M. 1950. Uniform Asymptotic Formulae for Functions with Transition Points. *Trans. Amer. Math. Soc.*, **68**, 224–257.

Chin S L, Rolland C, Corkum P B and Kelly P. 1988. Multiphoton Ionization of Xe and Kr with Intense 0.62 μm Femtosecond pulses. *Phys. Rev. Lett.*, **61**, 153–156.

Chirikov B V. 1979. A universal instability of many-dimensional oscillator systems. *Phys. Rep.*, **52**, 263–379.

Chirikov B V. 1989. *Les Houches School on Chaos and Quantum Physics* (Lectures (course II.3), session no. 52, August 1989). (Amsterdam: North-Holland).

Chirikov B V and Shepelyansky D L. 1986. Localization of dynamic chaos in quantum systems. *Radiofizika*, **29**, 1041–1049.

Chu S-I. 1985. Recent developments in semiclassical Floquet theories for intense-field multiphoton processes. *Adv. Atom. Molec. Phys.*, **21**, 197–253.

Connor J N L and Smith A D. 1981. Uniform semiclassical calculation of resonance energies and widths near a barrier maximum. *Mol. Phys.*, **43**, 397–414.

Crothers D S F. 1976. Perturbed symmetric resonance: the parabolic method. *J. Phys. B: Atom. Molec. Phys.*, **9**, 635–643.

Crothers D S F and Hughes J G. 1977. Stueckelberg close-curve-crossing planes. *J. Phys. B: Atom. Molec. Phys.*, **10**, L557–L560.

Damburg R J and Kolosov V V. 1983. Theoretical studies of hydrogen Rydberg atoms in electric fields. *Pages 31–71 of:* Stebbings R F and Dunning F B (eds), *Rydberg States of Atoms and Molecules.* (Cambridge: CUP).

Dando P A and Richards D. 1990. Ionization mechanisms of one-dimensional oscillators in high-frequency fields. *J. Phys. B: At. Mol. Opt. Phys.*, **23**, 3179–3204.

Delone N B and Kraĭnov V P. 1985. *Atoms in Strong Light Fields.* (Berlin: Springer).

Delone N B, Zon B A and Kraĭnov V P. 1978. Diffusion mechanism of ionization of highly excited atoms in an alternating electromagnetic field. *Sov. Phys.-JETP*, **48**, 223–227. (*Zh. Eksp. Teor. Fiz.*, **75**, 445–453, 1978).

Dörr M, Potvliege R M, Proulx D and Shakeshaft R. 1991. Multiphoton processes in an intense laser field. V. The high-frequency regime. *Phys. Rev. A*, **43**, 3729–3740.

Edmonds A R. 1973. Studies of the quadratic Zeeman effect I. Application of the sturmian functions. *J. Phys. B: Atom. Molec. Phys.*, **6**, 1603–1615.

Epstein P S. 1916. Zur Theorie des Starkeffektes. *Ann. Phys.*, **50**, 489–520.

Faisal F H M. 1973. Multiple absorption of laser photons by atoms. *J. Phys. B: Atom. Molec. Phys.*, **6**, L89–L92.

Fishman S, Grempel D R and Prange R E. 1982. Chaos, Quantum Recurrences and Anderson Localization. *Phys. Rev. Lett.*, **49**, 509–512.

Floquet G. 1883. Sur les équations différentielles linéaires a coefficients périodiques. *Ann. Ecole Norm. Supp. (2)*, **XII**, 47–88.

Friedrich H and Wintgen D. 1989. The hydrogen atom in a uniform magnetic field. *Phys. Rep.*, **183**, 37–79.

Gallas J A C, Walther H and Werner E. 1982. WKB solution of the Stark effect in hydrogen. *Phys. Rev. A*, **26**, 1775–1778.

Galvez E J, Sauer B E, Moorman L, Koch P M and Richards D. 1988. Microwave Ionization of H atoms: Breakdown of Classical Dynamics for High Frequencies. *Phys. Rev. Lett.*, **61**, 2011–2014.

Gavrila M and Kaminski J Z. 1984. Free-Free Transitions in Intense High-Frequency Laser Fields. *Phys. Rev. Lett.*, **52**, 613–616.

Gibson G, Luk T S and Rhodes C K. 1990. Tunneling ionization in the multiphoton regime. *Phys. Rev. A*, **41**, 5049 5052.

Goggin M E and Milonni P W. 1988. Driven Morse Oscillator: Classical Chaos, quantum theory, and photodissociation. *Phys. Rev. A*, **37**, 796–806.

Goldstein H. 1980. *Classical Mechanics.* Second edn. (London: Addison-Wesley).

Graham R. 1988. Quantization of Poincaré Maps. *Europhys. Lett.*, **7**, 671–675.

Graham R and Höhnerbach M. 1990. Quantum Map for Molecular Vibrations in High-Frequency Fields. *Phys. Rev. Lett.*, **64**, 637–640.

Graham R and Höhnerbach M. 1991. Quantum effects on the multiphoton dissociation of a diatomic molecule. *Phys. Rev. A*, **43**, 3966–3981.

Grempel D R, Prange R E and Fishman S. 1984. Quantum dynamics of a nonintegrable system. *Phys. Rev. A*, **29**, 1639–1647.

Halbach K and Holsinger R F. 1976. 'SUPERFISH', a computer program for the evaluation of RF cavities with cylindrical symmetries. *Part. Accel.*, **7**, 213–222.

Hauge E H and Støvneng J A. 1989. Tunneling times: a critical review. *Rev. Mod. Phys.*, **61**, 917–936.

Henneberger W C. 1968. Perturbation methods for atoms in intense light beams. *Phys. Rev. Lett.*, **21**, 838–841.

Horbatsch M. 1991. Suppression of ionization in short high frequency laser pulses of high intensity. *Phys. Rev. A*, **44**, R5346–R5349.

Jensen R V. 1982. Stochastic Ionization of Surface-State Electrons. *Phys. Rev. Lett.*, **49**, 1365–1368.

Jensen R V. 1984. Stochastic ionization of surface-state electrons: Classical theory. *Phys. Rev. A*, **30**, 386–397.

Jensen R V, Leopold J G and Richards D. 1988. High-frequency microwave ionization of excited hydrogen atoms. *J. Phys. B: At. Mol. Opt. Phys.*, **21**, L527–L531.

Jensen R V, Sanders M M, Saraceno M and Sundaram B. 1989a. Inhibition of Quantum Transport Due to "Scars" of Unstable Periodic Orbits. *Phys. Rev. Lett.*, **63**, 2771–2775.

Jensen R V, Susskind S M and Sanders M M. 1989b. Microwave Ionization of Highly Excited Hydrogen Atoms: A Test of the Correspondence Principle. *Phys. Rev. Lett.*, **62**, 1476–1479.

Jensen R V, Susskind S M and Sanders M M. 1991. Chaotic ionization of highly-excited hydrogen atoms: comparison of classical and quantum theory with experiment. *Phys. Rep.*, **201**, 1–56.

Jones R R and Bucksbaum P H. 1991. Ionization Suppression of Stark States in Intense Laser Fields. *Phys. Rev. Lett.*, **67**, 3215–3218.

Jowet J M, Month M and Turner S (eds). 1985. *Nonlinear dynamic aspects of particle accelerators.* Lecture Notes in Physics, vol. 247. (Berlin: Springer).

Keldysh L V. 1965. Ionization in the field of a strong electromagnetic wave. *Sov. Phys.-JETP*, **20**, 1307–1314. (*Zh. Eksp. Teor. Fiz.*, **47**, 1945–1957, 1964).

Knight P L. 1993. Private communication.

Koch P M. 1982. Interactions of intense fields with microwave atoms. *J. Physique Coll.*, **43 C2**, 187–201.

Koch P M. 1990. Microwave ionization of excited hydrogen atoms: What we do and do not understand. *Pages 441–475 of:* Campbell D K (ed), *Chaos/Xaoc: Soviet-American Perspectives on Nonlinear Science.* AIP Conference Proceedings. (New York: AIP).

Koch P M and Mariani D R. 1981. Precise measurement of the static electric-field ionization rate for resolved hydrogen Stark sub-states. *Phys. Rev. Lett.*, **46**, 1275–1278.

Koch P M, Moorman L, Sauer B E, Galvez E J, van Leeuwen K A H and Richards D. 1989. Experiments in Quantum Chaos: Microwave Ionization of Hydrogen Atoms. *Phys. Scr.*, **T26**, 51–58.

Koch P M, Moorman L and Sauer B E. 1992. Microwave Ionization of Excited Hydrogen Atoms: Experiments Versus Theories for High Scaled Frequencies. *Pages 173–191 of:* Gay J-C (ed), *Irregular Atomic Systems and Quantum Chaos.* (Philadelphia: Gordon and Breach).

Kramers H A. 1956. *Collected Scientific Papers.* (Amsterdam: North Holland).

Kulander K C, Schafer K and Krause J L. 1991. Dynamic Stabilization of Hydrogen in an Intense, High-Frequency, Pulsed Laser Field. *Phys. Rev. Lett.*, **66**, 2601–2604.

Landau L D and Lifshitz E M. 1971. *Classical Theory of Fields.* Third edn. Course of Theoretical Physics, vol. 2. (Oxford: Pergamon).

Landau L D and Lifshitz E M. 1976. *Mechanics.* Third edn. Course of Theoretical Physics, vol. 1. (Oxford: Pergamon).

Landau L D and Lifshitz E M. 1977. *Quantum Mechanics (Non-relativistic Theory).* Third edn. Course of Theoretical Physics, vol. 3. (Oxford: Pergamon).

Langer R E. 1937. On the Connection Formulas and the Solutions of the Wave Equation. *Phys. Rev.*, **51**, 669–676.

Ledermann W (ed). 1981. *Handbook of Applicable Mathematics.* Vol. 3. (New York: Wiley).

Leforestier C and Wyatt R E. 1982. Optical potential for laser induced dissociation. *J. Chem. Phys.*, **78**, 2334–2344.

Leopold J G and Percival I C. 1978. Microwave Ionization and Excitation of Rydberg Atoms. *Phys. Rev. Lett.*, **41**, 944–947.

Leopold J G and Percival I C. 1979. Ionization of highly excited atoms by electric fields III. Microwave ionization and excitation. *J. Phys. B: At. Mol. Phys.*, **12**, 709–721.

Leopold J G and Richards D. 1985. The effect of a resonant electric field on a one-dimensional classical hydrogen atom. *J. Phys. B: At. Mol. Phys*, **18**, 3369–3394.

Leopold J G and Richards D. 1986. The effect of a resonant electric field on a classical hydrogen atom. *J. Phys. B: At. Mol. Phys.*, **19**, 1125–1142.

Leopold J G and Richards D. 1989. Quasi-resonances for high-frequency perturbations. *J. Phys. B: At. Mol. Opt. Phys.*, **22**, 1931–1961.

Leopold J G and Richards D. 1990. On the quantum Kepler map. *J. Phys. B: At. Mol. Opt. Phys.*, **23**, 2911–2927.

Leopold J G and Richards D. 1991. A semiclassical ionization mechanism for excited hydrogen in high-frequency fields. *J. Phys. B: At. Mol. Opt. Phys.*, **24**, 1209–1240.

Leopold J G and Richards D. 1993a. Harmonic generation by one-dimensional systems. Submitted to *J. Phys. B: At. Mol. Opt. Phys.*.

Leopold J G and Richards D. 1993b. Robust scarred states. In preparation.

Lichtenberg A J and Lieberman M A. 1983. *Regular and Stochastic Motion.* (Berlin: Springer).

McWeeny R and Sutcliffe B T. 1969. *Methods of Molecular Quantum Mechanics.* (London: Academic Press).

Meerson B I, Oks E A and Sasarov P V. 1979. Stochastic instability of an oscillator and the ionization of highly-excited atoms under the action of electromagnetic radiation. *Sov. Phys.-JETPLett.*, **29**, 72–75. (*Pis'ma Zh. Eksp. Teor. Fiz.*, **29**, 79–82, 1979).

Miller W H. 1974. Classical-limit Quantum Mechanics and the Theory of Molecular Collisions. *Adv. Chem. Phys.*, **25**, 69–177.

Month M and Herrera J C (eds). 1970. *Nonlinear dynamics and the beam-beam interaction.* AIP Conference Proceedings, vol. 57. (New York: AIP).

Nauenberg M. 1990. Canonical Kepler Map. *Europhysics Lett.*, **13**, 611–616.

Olkhovsky V S and Recami E. 1992. Recent developments in the time analysis of tunnelling processes. *Phys. Rep.*, **214**, 339–356.

Percival I C. 1977. Semiclassical theory of bound states. *Adv. Chem. Phys.*, **36**, 1–61.

Percival I C and Richards D. 1982. *Introduction to Dynamics.* (Cambridge: CUP).

Perelomov A M, Popov V S and Terent'ev M V. 1966. Ionization of atoms in an alternating electric field. *Sov. Phys.-JETP*, **23**, 924–934. (*Zh. Eksp. Teor. Fiz.*, **50**, 1393–1409, 1966).

Perelomov A M, Popov V S and Kuznetsov V P. 1968. Allowance for the Coulomb interaction in multiphoton ionization. *Sov. Phys.-JETP*, **27**, 451–457. (*Zh. Eksp. Teor. Fiz.*, **54**, 841–854, 1968).

Perry M D, Szöke A, Landen O L and Campbell E M. 1988. Nonresonant Multiphoton Ionization of Noble Gases: Theory and Experiment. *Phys. Rev. Lett.*, **60**, 1270–1273.

Petite G, Agostini P and Yergeau F. 1987. Intensity, pulse width, and polarization dependence of above-threshold-ionization electron spectra. *J. Opt. Soc. Am. B*, **4**, 765–769.

Pont M and Gavrila M. 1987. The levels of atomic hydrogen in intence, high-frequency laser fields. *Phys. Lett. A*, **123**, 469–474.

Pont M and Gavrila M. 1990. Stabilization of Atomic Hydrogen in Superintense, High-Frequency Laser Fields of Circular Polarization. *Phys. Rev. Lett.*, **65**, 2362–2365.

Pont M, Walet N R, Gavrila M and McCurdy C W. 1988. Dichotomy of the Hydrogen Atom in Superintense, High-Frequency Laser Fields. *Phys. Rev. Lett.*, **61**, 939–942.

Pont M, Proulx D and Shakeshaft R. 1991. Numerical integration of the time-dependent Schrödinger's equation for an atom in a radiation field. *Phys. Rev. A*, **44**, 4486–4492.

Rath O. 1990. *The Dynamics of Excited Hydrogen Atoms in Strong Electric and Magnetic fields.* Ph.D. thesis, The Open University.

Rechester A B and Rosenbluth M N. 1978. Electron Heat Transport in a Tokamak with Destroyed Magnetic Surfaces. *Phys. Rev. Lett.*, **40**, 38–41.

Reiss H R. 1980. Effect of an intense electromagnetic field on a weakly bound system. *Phys. Rev. A*, **22**, 1786–1813.

Richards D. 1987. Ionisation of excited one dimensional hydrogen atoms by low-frequency fields. *J. Phys. B: At. Mol. Phys.*, **20**, 2171–2192.

Richards D. 1993. On Stabilization by high-frequency fields. Submitted to *J. Phys. B: At. Mol. Opt. Phys.*.

Richards D, Leopold J G and Jensen R V. 1989a. Classical and quantum dynamics in high-frequency fields. *J. Phys. B: At. Mol. Opt. Phys.*, **22**, 417–433.

Richards D, Leopold J G, Koch P M, Galvez E J, van Leeuwen K A H, Moorman L, Sauer B E and Jensen R V. 1989b. Structure in low frequency microwave ionisation of excited hydrogen atoms. *J. Phys. B: At. Mol. Opt. Phys.*, **22**, 1307–1333.

Richtmyer R D. 1957. *Difference Methods for Initial-Value Problems.* (New York: Interscience).

Rotenberg M. 1970. Theory and Application of Sturmian Functions. *Adv. Atom. Molec. Phys.*, **6**, 233–268.

Sauer B E, van Leeuwen K A H, Mortazawi-M A and Koch P M. 1991. Precise calibration of a microwave cavity with a nonideal waveguide system. *Rev. Sci. Instrum.*, **62**, 189–197.

Sauer B E, Yoakum S, Moorman L, Koch P M, Richards D and Dando P A. 1992. Dynamic Tunneling Ionization of Excited Hydrogen Atoms: A Precise Experiment versus Theories. *Phys. Rev. Lett.*, **68**, 468–471.

Schrödinger E. 1926. Quantisierung als Eigenwertproblem. *Ann. Phys.*, **80**, 437–490.

Schwarzschild K. 1916. Zur Quantenhypothese. *Sitzungsber. Preuss. Akad. Wiss.*, **1**, 548–568.

Shepelyansky D L. 1987. Localization of diffusive excitation in multilevel systems. *Physica D*, **28**, 103–104.

Shirley J H. 1965. Solution of the Schrödinger Equation with a Hamiltonian Periodic in Time. *Phys. Rev.*, **138**, B979–B987.

Su Q, Eberly J H and Javanainen J. 1990. Dynamics of Atomic Ionization Suppression and Electron Localization in an Intense High-Frequency Radiation Field. *Phys. Rev. Lett.*, **64**, 862–865.

Susskind S M and Jensen R V. 1988. Numerical calculations of the ionization of one-dimensional hydrogen atoms using hydrogenic and Sturmian basis functions. *Phys. Rev. A*, **38**, 711–728.

Tang X and Basile S. 1991. Dynamics of a one-dimensional model and a three-dimensional hydrogen atom in an intense high-frequency short-pulse laser. *Phys. Rev. A*, **44**, R1454–R1457.

van Kampen N G. 1981. *Stochastic Processes in Physics and Chemistry.* (Amsterdam: North Holland).

van Leeuwen K A H, v. Oppen G, Renwick S, Bowlin J B, Koch P M, Jensen R V, Rath O, Richards D and Leopold J G. 1985. Microwave Ionization of Hydrogen Atoms: Experiment versus Classical Dynamics. *Phys. Rev. Lett.*, **55**, 2231–2234.

Vos R J and Gavrila M. 1992. Effective Stabilization of Rydberg States at Current Laser Performances. *Phys. Rev. Lett.*, **68**, 170–173.

Walker R B and Preston R K. 1977. Quantum versus classical dynamics in the treatment of multiple photon excitation of the anharmonic oscillator. *J. Chem. Phys.*, **67**, 2017–2028.

Wisdom J. 1987. Chaotic behaviour in the Solar System. *Proc. Roy. Soc. Lond. A*, **413**, 109–129.

Xiong W and Chin S L. 1991. Tunnel ionization of potassium and xenon atoms by intense CO_2-laser. *Sov. Phys.-JETP*, **72**, 268–271. (*Zh. Eksp. Teor. Fiz.*, **99**, 481–487, 1991).

Yajima K. 1982. Resonances for the AC-Stark Effect. *Comm. Math. Phys.*, **87**, 331–352.

Yergeau F, Chin S L and Lavigne P. 1987. Multiple ionization of rare-gas atoms by a CO_2 laser (10^{14} Wcm^{-2}). *J. Phys. B: At. Mol. Phys*, **20**, 723–739.

Zaslavsky G M. 1981. Stochasticity in quantum systems. *Phys. Rep.*, **80**, 157–250.